THE UNIVERSITY
of EDINBURGH

The development of tools to explore the fundamentals of axonemal dynein heavy chain biology and improve the efficiency of genome editing.

Daniel Oliver Dodd

Thesis submitted for the degree of Doctor of Philosophy

The University of Edinburgh

2019

Declaration

I declare that the following work is my own and any work contributed by others has been indicated in the text of this document, all published work cited has been referenced. This thesis and its contents has been written for submission to the University of Edinburgh for the degree of Doctor of Philosophy and has not been previously submitted for any other purpose, nor will it be submitted for any other degree in the future.

Acknowledgements

I would like to acknowledge all those who have made the writing of this thesis possible, however due to the constraints on space and time I will limit these acknowledgements to the individuals who I think have helped me the most in this process. First amongst these I must thank my supervisor Pleasantine for allowing me to join her lab and always being encouraging and believing in my work even when I didn't. Secondly, my thanks to all the members of the Mill lab who welcomed and supported me from the beginning. In the early days of working in the Mill lab I was left in the very capable care of Rob, who I thank for showing me how to work with the mTmG system and teaching me tissue culture; and Girish, who is responsible for inducting me into the world of motile cilia and inspiring me to explore to the many facets of the field. I have constantly relied on the scientific and technical knowledge and support of Pete, Emma and Patricia, without whom I'm pretty certain I wouldn't have gotten anywhere. This project has relied heavily on the expertise of Margaret, who was responsible for creating and maintaining the *SNAP-Dnah5* mouse line, and Davie who has ably assisted me since Margaret's retirement.
I am privileged to work in an institute with a wealth of technical support, I am indebted to Lizzie and Stacey for all their work with me using the FACS and to Stephen and Jeff for sequencing, as well as to Sean, Pam, Joan and everyone else in the technical services department for their assistance. I have also benefitted from the world leading expertise and equipment provided by ESRIC and the HGU's imaging department, Anne, Matt and Laura. I must give special thanks to Laura for spending hours creating and optimising a way to count green fluorescent nuclei which has been invaluable for this project. Alison in Heriot Watt University also deserves special thanks for providing me with beautiful STED images. Thanks to Amelia at the University of Dundee also, for analysing my mTECs ciliary beat frequency and sending me the videos while on maternity leave. Another collaboration which, despite not being successful, deserves to be acknowledged is with the Jarman lab. I would especially like to thank Andy for inviting me to go to his departmental Firbush retreat and for being a good advisor on my committee. I would also like to acknowledge the time and effort that Petra put into teaching me how to inject fly embryos and for the many hours she spent injecting and screening them.

I would like to thank all of the Jackson and Hurd labs for their insights at Wednesday lab meetings. Special thanks to everyone in W1.11 Amy, Angus, Ivet, Tooba, Roly,

Melissa, Liv, Emma, Pete, Ioannis, Faye, Matt, Mark and Rob. Hopefully we will continue to have a fun and productive work environment. I of course have not forgotten to acknowledge my ballast, Fraser, who has been integral to the lab and office.

Thanks also to David Fitzpatrick and Andrew Wood for being on my committee and giving me so much good advice. Andrew is also directly responsible for allowing me into the IGMM and without him and Cathy Abbot I would not have had a chance of getting on the program.

Throughout the four years I have been at the IGMM our little year group of students have become firm friends and that support network has helped me navigate this difficult path. So thank you Yan, Nick, Issy, Andrea, Toby, David, Eleanor, Fiona, Tom, Irene, Tooba

My final acknowledgments are for my friends and family who probably won't read this but have made everything possible. I would like to thank mum, dad, Joe and Nazi for encouraging me to pursue academia. My close friends Jana, Alba, Valerie, Oonagh, Rinita and Alice for sticking with me despite the distance and the time. Most importantly I want to thank Rosie, for putting up with all the demands of the PhD and always being a voice of reason, everything is better and more bearable with you.

Abstract

Motile cilia are microtubule based projections that assist in the movement of fluid over the surface of cells, such as in the respiratory epithelium, or of cells through a fluid, such as in sperm. Ciliary movement is driven by axonemal dyneins (ADs), large molecular complexes which contain long heavy chain ATPase motor subunits. The stability of ADs has been shown to be dependent on multiple cytoplasmically localised proteins, which are involved in their assembly and trafficking to the cilia. The heavy chain subunits have been suggested to be particularly reliant on specialised chaperoning pathways in order to fold into the correct tertiary structure. Hereditary defects in genes encoding the proteins of the ADs or proteins involved in their assembly result in an incurable human disease, primary ciliary dyskinesia (PCD). PCD results in neonatal respiratory distress with lifelong respiratory complications and is also highly heterogenous with mutations in 40 genes associated with it so far. Despite the identification of many putative assembly factors, where and how they interact with AD proteins remains unknown.

In order to investigate AD complexes, from the translation of their subunits to their degradation, in greater spatial and temporal detail a heavy chain outer dynein arm subunit (ODA), *Dnah5*, was tagged with the adaptable SNAP tag in mice. *Dnah5* is the largest AD heavy chain and the most commonly mutated gene in PCD. When developing novel therapeutics the *SNAP-Dnah5* mouse could be used as a reporter for functional rescue in PCD mouse models which exhibit loss of these complexes from the cilia. The effectiveness of the therapy could then be graded on the restoration of SNAP-DNAH5 fluorescence in the motile cilia. As a secondary aim this project also sought to improve the efficiency of CRISPR/Cas9 induced gene correction, via a novel linkage method, to develop a genome editing therapy for PCD, which could be tested using *SNAP-Dnah5* mice.

Using the *SNAP-Dnah5* mouse tracheal epithelial cells I have directly imaged DNAH5's docking onto the motile axoneme from the distal end and have demonstrated that there is a very low level of ODA turnover in mature cilia. I have also shown that the *Dnah5* transcript localises to large apical clusters in ciliated tracheal epithelial cells and via preliminary pulldown experiments that SNAP-DNAH5 might interact with RNA regulatory proteins in maturing motile ciliated cells suggestive of translational regulation. This project demonstrates the utility of this mouse model for future studies.

Lay summary

Motile cilia are hair-like structures projecting from the surface of many of our body's cells that beat or wave in order to assist in the movement of fluids, like mucus out of our airways, or to propel cells, in the case of sperm. When mutations in our DNA mean that these cilia fail to beat, it can be the result of the hereditary disease primary ciliary dyskinesia (PCD). PCD causes neonatal respiratory distress, recurrent infections of the airways as well as infertility and complex problems in how our organs are positioned within our bodies. Currently mutations in 40 genes have been shown to cause PCD. As such, diagnosing and providing therapies for PCD is challenging, and currently there are only therapeutic interventions available to treat PCD symptoms. PCD urgently requires novel treatments to intervene early and prevent progressive airway damage.

Many of the affected genes in PCD make proteins which are important parts of large molecular motors, called axonemal dyneins (ADs), which drive the movement of motile cilia. These are made of very large and complex subunits which require specialised assembly factors to help them fold and form the correct macromolecular machines. These assembly factors are required for cilia motility and mutations in the genes that encode them cause PCD. Without these factors ADs fail to assemble properly and are absent from the cilia resulting in incorrect or no movement. One aim of this project is to use genome editing as a way to cure PCD, by cutting any PCD gene near the incorrect DNA sequence using molecular scissors called CRISPR/Cas9 and replacing it with the healthy sequence. As part of this aim I have been trying to improve the efficiency of this gene replacement using published drugs and a novel method of assembling the 'targeted' Cas9 scissor complex. The second aim of this project was to study the regulation and assembly of the mammalian AD proteins in real time to better understand disease mechanisms. To do this, I have used genome editing to attach a protein tag, named SNAP, to the dynein subunit *Dnah5* in mice (*SNAP-Dnah5* mouse model). This versatile tag can be used for live cell imaging or biochemistry by using different ligands. By adding different colours of dye to cells from these mice we can visualise where the protein is localised in a cell, its turnover and rates of trafficking. By doing this I established that the newly produced DNAH5 is incorporated at the growing tip of the cilia. Biochemical experiments that took advantage of the SNAP tag identified several novel putative DNAH5 interacting proteins which are also known to have a role in RNA regulation. To investigate whether *Dnah5* mRNA might be

specially regulated in order to make these motor subunits, I used a technique to directly visualise how many *Dnah5* transcript molecules exist and where they localise. I have shown that, in epithelial cells of the airways, transcripts of *Dnah5* cluster together beneath the upper surface of the cell where the cilia are located. This suggests *Dnah5* transcripts are actively transported to these clusters which may regulate its conversion into protein. In this study I have created and characterised the *SNAP-Dnah5* mouse line, which can be used to study the fundamental biology of ADs as well as record how well novel therapies work in restoring ADs in motile cilia of PCD models.

Table of Contents

List of figures

List of tables

Abbreviations

%	Percent
°C	Degrees Celsius
µg	Microgram
µl	Microlitre
µM	Micromolar
53BP1	p53-binding protein 1
A	Adenosine/Alanine
aa	Amino acid
AAA	ATPases Associated with diverse cellular Activities
AAV	Adeno-associated virus
AD	Axonemal dynein
ADP	**A**denosine **D**i**p**hosphate
AGT	O6-**a**lkyl**g**uanine-DNA alkyl**t**ransferase
AIH	Avian Influenza Haemagglutinin
AlkB5	Alpha-ketoglutarate-dependent dioxygenase
ALKBH5	AlkB Homolog 5, RNA Demethylase
alt-EJ	**Alt**ernative **E**nd **J**oining
APS	**A**mmonium **P**er**s**ulfate
ARL13B	ADP Ribosylation factor Like GTPase 13B
ARMC4	Armadillo repeat containing 4
AsCy3	**A**r**s**enical Cyanine 3
BFP	Blue Fluorescent Protein
BLM	Bloom
bp	Base pair
BPE	Bovine Pituitary Extract
BRCA1	**Br**east **Ca**ncer gene 1
BRCA2	**Br**east **Ca**ncer gene 2
Brf-A	Brefeldin-A
C11orf70	Chromosome 11 open reading frame 70
C21orf59	Chromosome 21 open reading frame 59
Cas9	CRISPR Associated protein 9
CCDC103	Coiled-Coil Domain Containing 103
CCDC114	Coiled-Coil Domain Containing 114
CCDC115	Coiled-Coil Domain Containing 115
CCDC164	Coilled-Coil Domain Containing 164
CCDC39	Coiled-Coil Domain Containing 39

CCDC40	Coiled-Coil Domain Containing 40
CCDC63	Coiled-Coil Domain Containing 63
CCDC65	Coilled-Coil Domain Containing 65
CCNO	Cyclin O
CDH1	**C**a**dh**erin 1
CDH23	Cadherin 23
CDK	Cyclin Dependent Kinase
cDNA	complementary DNA
CFAP300	Cilia Flagella Associated Protein 300
CG6971	Computed Gene 6971
CHoXAsH	di**ch**l**o**ro **X**anthen dihydroxy **A**r**s**enical **H**elix binder
CrAsH	**C**a**r**boxy-Fl**AsH**
Cre	**C**auses **re**combination
CRISPR	Clustered Regularly Interspaced Short Palindromic Repeats
crRNA	CRISPR RNA
C-terminal	Carboxy terminal
CtIP	C-terminal binding protein-Interacting Protein
DAPT	N-[N-(3,5-**d**ifluorophenacetyl)- L-**a**lanyl]-S-**p**henylglycine **t**-butyl ester
DBCO	**D**i**b**enzo**c**yclo**o**ctyne
DC1	Docking Complex 1
DC2	Docking Complex 2
DC3	Docking Complex 3
DDX3	DEADbox RNA helicase
DEPC	**D**i**e**thyl**p**yro**c**arbonate
DHC	Dynein Heavy Chain
DHC1	Dynein-1-alpha heavy chain, flagellar inner arm I1 complex
DHC10	Dynein-1-beta heavy chain, flagellar inner arm I1 complex
DHC11	Dynein Heavy Chain 11
DHC2	Dynein Heavy Chain 2
DHC3	Dynein Heavy Chain 3
DHC9	Dynein Heavy Chain 9
DHJ	Double Holiday Junction
DIC	Dynein Intermediate Chain
DLC	Dynein Light Chain
DM-CHX	N-(N′,N′-**D**i**m**ethylcarboxamidomethyl)**c**yclo**h**e**x**imide
DMEM	Dulbecco's Modified Eagle's Medium
DMSO	**D**i**m**ethyl **S**ulf**o**xide
DNA	Deoxyribonucleic acid

DNA2	DNA synthesis defective 2
DNAAF1	Dynein Assembly Factor 1, Axonemal
DNAAF2	Dynein Assembly Factor 2, Axonemal
DNAAF3	Dynein Assembly Factor 3, Axonemal
DNAAF4	Dynein Assembly Factor 4, Axonemal
DNAAF5	Dynein Assembly Factor 5, Axonemal
DNAAF6	Dynein Assembly Factor 6, Axonemal
DNAH1	Dynein Axonemal Heavy chain 1
DNAH11	Dynein Axonemal Heavy chain 11
DNAH17	Dynein Axonemal Heavy chain 17
DNAH5	Dynein Axonemal Heavy chain 5
DNAH6	Dynein Axonemal Heavy chain 6
DNAH8	Dynein Axonemal Heavy chain 8
DNAH9	Dynein Axonemal Heavy chain 9
DNAI1	Dynein Axonemal Intermediate chain 1
DNAI1	Dynein, Axonemal, Intermediate chain 1
DNAI2	Dynein Axonemal Intermediate chain 2
DNAI2	Dynein, Axonemal, Intermediate chain 2
DNAJB13	DnaJ Heat Shock Protein Family (Hsp40) Member B13
DNAL	Dynein Axonemal Light Chain 1
DNAL4	Dynein Axonemal Light Chain 4
DNA-PKCs	DNA-dependent protein kinase
dNTP	deoxy Nucleotide Tri-Phosphate
DOA	Dynein Outer Arm
DSB	Double Strand Break
DYF13	Intraflagellar transport protein 56
DynAP	Dynein Assembly Particle
DYNC1H1	Dynein heavy chain 1, cytosolic
DYNLL1	Dynein Light Chain LC8-Type 1
DYNLL2	Dynein Light Chain LC8-Type 2
DYNLRB	Roadblock-related dynein light chain
DYNLT1	Dynein Light Chain Tctex-Type 1
DYNLT3	Dynein Light Chain Tctex-Type 3
DYX1C1	Dyslexia Susceptibility 1 Candidate Gene 1 Protein
EAV	Equine Anemia Virus
EDTA	**E**thylene**d**iamine**t**etraacetic **a**cid
EGF	Epirdermal Growth Factor
EGFP	Enhanced Green Fluorescent Protein

EIF2S3Y	Eukaryotic Translation Initiation Factor 2 Subunit 3 structural gene Y-linked
EN2SA	Engrailed 2 Splice Acceptor
ENO1	Enolase 1
ENSG00000078674	**Ens**embl **G**ene 00000078674
ENSMUSG00000022262	**Ens**embl ***Mus*** *musculus* **G**ene 00000022262
EPB41L4A	Erythrocyte Membrane Protein Band 4.1 Like 4A
ESRIC	Edinburgh Super Resolution Imaging Consortium
Exo1	**Exo**nuclease 1
FACS	Fluorescence Activated Cell Sorting
FAP120	Flagellar Associated Protein 120
FCS	Fetal Calf Serum
FIV	Feline Immunodeficiency Virus
FKBP8	FK506 binding protein Prolyl Isomerase 8
FlAsH	**Fl**uorescin **A**r**s**enical **H**airpin binder
FLP	Flippase
FRT	Flippase Recognition Target
g	gram
G1	Growth phase 1
G2 phase	Growth phase 2
G3BP1	Stress Granule Assembly Factor 1
G3BP2	Stress Granule Assembly Factor 2
GAPDH	**G**lycer**a**ldehyde-3-**P**hosphate **D**ehydrogenase
GAS8	Growth Arrest Specific 8
GRCh38	Genome Reference Consortium Human Build 38
GRCm38	Genome Reference Consortium Mouse Build 38
gRNA	Guide RNA
GSTO1	Glutathione S-Transferase Omega 1
H2B	Histone-2B
HDR	Homology Directed Repair
HEATR	Huntingtin, elongation factor 3, protein phosphatase 2A, TOR1 Repeat
HEATR2	HEAT repeat 2
HEG	Hexa-Ethylene Glycol
HEK	Human Embryonic Kidney
HEK293	Human Embryonic Kidney 293 cells
HITI	Homology Independent Targeted Integration
HR	Homologous Recombination

HSP70	Heat Shock Protein 70
HSP90	Heat Shock Protein 90
HSP90aa1	Heat Shock Protein 90 Alpha Family Class A Member 1
HSPB11	Heat Shock Protein family B (small) member 11
hTERT	**h**uman **Te**lomerase **R**everse **T**ranscriptase
HYDIN	Hydrocephalus-Inducing Protein Homolog
IC1	Intermediate Chain 1
IC138	Intermediate Chain 138
IC140	Intermediate Chain 140
IC2	Intermediate Chain 2
IC3	Intermediate Chain 3
IC4	Intermediate Chain 4
IC5	Intermediate Chain 5
IC69	the 69,000 M(r) intermediate chain
IC78	the 78,000 M(r) intermediate chain
IC97	Intermediate Chain 97
IDA	Inner Dynein Arm
IDT	Integrated DNA Technologies
IF	Immuno-Fluorescence
IFT	Intra-Flagellar Transport
IFT88	Intra-Flagellar Transport 88
IGMM	Institute of Genetics and Molecular Medicine
ITR	Inverted Terminal Repeat
IVT	*In Vitro* Transcription
kDa	KiloDalton
KOD	*Thermococcus **kod**akaraenis*
KSFM	Keratinocyte Serum Free Medium
LB	Luria Broth
LC1	Dynein light chain 1, axonemal
LC10	Dynein light chain 10, axonemal
LC2	Dynein light chain 2, axonemal
LC3	Dynein light chain 3, axonemal
LC4	Dynein light chain 4, axonemal
LC5	Dynein light chain 5, axonemal
LC6	Dynein light chain 6, axonemal
LC7	Light Chain 7
LC7	Dynein light chain 7, axonemal
LC8	Light Chain 8

LC8	Dynein light chain 8, axonemal
LC9	Dynein light chain 9, axonemal
LIG4	DNA Ligase IV
LOX	**L**ysyl **Ox**idase
LoxP	**L**ocus **o**f crossing (**x**) over **P**1
LRRC50	Leucine-rich repeat-containing protein 50
LRRC56	Leucine Rich Repeat Containing protein 56
LRRC6	Leucine-rich repeat-containing protein 6
mAb	monoclonal Anti-Bodies
MARCKS	Myristoylated Alanine-Rich C-Kinase Substrate
MCIDAS	Multiciliate Differentiation And DNA Synthesis Associated Cell Cycle Protein
MEF	Mouse Embryonic Fibroblasts
mg	Milligrams
ml	Millilitre
mM	Millimolar
MMEJ	Microhomology Mediated End Joining
MNS1	Meiosis Specific Nuclear Structural 1
MOPS	3-(N-**mo**rpholino)**p**ropane**s**ulfonic acid
Mre11	Meiotic Recombination 11 Homolog 1
MRN complex	Mre11 Rad50 Nbs1 complex
mRNA	Messenger RNA
ms	Mass Spectrometry
MT	Microtubule
mTEC	mouse Tracheal Epithelial Cells
mTmG	MARCKS Tomato MARCKS GFP
MYL1	Myosin Light chain 1
MYND	myeloid, Nervy, and DEAF-1
Nbs1	Nibrin
NDK	Nucleoside Diphosphate Kinase
N-DRC	Nexin-Dynein Regulatory Complex
NEB	New England Biolabs
ng	Nanograms
NHEJ	Non-Homologous End Joining
nl	Nanolitre
nM	Nanomolar
Nm23-H5	NME/NM23 Family Member 5
Nm23-H7	NME/NM23 Family Member 7
NNO	Nasal Nitrous Oxide

nt	Nucleotide
N-terminal	Amino terminal
OCT	Optimal Cutting Temperature compound
ODA	Outer Dynein Arm
OFD1	Oral-Facial-Digital Syndrome 1 Protein
Opti-MEM	**Opti**mal Minimum Essential Medium
ORF	Open Reading Frame
P/S	Penicillin/Streptomycin
pAb	polyclonal Anti-Bodies
PAGE	**P**oly**A**crylamide **G**el **E**lectrophoresis
PAM	Protospacer Adjacent Motif
PARP1	Poly(ADP-Ribose) Polymerase 1
PAXX	Paralog of XRCC4 And XLF
P-body	Processing-body
PBS	Phosphate-Buffered Saline
PCD	Primary Ciliary Dyskinesia
PCM1	Peri-Centriolar Material 1
PCNA	Proliferating Cell Nuclear Antigen
PCR	Polymerase Chain Reaction
Pih1	Protein interacting with Hsp90 1
PIH1D3	PIH1 Domain Containing 3
Pol	Polymerase
Poly A	Poly-Adenosine
R2TP	Ruvb1-Ruvb2-Tah1-Pih1
Rad50	**Rad**iation sensitive 50
Rad51	**Rad**iation sensitive 51
Rad52	**Rad**iation sensitive 52
Rad54	**Rad**iation sensitive 54
RB	Royal Brompton
ReAsH	**Re**sorufin **A**r**s**enical **H**elix binder
Rep40	**Rep**lication protein 40
Rep52	**Rep**lication protein 52
Rep68	**Rep**lication protein 68
Rep78	**Rep**lication protein 78
RFP	Red Fluorescent Protein
RMI1	RecQ Mediated genome Instability
RNA	RiboNucleic Acid
RNAP II	RNA polymerase II

RP	Retinitis Pigmentosa
RPA	Replication Protein A
RPE-1	Retinal Pigmented Epithelial-1
RPGR	Retinitis Pigmentosa GTPase Regulator
RPM	Rotations Per Minute
rSAP	recombinant Shrimp Alkaline Phosphatase
RSP23	Flagellar radial spoke nucleoside diphosphate kinase
RSPH1	Radial Spoke Head Component 1
RSPH3	Radial Spoke Head Component 3
RSPH4A	Radial Spoke Head Component 4A
RSPH9	Radial Spoke Head Component 9
rtPCR	reverse transcription PCR
RvB	Holliday junction ATP-dependent DNA helicase
RvBL1	RuvB like AAA ATPase 1
RvBL2	RuvB like AAA ATPase 2
S phase	Synthesis phase
Sae2	Sporulation in the Absence of spo Eleven 2
SAM	S-Adenosyl Methionine
SDM	Site-Directed Mutagenesis
SDSA	Synthesis Dependent Strand Annealing
SFTPA1	Surfactant Protein A1
SGBS2	Simpson–Golabi–Behmel syndrome type 2
sgRNA	single guide RNA
SGS1	Slow Growth Suppressor 1
SiR	**Si**licon **R**hodamine
SIV	Simian Immunodeficiency Virus
smRNA FISH	small molecule RNA Fluorescence In-Situ Hybridisation
SPAG1	Sperm Associated Antigen 1
Sprtx-2	sperm-specific trx 2
SSA	Single Strand Annealing
ssDNA	Single stranded DNA
STED	**St**imulated **E**mission **D**epletion
SV40	Simian Virus 40
Tah1	TPR repeat-containing protein associated with Hsp90 1
TALEN	Transcription Activator Like Endo-Nuclease
TBE	Tris Borate EDTA
TBS	Tris-Buffered Saline
TCEA1	Transcription Elongation Factor 1 A

Tctex1	t-complex-testis expressed 1
TCTEX1D2	Tctex1 Domain Containing 2
Tctex2	t-complex-testis expressed 2
TE	**T**ris **E**DTA
TEM	Transmission Electron Microscope
TEMED	**Te**tra**m**ethyl**e**thylene**d**iamine
TIA1L	T-cell-restricted Intracellular Antigen-1 like
TLR	Traffic Light Reporter
TMR	Tetramethylrhodamine
Tn6677	Transposon 6677
TOP3	**Top**oisomerase 3
TPR	tetratricopeptide repeat
tracrRNA	Trans activating CRISPR RNA
T-REx	Tetracycline-regulated gene expression
TRMTS112	TRNA Methyltransferase Subunit 11-2
tRNA	Transfer RNA
Trx	Thioredoxin
TTC25	Tetratricopeptide Repeat Domain 25
TTC26	Tetratricopeptide Repeat Domain 26
Txl-2	Thioredoxin-like 2
TXNDC3	Thioredoxin Domain Containing 3
UoD	University of Dundee
UoE	University of Edinburgh
UoT	University of Tokyo
UTR	**U**n**T**ranslated **R**egion
V	Volts
VSVG	Vesicular Stomatitis Virus Glycoprotein
WDR92	WD40 Repeat 92
WT	Wild Type
x g	Times Gravity
XLF	XRCC4-Like Factor
XPF	Xeroderma Pigmentosum, Complementation Group F
XRCC4	X-Ray Repair Cross Complementing 4
ZMYND10	Zinc Finger MYND-Type Containing 10
α	Alpha
β	Beta
γ	Gamma
δ	Delta

η	Eta
θ	Theta

1. Introduction

1.1 Cilia: microtubular organelles with diverse functions

Cilia are a diverse group of cellular organelles that protrude from the surface of cells with a membrane continuous with the plasma membrane and a microtubule-based structure at their core termed the axoneme (Ledbetter and Porter 1964). The microtubules are composed of α and β tubulin which form nine outer-doublets arranged in a cylinder (Manton 1952; Manton and Clarke 1952) with the plus ends at the tip furthest from the cell. The doublets themselves contain one complete microtubular ring, the A tubule, and a second incomplete ring attached to it, the B tubule, as shown in **Figure 1.1 B)**. Cilia form as an extension of the basal body, which itself can either originate from a centriole or *de novo*, with nine microtubule triplets arranged in a similar pattern to the axoneme (Sorokin 1968; Sorokin 1962). The transition from basal body to axoneme is marked by a structure known as the transition zone, this has been shown to have a role as a gateway into the cilia, restricting the entry of proteins (Craige et al. 2010; Chih et al. 2012; Garcia-Gonzalo et al. 2011). The basal body also extends structures known as transition fibres into the membrane surrounding the cilium, which are important for the formation of cilia and regulating transport between the cilia and the cytoplasm (Wei, Ling, and Hu 2015). The movement of ciliary proteins in and out of the cilia is a highly regulated process known as intra-flagellar transport (IFT), which relies on the action of kinesin motors to bring material in and a dynein motor to transport it back out again as well as many other adaptor proteins (Cole et al. 1998; Kozminski et al. 1993). IFT is essential for the formation and maintenance of cilia as well as for their resorption and signalling responses, as reviewed by (Pedersen and Rosenbaum 2008). Once IFT trains reach the tip of the cilia, termed the distal region, components of the ciliary tip complex assist in remodelling of the trains for transport out of the cilium (Sale and Satir 1977; Dentler and Rosenbaum 1977; Dentler 1980; Marshall and Rosenbaum 2001; Sloboda 2005).

There are two common types of mammalian cilia, cilia with a central pair of doublets that run up the middle of the axoneme and cilia which lack this central pair, **Figure 1.1 A)**. Generally axonemes containing a central pair are motile, whereas the others are immotile. The immotile or primary cilium is found on almost every cell of the human body and was once thought to be vestigial having little or

no function. It has since become clear that the primary cilium is vital for many important cellular functions, such as chemosensation, signal transduction, mechanosensation and cell cycle control (Singla and Reiter 2006; Nachury and Mick 2019). Defects in primary cilia can result in several life threatening developmental disorders, such as Bardet-Biedl syndrome, short rib polydactyly and holoprosencephaly (Mitchison and Valente 2017). The motile cilia however, are found on only a few specialised subsets of cells, such as the respiratory epithelia cells or sperm cells. Mutations that effect the motility of cilia also cause human disease most commonly; male infertility due to defects in proteins specific to the sperm flagella or a more general effect on several motile cilia throughout the body causing primary ciliary dyskinesia (PCD). As this project focuses on motile cilia and PCD, the following introduction will specifically discuss how the proteins of the motile cilia relate to PCD and the potential for development of therapies for PCD.

1.2 The structure and composition of the motile axoneme

Motile cilia have been studied for 344 years, the motile cilium was the first organelle to be observed and studied, by Antony van Leeuwenhoek who described seeing the “incredibly thin feet, or tiny legs, which were moved very nimbly” of a puddle dwelling protist (Leeuwenhoek 1676; Peter Satir 1995). This early fascination with the movement of cilia led to the investigation into the cause of this movement and the detailed structural dissection of the cilium. Early light microscopy investigations of single celled flagellates, such as *Chlamydomonas reinhardtii* and *Tetrahymena thermophila*, and the gills of molluscs identified the presence of fibres within the cilia (Dellinger 1909). It was not until the development of transmission electron microscopes (TEMs) that the fine structure of these fibres and other parts of the motile cilia were visualised (Fawcett and Porter 1954). Using this knowledge of cilia structure, it was demonstrated that the microtubules slide and this results in cilia bending, producing their distinct movement (Satir, 1965), **Figure 1.1 B)**. In motile cilia the microtubule doublets are surrounded by multiple accessory protein complexes. The central doublet pair has a large protein complex, termed the central pair complex, associated with it that acts as a structural link to the rest of the axoneme allowing for fine control of ciliary beating (Goodenough and Heuser 1985; Smith and Yang 2004). The sliding of microtubules relative to one another is mediated by the axonemal dynein (AD) motors. The ADs form outer (ODAs) and inner dynein arms (IDAs) and are arranged along the A tubule of outer doublets at

96 nm intervals, this pattern is determined by a molecular ruler complex (Oda et al. 2014). The outer doublet pairs are connected to each other via the nexin-dynein regulatory complex (N-DRCs), which regulates the frequency and waveform of cilia beat via its connections to the IDAs (Heuser et al. 2009; Awata et al. 2015). The outer doublets are connected to the central pair complex via structures known as radial spokes, which transduce mechanical and chemical signals across the axoneme to regulate dynein function (Patel-King et al. 2004). The tips of motile cilia have a specialised tip complex. In rodents and many other vertebrates this consists of disc-like structures which link to an extra-cellular ciliary structure termed a crown (Dirksen and Satir 1972; Kuhn and Engleman 1978). It has been hypothesised that this crown and tip structure is a signal transducer for outside stimuli; pathogens can become adhered to the crown suggesting it might have an immune sensing role (Tuomanen 1990; Soares et al. 2019).

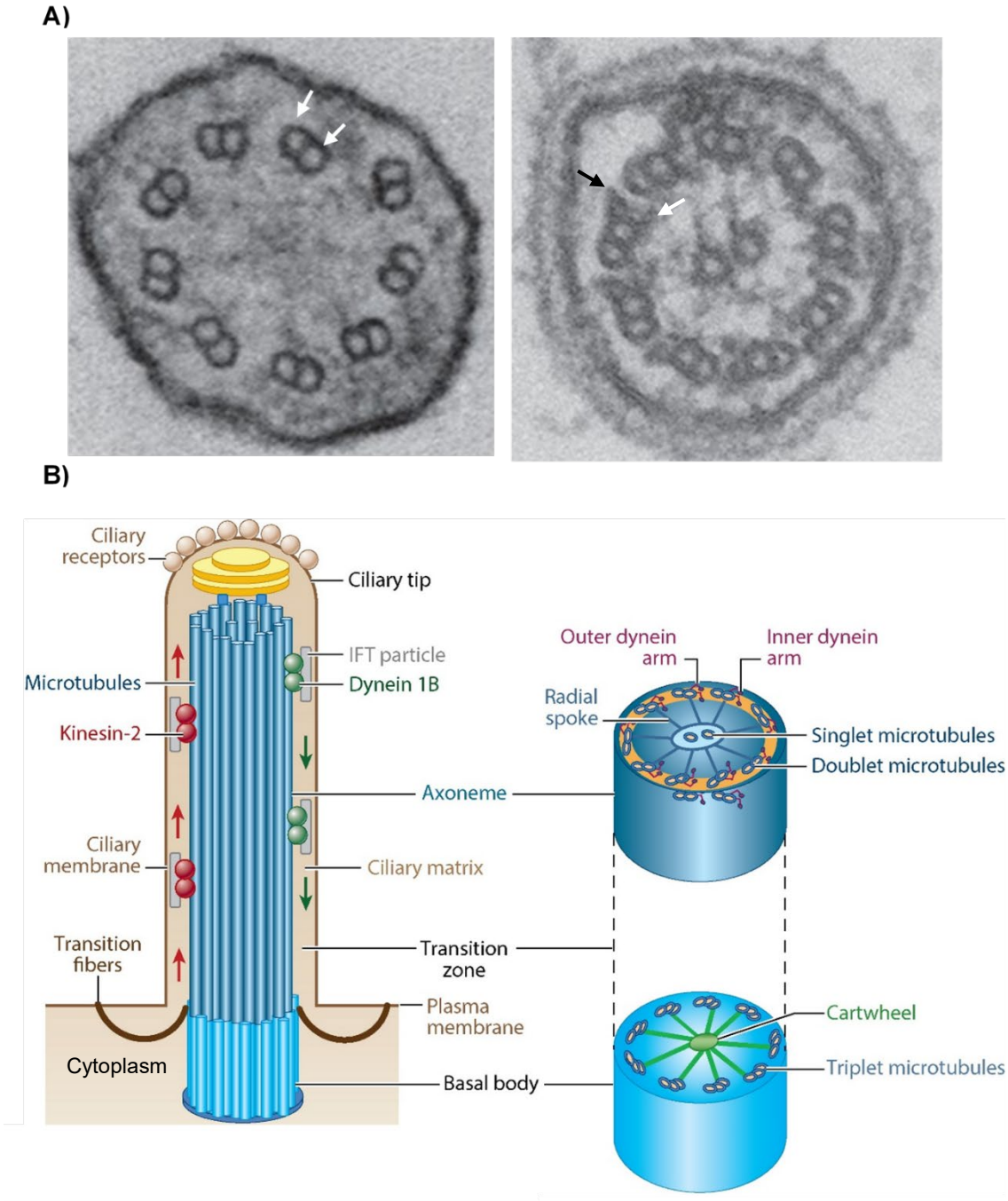

Figure 1.1 The structure of a 9 + 2 mammalian motile cilium

A) The TEM cross-section on the left shows a 9 + 0 primary cilium with the tubules highlighted by white arrows. The image on the right shows a motile 9 + 2 cilium with the ODAs and IDAs indicated by black and white arrows, respectively. Adapted from (Ishikawa, 2017).
B) The diagram on the left shows the longitudinal structure of the axoneme with the basal body underneath. Kinesin-2 is shown transporting IFT into the cilium and dynein 1b is shown directing IFT out of the cilium. The transverse view of the axoneme and basal body are shown on the right, highlighting the structures within. Adapted from (Tilley et al. 2015).

1.2.1 Axonemal dyneins: structures and functions

Axonemal dyneins (ADs), as described above are the motors which drive the movement of motile cilia via microtubule sliding and form the IDA and ODA complexes, which are indicated in the diagram in **Figure 1.1 B)**. The IDAs have been shown to be responsible for controlling the way in which motile cilia move, their waveform, while the ODAs control the frequency of ciliary beating (Brokaw 1994). The structure and composition of these complexes, generally containing heavy, intermediate and light chain subunits, has been determined by their biochemical isolation and fractionation into individual components as well as through electron microscopy. The ODAs seem to have less variation in their composition than IDAs, with bikonts such as *Chlamydomonas*, *Tetrahymena* and *Paramecium* all having three heavy chains or heads (Goodenough & Heuser, 1984; Johnson & Wall, 1983; Travis & Nelson, 1988), while opisthokonts such as sea urchins, tunicates, trout, cows and pigs have two heavy chains or heads (Sale, Goodenough, and Heuser 1985; Padma et al. 2001; Gatti et al. 1989; Belles-Isles et al. 1986; Hastie et al. 1986). IDAs have been well characterised in *Chlamydomonas* by observing various immotile mutants with electron microscopy (Burgess, Carter, Dover, & Woolley, 1991; Goodenough & Heuser, 1985; Mastronarde, O'Toole, McDonald, McIntosh, & Porter, 1992; Piperno & Ramanis, 1991) and fractionation of isolated complexes (Goodenough, Gebhart, Mermall, Mitchell, & Heuser, 1987), but are poorly characterised in other bikonts and in opisthokonts where evidence is only available for some IDAs in sea urchins (Ogawa and Gibbons 1976; Wada, Okuno, and Mohri 1991; Yokota and Mabuchi 1994; Inaba, Mohri, and Mohri 2005). The generalised structures of a selection of these dyneins are shown in **Figure 1.2**.

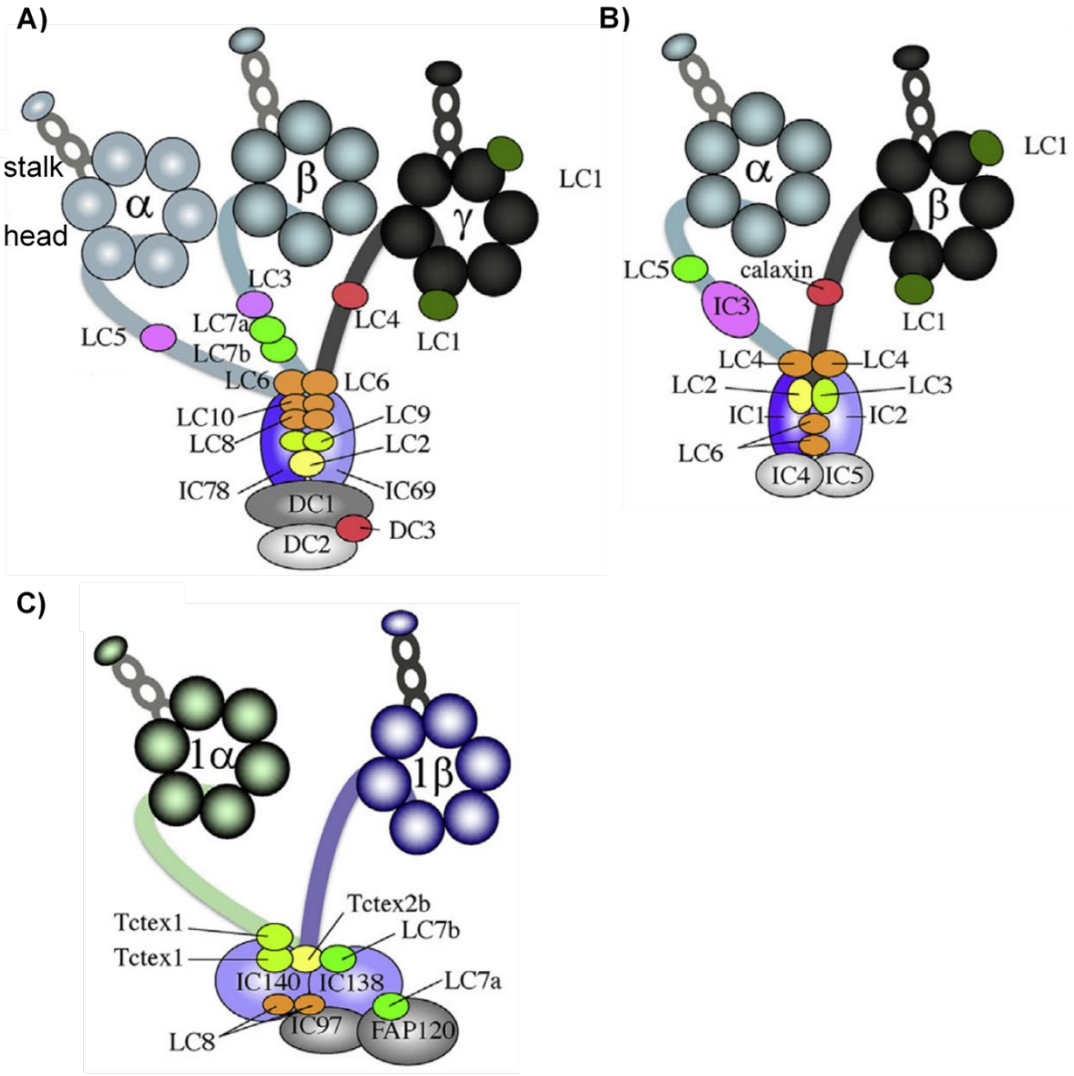

Figure 1.2 structure and composition of axonemal dyneins

A) The figure shows the hypothesised positions of the constituent proteins that make up the *Chlamydomonas* ODA complex, three Dynein Heavy Chains (DHCs) are labelled α, β, and γ and make up the stalk and head regions, the light and intermediate chains are also labelled and positioned according to available structural data and known interactions.
B) Diagram of an opisthokont ODA, specifically using information from studies of sea urchin and trout. The sea urchin α-DHC is an orthologue of *Chlamydomonas* β-DHC and sea urchin β-DHC is an orthologue of *Chlamydomonas* γ-DHC.
C) This figure shows the dimeric *Chlamydomonas* IDA dynein I1/f and its proteins. The diagrams shown are adapted from (Inaba, 2018).

1.2.1.1 Outer Dynein Arms

Human ODAs consist of two heavy chain proteins (DHCs), two intermediate chains (DICs) and potentially six light chains (LICs), based on information from (King 2018). They, like other opisthokont ODAs, lack the α-dynein heavy chain, which is the outermost heavy chain on the A tubule as shown in **Figure 1.2 B)**. Studies of *Chlamydomonas* mutants that lack α-DHC were shown to have increased ATPase activity but reduced movement, suggesting α-DHCs have a more regulatory role than the β and γ DHCs, (Sakato and King 2003; Furuta et al. 2009). The β-DHC provides the majority of the force in *Chlamydomonas* and sea urchin sperm ODAs, however it does not form an ATP dependent bond with microtubules *in vitro* (Sakakibara et al. 1993; Moss, Gatti, and Witman 1992). The γ-DHC has also been shown to be important for ODA force generation and flagellar movement in a study where only the N terminal domain was expressed (Liu et al. 2008). γ-DHC may bind to the B tubule via Light Chain 1 (LC1) in *Chlamydomonas*, which suggests that it might be able to act as a brake on the movement of the ODAs (Patel-King and King 2009).

The opisthokont β-DHC and γ-DHC are vital for the movement of the ODAs and losing one of these in humans results in the loss of the entire complex (Tan et al. 2007). Mammals have an expanded set of ODA heavy chains with three β-DHC (DNAH9, DNAH11 and DNAH17) two γ-DHC (DNAH5 and DNAH8) paralogues identified so far. It is thought that the β-DHC gene was duplicated twice in late metazoan evolution leading to mammals and many other vertebrates having three functionally distinct genes (Kollmar 2016). DNAH11 and DNAH9 are alternative partners of DNAH5 in the ODAs of the respiratory axoneme; DNAH11 occupies the proximal part of the axoneme whilst DNAH9 occupies the distal region (Dougherty et al. 2016). Loss of DNAH9 protein does not cause a reduction in the frequency of beating of respiratory cilia but does affect the way in which they move, due to the absence of ODAs from the distal portion of cilia. In cells that lack DNAH9 it was also shown that DNAH11 is confined to the proximal region of the cilia. However, the reverse is not true; loss of DNAH11 causes DNAH9 to mislocalise along the entire length of the cilia (Fassad, Shoemark, Legendre, et al., 2018; Loges et al., 2018). The difference in regulation and function between these paralogues is highlighted by evidence that mammalian DNAH11 is able to enter the motile cilium without DNAH5 or other essential components of the ODAs (Dougherty et al. 2016). DNAH17 and DNAH8 are only be expressed in the sperm

cells and make up the heavy chains of a distinct ODA complex in these cells (Whitfield et al. 2019; Samant et al. 2002). It's likely that these are the only ODA DHCs used in sperm (Mali et al. 2018) as DNAH5 and DNAH9 have only been seen in sperm axonemes in one study (Fliegauf et al. 2005). The variation in mammalian ODAs is further increased by the presence of alternative splice isoforms. In human ciliated cells *DNAH5* has an alternative first exon (Olbrich et al. 2002). In mouse embryos two splice isoforms of *Dnah11* were identified (Supp et al. 1999) and in mouse sperm cells *Dnah8* has multiple splice isoforms which localise in different regions of spermatocytes (Samant et al. 2002). Whereas in rat brains two isoforms of *Dnah9* were discovered (Tanaka, Zhang, and Hirokawa 1995). While it is clear that mammals have an abundance of variation within and between the heavy chains of the ODAs the mechanistic and functional consequences of these differences have yet to be determined.

1.2.1.2 Inner Dynein Arms

IDAs are the AD complexes that point into the centre of the axoneme and are responsible for regulating waveform, they are more diverse in their composition than the ODAs. IDAs, unlike ODAs, have not been successfully isolated from mammals however their structure and composition has been closely studied in *Chlamydomonas*. Biochemical purification of the IDAs and electron microscopy led to the initial characterisation of the IDA complexes (Piperno & Ramanis, 1991; Piperno, Ramanis, Smith, & Sale, 1990). Genomic comparison found there are at least eleven IDAs in *Chlamydomonas* with ten IDAs possessing one DHC and a single IDA, containing two DHCs, dynein I1/f (Wilkes et al. 2008; Kollmar 2016).

The most well studied IDA is the dimeric dynein I1/f, **Figure 1.2 C)**, which consists of two heavy chains (DHC1 and DHC10), three intermediate chains (IC140, IC138 and IC97), one light intermediate chain (FAP120) and five light chains (Tctex1, Tctex2b, LC7a, LC7b and LC8) (Porter and Sale 2000). *Chlamydomonas* mutants that lack this dynein have a slow swimming phenotype (Kamiya, Kurimoto, and Muto 1991). Dynein I1/f has been shown to be a regulator of microtubule sliding and possibly functions as a brake (Wirschell, Hendrickson, and Sale 2007). Phosphorylation of the intermediate chain IC138 has been shown to disable the motor domain of dynein I1/f (Habermacher and Sale 1997; P. Yang and Sale 2000) and de-phosphorylation activates it.

There have been few *Chlamydomonas* mutants isolated that have mutations in components of the single-headed IDAs. *ida9* is the only strain with a mutation in a DHC gene, *DHC9*. This affects a single IDA, dynein c, which results in a *Chlamydomonas* strain that swims slowly in viscous fluid compared with the wild type, but normally otherwise (Yagi et al. 2005). *ida4* mutants swim slowly and lack a common light chain, p28, resulting in the loss of inner dynein arms a, c, d and DHC11 (Kamiya, Kurimoto, and Muto 1991). The *ida5* strain has a mutation in actin, a component of many monomeric IDAs, these slow swimming mutants lack the IDAs a, c, d and e. *ida6*, which lacks only the IDA species e, has a mutation in an unknown gene and is also slow swimming (Kato et al. 1993).

While it is clear that the IDAs have a role in *Chlamydomonas* flagella their function in the motile cilia of mammals is less clear. DNAH1, the human orthologue of the *Chlamydomonas* DHC2 gene in IDA d, has the strongest evidence to support its importance for motility. Mutations in the mouse *Dnah1* gene, formerly *mDNHC7*, results in slow moving or immotile sperm as well as a reduction in the beat frequency of respiratory cilia (Neesen et al. 2001). Mutation of the orthologous human *DNAH1* results in more dramatic sperm defects, such as shortened, curled or narrow flagella, as well as immobility (Khelifa et al. 2014). There has been no assessment of whether mutations of human *DNAH1* cause a decrease in the beat frequency of respiratory cilia similar to that in mice. A missense mutation was identified in a single family that segregated with symptoms of PCD (Imtiaz et al. 2015), however no other patients have been identified suggesting that *DNAH1* is not commonly mutated in PCD. Similarly *DNAH6*, the human orthologue of *Chlamydomonas* DHC3, has been identified in one study as a potential modifier gene resulting in PCD in patients with heterozygous mutations in other known disease causing genes. The authors also showed that knocking *DNAH6* down in ciliated human nasal biopsies and mouse airway cells resulted in fewer and shortened cilia as well as causing a loss of motility. They showed a defect of the central pair but not an absence of dynein arms both upon *DNAH6* knockdown and in one of the patients with a mutation in this gene (Li et al. 2016). However, it is not clear why there would be an effect only in individuals with heterozygous mutations in known PCD genes when knocking down *DNAH6* seems sufficient to immobilise cilia in culture. While there have been other studies which claim to have found associations with IDA heavy chains and disease in humans there is insufficient data to confirm the validity of these links. This leaves *DNAH1* as the only IDA to so

far be ascribed a function in mammals. It's likely that each IDA has a subtle effect on cilia motility, which will require more detailed investigation to uncover.

1.2.1.3 Heavy chains

The heavy chain dynein subunits make up the bulk of the dynein complex, with DNAH5 being the largest of these in humans, at 529 kDa. The N-terminal domain is the distinguishing feature of heavy chains and contains binding sites for other dynein subunits (Kollmar 2016). It's followed by the linker region, which has been shown to transduce dynein's movement along microtubules either as part of a molecular winch (Burgess, Walker, Sakakibara, Knight, & Oiwa, 2003; Roberts et al., 2009) or grappling hook (Ueno et al. 2008). The heavy chains also contain four sequential AAA+ Walker ATPase domains that are separated from two more AAA+ domains by a microtubule binding domain, which is itself sandwiched between coiled-coil domains. The six AAA+ domains form a hexameric ring and hydrolyse ATP to provide the energy which allows dynein to move, together with the linker region this makes up the motor domain. The C terminal domain has been shown to be a regulatory cap in cytoplasmic dyneins (Nicholas et al. 2015). The domains of the heavy chains and their basic structure is shown in **Figure 1.3**.

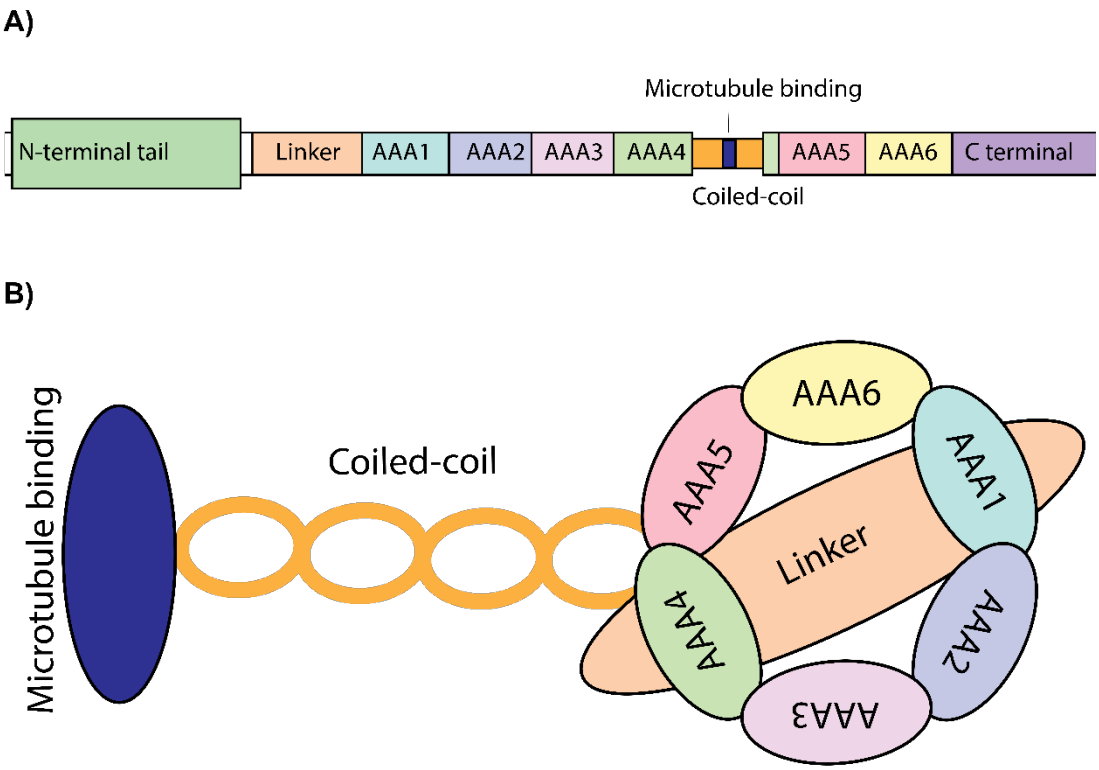

Figure 1.3 The arrangement of the dynein heavy chain domains

A) This figure shows the domains of a generic dynein heavy chain. The unstructured N-terminal tail is followed by the linker region. The AAA domains, numbered 1 to 6, are the ATPase enzymatic domains of the protein. AAA4 is interrupted by a coiled-coil region which has a microtubule binding domain in the middle of it.
B) This is an approximation of where these domains lie in the 3D structure of the protein, the AAA domains form a hexameric ring structure which is linked to the microtubule binding domain via the coiled-coil region. This structure is based on the crystal structure of the Dictyostelium cytoplasmic dynein motor domain (Kon et al. 2012).

The majority of high resolution structural information comes from cytoplasmic dynein and intraflagellar transport dynein (Schmidt, Gleave, and Carter 2012; Schmidt et al. 2015; Kon et al. 2012; Jordan et al. 2018) because, unlike ADs, they do not require assembly factors to form the correct structures. While the domains of the heavy chains are largely conserved between dyneins the number and diversity of heavy chains in the ADs is different. The cytoplasmic and intraflagellar transport dynein have two identical heavy chains, whereas outer arm dyneins can have two or three different heavy chains whilst inner arm dyneins can have a single heavy chain. The way in which the heavy chains are arranged in ODAs, with the hexameric rings stacked on top of one another (Ishikawa, Sakakibara, & Oiwa,

2007; Nicastro et al., 2006; Oda, Hirokawa, & Kikkawa, 2007), suggests that they might function in a different way to the homodimeric heavy chain dyneins (Roberts et al. 2009). The diversity of AD heavy chains points towards different functional roles, this has been shown to be the case in *Chlamydomonas* with the IDAs. Both the cytoplasmic dynein and the intraflagellar dynein have been shown to have inactive forms (Nicastro et al. 2006; Zhang et al. 2017; Jordan et al. 2018) these structures have yet to be identified in the ADs.

1.2.1.4 Intermediate Chains

While the heavy chains are the most studied and structurally characterised subunits the dynein intermediate chains (DICs) are also an important component of dynein. The classification of dynein components originally came from their molecular weight as observed in protein gels. Therefore the DICs are a group of proteins which weigh less than the heavy chains but more than the third group, the light chains. This grouping is not functionally assigned and it means that the intermediate chains encompass a wide variety of different proteins with diverse functions. The largest and most conserved group of DICs is the WD-repeat containing core intermediate chains; all oligomeric dyneins contain two of these DICs which differ mainly at their N and C termini (King, 2017). They are essential for the assembly of the dynein complex in both *Chlamydomonas* and humans, as demonstrated by the loss of ODAs in the absence of their DICs IC1 and IC2 in *Chlamydomonas* (Mitchell & Kang, 1991; Wilkerson, King, Koutoulis, Pazour, & Witman, 1995) and their human equivalents, DNAI1 and DNAI2 (Pennarun et al. 2002; Loges et al. 2008). One of the ways intermediate chains contribute to the assembly of dynein complexes is by acting as protein interaction partners. The WD repeat DICs have been shown to bind to several light chains in *Chlamydomonas* as well as to each other (Susalka et al. 2002; Hendrickson et al. 2004; King, Wilkerson, and Witman 1991; Mitchell and Rosenbaum 1986). Other than acting as linkers holding together the dyneins WD repeat DICs can also act as regulatory proteins, such as in the inactivation of dynein I1/f by phosphorylation of IC138 as mentioned in **Section 1.2.1.2**.

Not all DICs contain WD repeats, one group of DICs contain thioredoxin like modules, the N terminal of the sea urchin β-HC associated DIC IC1 has a thioredoxin unit with three Nucleoside Diphosphate Kinase (NDK) catalytic units downstream (Bell, Fronk, and Gibbons 1979; Ogawa et al. 1996). Similar proteins

are conserved in humans and found associated with motile ciliated cell types. This includes, *Sptrx-2* is expressed in sperm cells (Sadek et al. 2001) *Txl-2* is highly expressed in the testis and the lung (Sadek et al. 2003) while mutations in the thioredoxin *TXNDC3* have been shown to cause PCD (Duriez et al. 2007). Thioredoxins are a group of enzymes which catalyse reduction and oxidation reactions regulating the cellular protein disulphide/dithiol balance (Lu and Holmgren 2014). The redox environment of cells has been shown to directly regulate ciliary beating in *Chlamydomonas* and other organisms including mammals (Price and Sisson 2019; Wakabayashi and King 2006). It has been shown that ODAs react to the redox environment, although this is not necessarily mediated by the intermediate chains; *TXNDC3* and *TXL-2* are actually orthologues of the *Chlamydomonas* light chains LC3 and LC5, respectively. The NDK modules are also found in components of the axoneme and are presumably important for the regulation of ADs via phosphorylation. For instance, the Ca^{2+} NDK domain containing protein RSP23 is located on *Chlamydomonas* radial spokes and is an orthologue of the human gene Nm23-H7 (Patel-King et al. 2004). A similar protein, Nm23-H5, has been found associated with the axonemes of human ciliated cells (Munier et al. 2003). Therefore the DICs are important regulatory proteins within the AD complexes.

1.2.1.5 Light chains

The smallest and most functionally variable group of AD proteins are the dynein light chains (DLCs). The only DLC which has been associated with PCD so far is the human DNAL1 or LC1 in *Chlamydomonas* (Mazor et al. 2011). This protein has been shown to directly interact with the ODA γ-HC and its human orthologue DNAH5 (Horváth et al. 2005; Benashski, Patel-King, and King 1999), where it may act to modulate the timing of dynein beat via tethering to the B tubule (Patel-King and King 2009) The other core light chains fall into three groups: DYNLL, DYNLT and DYNLRB. The DYNLL group in humans (or LC8 group in *Chlamydomonas*) contains three classes of light chain, based on their similarity to LC8, LC10 and LC6. LC8 has two human homologues, DYNLL1 and DYNLL2, these proteins have been found to be essential components of multiple complexes in metazoans including cytoplasmic dynein (King, Barbarese, et al., 1996), myosin V (Espindola et al. 2000) and neuronal nitric oxide synthase (Jaffrey and Snyder 1996). Therefore loss of these DLCs in metazoan organisms leads to a lethal phenotype

early on in development (Dick et al. 1996). In *Chlamydomonas* however losing the function of any of these DLCs results in the development of distinct motility defects (Tanner et al. 2008). While LC6 is seemingly unique to *Chlamydomonas* LC10 is related to mammalian DNAL4, a gene which has been associated with mirror movement disorder in human patients (Ahmed et al. 2014). Despite being an AD protein expressed in the cilia of the mouse apical bronchial epithelium, it is also highly expressed during embryogenesis in the hypothalamus (Tanner et al. 2008). DNAL4 has also been associated with sperm defects and infertility in pigs (Wiedemann et al. 2018), showing it is has some axonemal function in addition to other non-ciliary roles.

DYNLT1, formerly Tctex1, is related to Tctex2 and the *Chlamydomonas* LC9. The T-complex or Tctex genes were originally identified as factors that resulted in non-Mendelian inheritance in mice due to immotile sperm cells (Lader et al. 1989; Huw et al. 1995). Tctex1 was subsequently found to be part of the mouse cytoplasmic dynein (King et al. 1996). Four DYNLT group DLCs are found in ADs; two dimeric Tctex1-like proteins and two monomeric Tctex2-like DLCs are localised to an uncharacterised axonemal complex, while both ODA and IDA I1/f have one Tctex2 (either LC2 or Tctex2b) and contain a dimer of Tctex1 (LC9 and Tctex1) in the *Chlamydomonas* axoneme (DiBella et al. 2001). In mammals, DYNLTs are associated with both cytoplasmic and axonemal dyneins with DYNLT1 and DYNLT3, formerly RP3, being associated with the cytoplasmic dynein and Tctex2 being present in subsets of both cytoplasmic and axonemal dyneins (DiBella et al. 2001). The *Chlamydomonas* Tctex2 orthologue LC2 is essential for the assembly of ODAs (Pazour et al. 1999), while Tctex2b and human version, TCTEX1D2, have been shown to be part of IFT dynein. Human mutations in TCTEX1D2 are associated with a severe developmental disorder, Jeune asphyxiating dystrophy (Schmidts et al. 2015), a disease caused by defects in primary cilia formation. Tctex2 orthologues in *Salmonid* and sea urchin sperm cells are activated via cAMP mediated phosphorylation and are essential for motility as they are in mice (Inaba, Kagami, and Ogawa 1999). Less is known about the exact function of the Tctex1-like proteins, other than their importance in sperm motility in mice and in *Drosophila* (Caggese et al. 2001). They have also been shown to be important for binding to the DICs in cytoplasmic and axonemal dyneins (DiBella et al. 2005; Lo et al. 2007).

The third group of DLCs, the DYNRB or Roadblock group, has only been studied in the ADs of *Chlamydomonas* where the DYNRBs, LC7a and LC7b, were discovered (Bowman et al. 1999). They are also found in mammalian cytoplasmic dyneins, where they are present as dimers (Jikui Song et al. 2005). Loss of LC7a in *Chlamydomonas* results in a significant slowing of flagellar beating similar to that seen in mutants with a loss ODAs, it seems to be important for ODA assembly as its loss results in fewer ODAs which are weakly bound to the axoneme (DiBella et al. 2004).

1.2.2 Axonemal dynein assembly

The ADs are large complexes, ~2 MDa in the *Chlamydomonas* ODA, which have been shown to exist in large cytoplasmic pools in some organisms (Auclair and Siegel 1966; Hisanaga and Sakai 1983). The process of making these complexes and ensuring that the correct subunits assemble together requires a multitude of cytoplasmic proteins, so called dynein axonemal assembly factors (DNAAFs). This is in contrast to cytoplasmic dynein which does not require assembly factors (Schlager et al. 2014). The first evidence showing a requirement for these factors was found in *Chlamydomonas* mutants, *oda7* and *oda10*, which were not able to assemble ADs into their flagella (Kamiya 1988; Fowkes and Mitchell 1998). Since then many other DNAAFs have been found with the majority being functionally conserved in mammals. However, despite the identification of these factors by association with AD assembly, their precise functions are mostly unclear.

The first DNAAF identified, *oda7* in *Chlamydomonas* and LRRC50/DNAAF1 in mammals, was shown to have a specific effect on ODAs in *Chlamydomonas* where it is essential for their formation in the cytoplasm. In the absence of *oda7* a specific ODA HC is depleted, preventing ODA formation (Fowkes and Mitchell 1998). In vertebrates, however, *DNAAF1* mutation also results in loss of some IDAs as well as ODAs and cause PCD in humans (Duquesnoy et al. 2009). This leucine-rich repeat protein was found to interact with Kurly in zebrafish, mammalian C21orf59, which itself is able to interact with another leucine-rich repeat protein LRRC6 in Xenopus (Jaffe et al. 2016). Both of these proteins are also essential for ODA and IDA assembly into the axoneme, suggesting that these three DNAAFs may be part of the same complex (Kott et al. 2012; Austin-Tse et al. 2013; Horani et al. 2013). Other studies suggests that LRRC6 might actually be responsible for AD transport or late stage formation of ODAs rather than assembly based on the evidence that

DNAI2, DNAH9 and DNAH5 are still present in the cytoplasm in its absence. However, the proteins do not mislocalise to the same place: the DHCs are sequestered in puncta and DNAI2 is diffuse throughout the cytoplasm, suggesting that the ODA precursor is not formed in the LRRC6 null cells, and therefore this is probably the stage at which LRRC6 is required (Inaba et al. 2016).

The most well studied complex involved in AD assembly is the R2TP chaperoning complex, which also interacts with LRRC6 orthologue Seahorse in zebrafish (Zhao et al. 2013). The R2TP complex was first isolated in yeast and contains two helicases (Rvbl1 and Rvbl2) and two non-enzymatic subunits (PIH1 and TAH1). It mediates the assembly of many different multi-subunit complexes in conjunction with HSP90 (Kakihara and Houry 2012). R2TP itself is therefore not a DNAAF specific chaperoning complex but there are multiple DNAAFs which share homology to its subunits and have been shown to interact with it. In vertebrates PIH1D3/DNAAF6 and DNAAF2 both have domains with homology to yeast PIH1. DNAAF2 and PIH1D3 are both important for the formation of ODAs and IDAs and were shown to interact with DNAI2 and HSP70 by mouse testis co-immunoprecipitation (Omran et al. 2008; Dong et al. 2014; Olcese et al. 2017). Interestingly however the known interactor of the R2TP complex, HSP90, was only found to interact with PIH1D3 but not DNAAF2 (Dong et al. 2014). The specific IDAs affected by PIH1D3 mutation were identified in human patients using EM tomography, showing a loss of IDAs I1/f a, I1/f b and the d and g complexes in some parts of the axoneme (Olcese et al. 2017), suggesting DNAAFs are at least partially specific for different dynein species.

Another DNAAF with homology to a R2TP complex subunit, SPAG1, has an RPAP domain similar to TAH1 and can bind to HSP70 and HSP90 (Benbahouche et al. 2014). Mutation of this gene causes PCD due to loss of ODAs and IDAs, which combined with its cytoplasmic localisation indicate that it is indeed a DNAAF (Knowles, Ostrowski, et al. 2013). It has been shown in *Drosophila* that SPAG1 makes up an R2TP interaction complex with WDR92, which is itself a DNAAF (Zur Lage et al. 2018). SPAG1 has also been shown to co-localise with DNAAF2 and another DNAAF, HEATR2, early on in the differentiation of human tracheal epithelial cells (Horani et al. 2018). If they are in a complex at this stage then it is possible SPAG1 represents a link between the early and late stages of assembly, as it has been suggested that WDR92 is a late stage recruiter of partially

assembled ADs to the R2TP (Zur Lage et al. 2018). Another important addition to the R2TP-like DNAAFs is DNAAF4/DYX1C1, which has been shown to interact with DNAAF2 as well as HSP70 and HSP90 (Tarkar et al. 2013; Chen et al. 2009). Both DNAAF4 and LRRC6 contain a p23 like domain, p23 has been shown to bind HSP70 and HSP90 (Buchner and Li 2013), which may mediate their binding to these chaperones rather than the R2TP complex itself. It is possible that there is an interaction between the R2TP complex and the R2TP-like DNAAFs, although the stage/s at which this happens and how exactly any interaction is mediated is unknown.

HEATR2 is not found to be associated with the heat shock chaperones or any other DNAAFs by immunoprecipitation, despite its co-localisation with SPAG1 and DNAAF2. It is a member of the HEAT repeat containing proteins, which makes it unique amongst DNAAFs, and it has been shown to be essential for AD assembly in flies and humans (Horani et al. 2012; Diggle et al. 2014). While it was not found to interact with either HSP70 or HSP90 HEATR2 was shown to interact with DNAI2, suggesting it may be part of a different complex to SPAG1.

ZMYND10 is another example of an HSP90 interacting DNAAF. *ZMYND10* mutations were shown to cause the loss of IDAs and ODAs in humans and mice (Zariwala et al. 2013; Mali et al. 2018; Cho et al. 2018). Where ZMYND10 is predicted to fit into the interaction network for DNAAFs is debatable as it was shown to interact with LRRC6, C21orf59, DNAAF4 and RUVBL2 in pulldowns (Cho et al. 2018). However, in another study these interactions were not seen endogenously and it was shown to interact with HSP90 and an immunophilin protein folding factor, FKBP8 (Mali et al. 2018). It has also been shown to be important for DIC stability, specifically for DNAII in transient expression with LRRC6 in HEK 293 cells (Cho et al. 2018) as well as DHC stability (Mali et al. 2018). It is possible that it does both and may form transient interactions with the identified proteins. Its effect on DHC is mirrored by other DNAAFs which seem to be important for the stability of these proteins, such as WDR92 (Patel-King et al. 2019), DNAAF2 (Omran et al. 2008) and DNAAF3 (Mitchison et al. 2012). It is predicted that due to the size and complexity of DHCs their interaction domains can become entangled with incorrect binding partners. It's also possible that due to the requirement for a large number of these proteins, ~900,000 ODAs in a multi-ciliated respiratory epithelial cell, the cellular space becomes abnormally crowded

with sticky protein domains which need to separated (King 2016). However, it has been demonstrated that not all DHCs require DNAAFs, DNAH11 is able to assemble on the axoneme without other ODA components and DNAAFs 1 or 3 (Dougherty et al. 2016). Vertebrates do not have pools of pre-assembled ADs and assemble them over a long time period (Jain et al. 2010). The existence of liquid like collections of assembly particles and dynein subunits in cells with growing cilia has been shown and could potentially aid this assembly (Huizar et al. 2018). More detailed observation of the temporal and spatial dynamics of this assembly will help to elucidate the mechanisms that underlie it.

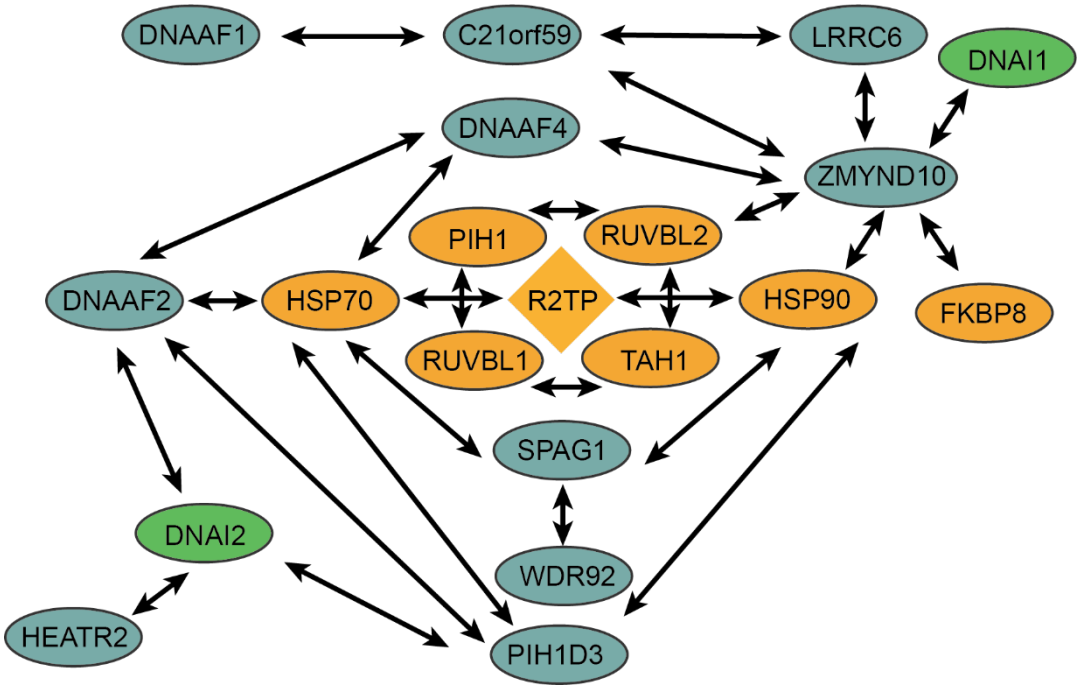

Figure 1.4 DNAAF interactors

The diagram shows the DNAAFs mentioned in the main text (in teal ovals). The R2TP complex with PIH1, TAH1, RUVBL1 and RUVBL2 are shown in the centre of the diagram in orange. Chaperone proteins are also shown in orange ovals. The ODA intermediate chains are shown in green ovals and do interact with one another despite not being connected in this map. Interactions are shown by black arrows, HSP90 and HSP70 interact with the whole R2TP complex.

1.2.3 Trafficking axonemal dyneins

Intra-flagellar transport (IFT) describes the action of active transport into and out of the cilia along the axoneme. Transport into the axoneme, anterograde, is mediated by the heterotrimeric kinesin-2 motor and a group of proteins which makes up the IFT-B complex, which travels along the B tubules at an average

speed of ~2.5 μm/s (Stepanek and Pigino 2016). Similarly retrograde transport in the opposite direction is mediated by the IFT-A complex which binds to cytoplasmic dynein 2/1b, also known as IFT dynein, which travels on the A tubules at an average speed of ~4 μm/s (Stepanek and Pigino 2016). This mechanism was described in *Chlamydomonas* (Kozminski et al. 1993) and was shown to be important for formation of cilia in mice and humans by homology to IFT-B gene *IFT88* (Pazour et al. 2000). The study of IFT has led to the discovery of 22 IFT proteins with the anterograde complex being further subdivided into the groups B-1, the core anterograde IFT proteins, and B-2, the peripheral anterograde IFT proteins (Taschner and Lorentzen 2016). Current research into the roles of these proteins suggest they act as transport adapters but may have various and diverse functions not all of which are in the cilium, such as the Golgi localised IFT20 (Follit et al. 2006).

Trafficking of ADs into the assembling and mature axoneme was demonstrated in early experiments that used a temperature sensitive *Chlamydomonas* mutant of kinesin-2 subunit *FLA10* (Piperno, Mead, and Henderson 1996). This mutant, when grown at the restrictive temperature, loses the ability to transport material into the flagella, which eventually causes its disassembly (Huang, Rifkin, and Luck 1977; Adams, Huang, and Luck 1982). In early experiments by Piperno et al. (1996), it was demonstrated that when the *FLA10* mutant was mixed with wild type in dikaryon rescue experiments that IDAs were not assembled in the cilium at the restrictive temperature but ODAs were, suggesting the IDAs are trafficked by IFT but ODAs are not. They also demonstrated that the IDAs were transported to the tip of the flagella and then were docked progressively towards the base (Piperno, Mead, and Henderson 1996). This was supported by more recent research, which also suggested that *Chlamydomonas* gene *ida3* interacts with IDA intermediate chain IC140 and is important for transporting I1 dynein (Viswanadha et al. 2014). Another IDA specific IFT adapter, TTC26/DYF13, was found to be part of the IFT-B complex in *Chlamydomonas*, mammalian cells and zebrafish and is partially responsible for IDA import in *Chlamydomonas* (Ishikawa et al. 2014). In contrast to the research by Piperno et al. the transport of ODAs was found to be reliant on an interaction with the N-terminal domain of an IFT-B protein, IFT46, and a specific IFT adapter, ODA16 (Ahmed and Mitchell 2005; Ahmed et al. 2008; Hou et al. 2007; Gao et al. 2010; Taschner et al. 2017). This was also shown in recent work in which the trafficking of ODAs was followed using a fluorescently tagged DIC,

IC2. In this study the trafficking of ODAs was shown to be bidirectional and slower than that of IDAs, this constant stopping may explain why ODAs dock along the length of flagella as they are trafficked rather than at the tip like IDAs (Dai et al. 2018). Further evidence for IFT-dependent AD transport comes from sequencing of known cilia related genes in the genomes of PCD patients, which identified mutations in *CFAP300/C11orf70* as causing loss of IDAs and ODAs. Analysis of the orthologues of this gene in *Paramecium* and *Chlamydomonas* showed that it is associated with IFT-A and is trafficked into the motile cilium but is predominantly cytoplasmic (Fassad et al. 2018; Zietkiewicz et al. 2019). Therefore both ODAs and IDAs are transported into the cilium via IFT, which is to be expected as the TZ inhibits diffusion of any complex larger than 50 kDa (Kee et al. 2012). It is clear that the different types of AD are recognised by specific IFT adaptors and this may contribute to their different distributions within the axoneme. A potential example of this specificity is the mammalian LRRC56 or *Chlamydomonas* ODA8 protein which has been shown to be present in assembling flagella. It interacts with IFT88 and its deletion results in impaired ciliary movement in humans causing laterality defects and pulmonary problems. However, only the distal ODAs were effected, with 6-9 arms missing, in a *T. brucei* mutation model, suggesting a very specific trafficking function for LRRC56 (Bonnefoy et al. 2018).

1.2.4 Axonemal dynein docking

The ADs are arranged in a very specific pattern in the axoneme and need to be tightly connected to the nexins and regulatory machinery as well as the axonemal microtubules. The stable docking of ODAs in 24 nm repeats has been shown to rely on three proteins which together make up the docking complex in *Chlamydomonas* (Wakabayashi et al. 2001; Ide et al. 2013; Owa et al. 2014). More recently the role of this docking complex has been further elucidated by *in vitro* reconstitution of ODAs (Oda et al. 2016), which shows that ODAs are capable of arranging themselves in the correct periodicity but are not tightly bound to the MTs. Therefore the docking complex is likely to keep ODAs bound in place rather than direct them to the correct position. This has been shown *in vivo* using a tagged ODA protein which can be seen to transiently bind in the absence of the docking complex (Dai et al. 2018). In *Chlamydomonas* the docking complex is made up of a protein with homology to calmodulin, DC3, (Casey et al. 2003) and two coiled-coil domain proteins, DC2 and DC1, (Takada et al. 2002; Koutoulis et al. 1997).

DC2 is the most widely conserved of these and has two orthologues in vertebrates CCDC63 and CCDC114. Loss of CCDC114 has been shown to result in the absence of ODAs, causing ciliary immobility and PCD (Onoufriadis et al. 2013; Knowles, Leigh, et al. 2013). CCDC63 is highly expressed in testes and has been shown to cause shortened sperm flagella when mutated in mice. However ODAs are still visible in its absence suggesting that it may not be a docking protein or that it is a docking protein but not required at the base of sperm flagella (Young et al. 2015). Another coiled-coil protein, MNS1, was found to be present in sperm and multi-ciliated epithelial cells, and was shown to interact with CCDC114. Mutations in MNS1 caused mild ODA defects in tracheal cilia with arms on MT doublets 2-4 missing in 50% of cross-sections, as well as causing severe sperm and laterality defects in mice and humans, with hydrocephaly in the mice (Zhou et al. 2012; Ta-Shma et al. 2018). Mutation in another ODA DC protein, ARMC4, was also shown to cause a slightly more severe loss of ODAs leading to PCD in affected individuals. Interestingly, DNAH5 was shown to be absent at the distal ends of ARMC4 null tracheal epithelial cells whilst DNAH9 was present along the entire length of the cilia not just at the tip. This mis-localisation of DNAH9 is also observed in the absence of the proximal β-DHC DNAH11, which suggests ARMC4 might be important for directing DNAH11 to the proximal region or for DNAH5 to the distal end (Loges et al. 2018).

CCDC115, another coiled-coil containing protein is found in metazoans and has been shown to have homology to the *Chlamydomonas* assembly factor ODA10 (Dean and Mitchell 2013). In *Drosophila*, it has been shown to have a role in assembly of IFT-dependent chordotonal neuron cilia, however not in the IFT-independent sperm flagella (Jerber et al. 2014). Mutations in CCDC115 also cause PCD, with loss of ODAs as well as ARMC4 and CCDC114 in affected individuals. Further evidence to suggest that these proteins form a docking complex comes from CCDC114's co-immunoprecipitation with CCDC115 in HEK 293 cells (Hjeij et al. 2014). Two more potential docking proteins that seem to be important for cilia motility in humans are TTC25 and CCDC103. TTC25 is widely conserved in opisthokonts and without it the other docking factors CCDC114, CCDC115 and ARMC4 fail to assemble suggesting that it is an essential part of the docking complex (Wallmeier et al. 2016). However, CCDC103 is predicted to not be part of the ODA docking complex and yet seems to be important for both IDAs and ODAs docking to the axoneme, where it has been shown to adhere very tightly with the

MT doublets at regular 12 nm intervals (Panizzi et al. 2012; King and Patel-King 2015). This protein is potentially a more general docking factor, in contrast to some of the other AD docking proteins suggesting a diverse array of docking complexes might exist.

1.3 PCD: a disease of motile cilia

The first records of primary ciliary dyskinesia (PCD) were made by Siewert who noted the correlation of people with *situs inversus* and bronchiecstasis (Siewert 1904). The coalescence of these conditions with chronic sinusitis was named Kartagener syndrome in 1933 by Kartagener, who also noted that it was likely to be heritable (Kartagener 1933). The link between this condition and motile cilia was not made until 1976 when Afzelius used electron microscopy, sperm motility and measurements of muco-ciliary clearance to show that Kartagener patients had defects in their motile cilia (Afzelius 1976). Afzelius initially named the disease immotile ciliary syndrome however when it was later discovered that some suffers did have some motility in their cilia it was renamed primary ciliary dyskinesia to reflect this.

There are as many defects associated with ciliary dyskinesia as there are different types of motile cilia in humans. There are at least five types of motile ciliated cell found within mammals, which are detailed in **Figure 1.5**. The sperm cells have a classical (9 + 2) organisation and are the most similar in terms of their function to the ancestral flagella from which motile cilia evolved, shown in **Figure 1.5 A)**. The flagella is divided into three regions: the connecting piece, the midpiece and the principal piece. The midpiece has been shown to be surrounded by outer dense fibres and mitochondria, which presumably provide the energy for flagella movement (Inaba 2011). While immotile sperm is a common symptom of PCD it is not always present, as sperm cells have a distinct set of axonemal DHCs (Vanaken et al. 2017). The most typical and defining motility defect of PCD is in the epithelial cells in the respiratory tract which cannot provide sufficient muco-ciliary clearance resulting in recurrent respiratory infections and inflammation, **Figure 1.5 C)**. These cells have 200-300 cilia each 5-6 μm in length and they beat in a co-ordinated meta-chronal wave, whereby they propel themselves forward in a stiff, straight conformation to push the mucus upwards and then have a recovery stroke in which they pull back in a more flaccid conformation (Wong, Miller, and Yeates 1993; Elgeti and Gompper 2013; Sears et al. 2013). These cilia also have a sensory role

in the respiratory tract and are able to increase their beat frequency in the presence of bitter tasting compounds (Shah et al. 2009). The epithelial lining of the brain ventricles and spinal cord is known as the ependyma and in the lateral ventricles it is lined with multi-ciliated epithelial cells, **Figure 1.5 D)**. These cells are much like those found on the epithelium of the respiratory tract, except there are only 2-40 cilia per cell and they are slightly longer at ~10 μm (Lechtreck et al. 2008; O'Callaghan, Sikand, and Chilvers 2012). The pattern in which ependymal cells beat in the human brain is not known but it has been hypothesised that they move CSF in compartmentalised circular flow systems from studies in other organisms (Olstad et al. 2019). Without this fluid flow PCD patients can develop hydrocephalus, however it is not very penetrant when compared to mice with immotile ependymal cilia, suggesting that there are other determinants involved (Lee 2013). The epithelial lining of the fallopian tubes is also covered in motile ciliated cells which assist in the movement of egg cells from the ovaries to the uterus. The cilia of these cells are approximately 10 μm in length (Satir 1992) and have a similar protein composition to those of the respiratory epithelia (Raidt et al. 2015). In female PCD patients this can be the cause of fertility problems as well as ectopic pregnancies (Blyth and Wellesley 2008). However, it is of variable penetrance with 61% of female PCD patients having fertility issues in one cohort (Vanaken et al. 2017); this observation suggests that ciliary movement is not the only method of fallopian tube transport (Raidt et al. 2015). Another classical symptom of Kartagener syndrome are situs defects, due to immotile cilia in the embryonic node. This is a specialised region of the developing embryo which is populated with motile mono cilia and surrounded by non-motile sensory cilia (McGrath et al. 2003). Unlike the epithelial motile ciliated cells these cells produce only a single cilium and in contrast to most motile cilia it lacks a central pair, **Figure 1.5 B)**. This cilium moves in a rotational motion and creates a fluid flow which is sensed, via an unknown mechanism, by the non-motile cilia and produces the left-right asymmetry of the body. In PCD patients there is a 50% chance that the symmetry will be reversed or abnormal (Nonaka et al. 2002; McGrath et al. 2003). These defects in symmetry, termed heterotaxy, can result in complex developmental problems, commonly within the heart (Shapiro et al. 2014).

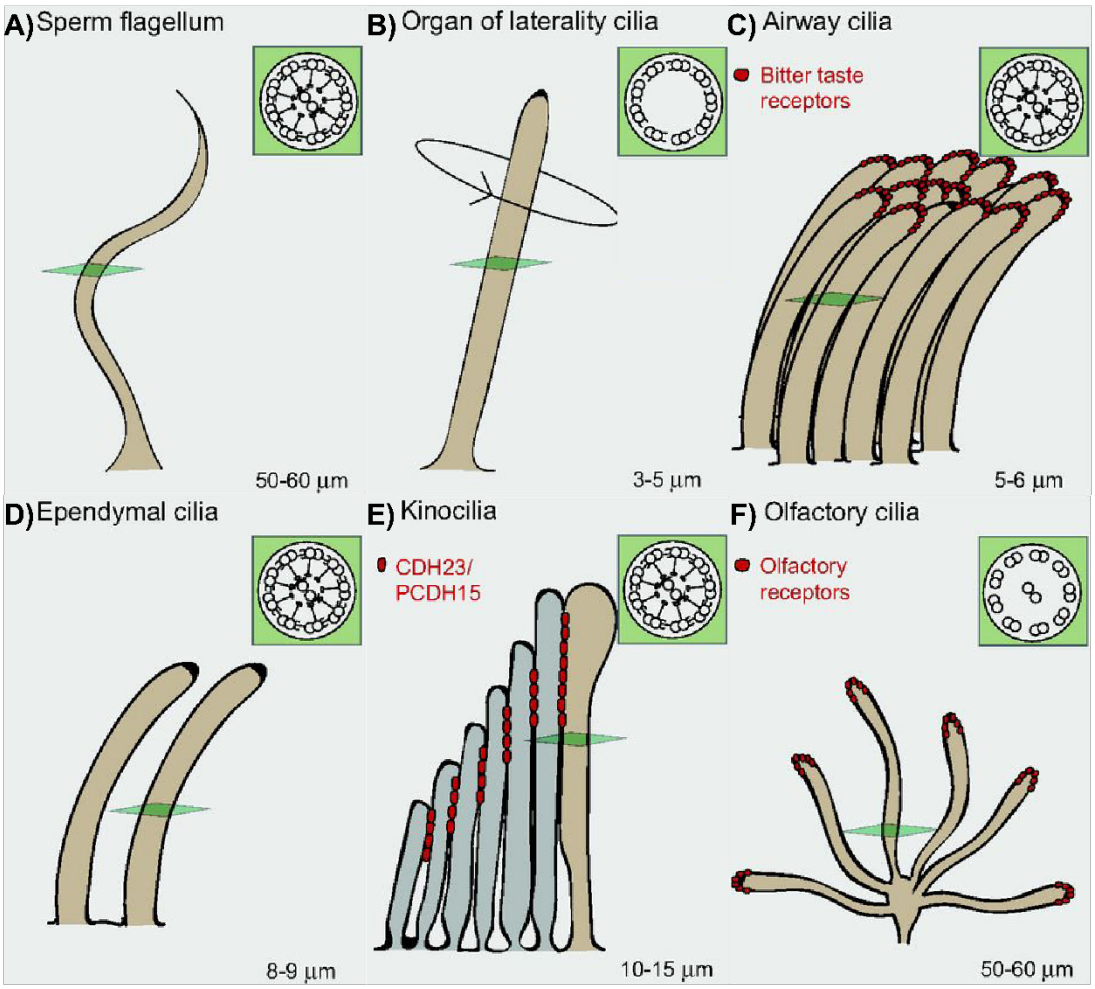

Figure 1.5 Mammalian motile and multi-ciliated cells

A) Diagram of the sperm tail flagella. The green panel is a cross section of the axoneme, showing its 9 + 2 structure microtubule structure and the motile machinery attached to the microtubules.
B) The embryonic cilia at the organ of laterality, the nodal cilia, is shown with the circular motion indicated by the black arrow around the cilium, the cross-section demonstrates that the axoneme has no central pair.
C) Respiratory cilia with the taste receptors highlighted, another classical 9 + 2 cross section.
D) Ependymal cilia, in this case there are only two which is common in the ependymal cells that line the spinal column
E) The Kinocilium, in brown, with the villi attached to it, in grey, by the CDH3 proteins. The cross section shows the same axonemal structure as the ependymal and respiratory cilia.
F) The olfactory cilia on the olfactory bulb, these cilia have no motility proteins but do have a 9 + 2 structure. These images are adapted from (Choksi et al. 2014).

While the nodal cilium is likely the only example of a (9 + 0) motile cilium in humans there are examples of (9 + 2) multi-ciliated cells which are not motile, such as the olfactory cells and the kinocilia, shown in **Figures 1.5 E)** and **F)**. The olfactory cilia are covered in chemo-sensors for the detection of odours, they do not contain the motile machinery. In contrast, the kinocilia are immotile despite having all the necessary components for motility. The kinocilium in humans is a temporary structure but is vital to allow for the development of actin-based stereo cilia in the inner ear. Hearing problems are a common symptom of PCD but this is often due to chronic infection or obstruction of the otitis media, middle ear. This is a result of impaired muco-ciliary clearance from the eustachian tube, an extension of the ciliary lining of the respiratory tract, and not defects of the kinocilia (Piatti et al. 2017). Similarly a reduced sense of smell is sometimes associated with PCD however, this is often attributable to the chronic nasal infections that occur due to muco-ciliary clearance defects (Rimmer 2018). The nasal epithelial cilia are non-motile but are controlled by the same transcriptional program of multiciliogenesis triggered by MCIDAS and CCNO. Mutations in these genes result in similar phenotypes to PCD but also affect the nasal cilia (Boon et al. 2014; Wallmeier et al. 2014; Choksi et al. 2014).

While the above symptoms describe the main consequences of impaired ciliary motility there are other functions of motile cilia which have been less well characterised. It has been shown that CSF flow creates a gradient of signalling molecules in the ventricles which guides the migration of neuroblasts in the brains of mice (Sawamoto et al. 2006). It is possible that a similar mechanism is disrupted in human brains leading to abnormal brain development in PCD patients, however this has not been well studied. While the majority of ciliated ependymal cells in the brain have more than 30 cilia, the spinal cords of mice have been shown to have a small population of bi-ciliated cells. These cilia have a (9 + 2) organisation and the cells begin to proliferate in response to spinal cord injuries (Alfaro-Cervello et al. 2012). However, whether the motility of these cilia is important for normal spinal cord growth and recovery is unknown, the lack of PCD related spinal symptoms suggests it is unlikely.

PCD is often quoted as affecting approximately 1 in 10,000 live births, a figure which comes from a study of patients by Afzelius in his native Sweden (Afzelius and Stenram 2006). However, the true incidence of the disease is hard to calculate,

it is likely to be underdiagnosed and therefore underestimated. In certain populations it can be a lot higher, such as in Volendam in North Holland which has an incidence of at least 1 in 400 (Onoufriadis et al. 2013) or in the British Asian (majority Pakistani) population of Bradford in England which has an incidence of 1 in 2265 (O'Callaghan, Chetcuti, and Moya 2010).

PCD is highly heterogeneous, as might be expected when the complexity of the motile cilia are considered. Currently there are 41 confirmed genes which are known to be loss of function causes of the disease, as shown in **Figure 1.6** (Leigh et al. 2019; Fassad, Shoemark, le Borgne, et al. 2018; Zietkiewicz et al. 2019). The first of these was the ODA intermediate chain *DNAI1* (Pennarun et al. 2002), since then many other ODA genes have been shown to be important for the correct function of cilia. However, it's interesting to note that while mutations in *DNAH9* cause laterality defects and dyskinetic cilia it does not result in a severe enough syndrome to be classed as PCD (Loges et al. 2018; Fassad et al. 2018). Similarly some IDA mutations result in motility defects of the tracheal cilia as well as sperm defects but do not cause PCD (see **Section 1.2.1.2** IDAs). Another example of this is the putative trafficking and assembly gene *LRRC56* which causes sub-threshold reductions in muco-ciliary clearance as well as laterality defects (Bonnefoy et al. 2018). Therefore it could be argued that PCD exists on a ciliopathy spectrum.

Defects in primary cilia often cause severe developmental conditions and as the fundamental blueprint of motile cilia these defects also result in PCD (Mitchison and Valente 2017). A spectrum of disorders, named Simpson–Golabi–Behmel syndrome type 2 (SGBS2), is caused by mutations in the X chromosome encoded gene *OFD1*, and includes PCD at the least severe end (Hannah et al. 2019). *OFD1* encodes a protein which is important for the regulation of centriolar length and the creation of distal appendages, therefore it is crucial for all cilia (Singla et al. 2010), however in hemizygous individuals the motile cilia are more severely affected. Another example of X-linked inheritance of PCD and another ciliopathy is *RPGR*, which causes retinitis pigmentosa resulting in degenerative blindness (Meindl et al. 1996; Krawczyński, Dmeńska, and Witt 2004; A. Moore et al. 2006). RPGR has been shown to be a part of the connecting cilium in photo-receptors and is found in the transition zone of respiratory motile cilia (Hong et al. 2003). The function of this gene remains unclear, both in photoreceptors and motile cilia, however it has

been suggested that in PCD patients with RPGR mutations the orientation of the cilia might be affected (Bukowy-Bieryłło et al. 2013).

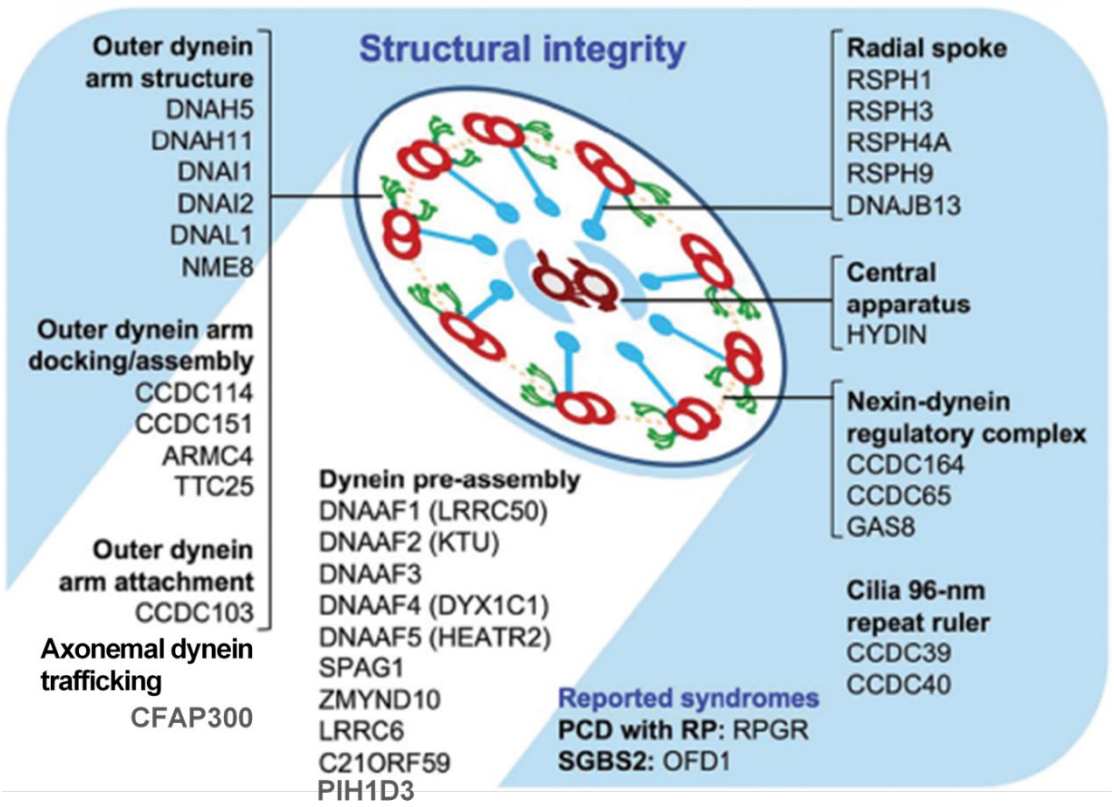

Figure 1.6 Genes associated with PCD

A summary of the genes currently associated with PCD and what their functions are in motile ciliated cells. The CFAP300/C11orf70 protein has recently been linked to PCD and is hypothesised to be an adapter for axonemal dynein transport into the cilia (Fassad, Shoemark, le Borgne, et al. 2018; Zietkiewicz et al. 2019). Similarly PIH1D3 has been found to be an essential DNAAF, DNAAF6, which causes x-linked PCD when mutated (Olcese et al. 2017; Paff et al. 2017). This figure is adapted from (Mitchison and Valente 2017).

The overlapping and variable symptoms that are present in PCD make it difficult to diagnose. The rarity of PCD also contributes to the long wait between presentation and diagnosis of the disease. PCD patients suffer respiratory distress shortly after birth, 12-24 hours, and often require oxygen supplementation for several days before leaving hospital. Despite the early signs of PCD people are often not diagnosed until early childhood. Diagnosis is made easier if they present with *situs inversus* however persistent wet cough and recurrent respiratory infections are also major indicators of PCD. Initial diagnosis of PCD is made by measuring nasal nitrous oxide (NNO) in patients above 5 years of age. If the NNO is low, being somewhere below 82 nl/minutes, then there is a high likelihood of PCD although other conditions may also cause low NNO, such as respiratory infection or some cases of Cystic Fibrosis. There may also be lung function tests and a CAT scan to look for organ positioning defects. The next stage of diagnosis involves referral to a specialist centre, there are only three of these in the UK. Either a nasal brush sample is sent to the centre or taken there, the nasal epithelial cells can then be monitored by high speed video microscopy to observe ciliary beat. TEM images will also be taken of the cilia to check for abnormal ciliary structure, the presence of motile cilia proteins can also be checked using immunofluorescence imaging. In addition to these tests the patient's DNA can be checked against a panel of known PCD causing genes using inexpensive sequencing techniques. There is still the possibility that these tests will miss certain cases of PCD as some gene mutations do not cause obvious structural defects, such as DNAH11 or LRRC56 (see **Sections 1.2.1.3** and **1.2.4**). The mutation may also not be on the panel of tested genes and beat frequency /waveform defects can also be subtle (Lucas et al. 2017; Shoemark and Lucas 2018). Treatment of PCD involves careful monitoring of lung condition, cardiovascular exercise with physiotherapy to help remove mucus and antibiotics to treat bacterial infections of the respiratory system. In more serious cases of chronic infection preventative application of antibiotics is recommended. The use of these interventions can help slow down the decline in lung function and reduce bronchiectasis however it does not treat the cause of the disease, immotile cilia (Shapiro et al. 2016).

1.4 Composition and development of the respiratory epithelium

As explained in the previous section the defining pathology of PCD is respiratory, with diagnosis and treatment being focused on PCD patients' poor lung function

and chronic respiratory infections. This is caused by the dyskinesia of the motile cilia in the epithelial tissues of the airways, resulting in defective muco-ciliary clearance and build-up of mucus that allows pathogens to infect the epithelial cells. The respiratory system can be broadly divided into two parts, the proximal and the distal, the proximal part, including the trachea, is lined with a pseudostratified epithelium while the distal lung is made up of specialised gas exchange structures called alveoli. While defects in the motile cilia of multi-ciliated respiratory cells defines PCD they are just one of a number of different cell types which comprise the proximal airway epithelium, as discussed in a recent review (Zepp and Morrisey 2019). The mucus itself comes from mucin proteins secreted by goblet cells, which are rarely found in mouse but are common in human. Other cells such as ionocytes, a cell type recently discovered by single cell RNA sequencing of the respiratory epithelium (Plasschaert et al. 2018; Montoro et al. 2018), regulate the production and the viscosity of mucus through ion channels such as CFTR. In addition to trapping particles in mucus and clearing them by ciliary action the respiratory epithelium has other cells and methods which help it cope with exposure to airborne pathogens and noxious substances. The brush cells for example have sensory villi on their apical surface allowing them to respond to allergens with inflammatory factors, similarly the secretory or club cells act to protect the epithelial lining by secreting various proteins and by detoxifying toxic substances. The epithelial cells also have a direct connection to the underlying mesenchymal smooth muscle cells through the pulmonary neuroendocrine cells which act to regulate muscle contraction and immune responses. These cells constitute the differentiated proximal airway epithelium.

The cells that make up the lung are specified early on in development in the ventral anterior foregut endoderm, at approximately 4.5 weeks gestation in humans and the 9th embryonic day in mice. However, the distal part of the lung, alveoli, only becomes fully developed at 4-6 weeks in mice and around 10 years in humans in a tissue remodelling process called alveologenesis. In contrast to the epithelium of the distal airways the pseudostratified epithelium of the proximal airways is essentially developed by embryonic day 16.5 in mice, with FOXJ1 positive multi-ciliated cells being present at this time (Rawlins et al. 2007). Epithelial cells of the proximal airways are replaced during normal homeostasis, albeit at a slower rate than other epithelia, and in response to injury. To do this the respiratory epithelium in mice has two types of progenitor cell which can give rise to all the other cells,

the basal stem cell which does not reach the airway lumen due to tight junctions formed above it, and the secretory or club cells. The basal stem cells are found only in the trachea and the large bifurcated bronchi in mice, but are present throughout the proximal respiratory epithelium of humans. It has been shown that these cells differentiate first into secretory cells and then into multi-ciliated cells during homeostasis, a process known as trans-differentiation, whereas in response to injury they can directly form either. The ability of the respiratory epithelium to repair itself in this way means effective therapies for diseases that affect this tissue, such as PCD, are more feasible as the epithelial cells can be replaced.

1.5 Gene therapy as a potential treatment for PCD

An ideal way to treat a genetic condition such as PCD would be to replace the mutated gene with a functioning version. The idea of genetically correcting a disease or gene therapy is not new, having been first attempted in humans in 1958 (Friedmann and Roblin 1972). The traditional approach to gene therapy involves adding a functional copy of the gene affected, termed gene replacement or gene augmentation (Wirth, Parker, and Ylä-Herttuala 2013). Gene therapy often requires viral vectors for efficient delivery of the replacement gene, which puts considerable constraints on its size. The most commonly used viral vectors are adenoviruses, adeno-associated viruses and lentiviruses, these have maximum packaging capacities of 8 kbp, 5 kbp and 8 kbp respectively (Thomas, Ehrhardt, and Kay 2003). This is particularly problematic for PCD, where the most commonly mutated gene, *DNAH5*, has a cDNA length of 13872 bp (Failly et al. 2009; Hornef et al. 2006). For long term expression of the replacement gene many therapies take advantage of the natural integrative capabilities of viruses like the lentiviruses. However, this integration event can be ineffective if the replacement is silenced or detrimental if it occurs either to disrupt an endogenous gene's expression or ectopically activate it, such as in oncogenes (Check 2002). The alternative to integration is transient expression of the therapeutic gene, however this requires expensive repeated delivery which increases the risk of an adverse host immune response.

Both integrative and transient gene therapy have been used for PCD in *ex vivo* and *in vivo* settings. The first of these studies used a lentiviral vector, Simian Immunodeficiency Virus (SIV) coated with Vesicular Stomatitis Virus Glycoprotein (VSVG), to deliver *DNAI1* to human airway epithelial cells *ex vivo*. The authors

were able to demonstrate that delivery of the *DNAI1* was able to restore beating in transduced patient cells with *DNAI1* mutations, with approximately 10% of the axonemes having nine ODAs by TEM which represents ~1/5 of the transduced cells (Chhin et al. 2009). The relevance of this research to the treatment of PCD *in vivo* is limited because the authors transduced cells which were grown in suspension, whereas the respiratory epithelium is made of a diverse collection of cells which form tight junctions with one another and is covered in a layer of mucus. Another study used a lentiviral vector, this time Equine Anemia Virus (EAV) coated with Avian Influenza Haemagglutinin (AIH), to deliver the *Dnaic1* gene. They showed a similar level of rescue in a Cre-inducible *Dnaic1* null mice, ~10% of cells showed recovery (Ostrowski et al. 2014). However, this study used an air liquid interface culture system which is closer to physiological conditions (You et al. 2002). They were also able to demonstrate *in vivo* through inducible deletion of *Dnai1* that only approximately 20% of wild type levels of *Dnai1*, which equates to 20% of cells if Cre recombination is 100% efficient, needs to be present in the nasopharynx for effective muco-ciliary clearance. Despite showing that the viral vector was able to transduce nasal epithelial cells after intranasal delivery of an EGFP reporter in wild type mice, there was no detectable *Dnai1* in the null mice. This highlights the potential difficulty of delivering therapeutics in PCD patients who suffer from chronic rhinosinusitis with thick layers of mucus in the respiratory tract. There may also be an increased number of immune cells in the respiratory epithelial lining in PCD patients due to chronic infection which could cause the viruses or infected cells to be recognised by the immune system and destroyed.

A way to avoid immune recognition of viral vectors is to package the DNA in a synthetically derived vector. Recently cationic lipid based vectors mixed with cationic peptides to allow DNA to pass through the mucosal layer have been developed and tested for use in PCD (Tagalakis et al. 2008; Munye et al. 2016). The authors showed that in combination with a small circularised transgene the lipid vector was able to transfect the lungs of wild type mice and was more effective than a full sized plasmid. Although they did not show whether it was effective in diseased tissue they were able to demonstrate successful expression of *DNAH5* in immortalised human bronchial epithelial cells. The ability to package a large gene such as *DNAH5* is a significant advantage of non-viral vectors over viral vectors which would not be able to do this. However, the disadvantage is that the therapy must be administered frequently as it was shown that 7 days after delivery

the level of gene expression was significantly reduced in the lungs of mice. An ideal approach to gene therapy is gene correction, whereby the disease causing mutation in the endogenous gene is corrected, as it would persist as long as the cell is alive.

1.6 Genome editing therapy for PCD

Genome editing is the process of altering the genome by using a targeted nuclease to make an intentional change and can be used for therapeutic gene correction. Genome editing provides the advantage of correcting the original mutation, leaving the gene to be regulated by its native promoter and preserving its splice sites. This has only been possible in recent years due to targeted nucleases, such as Meganucleases, Zinc Finger Nucleases, Transcription Activator Like Endo-Nucleases (TALENs) and Clustered Regularly Interspaced Short Palindromic Repeats (CRISPR)/ CRISPR Associated protein 9 (Cas9) (Cox, Platt, and Zhang 2015; Maeder and Gersbach 2016). These work by introducing a DNA double strand break (DSB) in a specified location, which is subsequently repaired by the cell's DNA repair machinery via non-homologous end joining (NHEJ) or if DNA with homology to the targeted site is present via homology directed repair (HDR). This can be used for mutagenesis by taking advantage of errors introduced by NHEJ or can be used for gene correction if a DNA template is used, the specifics of these repair pathways will be discussed in more detail in **Section 1.7**.

The most recent targeted nucleases to be developed are TALENS and CRISPR/Cas9. The TALEN system was adapted from the TALE proteins which the bacterial *Xanthomonas* species use to control the transcription of their plant hosts (Boch and Bonas 2010). These proteins were shown to be able to bind to specific base pairs of DNA via 33-35 amino acid residue repeats, with each repeat recognising a single base (Boch et al. 2009; Moscou and Bogdanove 2009). This system was later modified by the addition of the DNA nuclease FokI to the C terminal domain of TALE, creating TALENs (Miller et al. 2011). The single nuclease domain cuts one strand of DNA requiring a second TALEN to target the complementary strand to create a DNA DSB, as shown in **Figure 1.7**. This system was used to test the effectiveness of genome editing to treat PCD in an *ex vivo* system (Lai et al. 2016). The authors transduced patients' nasal epithelial cells grown in spheroid cultures with Feline Immunodeficiency Virus (FIV) coated with VSVG and showed that 20-29% of the previously immobile spheroids began to

rotate four days post transduction. The patients had mutations in *DNAH11* which does not result in completely immotile cilia but causes them to be stiff and have a significantly reduced range of motion. In order to repair this mutation the cells had to be transduced with three separate viruses, two to encode the TALENs and one for the 350 bp repair template. This highlights one of the major drawbacks of the TALEN system, the size of the proteins. There is also the added difficulty of requiring two nucleases to make a single cut and the need to re-engineer the entire TALE domain for each site targeted.

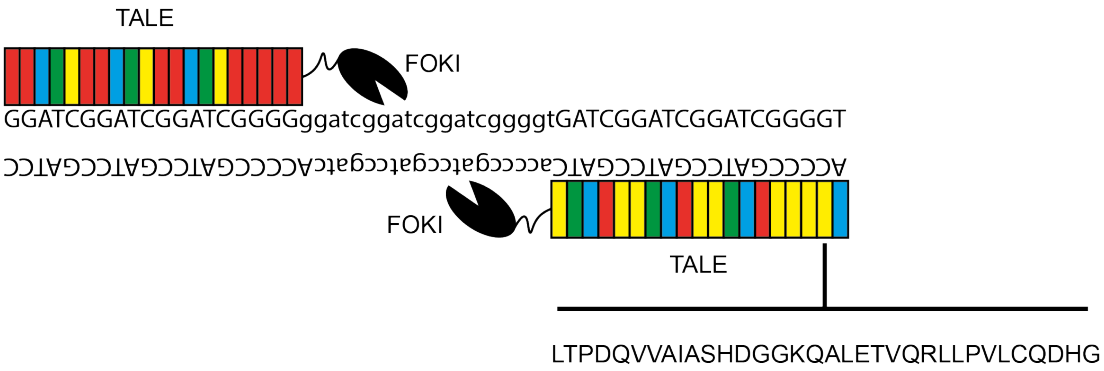

Figure 1.7 The principle behind TALEN editing

The diagram shows the TALE domains, coloured rectangles, each of which recognises a specific base, red for G, blue for A, green for T and yellow for C. Each of these domains is a 33 – 35 amino acid motif, the example for the C recognising motif is shown highlighted by the black line. The FOKI nuclease domains are shown as black ovals, which cut in a region between the two TALE arrays.

Some of these problems are curtailed by the use of the CRISPR/Cas9 system. The CRISPR sequences were first recognised as enigmatic repeats in the *E. coli* genome (Ishino et al. 1987). It was another two decades before the function of these repeats was hypothesised and proven to be part of an adaptive immune system in bacteria (Makarova et al. 2006; Barrangou et al. 2007). The palindromic CRISPR repeats were shown to flank sequences derived from bacteriophages and other bacterial pathogens, the sequences next to these were termed Protospacer Adjacent Motifs (PAMs). It was soon demonstrated that these repeats were transcribed and expressed RNA, CRISPR RNA (crRNA), which was complementary to the genomes of invading pathogens (Brouns et al. 2008). The crRNA was shown to direct nucleases, termed CRISPR associated proteins (Cas)

to these genomes with a second trans activating crRNA (tracrRNA) (Garneau et al. 2010; Deltcheva et al. 2011). In certain bacteria this process was mediated by a single protein, Cas9, which has been shown to have two nuclease domains as well as helicase and nucleic acid binding activity (Makarova et al. 2006; Sapranauskas et al. 2011). Cas9 can be guided to DNA containing the crRNA sequence followed by a PAM site, in the case of the commonly used *Streptococcus pyogenes* Cas9 the PAM sequence is NGG. The tracrRNA and crRNA can be combined to create a single guide RNA (sgRNA) (Jinek et al. 2012), as shown in **Figure 1.8**, to reduce the size of vector necessary. This system has been adapted in mammalian cells for experimental genome engineering and therapeutic gene correction, including *in utero* gene correction in the lungs of mice (Alapati et al. 2019).

The advantages of using CRISPR/Cas9 over TALENs and other genome editing methods are that it is easy to design a short, ~20 nucleotide, guide RNA in comparison to long TALE domains and it allows for the targeting of DNA DSBs to a large range of sequences using only a single protein. However, it is still subject to the same limitations as other targeted nucleases in that it relies entirely on the DNA repair mechanisms of the cell to make specific changes to the genome. This is a major limitation of genome editing compared with gene replacement as the efficiency of templated repair in most cells is much lower than that of virally mediated integration. However, recently it has been discovered that transposition can be directed by CRISPR/Cas ribonucleotide protein complexes which bind to bacterial transposases (Klompe et al. 2019), suggesting that RNA targeted integration may be possible.

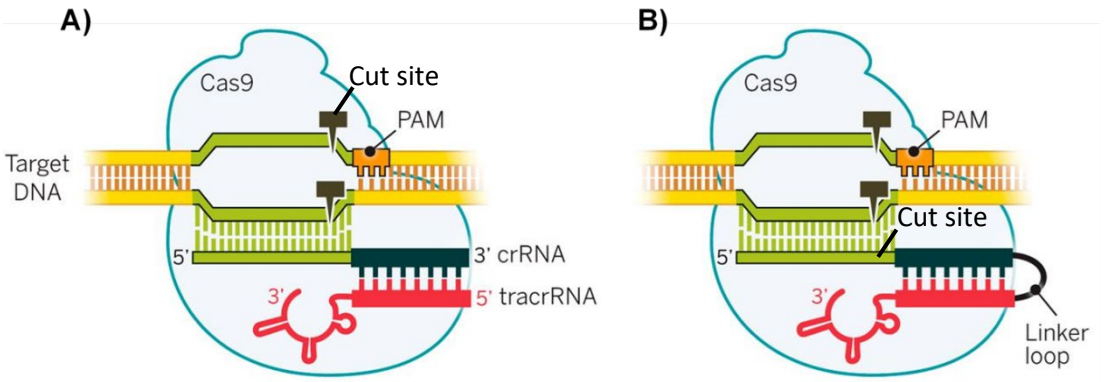

Figure 1.8 Overview of CRISPR/Cas9 genome editing

A) This drawing shows the Cas9 nuclease in complex with crRNA and tracrRNA binding to the target sequence. The black pins highlight where Cas9 cuts the DNA, the position of the PAM is also shown.
B) The crRNA and tracrRNA can be combined by use of a linker loop, as shown. These drawings are adapted from (Doudna et al. 2014).

1.7 DNA double strand break repair mechanisms

Eukaryotic cells have four conserved pathways which are used to repair DNA double strand breaks (DSBs), NHEJ, homologous recombination (HR), single strand annealing (SSA) and alternative end joining (alt-EJ). The HR and NHEJ pathways are the main mechanisms of repair whereas SSA and alt-EJ are less used. These pathways are summarised in **Figure 1.9**, further details about the detailed mechanisms of these pathways can be found in recently published reviews (Pannunzio, Watanabe, and Lieber 2018; Wright, Shah, and Heyer 2018; Sallmyr and Tomkinson 2018).

In mammals NHEJ is the most commonly used pathway to resolve DNA DSBs (Beucher et al. 2009), it is also vital for V(D)J recombination and immunoglobulin heavy chain class switching (Lieber 2016). The initiation event for NHEJ is the binding of protein heterodimer Ku70/Ku80 to the free double stranded DNA ends. This complex preferentially binds ends of DNA at DSBs and prevents exonucleases from digesting the DNA, essentially creating a cap (Mimitou and Symington 2010). One potential reason for the strong preference for NHEJ over other repair pathways is that the Ku complex is highly expressed in the cell (Chang et al. 2017). Once Ku is bound it recruits DNA-dependent protein kinase (DNA-PKCs) in complex with DNA nuclease Artemis. Auto-phosphorylation of DNA-PKCs when it arrives at the DNA DSB activates Artemis, presumably by phosphorylation of its inhibitory domain (Goodarzi et al. 2006; Gu et al. 2010). This

allows Artemis to cut any ssDNA to remove 3' and 5' overhangs and any mismatched sequence (Chang, Watanabe, and Lieber 2015; Chang and Lieber 2016). Artemis will only resect the DNA to leave maximum overhangs of ~4 nt, exposing short regions of homology. Artemis is required for repairing 20-50% of DSBs in cells exposed to ionising radiation (Kurosawa et al. 2008), suggesting that there are some types DSB which do not require resection and/or other nucleases exist which are able to process DSBs in NHEJ (Grundy et al. 2013). The complementary ssDNA ends bind each other to form a stable bond and any resected areas not bound are then filled in by the action of DNA polymerases. In NHEJ these polymerases are pol μ and pol λ, both of which are capable of template dependent and independent synthesis (Bebenek, Pedersen, and Kunkel 2014; Moon et al. 2014; Bertocci et al. 2006). The addition of non-templated nucleotides at the ends of DNA DSBs somewhat explains the error prone nature of NHEJ. Finally the DNA ends are ligated together by the action of DNA ligase IV in complex with XRCC4, which stimulates DNA ligase IV's activity (Grawunder et al. 1997).

During the S and G2 stages of the cell cycle the replication of chromosomes provides a template which can be used for HR. During S/G2 the CDK mediated phosphorylation of the CtIP protein activates the MRN nuclease complex, MRE11-RAD50-NBS1, with SAE2 to initiate bulk resection by removing the terminal 5' nucleotide at each end of the break. The ends are then chewed back 5' to 3' by the actions of EXO 1 nuclease in conjunction with nuclease DNA2 and the SGS1–TOP3–RMI1 complex (Symington 2014). The ssDNA is then coated in RAD51 which recruits RAD54 and other proteins that aid in the binding of this ssDNA to the homology template, termed strand invasion (Solinger, Kiianitsa, and Heyer 2002). The formation of bonds between the homology repair template and the DSB can form one of two types of DNA structure: a double holiday junction (DHJ), where there are two crossovers with a dsDNA repair template; or a synthesis dependent strand annealing (SDSA) junction, where only a single DNA strand anneals to one of the resected ssDNAs. This provides a template for DNA polymerases, pol δ and pol η, and accessory proteins, PCNA and RPA, to synthesise DNA complementary to the homology repair template (Sneeden et al. 2013). The ends are then ligated together to repair the break, in SDSA the repaired strand is then used as a template for the remaining broken strand. This ligation can result in crossovers at DHJs as is the case in meiotic recombination.

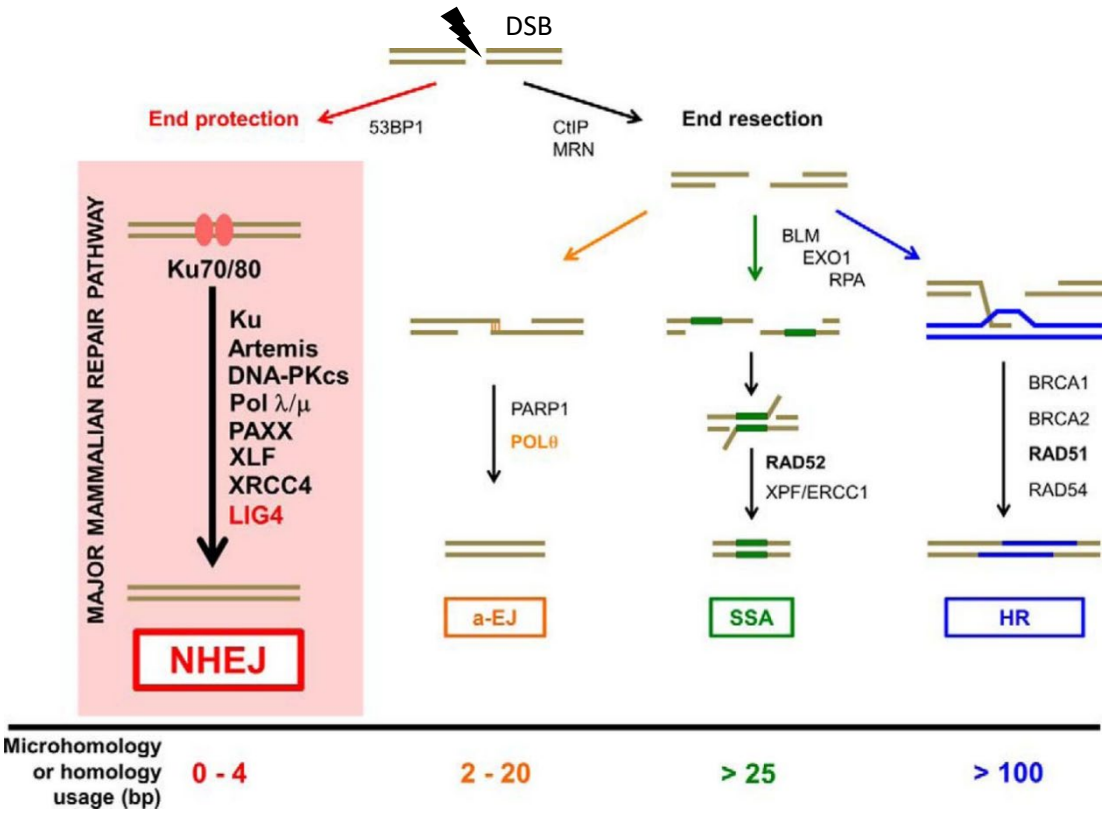

Figure 1.9 Double stranded DNA break repair mechanisms

This diagram highlights the mechanisms that eukaryotic cells use to repair DNA DSBs. These can essentially be split into those which use homology for repair and those which do not. The choice is determined by regulatory proteins 53BP1, NHEJ, and CtIP and MRN, homology pathways. The NHEJ pathway is shown as the major repair pathway in eukaryotes. The various lengths of homology used in each pathway are shown at the bottom of the diagram in order of ascending length from left to right. This diagram has been adapted from (Pannunzio, Watanabe, and Lieber 2018).

The other DNA DSB repair pathways are less commonly utilised in mammalian cells and can be viewed as back up pathways. They constitute two distinct pathways which have different requirements for homology lengths. The SSA pathway requires ssDNA homology of > 25 nt and uses similar complexes to the HR pathway. The alt-NHEJ pathway can be split into two different methods of repair depending on what homology is present. If there is homology between 2 and 20 nt then Microhomology Mediated End Joining (MMEJ) is used to repair the break. If the homology is < 2 nt then the ends are joined together through end joining (EJ), alt-EJ is usually used synonymously with MMEJ. The mechanism behind EJ is not known, however MMEJ is known to rely on DNA polymerase θ as

well as a number of other DSB repair proteins. The alt-NHEJ pathways were recently reviewed (Sallmyr and Tomkinson 2018).

The reliance of mammalian cells on NHEJ, even in G2/S where an estimated 80% of DSBs are repaired by NHEJ (Beucher et al. 2009), makes gene correction using genome editing and a homology repair template difficult. Numerous ways to overcome this DNA repair pathway problem have been explored and are summarised in **Chapter 5**.

1.8 Project objectives

Axonemal dyneins are large and complex molecular machines which play a vital role in human health, as demonstrated in the previous sections. The decades of research that have been conducted on motile cilia have uncovered a wealth of information about the structure, composition and regulation of these complexes. This work has largely taken advantage of single celled organisms with motile flagella, such as *Chlamydomonas reinhardtii*. However, data about axonemal dyneins in mammals is less comprehensive, especially with regards to how they are assembled and regulated. In order to investigate the dynamics of these processes with high temporal and spatial resolution it is necessary to be able to track proteins of interest and find their interactors at different stages of development. This project aimed to achieve this by:

1. Creating a library of tagged axonemal dynein proteins in *Drosophila* using a generic tagging strategy.
2. Tagging dynein proteins in mouse which were successfully tagged in *Drosophila*.
3. Using the tagged protein to pulldown interactors during assembly and at other stages of ciliary differentiation.
4. Following turnover of axonemal dynein complexes in mammalian cilia using dye pulse-chase imaging experiments that utilise the adaptable SNAP tag, as explained in **Chapters 3** and **4**.
5. Investigating the early translational regulation of the dynein heavy chains by observing the localisation of transcripts in motile ciliated cells.

The other aim of this project was to use the tagged axonemal dynein protein to quantify the rescue of PCD mutations by CRISPR/Cas9 genome editing in mice and cultured primary mouse cells. The ultimate aim being to rescue the PCD-like phenotype in mice using CRISPR/Cas9. To do this the first step was to try and improve the efficiency of CRISPR/Cas9 induced Homology Directed Repair (HDR) by:

1. Designing a fluorescent reporter system to quickly score the effectiveness of HDR.
2. Testing the effectiveness of published methods to improve HDR efficiency.
3. Linking the repair template to the Cas9 editing complex to boost HDR efficiency.

The first two results chapters cover the work done to understand axonemal dynein regulation in mouse motile ciliated cells, while the final results chapter details the research into improving HDR efficiency using CRISPR/Cas9.

2 Materials and methods

2.1 Sequence designs

2.1.1 Primer sequences

The primers used for genotyping, cloning and sequencing PCRs are shown in the **Table A1** in **Appendix 1**. Throughout the document, where there is mention of a primer being used it will be referred to by name and number. All oligonucleotide sequences, unless otherwise mentioned, were ordered from Sigma-Aldrich™.

2.1.2 Design of CRISPR guide sequences

CRISPR guides were designed for exon 1 of the mouse *Dnah5* gene ((GRCm38.p6) ENSMUSG00000022262), exons 2, 3, 38 and 39 of human *PCM1* ((GRCh38.p12) ENSG00000078674, PCM1-202), exon 1 and 2 of *Drosophila melanogaster* CG6971 and for *EGFP* using the online tool provided by Benchling (see **Section 2.16.2**) the guides shown below in **Figure 2.1** were ordered based on their scores, shown in **Table 2.1**. **Figure 2.1** shows the nucleotide and the amino acid residue sequences from CRISPR targeted genes. Genomic sequences were acquired from Ensembl genome browser (see **Section 2.16.1**) for mammalian sequences and from flybase (see **Section 2.16.1**) for *Drosophila melanogaster*.

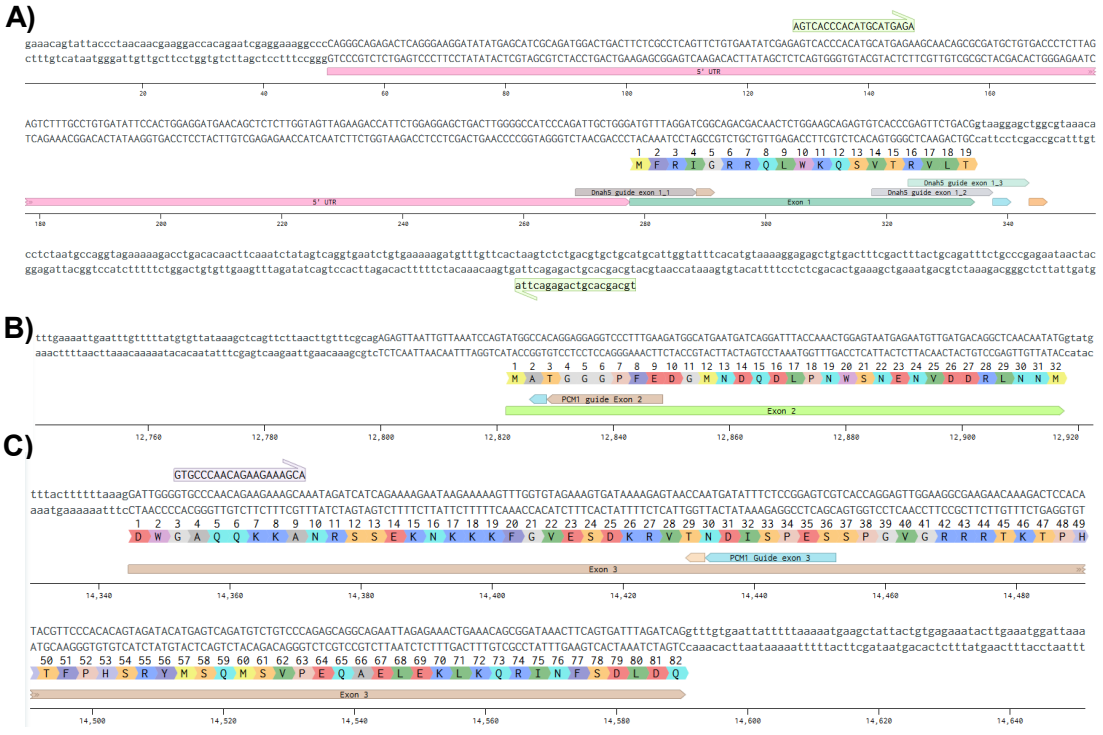

D)

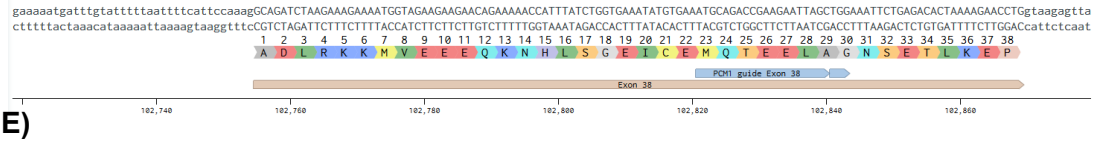

E)

F)

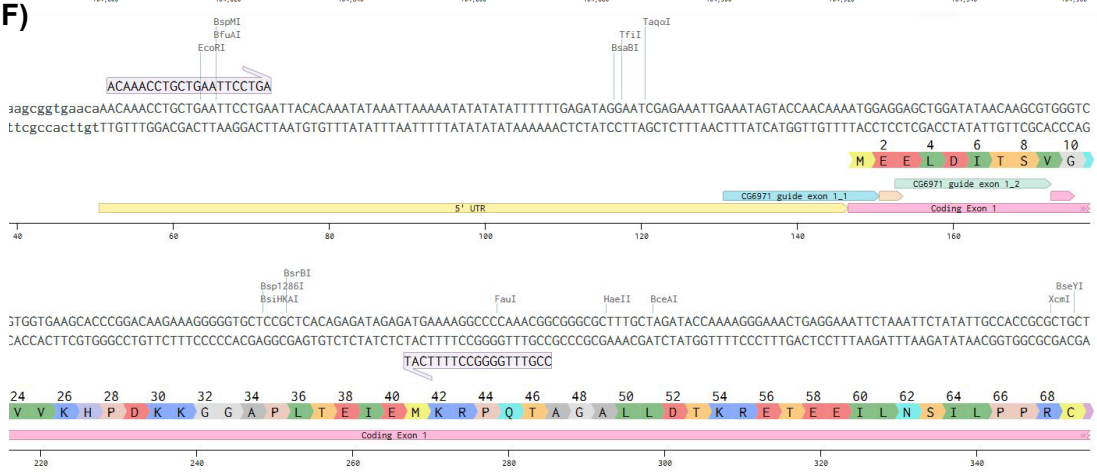

G)

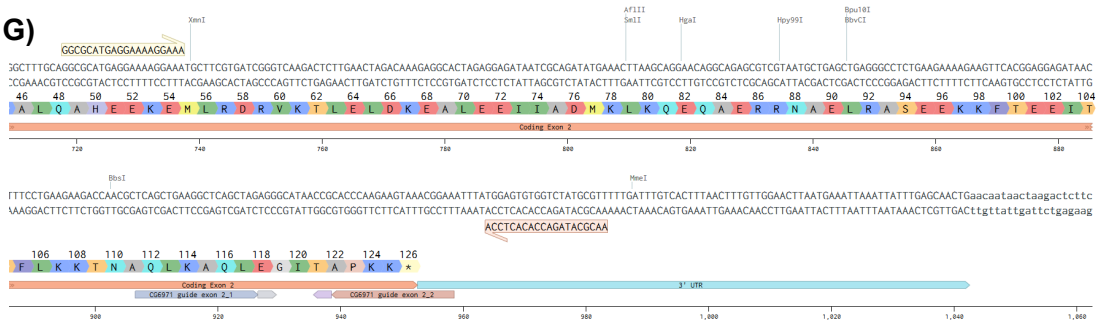

H)

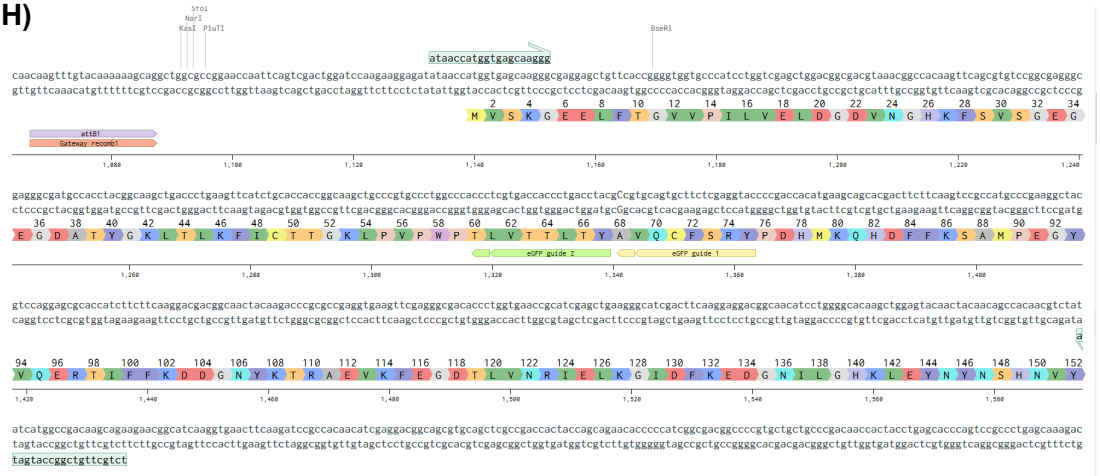

Figure 2.1 Positions of guide RNA sequences in their target sequences.

A) Position of mouse *Dnah5* targeting guides (indicated by the labelled arrows) on the 1st two exons of the gene, the direction of the arrows indicates the orientation of the guide 5' to 3'. The smaller arrow immediately after the guide marks the position of the guide's PAM site.
B) Position of human *PCM1* targeting guide on the 2nd exon of the gene.
C) Position of human *PCM1* targeting guide on the 3rd exon of the gene.
D) Position of human *PCM1* targeting guide on the 38th exon of the gene.
E) Position of human *PCM1* targeting guide on the 39th exon of the gene.
F) Positions of *Drosophila melanogaster* CG6971 targeting guides on the 1st exon.
G) Positions of *Drosophila melanogaster* CG6971 targeting guides on the 2nd exon.
H) Position of the *EGFP* targeting guides in the Flp-in recombination site of T-REx HEK 293 Flp-in cells.

Name	Sequence	PAM	Specificity Score	Efficiency Score
Dnah5 guide exon 1_1	ATTGCTGGGATGTTTAGGAT	CGG	54.03	59.76
Dnah5 guide exon 1_2	TCACCCGAGTTCTGACGgta	agg	90.62	59.90
Dnah5 guide exon 1_3	GAGTTCTGACGgtaaggagc	tgg	70.46	54.34
PCM1 guide exon 2	TTCAAAGGGACCTCCTCCTG	TGG	38.95	61.82
PCM1 guide exon 3	CGACTCCGGAGAAATATCAT	TGG	80.42	58.48
PCM1 guide exon 38	ATGCAGACCGAAGAATTAGC	TGG	53.85	54.65
PCM1 guide exon 39	ttctgtttttcagAAACGGT	GGG	55.41	57.34
CG6971 guide exon 1_1	AAATAGTACCAACAAAATGG	AGG	45.62	68.80
CG6971 guide exon 1_2	GAGCTGGATATAACAAGCGT	GGG	49.68	63.57
CG6971 guide exon 2_1	TCAGCTGAAGGCTCAGCTAG	AGG	49.11	59.78
CG6971 guide exon 2_2	TTCCGTTTACTTCTTGGGTG	CGG	48.85	45.30
EGFP guide 1	gtaggtcagggtggtcacga	ggg	63.56	71.76
EGFP guide 2	gtacctcgagaagcactgca	cgG	64.50	65.30

Table 2.1 Guide sequences

CRISPR guide sequences (shown in **Figure 2.1**) as designed using Benchling against target sites in this study. The sequence of the PAM is also shown. The specificity score is calculated by using the algorithms in (Hsu et al. 2013) and the efficiency score is calculated using algorithims from (Doench et al. 2016).

2.1.3 Repair sequence design

Repair templates for CRISPR/Cas9 editing were designed using the sequences shown in **Figure 2.1**. They were designed to insert a new sequence and/or alter the existing sequence to destroy the PAM site and prevent further cutting

Mouse *Dnah5* was targeted at the N terminus based on the evidence that this region has no predicted structural domains and that fusion of GFP to the mouse paralogue *Dnah11* gene at the N terminus was non-disruptive (McGrath et al. 2003). Homology arms were designed to be 779 bp on the 5' side of the insertion and 800 bp on the 3' side of the insertion, as summarised in a diagram of this repair template, **Figure 4.1**. The insertion site was chosen 3 bases upstream of the predicted site of cutting by the CRISPR guide "Dnah5 guide exon 1_2" as shown in **Table 2.1**. The plasmid repair template was synthesised by Geneart®, Thermo Fisher Scientific Invitrogen™.

The repair template for the *EGFP* G68A locus to convert the GFP from non-fluorescent to green fluorescence was made to be asymmetrical, because this was shown to be more efficient (Richardson et al. 2016). The sequence converts a single nucleotide from cytosine to guanine creating the corresponding amino acid change from glycine to alanine, see **Figure 2.2**, this also destroys the PAM of *EGFP* guide 1.

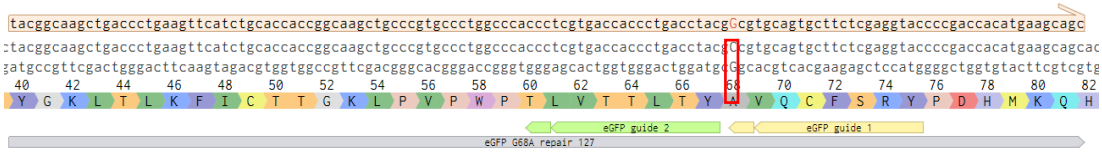

Figure 2.2 Site of *EGFP* G68A repair template

The figure above shows the sequence of the *EGFP* G68A allele. The guide RNAs shown in **Figure 2.1** are aligned to this sequence along with the *EGFP* G68A repair template. The template is 127 nt with an 85 nt long 5' homology arm and a 41 nt long 3' homology arm. The switch of the cytosine, highlighted by the red box, to guanine shown in red font causes the 68th amino acid alanine to change to glycine, making *EGFP* fluorescent. This also results in the change of the PAM for *EGFP* guide 1 from CGG to CGC rendering the guide unable to cut if the locus is correctly repaired.

2.1.4 Design of plasmid for universal tagging

The universal tagging plasmid was created by Lackner et al. (2015) to be a non-homologous end joining based tagging system that can be used with any

sequence. The plasmid Lackner et al. designed contains recognition sites for a guide RNA that targets the zebrafish gene *tia1l* gene which flank the insertion site for the tag. The plasmid also expresses the guide RNA allowing the tag to be cut out of the plasmid when Cas9 is present. Information about cloning strategy can be found in **Section 2.3.6** and more information about the use of this plasmid can be found in **Section 3.2**.

2.1.5 Design of Cas9-Rep78 fusion

To make a Cas9 nuclease capable of binding to the AAV genome and targeting repair templates to the site of Cas9 editing the *Streptococcus pyogenes* Cas9 protein was fused to the first 244 amino acids of the Adeno Associated Virus (AAV) protein Rep78 which has been shown to be sufficient to mediate binding to the ITR (Inverted Terminal Repeat) sequences of the AAV genome (Cathomen, Collete, and Weitzman 2000). The linker region was taken from the Cas9-RFP fusion (Mircetic et al. 2017) and was used to fuse Rep78 to the C terminus of Cas9, the sequences used to create Cas9-rep78 are shown in **Figure 2.3**.

A)

B)

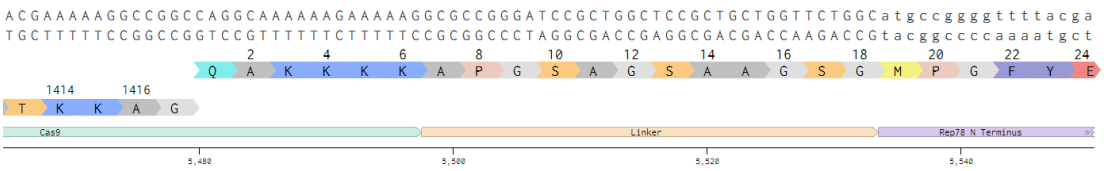

Figure 2.3 pX330 Cas9-Rep78 sequence

A) The plasmid map shows the fusion of the C-terminal domain of the *S.p.* Cas9 (green) with the 1st 244 amino acids of the AAV Rep78 protein (purple) separated by a 12 amino acid linker (orange). The positions of genotyping primers Cas9-Rep F and Cas9-Rep R are shown. The plasmid backbone is pX330 (Addgene catalogue number 42230).
B) This shows the nucleotide and amino acid sequence of the fusion site between the two proteins.

2.1.6 mTmG reporter repair templates

Several repair templates were used in this project which work in conjunction with the mTmG mouse (Muzumdar et al. 2007) to report on the DNA repair outcomes of genome editing, a summary of this system is shown in **Figure 5.1**. **Figure 2.4 A)** shows a plasmid with homology arms to the mTmG locus which converts the membrane localised *EGFP* to a nuclear *EGFP* by switching the MARCKs sequence for an *H2B* sequence. **Figure 2.4 B)** shows a *TagBFP* sequence in a minicircle with a recognition site for the CRISPR guide RNA used to target adjacent to the Loxp sites in the mTmG locus. The third template used is the plasmid from **Figure 2.4 A)** but packaged in an AAV2/2 genome, shown as a cartoon in **Figure 5.6**.

A)

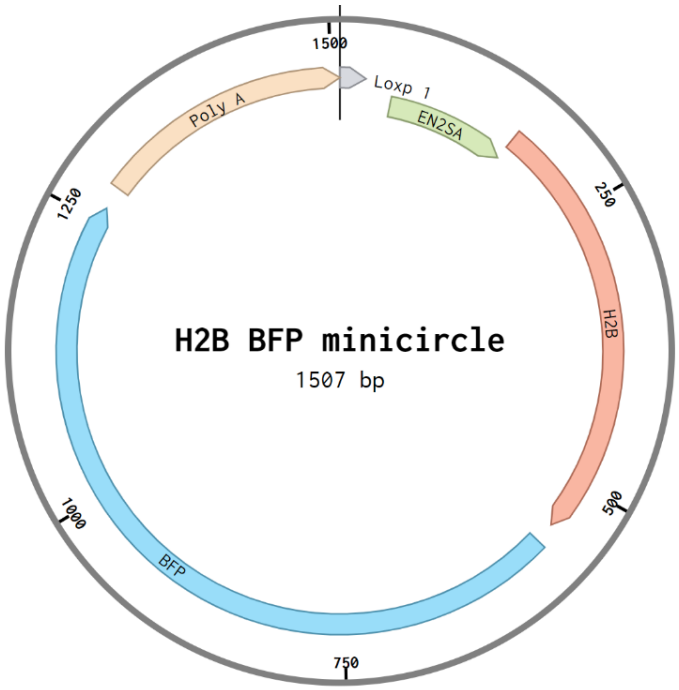

B)

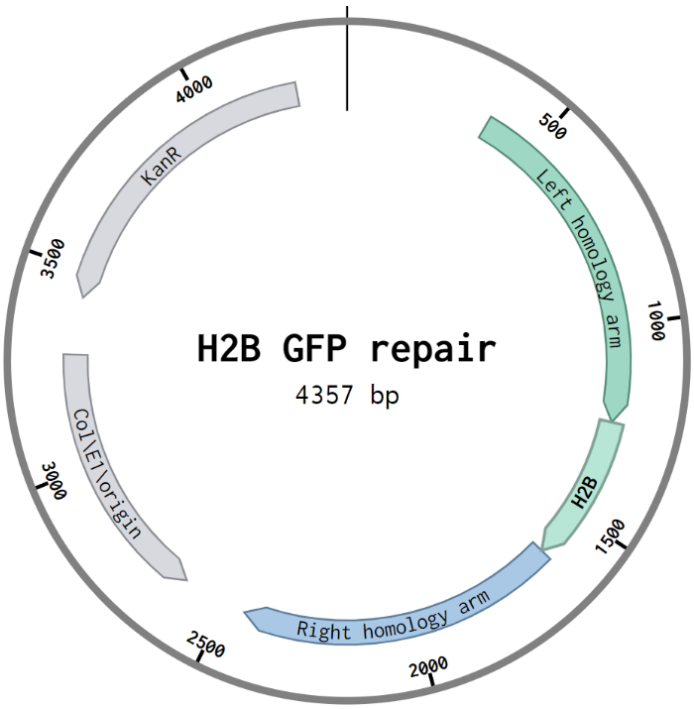

Figure 2.4 mTmG repair templates

A) The plasmid map shows the *H2B* gene flanked by a left homology arm (878 bp) and right homology arm (823 bp) which targets the *H2B* gene (378 bp) to the N terminus of *EGFP* in the mTmG locus.
B) The plasmid map shows the H2B (orange) BFP (blue) fusion downstream of a EN2SA splice acceptor site (green) and upstream of a strong Poly A sequence (orange). The minicircle is cut at the LoxP1 recognition site (grey) by Cas9 targeted by the Loxp1 guide RNA, which linearises it for integration.

2.2 Cas9 editing digests

2.2.1 Surveyor assay

The surveyor assay detects CRISPR/Cas9 editing using the Surveyor Nuclease, a restriction enzyme that cleaves at mismatched sequences, supplied in a kit from IDT™ (catalogue no. 706025). 50 ng/µl of purified PCR product was annealed and digested according to the manufacturer's instructions, except that instead of digesting in polymerase buffer the PCR products were purified and put into a 1x Surveyor buffer (Jiang, Yao, and Liu 2013), recipe in **Section 2.16.1**.

Reaction mixes were made as follows for volumes 20 to 40 µl:

Hybridised DNA	200–400 ng
0.15 M MgCl2 Solution	1/10th volume
10x Surveyor buffer	1/10th volume

Surveyor Enhancer S	1 µL
Surveyor Nuclease S	1 µL
Nuclease free water	To final volume

Digests were carried out at 42 °C for 45 minutes before stop solution was added to stop the digestion.

2.2.2 Cas9 *in vitro* digest

In vitro digests with Cas9 nuclease were used to test the efficacy of guide RNAs. This was done by incubating for 1 hour at 37 °C, using the mixture below:

10x BSA (diluted from 100x, NEB™: B9000S)	1/10thfinal volume
10x NEB buffer 3 (NEB™: B7003S)	1/10th final volume
Cas9 protein (Invitrogen™: B25640)	150 ng
Guide RNA	400 ng
Target dsDNA	70 - 300 ng
Nuclease free water	To final volume

Once digested the reactions were heated to 95 °C for 5 minutes and then placed onto ice.

2.3 Sequence synthesis and creation

2.3.1 Synthesis of guide RNA

Guide RNA was made using the Invitrogen GeneArt™ Precision gRNA Synthesis Kit (Catalogue no. A29377). This kit provides primers to amplify custom made oligonucleotides designed by the user to encode their guide RNA sequence, which is the target sequence immediately preceding the PAM, and to add a transcriptional T7 promoter as well as sgRNA scaffold (crRNA/tracrRNA). This is shown in **Figure 2.5**.

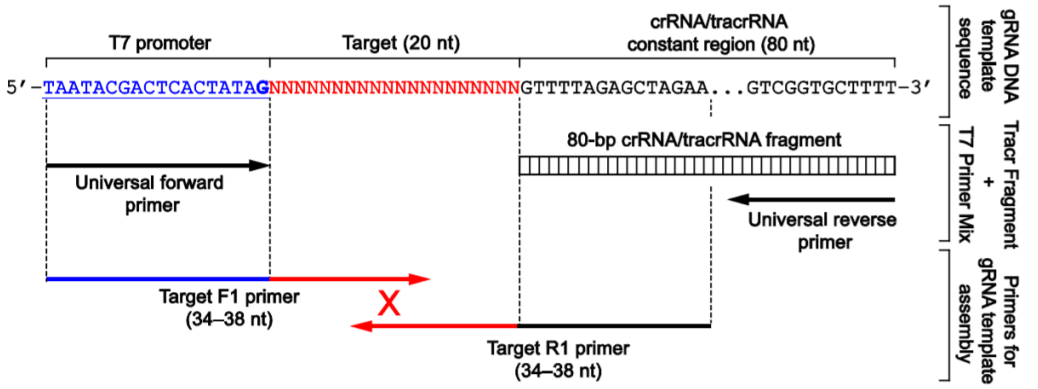

Target F1: TAATACGACTCACTATAG **+ first 16–20 nt of the target sequence**

Target R1: TTCTAGCTCTAAAAC **+ first 19–20 nt of the target sequence reverse complement**

Figure 2.5 Design of primers for Geneart™ IVT gRNA synthesis (adapted from Thermo Fisher Scientific™ 2016)

The diagram shows the positions of the primers that are used to make the DNA template for sgRNA synthesis, the sequences that are added to the primers encoding the guide or target sequence itself are shown below the diagram.

These primers are used in a PCR reaction to create the DNA template for *in vitro* transcription using Pfusion™ polymerase (Geneart™). The PCR product is then used to synthesise the guide RNA using the Transcriptaid RNA polymerase at 37 °C for 2-4 hours. This product is then treated with DNAseI to remove the template DNA and the RNA is purified using the Genejet™ RNA purification micro-columns provided. Detailed instructions for this protocol can be found on the Fisher Scientific Invitrogen™ Geneart™ website. RNA was heated to 70 °C for 2 minutes then placed directly into ice to denature before being analysed using the Agilent™ Bioanalyzer 2100 with RNA nanochip to assess the RNAs' concentration and the purity.

2.3.2 cDNA synthesis for reverse transcription PCR of *EGFP* Flp-In HEK 293 T-REx cell lines

cDNA was synthesised from 1 µg of RNA for each sample using the Transcriptor First Strand cDNA Synthesis Kit (catalogue no. 04379012001) from Roche™, except for the reaction with control RNA which used 10 ng.

The following master mix was set up with random hexamer primers for 10 x 13 µl reactions:

Hexamers (600 µM)	20 µl
Nuclease free water	74 µl

This was added to 1 µg of RNA made up to a volume of 3.6 µl and 10 ng in the case of the control. The reaction was incubated at 65 °C for 10 minutes and then put straight on ice.

The following master mix was made while the reaction above was incubating:

Transcriptor buffer (5x)	40 µl
dNTPs (10mM each)	20 µl
Transcriptor reverse transcriptase	5 µl
Nuclease free water	5 µl

7 µl of this was then added to the other reaction mixes and the reactions were incubated using the following settings:

Temperature (°C)	Time
25	10 mins
55	30 mins
85	5 mins
4	Forever

2.3.3 Reverse transcription PCR for *EGFP* G68A Flpin Cell line

2 µl of the cDNA produced in the reaction described in **Section 2.3.2** was used as a template for the following reactions. In addition a pool of all the RNA (1 µg each) was used as a negative control after being diluted 1 in 100. 10 ng of the G68A plasmid was used as a positive control. Incidentally the same PCR was used with genomic DNA as well, for genotyping.

The following 12 x master mix was set up:

DreamTaq green (2x)	120 µl
primer mix (21 and 22) (10uM)	4.8 µl
nuclease free water	91.2 µl

18 µl of this mix was added to 2 µl of each sample.

These were then amplified using the DreamFLP PCR program:

Temperature (°C)	Time (s)	Cycles
95	150	1
95	30	30
54	30	
72	30	
72	420	1
4	forever	1

The control RNA reaction was amplified using its own primers and program as described in the First strand cDNA synthesis protocol except that 95°C instead of 94°C was used and DreamTaq polymerase was used instead of quick start.

2.3.4 Site-directed mutagenesis to create EGFP G68A plasmid

To make a null *EGFP* integrated into a cell line to act as a fluorescent reporter *EGFP* FRT plasmid (EGFP PCDNA5) (840 ng/µl) was targeted for site directed mutagenesis as shown in the plasmid sequence in **Figure 2.6** the primers were designed to have a 20 nt overlap region and the forward primer (no. 11) had the insertions to introduce an XhoI site downstream of a G to C transition resulting in a change in the 68th amino acid from glycine to alanine. Reagents to perform this site-directed mutagenesis were a gift from Dr. Mark Handley and the EGFP PCDNA5 plasmid was a gift from Dr. Matthew Ford.

The following reaction was set up to methylate the plasmid DNA:

NEB buffer 2 (10x)	1.6 µl
SAM (10x) made from 200x stock	1.6 µl
EGFP PCDNA5 plasmid (100 ng)	0.12 µl
Ss1 (DNA methylase)	1 µl
Nuclease free water	11.68 µl

This was incubated using program SDMMETHY (37°C for 1 hour then 20 minutes at 65 °C and held at 4 °C). 6 µl of this template was used to set up the following PCR reactions:

Betaine (5 M)	30 µl
KOD DNA polymerase buffer (10x)	15 µl
dNTPs (5 mM)	15 µl

MgSo4 (25 mM)	6 µl
Template DNA	6 µl
Forward primer no. 11 (10 µM)	4.5 µl
Reverse primer no. 12 (10 µM)	4.5 µl
KOD DNA polymerase	1.5 µl
Nuclease free water	67.5 µl

50 µl of this was aliquoted into each of three 200 µl tubes and run on the program SDM PCR, below:

Step	Temperature (°C)	Time	Cycles
Initial denaturation	98	30s	1
Denaturation	98	10s	20
Annealing	55-60	30s	
Elongation	72	3 min 15s	
Final extension	72	10 mins	1
Storage	4	Forever	1

A gradient was set up from 55 to 60°C, with tube 1 at 55°C, tube 2 at 58°C and tube 3 at 60°C.

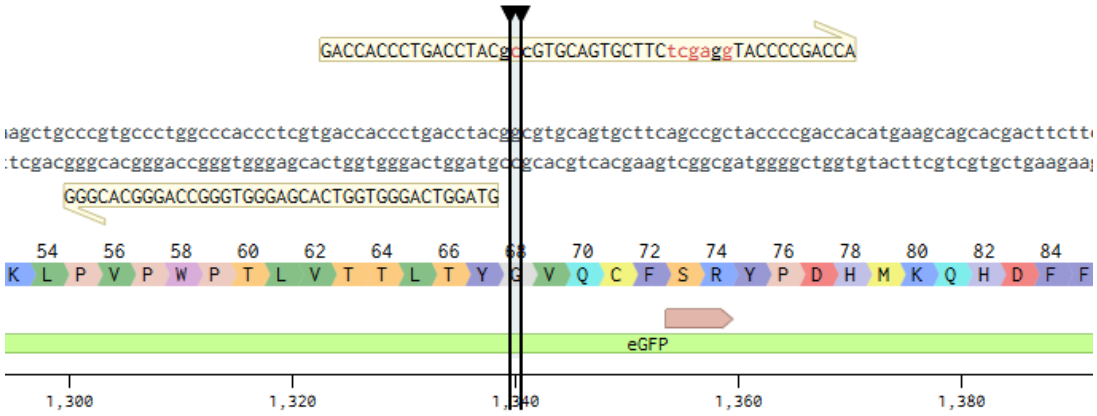

Figure 2.6 Site Directed Mutagenesis to make *EGFP* G68A reporter plasmid

The figure shows the site mutagenised by the primers, shown as yellow arrows. The highlighted base guanine in the reference sequence and cytosine in the primer is the site which results in the switch from glycine to alanine. The red coloured letters are the bases which are different between the original plasmid and the mutagenised one. The area above the brown arrow is the site where the XhoI recognition sequence was introduced.

2.3.5 Cloning CRISPR guides into plasmid backbone

The protocol used to clone CRISPR guide sequences into the Cas9 expressing plasmid pX330-U6-Chimeric_BB-CBh-hSpCas9 (pX330). The plasmid map shown in **Figure 2.7**, developed by the Zhang lab (Cong and Zhang 2014), has a site for the insertion of CRISPR guide sequences under the control of the human U6 promoter. The guide sequences are ordered as 5' phosphorylated oligonucleotides with overhangs that are compatible with overhangs created by BbsI restriction digest of the plasmid, the design of these primers is shown below.

Guide oligonucleotide design for cloning into pX330:

5' – CACCGNNNNNNNNNNNNNNNNNN – 3'

3' – CNNNNNNNNNNNNNNNNNNNCAAA – 5'

The protocol followed for this cloning was identical to that described in the article except that instead of digesting and ligating simultaenously the steps were separated and the DNA was purified using the Invitrogen™ Purelink™ PCR purification kit, see **Section 2.7.1.5** for details, before being ligated to annealed oligonucleotides overnight.

The plasmid was digested using either BpiI (Thermo Scientific™ Catalogue no. ER1011) or BbsI (NEB™ catalogue no. R0539S).

Px330 digestion @ 37 °C for 1 hour:

BpiI 6 U/ BbsI 10 U
pX330 plasmid 1 µg
1 x Buffer G (BpiI Thermo)/ 1x Cutsmart (BbsI NEB)
Water to volume total

Denature @ 65 °C for 20 minutes.

To be inserted into the plasmid the oligonucleotides need to be re-suspended in nuclease free water or pH 8 TE buffer at 100 µM then diluted to 10 µM together. Then they are annealed to each other using the recommended settings from Ran et al. (2015), which heat the DNA to 95 °C before cooling gradually to 25 °C.

Settings used to anneal guide inserts		
Time (min)	Temperature (°C)	Speed (°C/S)
10	95	
1	95	2
1	85	0.3
1	75	0.3
1	65	0.3
1	55	0.3
1	45	0.3
1	35	0.3
1	25	
Forever	4	

Once the digested plasmid was purified it was ligated with the annealed guide oligonucleotides.

Ligation of pX330 and guide oligonucleotides at 16°C for 16 hours:

T4 DNA ligase buffer (NEB)	1 µl
Annealed oligonucleotides (1:200 dilution)	1 µl
pX330 plasmid digest (50 ng)	1 µl
T4 DNA ligase (NEB)	1 µl
Nuclease free water	6 µl

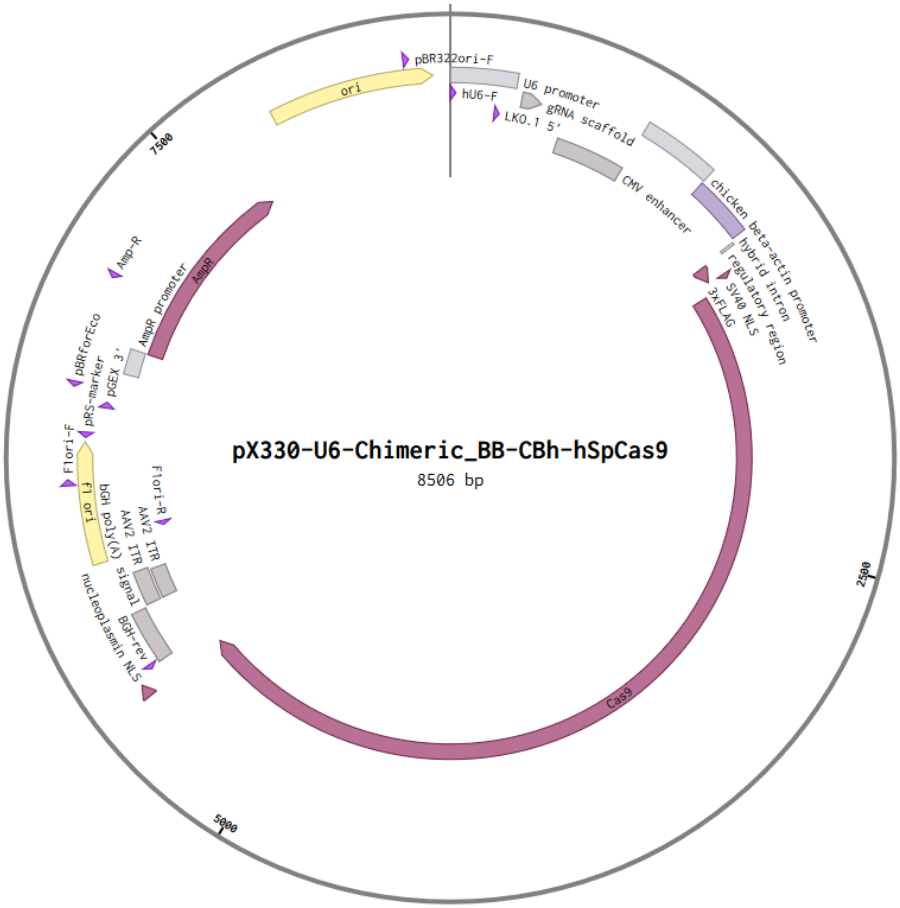

Figure 2.7 pX330 plasmid

The diagram shows a plasmid of the pX330 vector which contains the *S.p.* wild type Cas9 protein under the control of the chicken beta-actin promoter as well as a BbsI restriction site downstream of the human U6 promoter and upstream of the sgRNA guide scaffold containing the 3' end of the gRNA sequence attached to the tracrRNA sequence.

2.3.6 Cloning tags into the generic tagging plasmid

The protocol used to clone tags into the generic tagging vector (Lackner et al. 2015) was designed to clone the tags into the three different frames either 0, +1 or +2 as mentioned in the original article. The multiple cloning site for the vector is between two guide RNA target sites from the Zebrafish *tia1l* gene and has BamHI at the 5' end and HindIII at the 3' end of the tag insertion site. The tags were amplified with primers to add the BamHI and HindIII restriction sites to the ends of the tags. The primer designs for the different frame shift insertions and the plasmid map are shown in **Figure 2.8**.

A)

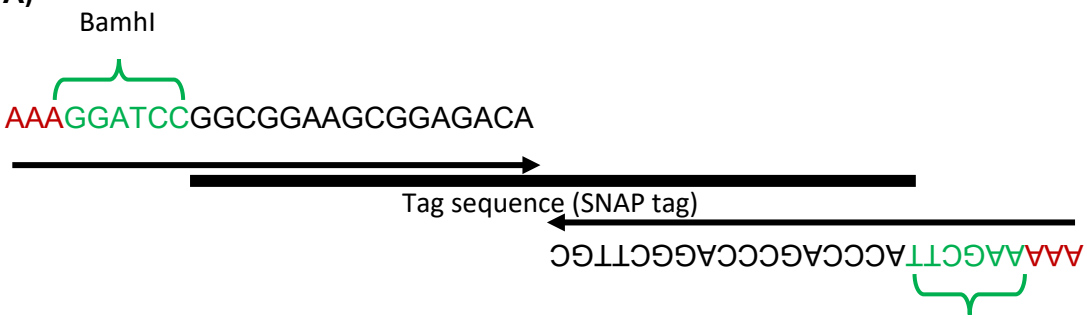

B)

SNAP BAMH1 cloning F +0 ORF	AAAGGATCCGGCGGAAGCGGAGACAAAGA
SNAP HindIII cloning r +0 ORF	AAAAAGCTTACCCAGCCCAGGCTTGCCCA
SNAP BAMH1 cloning F +1 ORF	AAAGGATCCGGGCGGAAGCGGAGACAAAGA
SNAP HindIII cloning r +1 ORF	AAAAAGCTTTCACCCAGCCCAGGCTTGCCCA
SNAP BAMH1 cloning F +2 ORF	AAAGGATCCGAGGCGGAAGCGGAGACAAAGA
SNAP HindIII cloning r +2 ORF	AAAAAGCTTTACCCAGCCCAGGCTTGCCCA

C)

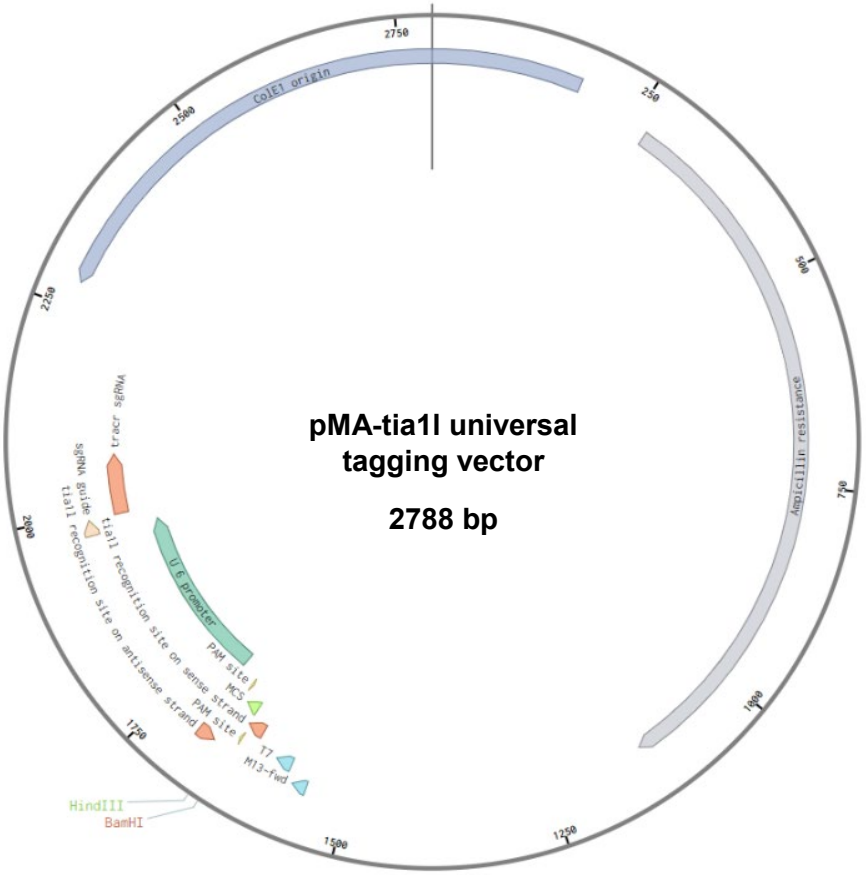

Figure 2.8 Cloning a tag into pMA-tia1l tagging vector.

A) The design of the primer sequences to amplify tags is shown in this image. The example given is for the SNAP tag. 20 nt primers were designed with either the BamHI recognition site on the 5' end of the forward primer or a HindIII recognition site at the 5' end of the reverse primer, shown in green. Triple adenosine, shown in red, was added to the ends of primers to allow the PCR products to be efficiently cleaved by the restriction enzymes.
B) To ensure that the tag is inserted in the correct frame. Extra base pairs are added into the primer sequences as shown in the table, these are coloured in blue, to shift the frame 1 base a G is added to the forward primer while a TC is added to the reverse, to shift the frame 2 bases GA is added to the forward while C is added to the reverse.
C) The whole plasmid map of pMA-tia1L is shown with the presence of the tag insertion site, the tia1l expression site and target sites annotated.

The PCR to add the restriction sites to the tag for insertion into pMA-tia1l, shown in **Figure 2.8** was performed as described below.

20 µl reactions were set up in 0.5 ml Eppendorf tubes as follows:

Primer F (10 µM)	0.4 µl
Primer R (10 µM)	0.4 µl
Mixed dNTPs (10 mM) (Thermo Scientific™: R0181)	0.4 µl
GC buffer (10 x) (Thermo scientific™: F519L)	0.44 µl
Nuclease free water	13.4 µl
Hotstart II Phusion DNA polymerase (Thermo scientific™: F549L)	0.2 µl
(Thermo scientific™: F549L)	
SNAP tag plasmid template (9.7 ng/µl)	1 µl

These were run using the PCR program Phugrad:

Step	Temperature (°C)	Time	Cycles
Initial denaturation	98	30s	1
Denaturation	98	10s	25
Annealing	62	20s	
Elongation	72	20s	
Final extension	72	5 minutes	1
Storage	4	forever	1

Once amplified the inserts and the pMA-tia1l universal tagging vector are digested by BamHI-HF and HindIII-HF (NEB™ catalogue no. R3136S and R3104S, respectively) in 1 x Cutsmart buffer (NEB™ catalogue no. B7204S) for 2-3 hours at 37 °C the enzymes were deactivated at 65 °C for 15 minutes.

Once digested the pMA-tia1l plasmid was de-phosphorylated by having 1 unit of rSAP (NEB™ catalogue no. M0371L) per µg added to it with Cutsmart buffer to make it 1x and was incubated at 37 °C for 1 hour and heat deactivated at 65 °C for 15 minutes.

Inserts and plasmid digest were purified using the Invitrogen™ Purelink™ PCR purification kit (catalogue no. K310001), see **Section 2.7.1.5**. They were then ligated together in a molar ratio of 1:3 (vector:insert) using the same protocol as described in **Section 2.3.5**. After ligation samples were digested with 0.8 µl of EcoRV-HF (NEB™ catalogue no. R3195L) and 1.2 µl of Cutsmart buffer for 1.5 hours at 37 °C and were heat inactivated at 65 °C for 15 minutes to remove undigested plasmid which would contain an EcoRV restriction site between the BamHI and HindIII restriction sites.

2.3.7 Cloning of Cas9-Rep78

As described in **Section 2.1.5** Cas9-Rep78 is a fusion of the N-terminal domain of AAV Rep78 to the C-terminal domain of *S.p.* Cas9 with a flexible linker of amino acid sequence APGSAGSAAGSG from (Mircetic et al. 2017) in between. The linker-Rep78 fragment was made using primers for 2 rounds of PCR firstly to amplify the N-terminal domain of the Rep78 gene from the cloning vector pAAV-RC/AAV2 Rep78 plasmid (Genbank accession no. AF369963.1) while adding the linker sequence at the 5' end and an EcoRI restriction site at the 3' end, **Figure 2.9 A)**. The next PCR used the product of the first PCR as a template and added the end of the Cas9 protein and MCS from pX330 moving the FseI site to the 5' end of the linker sequence and placing a stop codon at the 3' end, as shown in **Figure 2.9 B)**. The inserts and the pX330 plasmid vector were then digested with EcoRI-HF (NEB™ catalogue no. R3101L) and FseI (NEB™ catalogue no. R0588S) for 2 hours at 37°C before being purified and then ligated.

A)

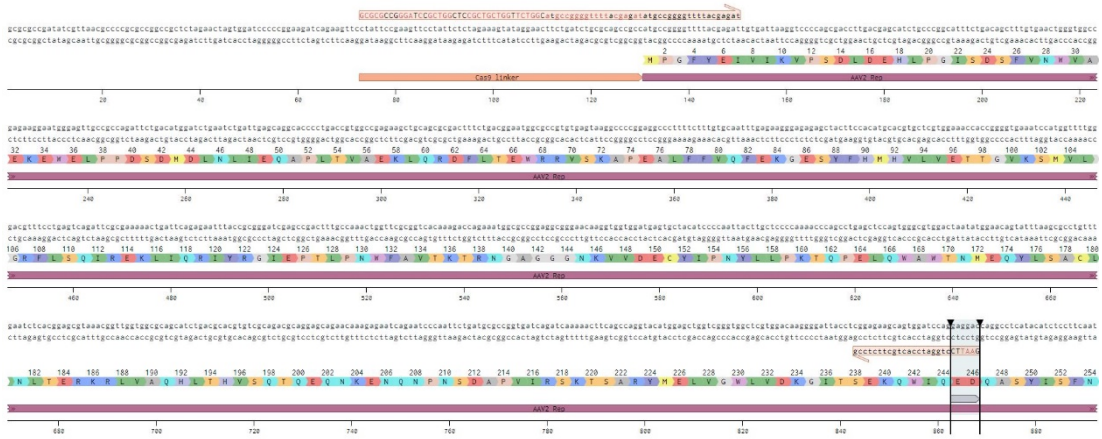

B)

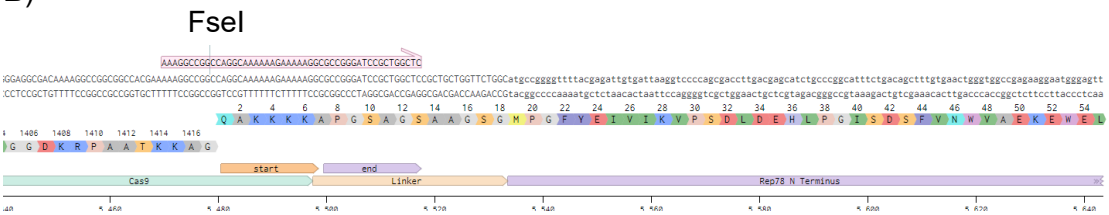

Figure 2.9 Cas9-Rep78 construction

A) The sequence shown is from the AAV2 Rep78 plasmid and has the forward primer Linker Rep78 F and the reverse primer EcoRI Rep78 R attached, the grey arrow indicates the EcoRI recognition site added and the orange bar is the linker sequence.
B) This shows the end of the Cas9 sequence and the junction with Rep78, the primer FseI Rep78 adds the 3' end of Cas9 which is removed by FseI EcoRI digestion back onto the 5' end of the linker sequence with the FseI left intact as indicated by the "start" arrow, the "end" arrow indicates the part of the linker the primer contains.

Rep78 was amplified from the AAV2 Rep78 plasmid using the following reaction:

Template DNA (10 ng/µl)	1µl
Phusion Hotstart II	1 µl
HF buffer (5x) (Thermo Fisher scientific™ catalogue no. F518L)	10 µl
Primer mix of EcoRI Rep78 R and Linker Rep78 F (10 µM)	1 µl
dNTPs	1 µl
Nuclease free water	36 µl

This reaction was run using PCR program PhuGFP60:

Step	Temperature (°C)	Time	Cycles
Initial denaturation	98	30s	1
Denaturation	98	10s	25
Annealing	60	20s	
Elongation	72	40s	
Final extension	72	5 minutes	1
Storage	4	forever	1

After this the samples were purified using the Invitrogen™ Purelink™ PCR purification kit and a second round of PCR was performed with primers FseI Rep78 F and Stop Rep78 R with the same conditions and amounts as the first round of PCR.

Digests and ligations were performed as described for the pMA-tia1l cloning in **Section 2.4.5**. The primers mentioned are below with restriction sites coloured green and extra sequence in blue:

EcoRI Rep78 R	GAATTCctggatccactgcttctccg
Linker Rep78 F	GCGCGCCGGGATCCGCTGGCTCCGCTGCTGGTTCTGG Catgccgggggttttacgagat
FseI Rep78 F	AAAGGCCGGCCAGGCAAAAAAGAAAAAGGCGCCGGGATCCGCTGGCTC
Stop Rep78 R	AAAAGAATTCTTActggatccactg

2.4 Transformation

DH5α (Thermo Fisher: catalogue no. 18265017) *E. coli* were used for cloning transformations according to the protocol provided and were grown with LB. For SDM TOPO Oneshot (Thermo Fisher Scientific™ catalogue no. C404003) *E. coli* were used instead, according to the protocol provided with them.

2.5 PCR conditions used for genotyping

2.5.1 *SNAP-Dnah5* genotyping

The following conditions were used for PCRs to genotype the insertion of the SNAP tag into *Dnah5*.

PCRs from the SNAP tag into exon 1 and the 5' UTR was performed in 20 µl reaction volumes:

DreamTaq green master mix (2x)	10 µl
Earclip DNA/ 100 ng purified genomic DNA	1 µl
Primer mix SNAP_r and DNAH5nterm F (10 µM)	0.4 µl
Nuclease free water	9.6 µl

Reaction conditions used interchangeably for this genotyping PCR:

Program: PCM1SNAP or DNAH5SNA			
Step	Temperature (°C)	Time	Cycles
Initial denaturation	95	3 min	1
Denaturation	95	30 s	30
Annealing	58/62	30 s	
Elongation	72	30 s	
Final extension	72	5 min	1
Storage	4	forever	1

Expected product size of 426 bp

PCRs to span the SNAP tag insertion site in *Dnah5* were performed in 20 µl reaction volumes as follows:

DreamTaq green master mix (2x)	10 µl
Earclip DNA/ 100 ng purified genomic DNA	1 µl
Primer DNAH5nterm F and DNAH5nterm R (10 µM)	0.4 µl
Nuclease free water	9.6 µl

Reaction conditions used for this genotyping PCR are below:

Program: DNAH5NLO			
Step	Time	Temperature (°C)	Cycles
Initial denaturation	3 min	95	1
Denaturation	30 s	95	33
Annealing	30 s	58.5	
Elongation	1 min	72	
Final extension	15 min	72	1
Storage	forever	4	1

Product size with no insertion is 328 bp and with the insertion of the SNAP tag the size is 874 bp.

PCR to amplify from the SNAP tag into the 1st exon and intron of *Dnah5* were performed in reaction volumes of 20 µl as follows:

DreamTaq green master mix (2x)	10 µl
Earclip DNA/ 100 ng purified genomic DNA	1 µl
Primer (24) and Primer (A55) (10 µM)	0.4 µl
Nuclease free water	9.6 µl

Reaction conditions used for this PCR are below:

Program: PCMSNAP3			
Step	Time	Temperature (°C)	Cycles
Initial denaturation	3 min	95	1
Denaturation	30 s	95	30
Annealing	30 s	61.8	
Elongation	1 min	72	
Final extension	15 min	72	1
Storage	forever	4	1

The PCR product size for this reaction is 190 bp.

PCRs to amplify from the SNAP tag into the *Dnah5* gene outside of the homology arms were performed in reaction mixes of 30 µl as follows:

DreamTaq green master mix (2x)	15 µl
Earclip DNA	2.5 µl
Primer (A100) and primer (A101) (10 µM)	0.6 µl
Nuclease free water	12.1 µl

Reaction conditions used for this PCR are below:

Program: D5SNAHOM			
Step	Time	Temperature (°C)	Cycles
Initial denaturation	3 min	95	1
Denaturation	30 s	95	33
Annealing	30 s	62.4	
Elongation	1 min	72	
Final extension	10 min	72	1
Storage	forever	4	1

Expected product size of 980 bp.

2.5.2 PCM1^{SNAP} genotyping

The following PCR conditions were used to identify and characterise the insertion of the SNAP tag into the *PCM1* locus in HEK 293 cells.

Step	Temperature (°C)	Time	Cycles
Initial denaturation	95	3 min	1
Denaturation	95	30 s	30
Annealing	x	30 s	
Elongation	72	1 min	
Final extension	72	10 min	1
Storage	4	forever	1

All reactions were performed using the DreamTaq green master mix (2x) in 20 µl volumes with 0.2 µM final concentration of primers. The reaction conditions for all but the exon spanning PCR, PCM1ex3 which had an elongation time of 50 seconds, are identical to those below except the annealing temperatures were altered, **Table 2.2** summarises the different PCRs used.

Purpose of PCR	Name of program	Annealing temperature (°C)	Forward primer	Reverse primer	Product size (bp)
Exon 2 to 5' SNAP	PCMSNAP2	56.1	PCM1 ex2_f	Primer SNAP_r	375
Exon 3 to 5' SNAP	PCM1SNAP	58	PCM1-ex3_f	Primer SNAP_r	329
Exon 38 to 5' SNAP	PCM1SNAP	58	PCM1 ex38_f	Primer SNAP_r	341
Exon 39 to 5' SNAP	PCM1SNAP	58	PCM1 ex39_f	Primer SNAP_r	435
Exon 3 to 3' SNAP	PCMSNAP3	61.8	GGSGSNAP 888-906	PCM1-ex3_r	198
Spanning exon 3	PCM1ex3	59	PCM1-ex3_f	PCM1-ex3_r	785

Table 2.2 PCR conditions for SNAP insertion into *PCM1*.

The table summarises where the *PCM1* PCRs are designed to amplify, the name of the PCR program, the name of the primers used, the annealing temperature and the product sizes expected with a SNAP tag insertion in the correct position.

2.5.3 PCR for *D. melanogaster* genotyping

The following PCRs were used to test for the insertion of the SNAP tag into the second exon of *CG6971*, all reactions were done using the DreamTaq green master mix (2x) in 20 µl volumes with 0.2 µM final concentration of primers. The reaction conditions are shown below.

PCRs to amplify from the gene sequence into the 5' end of the SNAP tag were performed in reaction mixes of 20 µl as follows:

DreamTaq green master mix (2x)	10 µl
Embryonic DNA	1 µl
Primer C-1F *CG6971* and SNAPCR *CG6971* (10 µM)	0.4 µl
Nuclease free water	9.6 µl

Reaction conditions used for this PCR are below:

Program: 6971SNAP			
Step	Temperature (°C)	Time	Cycles
Initial denaturation	95	3 min	1
Denaturation	95	30 s	25
Annealing	58.5	30 s	
Elongation	72	1 min	
Final extension	72	5 min	1
Storage	4	forever	1

Expected product size of either 273 bp for guide C1 or 255 bp for guide C2.

PCRs to amplify across the SNAP tag integration site were performed in reaction mixes of 20 µl as follows:

DreamTaq green master mix (2x)	10 µl
Embryonic DNA	1 µl
Primer C-1F CG6971 and C-1R CG6971 (10 µM)	0.4 µl
Nuclease free water	9.6 µl

Reaction conditions used for this PCR are below:

Program: 6971SPA			
Step	Temperature (°C)	Time	Cycles
Initial denaturation	95	3 min	1
Denaturation	95	30 s	30
Annealing	60.2	30 s	
Elongation	72	1 min	
Final extension	72	5 min	1
Storage	4	forever	1

Expected product size of either 266 bp with no insertion or 851 bp with an insertion.

2.6 Gel electrophoresis

2.6.1 Agarose gels

Agarose gels were made up in 1 x TBE buffer with Hi-Pure Low EEO (Biogene™ catalogue no. 300-300), to either 1% W/V or 2% W/V. Either 0.00002% ethidium bromide or 0.0001% SYBR SAFE was added to image the DNA bands.

2.6.2 Polyacrylamide gels

PolyAcrylamide Gel Electrophoresis (PAGE) was used for both protein analysis as well as for nucleic acid analysis and purification for modified guide RNA and repair DNA.

PAGE for proteins

Beads from immunoprecipitation or protein lysate were suspended in 1X **protein loading buffer** (see **Section 2.16.1**) with final volumes of ~30 µl for a 10 well gel or ~20 µl for a 12 well gel, samples were heated to 72 °C for 10 minutes before loading.

PAGE for PCM1 used the NuPage® 4-12% Bis-Tris gel system (Thermo Fisher Scientific™ catalogue no. NP0321BOX) with the NuPage® MOPS SDS running buffer (catalogue no. NP0001) diluted from 20x to 1x with distilled water. The gel was run at 150 V for 55 minutes.

PAGE for DNAH5 used the NuPage 3-8% Tris-acetate gel system (Thermo Fisher Scientific™ catalogue no. EA0375BOX with the NuPage Tris-acetate SDS running buffer (catalogue no. LA0041) diluted from 20x to 1x with distilled water with NuPage sample reducing (10X) (catalogue no. NP0009) agent added to the top chamber only. The gel was run at 150 V for 65 minutes.

PAGE for nucleic acids

15 % polyacrylamide 8M urea gels were made with 1.0 mm thick wells for analysis and 1.5 mm thick wells for purification. The recipe for 15 ml of gel is below:

TBE (1x)	9 ml
Acrylamide (30%)	6 ml

Urea	6.3 g

Urea was added to liquid and left at 65 °C for 5 minutes then mixed until clear.

150 µl of 10% APS and 15 µl of TEMED were added and the gel was pipetted into a Biorad™ (catalogue no. 1702982) 1.5/1.0 mm glass plate. Gels were left to set for ~60 minutes.

The wells were flushed with 1x TBE running buffer to remove urea, they were then pre-run before the nucleic acid was loaded.

Nucleic acids were mixed with RNA gel loading dye (2x) (Thermo Fisher Scientific™ catalogue no. R0641) before being loaded into the gel. Gels were run at between 65 and 90 V for 1 to 2 hours.

Gels were post-stained with SYBR Gold (Thermo Fisher Scientific™ catalogue no. S11494) diluted 1 in 10,000 in 1 x TBE. The gel was left to soak gently rocking at 4 °C for 30 minutes.

2.7 Extraction and purification

2.7.1 DNA extraction and purification

2.7.1.1 Sodium hydroxide extraction

Mouse earclips were submerged in 25 mM sodium hydroxide heated to 95 °C for 20 minutes before being neutralised with an equal volume of 40 mM Tris-HCl.

2.7.1.2 Quick lysis with proteinase K

Single colonies of mammalian cell lines from the *PCM1* SNAP tagging experiment were pelleted and lysed with QuickExtract™ DNA Extraction Solution 1.0 (Epicentre™ catalogue no. QE0905T) overnight at 56 °C using the following volumes of reagents:

Pelleted cells	1/10 96 well
QuickExtract™ solution 1.0	40 µl
Proteinase K (20 µg/µl)	5 µl

2.7.1.3 DNA extraction from fly embryos

Injected *Drosophila melanogaster* embryos were picked up with forceps and placed on a 200 µl pipette tip before being squashed against the side of a 0.5 ml

Eppendorf tube. 20 µl of **Smashing Buffer** (**Section 2.18.1**) with added proteinase K was added to each embryo. The embryos were incubated at 37°C for 30 minutes then 95°C for 5 minutes.

2.7.1.4 Qiagen DNeasy blood and tissue kit

This kit was used as described in the manufacturer's protocol, samples were always heated to 56 °C for 10 minutes and eluted in 30-50 µl of elution buffer.

2.7.1.5 Invitrogen™ Purelink™ PCR purification kit

Restriction digests and PCRs were purified using the Invitrogen™ Purelink™ PCR purification kit following the manufacturer's instructions except eluting in smaller volumes between 10-20 µl.

2.7.1.6 Invitrogen™ Purelink™ Quick Plasmid Mini-prep kit

Bacterial colonies were grown in 5 ml of LB overnight then the Invitrogen™ Purelink™ miniprep kit (catalogue no. K210010) was used according to the protocol provided, DNA was eluted in 40 µl.

2.7.1.7 Invitrogen™ Purelink™ HiPure Plasmid Filter Maxiprep kit

100 ml of LB was inoculated with 200 µl of LB with *E. coli* grown for 4-6 hours at 37 °C and shaking at 250 rpm. The 100 ml of LB was left to grow overnight with the same conditions. All steps of the protocol provided with the Purelink™ HiPure kit (catalogue no. K210007) were followed except the following:

- When loading the precipitated lysate into the column the column was first covered with gauze to prevent precipitate from potentially blocking the column.
- The column was eluted into 30 ml Corex, DNA binding glass, tubes instead of plastic falcons.
- The ethanol was dried first with paper and then left to evaporate.
- The pellet was left to dissolve in pH 8 TE overnight at 4 °C to increase the yield of the DNA.

2.7.1.8 Plasmid clean-up for zygote injection

The repair template for *Dnah5* tagging was further purified by running through an Amicon column (Merck Millipore™ catalogue no. UFC503096) as follows:.

1. The plasmid was diluted to 100 ng/µl in distilled water.
2. 50 µl of this was added to a 30 kDa centrifugal filter.
3. The column was spun at 13,000 rpm for 5 minutes.
4. 100 µl of wash buffer (1 mM Tris-HCl, 1 mM EDTA) was added to the column.
5. The column was spun at 13,000 rpm for 5 minutes.
6. The column was washed with 100 µl of wash buffer.
7. The column was spun at 13,000 rpm for 10 minutes.
8. 10 µl wash buffer was added to the column.
9. The column was incubated at room temperature for 1 minute.
10. The column was inverted into a clean collection tube.
11. The column was spun at 13,000 rpm for 3 minutes.
12. Add 40 µl Transfer buffer (10 mM Tris-HCl, 0.1 mM EDTA, pH 8).

2.7.2 RNA extraction from Flp-In T-REx HEK 293 cells

HEK 293 cells that had *EGFP* either 68G or 68A were grown in 6 well plates, trypsinised and 90% were pelleted, frozen on dry ice and then had their RNA extracted using the Qiagen™ RNeasy Plus mini kit (catalogue no. 74134) as follows:

1. Pelleted cells were resuspended in 600 µl of RLT plus buffer by vortexing for 30 seconds.
2. The lysate was then transferred to QiaShredder columns (catalogue no.79654) and spun for 2 minutes at maximum speed in a benchtop centrifuge.

3. The lysate was transferred into gDNA Eliminator spin columns and placed in 2 ml collection tubes.

4. The column was centrifuged for 30 seconds at ≥8000 x g (≥10,000 rpm). The column was discarded and the flow-through was saved. 600 µl of 70% ethanol was mixed well with the flow-through by pipetting. Do not centrifuge.

5. 700 µl of the sample, including any precipitate, was transferred to an RNeasy spin column placed in a 2 ml collection tube, the remaining 500 µl was also transferred to another RNeasy spin column. The lids were closed and the columns were centrifuged for 15 seconds at ≥8000 x g, the flow-through was discarded.

6. 700 µl of Buffer RW1 was added to the RNeasy Mini spin column (in a 2 ml collection tube). The lids were closed and the columns were centrifuged for 15 seconds at ≥8000 x g and the flow-through was discarded.

7. 500 µl of buffer RPE was added to the RNeasy spin column. The lids were closed and the columns were centrifuged for 15 seconds at ≥8000 x g and the flow-through was discarded.

8. 500 µl of buffer RPE to the RNeasy spin column. The lids were closed gently and the columns were centrifuged for 2 minutes at ≥8000 x g (≥10,000 rpm).

9. The RNeasy spin columns were placed in new 1.5 ml Eppendorf tubes. 30 µl of RNase-free water was added directly to the spin column surface of the columns with 700 µl added in step 5 and 20 µl to columns with 500ul added in step 5. The lids were closed and the columns were centrifuged for 1 minutes at ≥8000 x g to elute the RNA.

RNA content was measured using Nanodrop^{TM} and the RNA concentrations were between 276 and 1712 ng/µl for all tubes except HEK 293-Flpin EGFP^{WT} G6, which had fewer cells.

2.7.3 Purification from polyacrylamide gels for DNA-RNA fusions

The click chemistry reaction products were analysed in polyacrylamide gels as described in **Section 2.6.2**. Products which appeared to be of the right size were

extracted by first imaging the stained gels on a blue light illuminator and using a razor to cut the bands of the correct size out of the gel, making sure to only cut out the centre of the band at the brightest part. The bands can then be stored at -80 °C for a week.

Extraction:

1. Excised acrylamide bands were placed in 0.5 ml Eppendorf tubes that had a hole made in them by using a 21 G needle, these were then placed in a 1.5 ml Eppendorf and spun at 21,100 x g for 5 minutes.
2. The slurry at the bottom of the big centrifuge tube was covered with 150 µl of TE pH 7.4.
3. The samples were then frozen at -80 ° C for ~30 minutes
4. Samples were thawed for 5 minutes at 55 °C before being left at 4°C overnight shaking at 40 rpm on a rotary shaker.

Precipitation:

1. The gel slices left in TE overnight were spun with elution buffer at 21,100 x g for 3 minutes.
2. The liquid was then transferred to a 0.2 µm filter spin column (Co-star™ catalogue no. CLS8161-100EA) and spun at the same speed for 1 minute to remove the bits of gel.
3. The volume of the flow-through was then measured using a pipette. In this example ~90 µl.
4. 9 µl or ~1/10 the volume of the flow-through of precipitation buffer was added (3 M sodium acetate pH 5.19).
5. 225 µl or 2.5 volumes of 96 % ethanol was added with 1 µl (15 ng) of Glycoblue Coprecipitant (Thermo Fisher Scientific™ Catalogue no. AM9516).

The sample is vortexed and then left at -20°C overnight to several days.

Wash:

1. The precipitated material was then pelleted by spinning at 21,100 x g at 4 °C for 30 minutes.
2. The supernatant was removed and 10 µl of ice cold 96% ethanol was added to the pellet.
3. The tube was spun at the same temperature and speed for an additional 10 minutes.
4. The ethanol was removed and the tube was spun with the lid open for 1 minute at maximum speed to dry the pellet.
5. The pellet was re-suspended in 10 µl of TE pH 7.4.
6. The concentration was estimated by measuring absorbance at 260 nm and averaging between ssRNA and ssDNA multipliers.

2.7.4 Protein lysis and Immunoprecipitation

Tissues and cells were lysed for immunoprecipitation of their proteins using the SNAP antibody and western blot analysis as follows:

Lysis:

Three different samples were used for immunoprecipitation in this project **(1)** mTECs, **(2)** HEK 293 cells and **(3)** mouse tracheas.

(1) mTECs were rinsed 2x with PBS (Dulbecco's PBS pH 7.5) in transwells.

(2) HEK 293 cells were pelleted before being rinsed 1x with PBS.

(3) Mouse tracheas were dissected, placed into PBS and snap frozen in liquid nitrogen for storage before lysis.

All cells and tissues were lysed in the same buffer, **IP lysis buffer** (see recipes **Section 2.18.1**).

(1) mTECs had lysis buffer directly added to them and were scraped and re-suspended with a pipette.

(2) Similarly HEK 293 pelleted cells were re-suspended in lysis buffer.

(3) While tracheas were put into lysis buffer and homogenised using a motorised hand pestle for several minutes.

Lysis was carried out at 4 °C for 10 minutes with agitation.

Measure Protein concentration:

Protein concentrations were estimated using absorbance with a Denovix™ spectrophotometer. For **(1)** mTEC IP 1 transwell/replicate was used.

Optional: SNAP label.

For **(2)** HEK 293 *PCM1*^{SNAP} cell IPs 10 µM fluorescent SNAP-cell 647 SiR (NEB™ catalogue no. S9102S) was added to 1 mg protein for 30 minutes at 37 °C.

Optional: Preclear lysate.

1. PureProteome beads (Millipore Merck™ catalogue no. LSKMAGAG10) were resuspended by gently rotating on roller.
2. A volume equal to the number of IPs x 30 µl of beads was transferred to a fresh tube, placed on a magnetic rack for <2 minutes and aspirated with fine-tip pastette.
3. Beads were pre-equilibriated by adding X µl IP lysis buffer (where X is the amount in µl of lysate added to antibody x no. IPs) for 5 minutes and were left to gently rotate on a roller.
4. The beads were placed on a magnet tube rack <2 minute and the buffer was aspirated off with a fine-tip pastette.
5. Beads were re-suspended in (no. IPs X 30) µl of lysis buffer.
6. 1 µl of Benzonase (Merck Millipore™ catalogue no. E1014) was added to 1 mg of lysate.
7. 1 mg of protein was incubated with 30 µl of beads.

Binding of antibody to target protein in cell lysates

1. If preclearing was done then PureProteome beads were magnetically separated from the lysate.

2. The lysate was incubated with 10 µl or 8 µl **(1)** SNAP tag antibody (NEB™ catalogue no. P9310S) per ~1 mg/transwell **(1)** of lysate.
3. Lysates were incubated with antibody overnight at 4 °C with mild agitation (side-to-side, 18 rpm, setting 90).

Immunoprecipitations of immunocomplexes using PureProteome Beads

1. PureProteome beads were re-suspended by gently rotating on a roller.
2. A volume of beads equal to the number of IPs x 30 µl of beads was transferred to a fresh tube, placed on a magnetic rack for <2 minutes and aspirated with fine-tip pastette.
3. Beads were pre-equilibriated by adding X µl IP lysis buffer (where X is the amount in µl of lysate added to antibody x no. IPs) for 5 minutes and gently rotating on roller.
4. The beads were placed on a magnet tube rack <2 minutes and the buffer was aspirated off with a fine-tip pastette.
5. Beads were re-suspended in (no. IPs X 30) µl of lysis buffer.
6. They were then incubated for 30-45 minutes (always < 1 hour) on a roller to concentrate immuno-globulin complexes on the beads.
7. 8 washes in X µl of wash buffer (where X is the volume of the lysate added to the antibody) were performed by adding the wash buffer to the beads and agitating at 4 °C for 2-5 minutes before briefly centrifuging for ~5-10 seconds and placing in the magnetic rack to remove the liquid from the beads with a fine tip pastette, each time ensuring all liquid is aspirated away. The wash buffers used had decreasing amounts of detergent as detailed below:
    a. 2 x washes with **IP wash buffer 1** (see **Section 2.18.1**).
    b. 2 x washes with **IP wash buffer 2** (see **Section 2.18.1**).
    c. 4 x washes with **IP wash buffer 3** (see **Section 2.18.1**).
8. After the final wash before aspirating the suspended beads were transferred to a new tube and then the liquid was carefully removed using a fine tip pastette. The dried beads were stored at -80 °C for later use in Western blotting or mass spectrometry.

2.8 Western blotting

The blots shown in this document were both to measure the effectiveness of immunoprecipitation of the SNAP tag from an endogenously tagged cell line and mouse. The details of the protocols used are below and the antibodies used for these experiments are listed in **Table 2.3.**

Protein gels were blotted by removing the gels from their plates, washing in water or 20% ethanol and then transferring to nitrocellulose membranes (Thermo Fisher Scientific™ catalogue no. IB23001) with the iBlot 2 dry blotting system (Thermo Fisher Scientific catalogue no. IB21001) using the 7 minute 25 V program 0 for PCM1 and a custom program of 8 minutes at 20 V was used to transfer the much larger DNAH5 protein.

Manual method of western blotting, used for PCM1:

1. The transferred blot was blocked in blocking solution, which is 1x TBS with 0.1% (w/v) Tween-20 detergent (TBST) and Marvell's Milk Powder 5% (w/v) added to it, for 1 hour at 4 °C.
2. The block was then removed and replaced with block containing primary antibody, anti-SNAP tag antibody diluted 1 in 250, this was left to incubate overnight at 4°C.
3. The blot was washed twice to remove primary, then 3 times for 10 minutes each time in TBST shaking at 4°C.
4. Secondary antibody, HRP-conjugated rabbit heavy-chain, diluted 1 in 10,000 was added to the blot in blocking solution for 50 minutes at room temperature and then 2 hours at 4°C.
5. The blot was washed three times in TBST for 12 minutes per wash.
6. The blot was then submerged in SuperSignal™ West Femto Maximum Sensitivity Substrate (Thermo Fisher Scientific catalogue no. 34095) for 5 minutes.
7. Chemi-luminescence was imaged using an Imagequant LAS 4000 series imager.

iBind Western Device (Thermo Scientific catalogue no. SLF1000) used for DNAH5:

1. 5 ml of 1x iBind buffer was made as follows:
    a. 1 ml of 5x FD buffer
    b. 50 µl of 100 x additive
    c. 3.95 ml of distilled water
2. Blots were placed in water after transfer then moved into 50 ml Falcon tubes with 2 ml of 1x iBind buffer and were left to roll at 4 °C for 30 minutes.
3. The iBind buffer was replaced with 2 ml of iBind buffer containing primary antibody, which was left rolling overnight at 4 °C.
4. The rest of the steps are described in detail in the iBind manual, secondary antibody was diluted 1 in 10,000.
5. Blots were imaged in the same way or with photographic film.

Blots were stripped using Thermo Fisher Scientific's Restore™ Western Blot Stripping Buffer (catalogue no. 21059).

Protein detected	Animal raised in	Manufacturer	Catalogue no.	Concentration used
SNAP tag	Rabbit pAb	NEB™	P9310S	1 in 250
DNAH5	Rabbit pAb	A gift from Dr. H. Takeda	N/A	1 in 2000
DNAI1	Rabbit pAb	Abcam™	AM9516	1 in 2000
DNAI2	Mouse mAb	ABNOVA™	H00064446-M01	1 in 1000
PCM1	Mouse pAb	Novus Biologicals™	H0005108-B01P	1 in 250

Table 2.3 Primary antibodies used for western blotting

The table above shows the polyclonal (pAb) and monoclonal (mAb) antibodies used to analyse the western blots of SNAP Tag IPs.

2.9 Mouse work

Mice were housed in a Specific Pathogen Free environment. Experiments on these mice were performed following the guidelines issued by the Medical Research Council in 'Responsibility in the Use of Animals in Medical Research' (July 1993). Licence to do this work was granted by the Home Office under the Animals (Scientific Procedures) Act 1986.

2.9.1 Injection mix preparation for *SNAP-Dnah5* tagging

S. pyogenes GeneArt™ Platinum™ Cas9 Nuclease (Thermo Fisher Scientific™ (catalogue no. B25640) was mixed with *in vitro* synthesised guide RNA *Dnah5* guide exon 1_2 up to 1 hour before injection using the following reagents and volumes in a 1.5 ml Eppendorf.

Repair Plasmid (10 ng/µl)	6 µl
Cas9 protein (100 ng/µl)	2 µl
sgRNA (25 ng/µl)	15 µl
Transfer buffer	37 µl

This mix was incubated at room temperature for 5 minutes to allow RNP complexes to form. This was then placed on ice.

2.9.2 Tracheal dissection and mTEC derivation

Mice aged between 9 days and 1 year were dissected to remove their tracheas to either generate primary cell cultures from their tracheal epithelial cells or for lysis to analyse the expression of tagged DNAH5 protein.

Mice were culled with either CO_2 asphyxiation or by using intraperitoneal injection of a lethal dose of anaesthetic, in order to preserve the trachea. The mice were then dissected, as previously described in detail (Vladar and Brody 2013). The protocol to make mouse tracheal epithelial cells (mTECs) is also provided by Vladar and Brody 2013, it was followed exactly up until the point of seeding. Another publication (Eenjes et al. 2018) showed it was possible to expand mTECs in culture for an extended period of time to increase the number of cells grown from each trachea. Therefore instead of being seeded into transwells directly the mTECs were instead grown in T75 flasks for 1 to 2 weeks before being seeded

into transwells, this was done by growing the cells in KSFM media, see **Section 2.18.3** for the recipe.

The steps after this were the same as the original publication except that Life Technologies DMEM was substituted for advanced DMEM F12 (Catalogue no. 12634028) instead of DMEM F12 (Catalogue no. 11330-032) and the PLUS proliferation media was supplemented with Y-27632 as well as the KSFM media, at the same concentration the recipe for PLUS and NS media can be found in Vladar and Brody 2013.

2.10 Tissue culture

2.10.1 mTEC tissue culture techniques

2.10.1.1 Dissociating and seeding or freezing mTECs

Dissociating

mTECs being grown in T75 flasks were dissociated using a **dissociation media** described previously (Eenjes et al. 2018), the (recipe in **Section 2.18.3**), 3 ml of dissociation buffer was added to each T75 flask of mTECs and the flasks were left to incubate at 37°C 5% CO_2 for 10-15 minutes. Once the cells began to detach from the flask the trypsin was neutralised with 300 µl of FCS. The cells were pipetted up and down to evenly disperse them and then they were spun in 50 ml Falcon tubes at 400 x g for 10 minutes.

Seeding

To seed mTECs, Transwells® (Corning®) were coated with collagen coating solution from 4 hours to overnight and the cells were then seeded on these (Vladar and Brody 2013). The pelleted cells from the mTEC flasks were re-suspended in PLUS media and were either counted using the Sceptre cell counter (Millipore Merck™) to seed between 40,000 and 200,000 cells per well or the cells from a single T75 flask were divided equally between 5 to 15 Transwells. The tendency of the cells to aggregate can make counting difficult, therefore excess cells were often seeded, this approach did not appear to harm the ability of mTECs to grow and differentiate.

Freezing

Pelleted cells can be re-suspended in **freezing media** (**Section 2.18.3**) similar to other cell lines used in this work. mTECs were frozen in 500 µl of freezing media at a high density between 1/3 and 1/2 of a T75 flask per Cryo-vial (Thermo Fisher Scientific catalogue no. 10004220).

2.10.1.2 Reverse seeding, differentiating and SNAP dye imaging

Reverse seeding

Imaging of mTECs live is made difficult due to the high auto-fluorescence on the membrane of the transwells and the thickness of the membrane. To overcome this a method to grow the mTECs on the underside of the transwell inserts was developed in this project, such that the cilia of the cell point down towards the lens of the inverted microscope. This was accomplished by putting the transwells upside down in a 12 well plate and then placing a short piece of plastic tubing over the bottom of the insert, the chamber normally named the apical chamber is now facing downwards. The apical chamber is filled with 200 µl of PLUS media which is kept in place by surface tension. Then the upwards pointing side of the membrane has the cells seeded onto it. These are left overnight at 37°C 5% CO_2 to adhere and then the inserts are put back into a 24 well plate, in the normal orientation, with 500 µl of PLUS media in each well and the temporary chamber is removed.

Differentiating mTECs

mTECs are differentiated as described (Vladar and Brody 2013), by removing the PLUS media and replacing only the basal chamber media with NS differentiation media. The stage at which mTECs are ready to be differentiated was difficult to ascertain and therefore proliferation time varied considerably between cultures.

SNAP dye imaging

mTECs derived from *SNAP-Dnah5* mice had SNAP cell permeable dyes added to them. The most effective dyes, concentrations and protocols for staining were found to be as follows:

1. Addition of 0.6 mM SNAP-Cell TMR-Star (NEB™ catalogue no. S9105S) in DMSO at 0.5 µM final concentration or 0.6 mM SNAP-Cell 647-SiR (NEB™

catalogue no. S9102S) in DMSO at 0.3 µM final concentration to NS media with retinoic acid, mixed thoroughly by pipetting.

2. 500 µl of this dye solution was added into the basal chamber of the mTECs, which were incubated at 37°C 5% CO2 for 24 to 48 hours.
3. The dye is then washed off as follows:
    a. 1st wash: media was aspirated off, replaced with new media
    b. 2nd wash: media was immediately removed and replaced with more media.
    c. 3rd wash: after 1 hour at 37 °C 5% CO_2 the media was removed and replaced with new media before incubated at 37 °C 5% CO_2.
    d. 4th wash: 1 hour later the media was removed and replaced with new media.
4. DNAH5 will be stably labelled now for at least ~32 days, the longest timepoint studied in this thesis.

2.10.2 Flp-In™ T-REx™ HEK 293 Cell Line

2.10.2.1 Integration of *EGFP* G68A vector into Flp-in cells

The Flp-In HEK 293 cells have a detailed manufacturer's protocol that explains how to maintain them and how to integrate constructs, as such this will be a brief overview highlighting where the approach taken differs from the published protocols.

2.10.2.1.1 Transfection of the Flp-In HEK 293 cell line

Cells were grown to 70% confluence and were transfected with Lipofectamine 2000 (Thermo Fisher Scientific™ catalogue no. 11668019) with a ratio of 1 µg to 4.5 or 6 µl of DNA to Lipofectamine 2000 (see **Section 2.10.4.1**). The ratio of EGFP pcDNA FRT plasmid, the plasmid which is integrated, was 1 to 10 of the pOG44 plasmid which contains the Flp recombinase. This makes multiple integrations of the *EGFP* gene less likely. This is a summary of the transfection protocol used:

1. The following master mixes were made with Opti-MEM (Thermo Fisher Scientific™ catalogue no. 31985070), lipofectamine 2000 and either plasmid DNA in TE or plasmid DNA diluted in Opti-MEM.

2. 6 µg of DNA in total was added to each of the wells in the 6 well plates.
3. The table below summarises the different reactions, wells 1-5 are the experimental wells whereas wells 6-12 are the controls.

Plasmid	G67A FRT + poG44		eGFP FRT + poG44		pMAX eGFP		pOG44		eGFP		No DNA	
Well number	1	4	2	5	3	6	7	10	8	11	9	12
Lipofectamine (µl)	9	12	9	12	9	12	9	12	9	12	9	12

4. The media was replaced 4 hours after transfection with antibiotic free media.
5. The media was changed the next day to media containing penicillin and streptomycin.

2.10.2.1.2 Hygromycin selection

The transfected cells had their media changed to DMEM containing 100 µg/ml Hygromycin 2 days after transfection. They were then transferred from 6 well plates into 10 cm dishes, the like wells were pooled. Cells began to die within 2 days and were under selection for 12 days before colonies of cells could be observed to have grown.

2.10.2.1.3 Transferring cell colonies from 10 cm dish

When the colonies of Hygromycin resistant cells were visible to the naked eye they were drawn around with a marker pen. The circled areas had a drop of TrypLE express (Thermo Fisher Scientific™ catalogue no. 12605010) put onto them and were carefully pipetted up and down to dislodge the cells, they were then transferred into 24 well plates with 500 µl of DMEM with Hygromycin in each of the wells.

2.10.2.1.4 Inducing *EGFP* expression in Flp-in T-REx HEK 293 cells

The Flp-in locus in T-REx HEK 293 cells is under the control of the tetracycline repressor operon, therefore in order to have consistent expression of *EGFP* from these cells 1 µg/ml Doxycycline in the selection media was added at least 24 hours before analysis of the cells.

2.10.3 Mouse Embryonic Fibroblasts

Mouse Embryonic Fibroblasts (MEFs) from mTmG mice, immortalised with the large T antigen from Simian Virus 40 (SV40), were cultured as an editing reporter system. In this study they have been used to test the effectiveness of putative small molecule enhancers of Homology Directed Repair (HDR) and Cas9-rep78 in improving Cas9 nuclease induced HDR. These cells were grown in modified Opti-MEM, the recipe for **MEF Media** can be found in **Section 2.18.3**.

2.10.4 Transfection and transduction

2.10.4.1 Lipofectamine 2000

Flp-in HEK 293 cells were transfected with Lipofectamine 2000 for the creation of the EGFP reporter line as described in **Section 2.10.2.1.1** and to tag the endogenous *PCM1* locus with SNAP. The SNAP tagging was done in the same way, except with equal masses of pX330 with PCM1 guides to SNAP tagging pMA-tia1l plasmids were added in a 24 well plate.

2.10.4.2 Lipofectamine CRISPRMAX

Lipofectamine CRISPRMAX (Thermo Fisher Scientific™ catalogue no. CMAX00015) was used to transfect EGFP Flp-In T-REx HEK 293 cells with Cas9 nuclease and *EGFP* guides and repair. This was done in accordance with the protocol.

7.62 pmol of guide RNA and repair DNA were added to 7.62 pmol of Cas9 nuclease with 2 µl of Plus reagent in 50 µl of Opti-MEM and were mixed and left to incubate for 5 minutes at room temperature. 50 µl of Opti-MEM was mixed with 3 µl of lipofectamine. The RNP plus mix was added to the lipofectamine and was incubated at room temperature for 10 minutes. The solutions were then added to the Flp-In T-REx HEK 293 $EGFP^{68A}$ cells and were left to incubate overnight with the cells before removing.

2.10.4.3 Neon transfection system

MEFs were transfected using the Neon transfection system (Thermo Fisher Scientific™) as follows:

1. Cells were trypsinised (**Section 2.10.5.1**) and were re-suspended in 1x Dulbecco PBS before being counted using the sceptre cell counter.
2. 10% excess of cells and plasmid DNA was used to make sure there was enough.
3. 110,000 cells were counted and re-suspended in 22 µl R buffer.
4. The plasmids, pX330 and pX330-Rep78 were mixed with R buffer, two 2.2 µg of plasmid pX330-Rep78.
5. The cells were then electroporated in two transfections with one 10 µl tip per well.
6. The cells were electroporated with 1350 V, width 30 ms and 1 pulse.
7. Cells were then put into **MEF media** in a 24 well plate at 37 °C 5% CO_2.

2.10.4.4 Electroporation and small molecule treatment of MEFs

MEFs were transfected using the Neon electroporator, as described in the previous section, with Cas9 protein (1 µg/well), Loxp 1 guide RNA (180 ng/well), H2B GFP repair plasmid (500 ng/well) and H2B BFP minicircle (500 ng/well) diluted in Opti-MEM. Each well was a technical replicate and contained 100,000 MEFs, the mixes were left to stand for 5 minutes at room temperature before adding to the cells and electroporating. This electroporation was done in two separate experiments, the first used three technical replicates and had only H2B GFP repair plasmid added (1 µg/well) while the second had five replicates and H2B BFP minicircle in addition to H2B GFP repair plasmid. Once electroporated, cells were pipetted into wells containing 2 ml of **MEF media** with the small molecules (dissolved in DMSO) at the concentrations listed in the table below:

Molecule	Final concentration (µM)
DMSO (vehicle control)	70
RS-1 (Sigma-Aldrich™ catalogue no. R9782)	10
SCR7 (Sigma-Aldrich™ catalogue no. SML1546)	0.1
L-755,507 (Sigma-Aldrich™ catalogue no. SML1362)	5
Brefeldin A (Sigma-Aldrich™ catalogue no. B7651)	0.1
Nu-7441 (Tocris Bioscience™ catalogue no. 3712)	2

2.10.4.5 AAV2 transduction of MEFs for HDR reporting

MEFs were transduced with AAV2/2 H2B GFP repair virus after being transfected with the Neon system, this was done by adding virus to cells immediately after transfection at an MOI of 100,000.

2.10.5 General tissue culture techniques

2.10.5.1 Trypsinisation

Unless otherwise stated passaging and dissociation of cells was carried out as follows:

1. The media was removed from the flask or plate.
2. The cells were covered in TrypLE™ express (Thermo Fisher™).
3. The cells were left to incubate at 37 °C 5% CO_2 for several minutes until cells detached.
4. The media was neutralised with an equal or greater amount of culture media.
5. Cell suspensions were either pelleted at 1,300 x g for 3 minutes or transferred to new culture vessels for passaging.

2.10.5.2 Freezing cells in liquid nitrogen

Cells centrifuged at 1,300 x g for 3 minutes and re-suspended in **freezing medium** (**Section 2.18.3**) for long term storage in liquid nitrogen.

To revive cells for culture they were thawed at 37 °C before being seeded into culture media.

2.11 Fixed tissue experiments

2.11.1 Para Formaldehyde fixation: for cells

mTECs were fixed for immunofluorescence and for RNA FISH while MEFs were fixed for imaging.

1. 4% paraformaldehyde (PFA) was made up fresh by diluting 16% PFA (Sigma-Aldrich™ catalogue no. 28908) with 1x PBS.

2. Cells were washed twice with 1x PBS and then covered in 4% PFA for 5 minutes.
3. PFA was washed off the cells and replaced with 1x PBS.
4. PBS was washed off and replaced with more PBS.
5. This PBS was washed off after 5 minutes and was either replaced with 1x PBS with 0.001% Sodium Azide added for storage of the cells or the cells were used immediately for immunofluorescence (**Section 2.9.2**).

2.11.2 Fixation for cryosectioning

Mouse tracheas were fixed for cryo-sectioning and smRNA FISH (**Section 2.11.4.2**), all solutions were diethylpyrocarbonate (DEPC) treated and autoclaved to minimise RNAse contamination.

1. The dissected tracheas were placed in 4% PFA and were left for 1 hour on a roller at 4 °C.
2. The tracheas were then rinsed twice with 1x PBS.
3. Tracheas were then placed in 20 % sucrose (w/v, made up in 1x PBS) overnight on a roller at 4 °C.
4. The tracheas were then placed upright into cryo-moulds (Agar Scientific™ catalogue no. AGG4581) dry ice.
5. While being held up with forceps the tracheas were submerged in OCT (VWR™ catalogue no. 361603E) until the compound hardened enough for the trachea to stand, ~2 minutes, and then another 30 minutes until the OCT had hardened fully.

Tracheas were sectioned transversely using a cryostat set at -20 °C. Sections were cut at a width of 8 µm, then placed on microscope slides and air dried before being stored at -80 °C.

2.11.3 Immunofluorescence mTEC protocol

Fixed cells were incubated with primary antibody to visualise the localisation of specific proteins. The antibodies used for these experiments are shown in **Table 2.4**. This was done using the following protocol:

1. PBS was removed from the surface of cells, for mTECs washes apply to both top and bottom chambers.
2. The wells were filled with TBST (TBS with 0.1% Triton X-100) and left to incubate at room temperature for 5 minutes.
3. Blocking buffer was made with TBST containing 5% donkey serum (Sigma-Aldrich™ catalogue no. D9663).
4. The top and bottom chambers had blocking buffer added to them and the cells were left to incubate with block for 30 minutes at room temperature.
5. The bottom chamber had 1% donkey serum in TBST added to it while the top chamber had 1% donkey serum in TBST with primary antibody added to it.
6. The cells were then left at 4 °C overnight to incubate with primary antibody.
7. Primary antibody was washed off with TBST, three times 5 minute washes.
8. 1% donkey serum in TBST was put into the bottom chambers and the top chambers had 1% donkey serum in TBST with secondary antibody added.
9. After 1 hour at room temperature the secondary antibody was washed off, three times 5 minute washes.
10. mTECs transwells were then removed from their wells and the membranes were cut off using a razor. Membranes were placed face up on microscope slides (Thermo Fisher Scientific™ catalogue no. 10149870). Samples were covered with mounting medium ProLong-Gold (Thermo Fisher Scientific™ catalogue no. P36930) and then a coverslip and allowed to cure as per the manufacturer's protocol.
11. Slides were usually imaged the same day or the next day and were kept at room temperature for up to ~2 months.

Protein detected	Animal raised in	Manufacturer	Catalogue no.	Concentration used
SNAP tag	Rabbit pAb	NEB	P9310S	1 in 250
DNAH5	Rabbit pAb	Gift from Dr. H. Takeda	N/A	1 in 1000
DNAI2	Mouse mAb	AbNova	H00064446-M01	1 in 300
SENTAN	Rabbit pAb	Gift from Dr. A. Kubo	N/A	1 in 400
Acetylated α-tubulin	Mouse mAb	Sigma-Aldrich	T 6793	1 in 800

Table 2.4 Antibodies used in immunofluorescence

The table above shows the polyclonal (pAb) and monoclonal (mAb) antibodies used for immunofluorescence imaging of fixed cells and tissues with the source, catalogue number of each note.

2.11.4 Single molecule RNA FISH using Stellaris probes

2.11.4.1 RNA FISH and immunofluorescence for adherent cells

Single molecule RNA fluorescence in situ hybridization (smRNAFISH) was performed as described in the Stellaris® combined immunofluorescence and RNA FISH protocols (https://www.biosearchtech.com/support/resources/stellaris-protocols). Custom Stellaris® FISH Probes, 48 in total, were designed against mouse *Dnah5* (catalogue number SMF-1065-5) by utilising the Stellaris® FISH Probe Designer (Biosearch Technologies, Inc., Petaluma, CA) available online at www.biosearchtech.com/stellarisdesigner. The mTECs were hybridised with the *Dnah5* and mouse *Gapdh* (catalogue number SMF-3140-1) Stellaris® FISH Probe set labelled with Quasar 670 dye (Biosearch Technologies, Inc.), following the manufacturer's instructions for simultaneous IF and FISH.

The following exceptions and additions to the protocol were made:

- All steps except mounting were performed within the wells. Fixative and hybridisation buffer were only applied to the top chamber.
- Cells were left to permeabilise in 70% ethanol at 4°C for 2-3 days.

- RNase treated cells that are fixed and permeabilised were washed with PBS and incubated with 50 µg/ml RNase A (Thermo Fisher Scientific™ catalogue number K2100-27) diluted in 1x PBS, for 1 to 2.5 hours at 37°C. *note it is important to keep these RNase treated samples away from the experimental samples*
- 10x the recommended amount of probe (10 µl or 1.25 µM concentration) was used when hybridising with cells.
- Hybridisation was always carried out overnight in a 37°C degree oven inside a box with wet tissue paper.
- Mounting was the same as that in the protocol for immunofluorescence.

2.11.4.2 smRNA FISH and immunofluorescence of cryosections

The tracheal cryosections produced as described in **Section 2.11.4.1** were processed as described in the protocol in the previous sections combined with the protocol for frozen tissue provided by Stellaris on their website. These samples had the recommended concentration of probes added.

2.12 Microscopy and imaging analysis

2.12.1 Confocal microscopy

The confocal images shown were captured using the Andor™ Dragonfly Spinning Disc confocal with the high sensitivity Xyla camera. Images were acquired using a 100x or 40x lens on the multimodal Imaging Platform Dragonfly (Andor technologies, Belfast UK) equipped with 405, 458, 488, 514, 561, 640 and 680nm lasers built on a Nikon™ TiE microscope body with a Perfect focus system (Nikon™ Instruments, Japan). Data were collected in Spinning Disk 40 µm pinhole mode on the iXon888 EMCCD camera using a Bin of 1 and frame averaging of 1 using Fusion v1.4 software.

2.12.2 Widefield microscopy and automated acquisition

Acquisition to quantify levels of HDR in edited mTmG MEFs was performed using a Nikon wide field microscope and Nikon™ JOBs software set to acquire either 240 or 148 images per well from the centre of each the wells at 20x magnification using the perfect focus system.

2.12.3 Stimulated Emission Depletion Microscopy

Super resolution images were captured using the Leica™ SP8 3X STED system using the pulsed 770 nm laser. All STED images were captured by Dr. Alison Dunn, Edinburgh Super Resolution Imaging Consortium (ESRIC), Heriot-Watt University.

2.12.4 High-speed video microscopy and transmission electron microscopy

High-speed video microscopy was used to assess ciliary beat patterns (speed and changes in shape) of *Dnah5*$^{SNAP/SNAP}$ MTEC axonemes compared to littermate control. These procedures were carried out by Dr. Amelia Shoemark (University of Dundee). Transmission electron microscopy was used to examine the ultrastructure of *Dnah5*$^{SNAP/SNAP}$ MTEC axonemes compared to littermate control performed by Dr. Farheen Daudvohra (Royal Brompton & Harefield NHS foundation trust) as described in (Fassad, Shoemark, le Borgne, et al. 2018).

2.12.5 CellProfiler analysis to quantify percentage GFP positive nuclei

Images acquired were analysed using the free open source software CellProfiler (https://cellprofiler.org/) (Doan et al. 2016). The pipeline was developed by Dr. Laura Murphy. Briefly, it identifies nuclei and then measures mean GFP intensity within the nucleus as compared with the area directly surrounding the nucleus. This ratio was then used to score nuclei as either GFP positive or not and was found to be the most effective way to distinguish between GFP positive nuclei and GFP positive membranes.

2.12.6 Image J analysis for general image manipulation

Image J 2.0 with 64 bit Java 8 (https://imagej.nih.gov/ij/) was used post-acquisition, primarily to process images and convert them to other file types (Schindelin et al. 2012).

2.12.7 Imaris processing and analysis of large stacks

Imaris was used to analyse confocal images and make 3D images from large stacks. Imaris v 9.2, Bitplane AG software available at http://bitplane.com.

2.13 Mass spectrometry analysis

Mass spectrometry analysis of the immunoprecipitated samples was performed by the mass spectrometry facility at the IGMM, specifically by Dr. Alex von Kriegsheim

and Dr. Alfonso Bolado using an IP/MS workflow carried out according to (Turriziani et al. 2014). MaxQuant software was used to analyse mass spectra and obtains label-free quantification intensity values which were used to calculate enrichment (log_2 fold change of SNAP vs WT IPs). Statistical significance was measured using a T-test based on these results.

The volcano plot created was made using a pipeline designed by Dr. Jimi Wills using LIMMA analysis software.

2.14 Fluorescence activated cell sorting

MEFs were trypsinised and pelleted as described in **Section 2.10.5.1**. The pellets were then re-suspended in 200-400 µl of PBS. This cell suspension was transferred into 4.5ml FACS tubes (BD™ Falcon). Samples were analysed using the LSR Fortessa (BD™ Biosciences). Sorting gates were manually set on all machines. For EGFP and Tomato an excitation filter of 488/50 and 561/20 was used with an emission filter of 525/50 (488-525/50) and 610/20, respectively. Cell counts were usually between 50-100,000 cells. FACS was performed by the technicians at the Institute of Genetics and Molecular Medicine (IGMM), Elisabeth Freyer and Stacey Thomson.

2.15 Sanger sequencing

Sanger sequencing was performed by the IGMM technical services department on an Applied Biosystems 3130 (4-capillary) Genetic Analyzer or a 48-capillary 3730 DNA Analyzer (Both Thermo Fisher™). Sequencing and the Agilent™ Bioanalyzer were both run by the IGMM technical service team members, Stephen Brown and Jeffrey Joseph.

2.16 Genome browsers, DNA sequence design and analysis

2.16.1 Genome browsers

Mammalian genomic sequences were downloaded from Ensembl genome browser 90, 2017 (https://www.ensembl.org/index.html) (Kersey et al. 2018).

Drosophila DNA sequences were downloaded from Flybase (https://flybase.org) FB2016_03, Dmel Release 6.11 (Thurmond et al. 2019).

2.16.2 DNA sequence design and analysis

DNA sequences were deposited and re-designed in the online biology software tool Benchling (https://benchling.com 2016-2019) to create genomic reference sequences for tagging as well as for plasmid Chromatic DNA traces and sequences from Sanger sequencing were aligned to these sequences. Benchling was also used to design the CRISPR guide RNA sequences used in this project. All pictures of DNA sequences, alignments and plasmid maps are from Benchling.

2.17 Miscellaneous software used

2.17.1 Primer design

Primers were designed using the online primer design software Primer3 (Koressaar and Remm 2007; Untergasser et al. 2012).

2.17.2 Statistical analysis and graphing

All statistical analysis and graphs shown were generated using GraphPad Prism version 8.2.0 for Windows, GraphPad Software, La Jolla California USA, www.graphpad.com.

2.17.3 Figures and illustrations

All figures and illustrations were made with Adobe Illustrator 2019, Adobe Indesign 2019 and Adobe Reader DC 2019. Some images were created using www.Biorender.com

2.18 Recipes

2.18.1 Buffers

20x TBE (1000ml):

Tris base	216.0 g
Boric Acid	110.0 g
0.5 M EDTA, pH 8.5	80 mL

Add deionised water to 1000ml

1x PBS (1000ml):

Deionised water 800 ml

NaCl	8.00 g
KCl	0.20 g
Na_2HPO	41.44 g
KH_2PO4	0.24 g

Adjust pH to 7.4 with HCl

Add deionised water to 1000 ml

10x Surveyor Buffer (10 ml):

100 mM HEPES buffer 10 ml

KCL	100 mM
MgSO4	100 mM
BSA	20 µg
Triton-x-100	0.02%

HEPES was made to pH 7.5 and all other ingredients were added to make a solution. This was stored at 4 °C and 3 ml was kept at -20°C.

Protein Loading Buffer (1x)

NuPage™ LDS sample buffer (4x)
(Thermo Fisher Scientific™ catalogue no. NP0007) 1/4 total volume
NuPage™ sample reducing buffer (10x)
(Thermo Fisher Scientific™ catalogue no. NP0004) 1/10 total volume
Deionised water to total volume

Ip lysis buffer

Tris-HCl pH 7.5	50 mM (from 1 M solution)
NaCl	100 mM (from 5 M solution)
Glycerol	10% (from 100%)
EDTA	0.5 mM (from 500 mM solution)
IGEPAL	0.5% (from 10% stock)

Add HALT protease inhibitor (1/100) fresh to lysis buffer.

IP wash buffer 1

Tris-HCl pH 7.5	50 mM (from 1 M solution)
NaCl	100 mM (from 5 M solution)
Glycerol	10% (from 100%)

EDTA	0.5 mM (from 500 mM solution)
IGEPAL	0.5% (from 10% stock)

IP wash buffer 2

Tris-HCl pH 7.5	50 mM (from 1 M solution)
NaCl	100 mM (from 5 M solution)
Glycerol	10% (from 100%)
EDTA	0.5 mM (from 500 mM solution)
IGEPAL	0.2% (from 10% stock)

IP wash buffer

Tris-HCl pH 7.5	50 mM (from 1 M solution)
NaCl	100 mM (from 5 M solution)
Glycerol	10% (from 100%)
EDTA	0.5 mM (from 500 mM solution)

Smashing buffer (1x)

Tris-HCl (pH 8.2)	10 mM
NaCl	25 mM
EDTA	1 mM
Triton x100	0.2% (v/v)

Just before use, dilute Proteinase K into buffer at 200 ug/mL

2.18.2 Bacterial solutions

Luria-Bertani Broth (LB) (1000 ml):

Tryptone 10.00 g
Yeast Extract 5.00 g
NaCl 10.00 g
Glucose 1.00 g
Add deionised water to 1000 ml
Add Ampicillin (100 µg/ml) or Kanamycin (50 µg/ml)

Freezing Media:

Luria Broth 70%
Glycerol 30%

LB-Agar (1000 ml):

Tryptone 10g
Yeast Extract 5 g
NaCl 10 g
Glucose 1 g
Agar 15 g
Add deionised water to 1000 ml
Add Ampicillin (100 µg/ml) or Kanamycin (50 µg/ml) as required

2.18.3 Tissue culture solutions

MEF Growth Media (500ml):

Opti-MEM (Thermo Fisher™ catalogue no.31985070)	445 ml
FCS	50 ml
P/S	5 ml

KSFM mTEC proliferation media (500 ml):

KSFM (Gibco™ catalogue no. 17005034)	491 ml
P/S	5 ml
EGF (Peprotech™ catalogue no. 315-09)	2.5 ml
BPE (Gibco™ catalogue no. 13028014)	1 ml
Isoproterenol (Sigma™ catalogue no. I-6504)	500 µl

Add fresh to aliquots when used:

Y-27632 1 in 1000 dilution (Cayman Chemical™ catalogue no. 10005583)
DAPT 1 in 1000 dilution (Sigma Aldrich™ catalogue no. D5942)

mTEC dissociation buffer (50 ml):

EDTA 0.5 M	270 µl
Trypsin	125 mg
Non-enzymatic 1x (Sigma) to make 50 ml	49.73 ml

Filter sterilise with 0.22 um filter.
Final concentrations: 0.25% Trypsin and 2.7 mM EDTA

Store at 4 °C

Freezing media (1000 ml):

Ham's F10 (Thermo Fisher Scientific™ catalogue no. 31550)	480 ml
Tryptose Phosphate Broth (Sigma-Aldrich™ catalogue no. T8159)	400 ml
DMSO (Sigma-Aldrich™ catalogue no. D2650)	120 ml

3 The design and testing of a high throughput endogenous axonemal dynein tagging strategy for *in vivo* analysis

3.1 Introduction

3.1.1 Axonemal dynein assembly, regulation and challenges to study

Axonemal dyneins (ADs), as introduced in **Section 1.2.1**, are large molecular complexes responsible for the movement of motile cilia and flagella. While a lot is understood about how these molecular machines function from work in model organisms (reviewed (Dutcher 1995; Luck 1984)) and by studying people with diseases of motile cilia (Afzelius and Stenram 2006) there are still many unanswered questions. ADs are assembled in the cytoplasm with the help of several assembly factors (Fowkes and Mitchell 1998), which recruit chaperoning proteins to sites of dynein assembly (Diggle et al. 2014; Dong et al. 2014). To date, most studies on AD assembly and function rely on antibody detection in fixed samples, and while these are able to provide a snapshot of AD localisation in motile ciliated cells, they do not convey the temporal information that is important for understanding how ADs are regulated. Therefore, being able to follow AD localisation over time, for example during motile ciliogenesis, is of great value in helping to understand how these molecular machines are made, regulated and turned over. Transiently expressing cDNAs with functional protein tags has been the standard method used to study many biological processes, including AD assembly (Mali et al. 2018; Kobayashi et al. 2017). However, the ADs are only expressed in a few motile ciliated cell types which are not easily transfected or cultured. Therefore endogenous tagging *in vivo* is necessary to investigate AD localisation in a dynamic and relevant system. While fluorescently tagged ADs do exist, expressed both endogenously (McGrath et al. 2003) and from ectopic genomic sites (Diggle et al. 2014), there are many more genes which remain untagged. The recent emergence of precise genome editing tools mean it is now much easier to tag genes endogenously, opening up a path to a better understanding of complex biological processes in their physiological contexts.

3.1.2 Endogenous tagging strategies

In order to investigate the dynamics and regulation of AD proteins endogenous tagging was employed. The ability to integrate protein tags into a locus of choice has been greatly aided by the recent development of easy-to-use genome editing

tools, such as CRISPR/Cas9. Many different strategies to endogenously tag genes of interest using CRISPR/Cas9 have been developed utilising different endogenous DNA repair pathways. The traditional method of genetic engineering requires the tag to be flanked by long stretches of sequence homologous to the targeted locus. Both single stranded and double stranded templates (Mali et al. 2013) have been used for this type of homology directed repair (HDR) to introduce changes in mammalian genomes. Although recent work has shown that long single stranded DNA is an effective template for endogenous tagging with larger insertions in mouse embryos (Quadros et al. 2017), in general, single stranded repair templates tend to be more suitable for shorter tags such as HA or V5 due to the difficulty and expense of synthesising long single stranded DNA.

While HDR is a well proven method for the insertion of a tag into the genomes of whole organisms and cells it either requires lengthy generation of double stranded homology arms or costly synthesis of single stranded DNA. Therefore methods of endogenous tagging have been developed that utilise the homology independent DNA repair pathways, non-homologous end joining (NHEJ) (Auer et al. 2014) and micro-homology mediated end joining (MMEJ) (Nakade et al. 2014). The main advantages of these approaches are the aforementioned savings on time and cost and the fact that mammals suppress homologous recombination in the G1 phase of the cell cycle (Orthwein et al. 2015). Without the constraints of homology arms a single tagging vector can be used to tag any gene within the genome and in any place where a guide sequence is present, significantly reducing the amount of time and resources needed to create a library of tagged genes. For these reasons the generic NHEJ tagging system (Lackner et al. 2015) is the strategy employed in this project for the tagging of AD proteins in *Drosophila melanogaster*, see **Section 3.2.1** and **Figure 3.1**.

3.1.3 Adaptable protein tags

In order to study AD assembly and regulation in detail, high temporal and spatial resolution of the underlying processes is required. Ideally it would be possible to follow the known components of ADs over time in a live cell and uncover their localisation, their turnover rate and what they are interacting with from their synthesis to their degradation. A first step to achieving this goal is to directly label the proteins of interest. While fluorescent protein tags such as GFP provide a way to visualise the protein of interest in live cells and have been used for a long time,

they do not offer flexibility of function. In recent years modular tagging systems have been developed, in which the protein tag binds covalently to substrates linked to a variety of moieties including fluorescent dyes, magnetic beads and biotin. Examples include the HALO-tag (Los et al. 2008), SNAP tag (Keppler et al. 2003) and CLIP tag (Gautier et al. 2008). A slightly different modular tagging system involves the use of activatable biarsenical fluorescent dyes, such as FlASH (Griffin, Adams, and Tsien 1998), CrASH (Cao et al. 2006), CHoXAsH, ReASH (Adams et al. 2002) and AsCy3 (Cao et al. 2007), which fluoresce when bound to a tetracysteine tag sequence. The SNAP tag was chosen for this project because of its small size, 19.4 kDa, making it less likely to be disruptive and reducing the size of the tagging vector. It has also been used extensively for various purposes, particularly imaging at high resolution, reviewed in (Kolberg et al. 2013), and can be used alongside the CLIP tag with very similar reagents for imaging experiments involving two tagged proteins. The SNAP tag is a modified human O^6-alkylguanine-DNA alkyltransferase (AGT) which irreversibly binds to O^6-benzylguanine (Keppler et al. 2003). The O^6-benzylguanine group is easily synthesised and can be attached to a multitude of fluorescent dyes, creating a greatly expanded repertoire of potential fluorescent labels for *in vivo* use. The O^6-benzylguanine group can also be attached to a variety of other substrates including biotin and magnetic beads allowing the SNAP tag to be the 'Swiss Army knife' of protein tags, see the diagram in **Figure 3.1 A)**. The ability to sequentially add dyes of different colours makes it possible to observe the dynamics of protein turnover and localisation over a wide range of time periods, **Figure 3.1 B)**. With a library of SNAP tagged ADs it would be possible to study AD assembly in the cytoplasm, visualise exactly when the ADs enter the cilium during differentiation and determine turnover rates at the motile axoneme.

3.2 A generic tagging strategy to produce a library of SNAP tagged axonemal dynein proteins

In order to generate a library of AD proteins and assembly factors, of which there are 18 genes and 7 genes in humans, respectively, a high-throughput method needs to be considered. To circumvent the challenges presented by the large size of the ADs and the need to study primary motile ciliated cells, we pursued a strategy of endogenous tagging (Lackner et al. 2015). The generic tagging strategy, **Figure 3.1 C)**, consists of a plasmid encoding sgRNA targeting the zebrafish gene *tia1l* under the control of the human U6 promoter and the tag

flanked by recognition sites for the *tia1l* sgRNA upstream of a PAM site. This plasmid is co-transfected into cells with a plasmid expressing Cas9 nuclease and a sgRNA recognising the target site within the cell's genome. Upon Cas9 expression, the tagging plasmid is cut, releasing the tag sequence and cutting the genome at the desired site, resulting in simultaneous double stranded DNA breaks and allowing the tagged sequence to be integrated into the genome via NHEJ. The lack of homology means that the tag can be integrated in either orientation and that the genomic cut site must be in a coding region to work. This necessitates the creation of plasmids in different reading frames and careful screening to ensure functional tagging. However, the tagging vector can be used for any gene and due to the facile nature of the cloning protocol it's possible to generate many plasmids with different tags relatively quickly.

The aim of endogenously tagging multiple ADs for *in vivo* study requires the use of many animals, and while the main focus of this project is in understanding AD regulation in the context of mammalian biology and human disease, mammalian animal models are slow to generate and expensive to maintain. It is more economical and practical to perform initial pilot experiments in non-mammalian animal models, such as *Drosophila melanogaster*, which breed more quickly and are relatively cheap to maintain. *Drosophila* and humans have many orthologous AD and motile cilia genes, despite *Drosophila* only having two motile ciliated cell types, making them good models for motile cilia biology and well suited to PCD candidate gene screening (zur Lage, Newton, and Jarman 2019). The initial tagging screen, conducted in collaboration with Prof. Andrew Jarman and outlined in **Figure 3.1 D)**, aimed to tag multiple *Drosophila* AD proteins at different locations with SNAP. These could be quickly screened for tag functionality by imaging with fluorescent SNAP dyes. Non-disruptive tagging can be confirmed in homozygous flies by a gravitaxis assay, a test of chordotonal neuron function which is disrupted by defects in the motile ciliary machinery. Once established as a viable fusion protein in the *Drosophila* model the orthologous gene in mice would be targeted and tagged at the same end with SNAP for further analysis. This approach would create multiple SNAP AD fusion lines in flies, which could be used for biochemical and imaging studies to address AD localisation and stability, as well as detection of novel interacting partners. Importantly, they would also provide valuable information about which genes, and where in the gene, would be the best targets for SNAP tagging and analysis in mice.

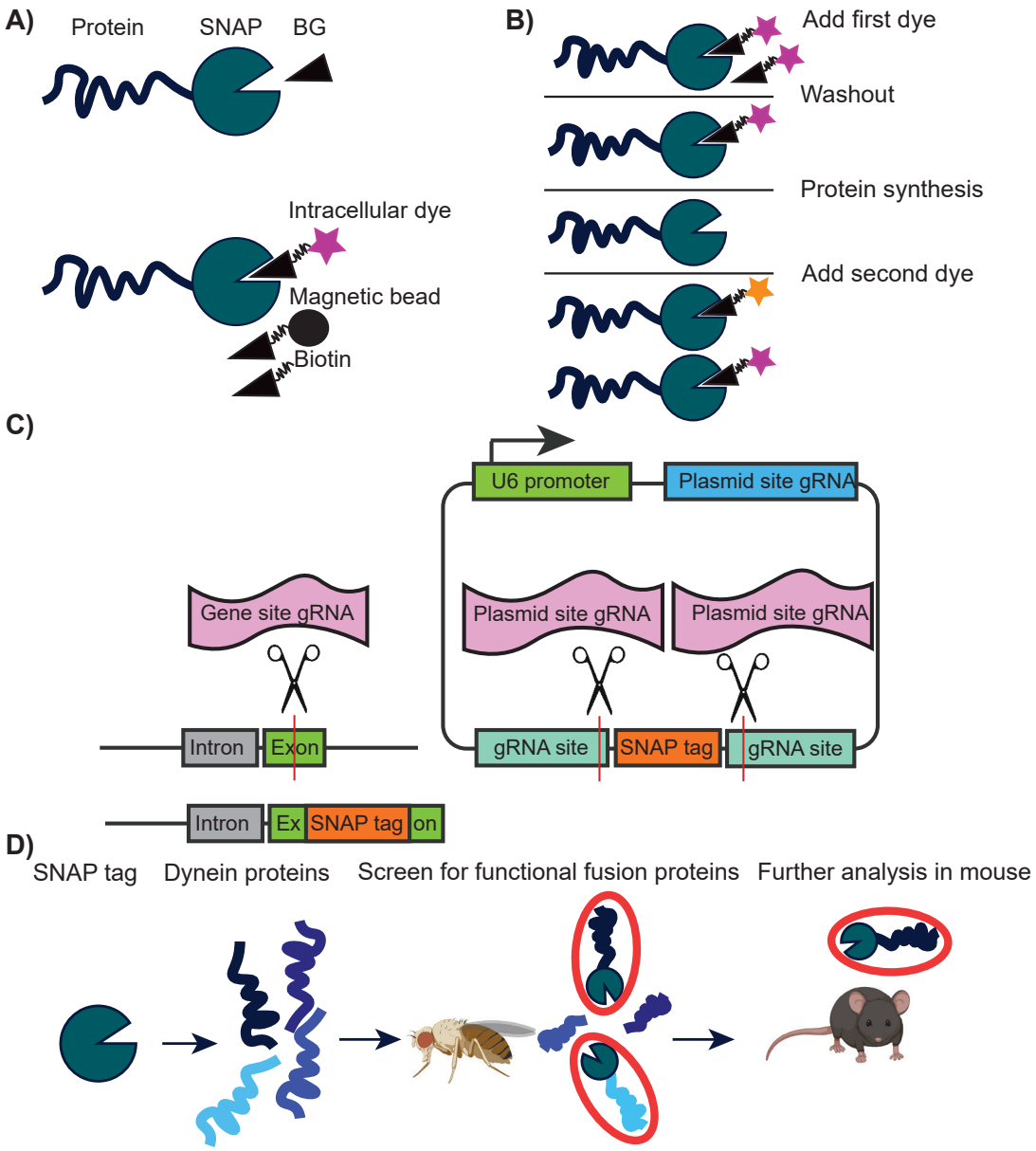

Figure 3.1 Universal SNAP tagging strategy

A) The SNAP tag (pie shape) covalently binds to benzyl-guanine (black triangle), which can itself be linked to fluorescent dyes, biotin adapters or magnetic beads.
B) The SNAP tag can be used to identify newly translated protein by adding a dye in one colour, washing it out and adding a dye in another colour. The second dye will label only those proteins produced after the 1st dye was washed out.
C) The generic tagging strategy utilises two plasmids, the one shown encodes a guide RNA which cleaves the tag from the plasmid when it is co-transfected with another plasmid expressing Cas9 (scissors) and a guide targeting the gene of interest. This results in the tag being released from the plasmid at the same time that the gene is cut, allowing the tag to integrate at the DSB with NHEJ.
D) The aim is to use this generic strategy to tag multiple dynein genes with SNAP in flies. This would serve to build up a library of tagged genes in Drosophila and also to screen for functional SNAP-dynein fusion proteins, which would indicate which orthologues to tag for further analysis in mice.

3.3 Testing the feasibility of creating a library of SNAP-tagged axonemal dyneins in *Drosophila*

The SNAP tag was cloned into the generic tagging vector with a flexible N-terminal linker and used to tag *Pericentriolar Material 1* (*PCM1*) in Flp-In T-REx HEK 293 cells. This was to test the SNAP tag with equipment and reagents previously validated in the lab and to check that the generic tagging strategy would work for the purposes of endogenous insertion of SNAP. *PCM1* is the core structural component of centriolar satellites, protein rich particles that surround the centrioles (Kubo et al. 1999). It was chosen as the test case because it was already known that *PCM1* was able to tolerate a SNAP tag in mice and the cell line would be useful for experiments being conducted by others. HEK 293 cells were chosen because they were readily available and easy to transfect with plasmid DNA.

Guide RNA sequences were designed that targeted exons 2, 3, 38 and 39 and these were then cloned into an *S. p.* Cas9 expressing vector, pX330. The cells were transfected with the guide plasmids and the SNAP tag in the generic tagging vector in either a +1 frame or a +2 frame depending on where the predicted cut site was. After transfection the cells were screened for insertion of the SNAP tag using PCR, **Figure 3.2 A)**. The cells from the exon 2 transfection did not yield enough DNA for PCR, however of the 3 tested populations it appeared that the SNAP tag had been inserted at a detectable level into *PCM1* in exons 3 and 39, with exon 3 having the stronger band. Therefore this population was then diluted and seeded into wells such that each well contained 1-3 cells. This was to increase the number of SNAP positive cells to make imaging easier to optimise. These colonies of SNAP-*PCM1* cells were screened with PCR to find the clonal population with the correct insertion. A quick lysis method was used to extract DNA from the colonies, which were then screened by PCRs (data not shown). The colonies which returned positive bands for the SNAP insertion were then grown on and DNA was extracted from them for further characterisation. The cells were screened by PCRs that amplified from SNAP upstream, from SNAP downstream and across the insertion site, shown in **Figure 3.2 B)**. Doing this showed that only one colony seemed to have PCR products of the correct size, colony 52, although other bands were observed. This is likely due to concatemers of SNAP being inserted at other alleles in the same cell or in other cells, similarly smaller bands could be the result of deletions

These cells were then further characterised by immunoprecipitation with the anti-SNAP antibody and blotting with anti-PCM1, **Figure 3.3 A)**. The band for PCM1, around 260 kDa, in the sample immune-precipitated with anti-SNAP from colony 52 cells was stronger than that in the wild type immunoprecipitation, indicating that endogenous SNAP-PCM1 is expressed in these cells. SNAP dye was also added to the lysate before incubating with anti-SNAP, however no fluorescent band could be seen (data not shown), this suggests that either the lysis denatured the protein or that the fluorescence was too weak to be detected, see **Section 4.5** for discussion.

The cells were also imaged using the cell permeable SNAP dye SNAP-cell SiR-647, **Figure 3.3 B)**. This initially did not work in the pool of cells, however with optimisation of the protocol clusters of PCM1 could be observed in the cytoplasm of colony 52. The staining is consistent with centriolar satellite localisation, as published for PCM1 (Kubo et al. 1999). This demonstrates that the generic tagging system is suitable for the integration of SNAP into endogenous loci and that SNAP can be used for live cell imaging.

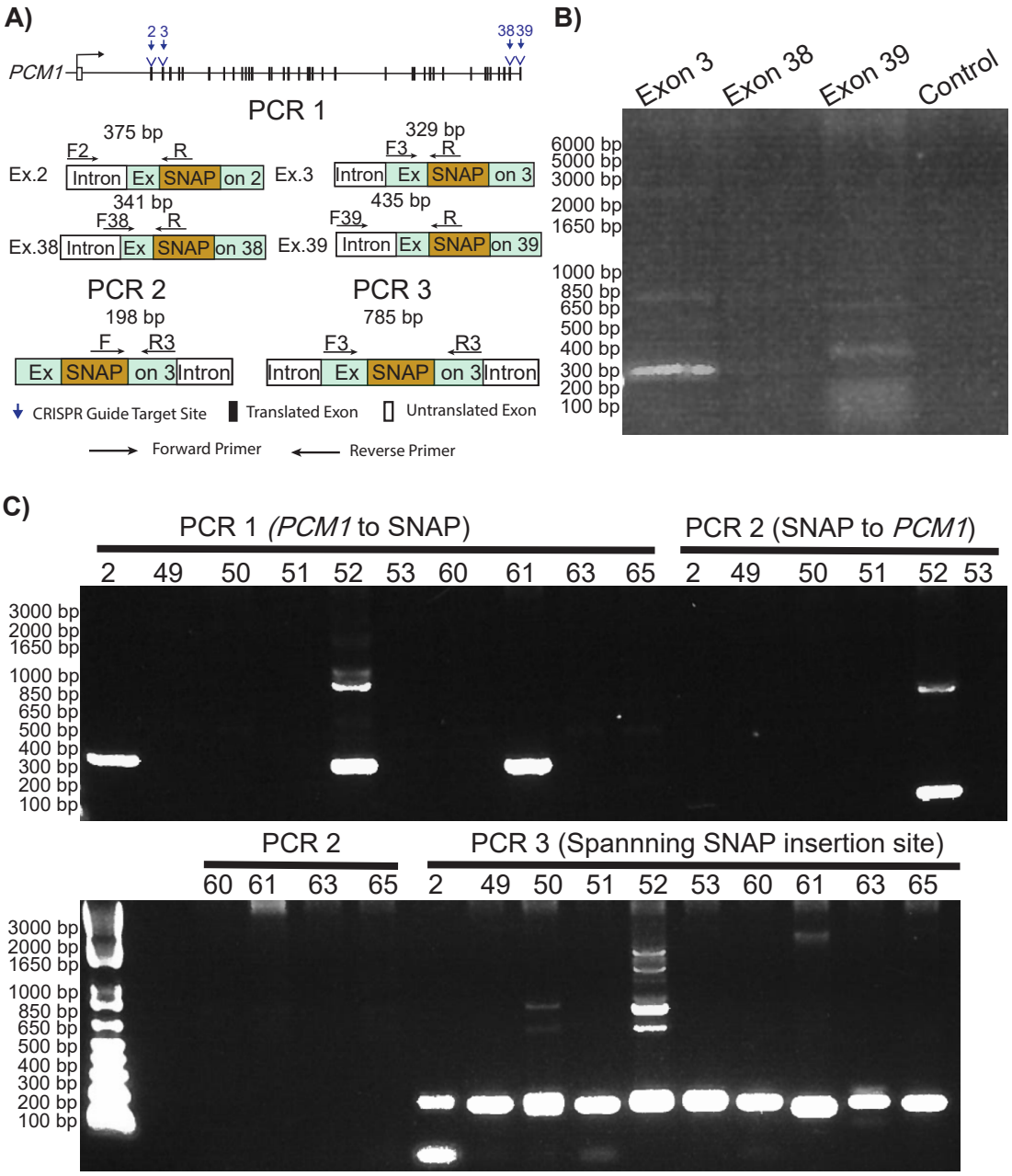

Figure 3.2 PCR screening for SNAP insertion into *PCM1*

A) Schematic showing the exon structure of *PCM1* and where the guide RNA targets are. The PCRs used to screen for SNAP insertion are also shown, PCR 1 amplifies from *PCM1* into the 5' end of SNAP, PCR 2 amplifies from the 3' end of SNAP to *PCM1* and PCR 3 spans the insertion site, the same SNAP primer (R) was used for PCRs of all three exons, expected product sizes with insertion are indicated. **B)** The gel shows PCRs of DNA from transfected HEK293 cells, PCR 1 was used for all exons the expected sizes are 329, 341 and 435 bp for exons 3, 38 and 39, respectively. There was no DNA from the exon 2 targeted transfection. **C)** These gels show PCRs 1, 2 and 3 of exon 3 from single, double and triple cell colonies, the numbers denote the colony. SNAP to *PCM1* PCR 2 gives an expected band size of 198 bp. Spanning PCR 3 gives an expected band size of 785 bp with SNAP, 200 bp without SNAP. Colony 52 appears to have SNAP inserted in the correct place.

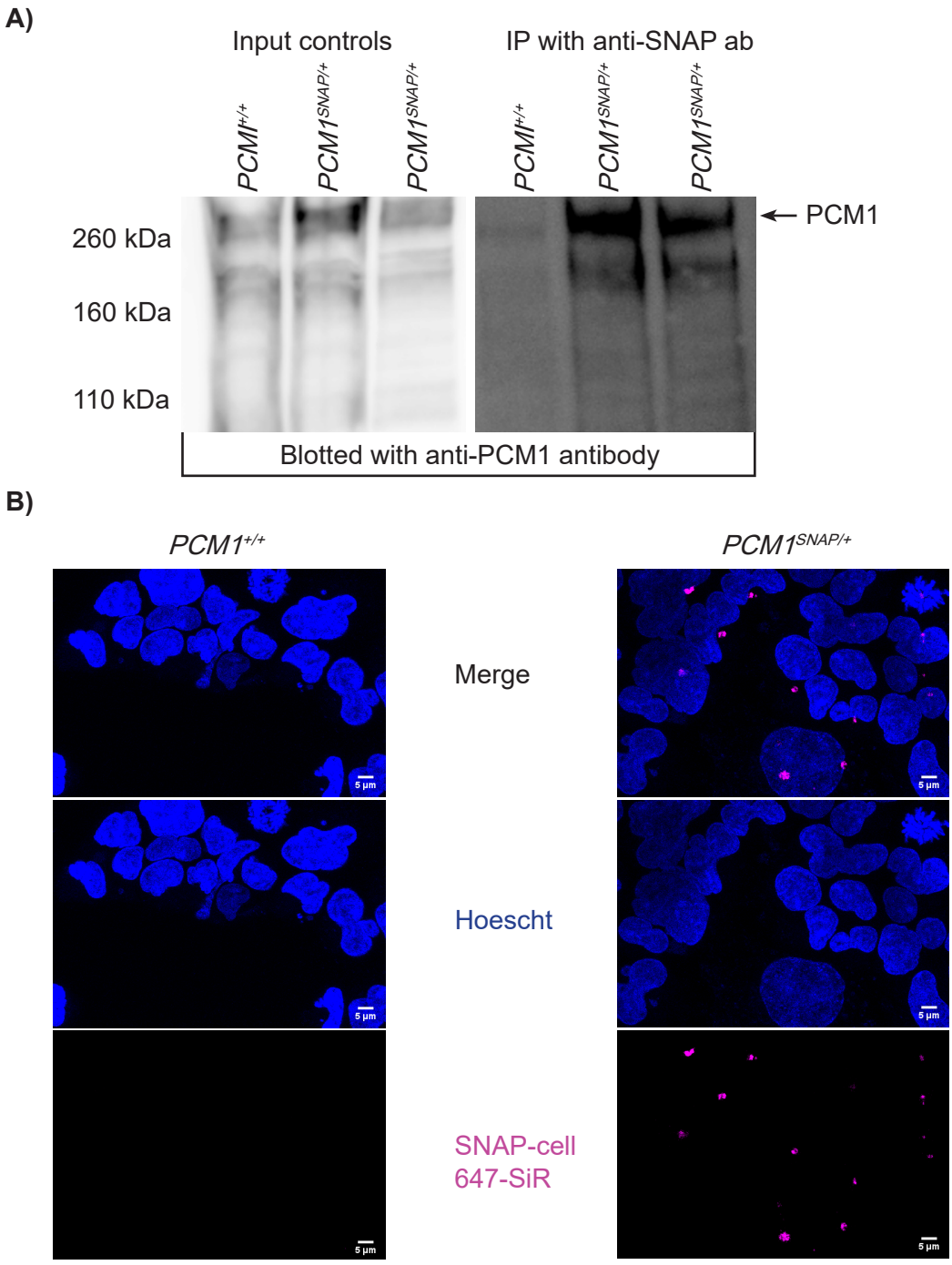

Figure 3.3 Integrating the SNAP tag into *PCM1*

A) Lysed HEK 293 cells from SNAP PCR positive and negative colonies with either SNAP-cell 647-SiR added or not were pulled down with the anti-SNAP antibody and were blotted with anti-PCM1 antibody on western blots.The band corresponding to PCM1 is indicated by the black arrow.
B) HEK 293 cells were incubated with SNAP-Cell 647-SiR (magenta) and Hoescht (blue) for imaging. The images show the accumulation of tagged PCM1 in large puncta near the nucleus, which is consistent with centriolar satellite localisation. Not every cell expresses SNAP-PCM1, reflecting the multi-clonal nature of these cells.

After establishing the effectiveness of the generic tagging vector and the cell permeable SNAP dyes in mammalian cells, further proof of principle studies were conducted in *Drosophila*. *CG6971*, an orthologue of the human Dynein Axonemal Light Intermediate chain 1 (*DNALI1*), was targeted for SNAP tagging at the C terminus because it was already known to be functional with a C terminal mVenus fusion (Diggle et al. 2014). Additionally an endogenously expressed SNAP *CG6971* or *Dnali1* in mouse would be a useful tool for the study of AD regulation and assembly. Two guides were designed to target the C terminus of *CG6971*, to optimise the chance of a successfully tagged gene. The guides were tested against PCRs from the C terminus of *CG6971* by *in vitro* digestion, this showed that both guides were very active in their ability to cut at the required sites with guide C2 being slightly more efficient, shown in **Figure 3.4 A)**. Injections into fly embryos were attempted with guides expressed from plasmids and with RNA and Cas9 protein mixed with the SNAP tagging plasmids. Embryos were allowed to gestate for 24 hours and then were screened for insertion of SNAP by PCR, **Figure 3.4 B)**, injections and screening were conducted in collaboration with Dr. Petra zur Lage (Dr. A. Jarman lab University of Edinburgh). Despite PCRs spanning the tagging site producing a product of the correct size for SNAP insertion subsequent PCRs for the tag and sequencing showed the tagging to be unsuccessful, suggesting that the large product produced could have been the result of aberrant amplification. No editing could be detected when a selection of injected embryos were screened using PCR to amplify over the edited region and were digested with the Surveyor nuclease to detect mismatched bases introduced by Cas9 editing, **Figure 3.4 C)**. This suggests the CRISPR/Cas9 activity at the targeted region was inefficient *in vivo* and this is probably the reason no SNAP was detected in the screening PCRs.

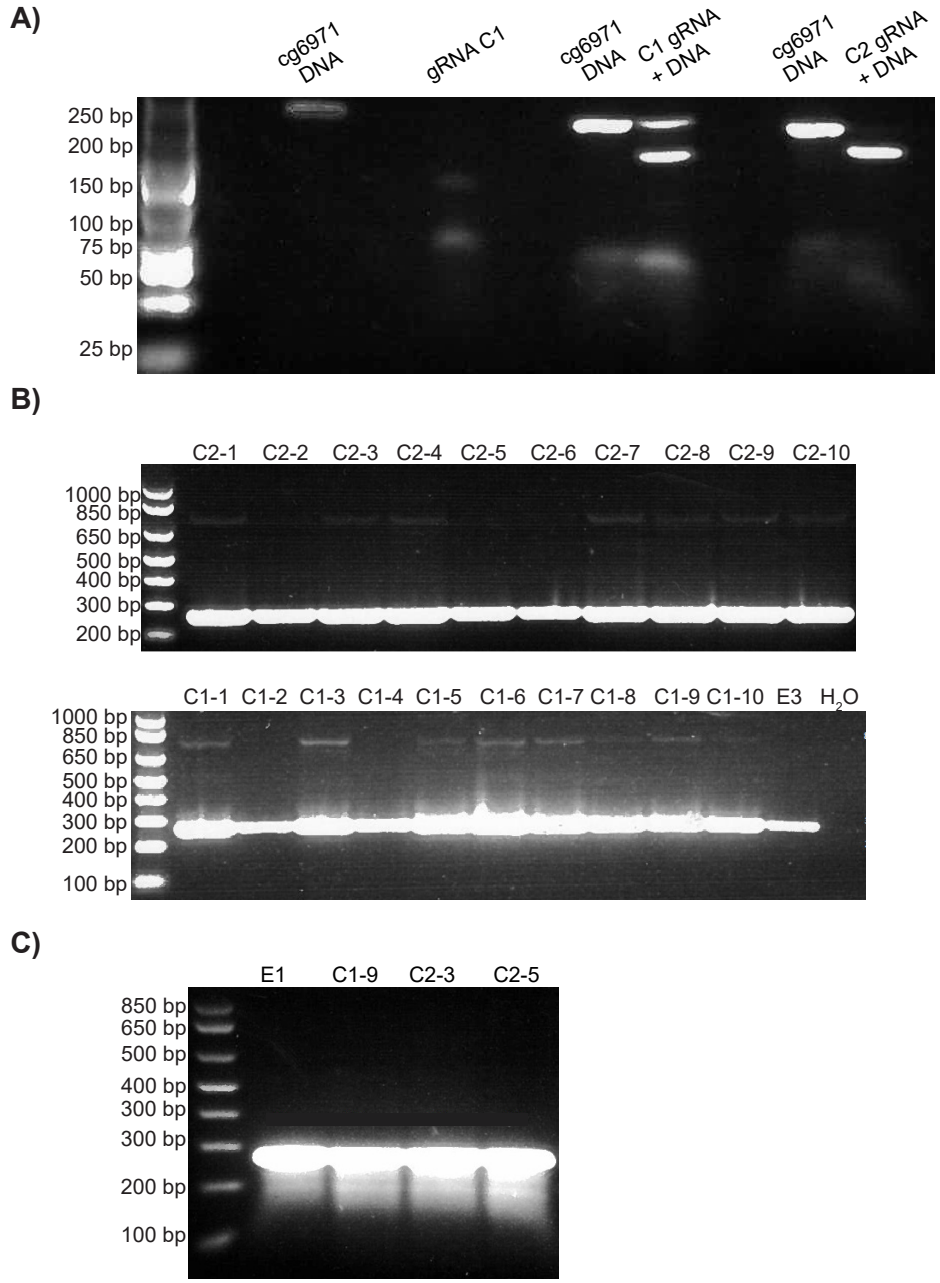

Figure 3.4 Testing guides for endogenous tagging in the fly

A) The gel shows that digestion of a PCR product from the C terminus of the CG6971 gene is possible with either guide C1 or C2, however C2 would appear to be more efficient. The expected sizes of the digest are 224 bp and 42 bp for guide C1 and 206 bp and 60 bp for guide C2. The control lanes contain either the PCR DNA with no guide or the guides without the DNA.
B) DNA extracted from injected embryos was used for PCR to amplify over the insertion site, all embryos injected with guide C1 are labelled with C1 and those injected with C2 are labelled with C2. E3 is an uninjected embryo control and H_2O had water added as a template as a negative control. The expected band sizes are 266 bp without the SNAP insertion and 854 bp with.
C) Surveyor digest of 3 fly embryos either injected with guide C1 (C1-9) or guide C2 (C2-3 and C2-5) produced results identical to the uninjected control E1.

3.4 Discussion

By creating an extensive library of tagged AD proteins it was hoped that the fundamental biology of their assembly and regulation could be teased apart in the fly model and that successful tagging candidates would be prioritised for more detailed analysis in mice. However, despite successfully demonstrating that the strategy would work well within a human cell line it appears to be incompatible or at least much more difficult to implement in the intended *Drosophila* model. There are many reasons why a CRISPR/Cas9 based tagging strategy designed for immortalised human cell lines may not work in another organism.

First and most fundamentally the two species are separated by 782.7 million years of evolution, when their most recent common ancestor existed, and humans have homologues to only 14.9% of *Drosophila* genes (Shih, Hodge, and Andrade-Navarro 2015; Hedges, Dudley, and Kumar 2006). These differences likely contributed to the failure of SNAP tagging in the targeted genes, potentially due to the promoters used being sub-optimal for expression in flies. The guide RNAs used were expressed under the control of the human *U6* promoter. The *U6* promoter is responsible for controlling the expression of Small Nuclear RNA *U6*, an important structural component of the *U6* small nuclear ribonucleoprotein splicing complex which is conserved amongst most eukaryotes (Brow and Guthrie 1988). There is evidence of expression of small inhibitory RNA from human *U6* and *Drosophila U6* at equal levels in *Trichoplusia ni* insect cells (Kim et al. 2012), suggesting that there might be enough conservation between the two promoters to allow for expression in the distantly related *D. melanogaster*. Despite this, there is no published record for the use of the human *U6* promoter in *Drosophila*, with most studies preferring to use one of the three *Drosophila* encoded *U6* promoters. Even within these promoters there appears to be wide variation in the levels of guide RNA expression (Port et al. 2014). Therefore the guide RNA is unlikely to be expressed at as high a level with human *U6* promoter as if it were under the control of one of the *Drosophila U6* promoters. The levels of guide RNA expression and Cas9 editing could be enhanced by using a system which has been optimised for use in flies.

Another way to avoid sub-optimal expression of guides and Cas9 nuclease is to add the editing complexes as ribonucleoproteins, obviating the need for promoters. This was attempted with C2 guide RNA and *tia1l* guide RNA for SNAP tagging, however again no tag insertion was detected (data not available). This could be

due to cleavage of the tagging plasmid before injection into the embryo resulting in linearised DNA being injected with the editing complexes targeted to the gene. Linear DNA was shown to be unable to integrate in the original publication of the generic tagging system (Lackner et al. 2015).

It is also a possibility that the DNA repair mechanisms in *Drosophila* do not allow for the incorporation of exogenous DNA by NHEJ, potentially another consequence of divergence between humans and flies. However, the lack of editing observed with the Surveyor nuclease assay points towards poor expression of the editing complexes as the cause of the failure to tag *CG6971*. To improve this a *Drosophila* line which constitutively expresses Cas9 could be used as well as the endogenous U6:3 promoter for guide expression, both of which have been shown to boost editing to up to 100% (Port et al. 2014). The addition of an easily identifiable selection marker, such as the *mini-white* gene (Roseman, Pirrotta, and Geyer 1993), would also vastly decrease the time taken to screen for the rare insertion of SNAP. Given these technical hurdles it was decided that the initial tagging of AD genes in flies would be bypassed and that instead the mouse genes would be targeted directly.

4 Generation and validation of a novel *SNAP-Dnah5* mouse line to study of mammalian axonemal dynein regulation.

4.1 Introduction

4.1.1 Axonemal dynein heavy chains: subtle variations between giants.

Axonemal dyneins (ADs) are large and molecularly complex motors up to 2 megadaltons in size, with a variety of subunits that can be incorporated. The largest of these subunits are the heavy chains, which contain six AAA ATPase domains and in humans are as long as 4624 residues, as introduced in **Section 1.2.1.3**. There are seventeen classes of dynein heavy chain proteins across all phyla and ten in humans; despite this diversity they have high structural conservation (Kollmar 2016). Yet differences exist in which cell types as well as in what part of the axoneme the various AD heavy chains can be found, suggesting that each heavy chain has a distinct function. For example, it has been shown that the β Outer Arm Dynein (OAD) heavy chains DNAH11 and DNAH9 have distinct proximal and distal, respectively, localisations along the motile axonemes of multi-ciliated respiratory cells, and cannot functionally substitute for one another as shown in dyskinetic cilia from patients with pathogenic mutations in either gene (Dougherty et al. 2016; Loges et al. 2018; Fassad, Shoemark, Legendre, et al. 2018). In contrast, DNAH5, their partner heavy chain in the ODA, is localised along the entire axoneme (Oltean et al. 2018; Dougherty et al. 2016). How these molecularly defined boundaries are established is not clear and moreover may vary between cell types. For example, DNAH11 is expressed along the full length of the axoneme of embryonic node monocilia (McGrath et al. 2003). Clear tissue specific paralogues also exist; mammalian DNAH9 and DNAH11 are not expressed in sperm (Mali et al. 2018) whilst DNAH17 is, causing male infertility when mutated (Whitfield et al 2019). Given the variety of ways in which different types of cilia move across these cell types, it is likely that these different heavy chains are responsible for altering the frequency, direction and/or the waveform of the beating cilia in mammals as they do in single celled flagellates (Brokaw and Kamiya 1987; Edwards et al. 2018). This suggests that the cell is able to alter the movement of cilia by docking different dynein arms in a modular fashion.

4.1.2 Axonemal dynein docking.

Although this process is clearly regulated, very little is known about what determines which AD is docked where in the cilium and how this is controlled. It has been shown that ADs dock at the assembling ciliary tip in *Chlamydomonas reinhardtii* (Viswanadha et al. 2014) and in *Trypanosoma brucei* (Georgikou et al. 2017) and that in *Trypanosoma* there is very little turnover of these proteins. It has also been heavily implied that this mechanism of AD docking is highly conserved and active in mammals (Oltean et al. 2018). While most axonemal proteins dock at the growing tip Inner Dynein Arm (IDA) complexes I2 and I3 were shown to be proximally localised and to dock only in the final stage of ciliary growth in *Chlamydomonas* (Piperno and Ramanis 1991). This demonstrates that the spatial separation of different AD complexes is not restricted to mammals. *Chlamydomonas* have also been used to show that there are differences in how ODAs and IDAs dock in dikaryon rescue experiments, with ODAs seemingly docking along the entire length of the axoneme and IDAs docking from only the tip of the axoneme (Piperno, Mead, and Henderson 1996; Dai et al. 2018; Viswanadha et al. 2014). While this type of rescue experiment may not be physiologically relevant it does indicate that mature axonemes can still accommodate new ADs. It has also been shown that the ADs are replaced in the mature axonemes of *Chlamydomonas* (Dai et al. 2018) and sea urchin embryos (Stephens 1997), although not in *T. brucei* (Georgikou et al. 2017).

The study of axonemal docking lags behind in mammals, where there has been no direct observation of AD docking at the ciliary tip or any investigation into AD turnover in the mature cilium. This is mainly due to the lack of genetic tools, such as temperature sensitive mutants and inducible fluorescently tagged AD genes. This was the reasoning behind the creation of the *SNAP-Dnah5* mouse line, which would allow AD complexes to be tracked over time and space giving valuable insights into how they are regulated, in healthy and diseased cell types.

4.1.3 Cytoplasmic axonemal dynein assembly.

Individual AD subunits are assembled to form their quaternary complexes in the cytoplasm (Fok et al. 1994) and it is assumed that there are shared regulatory pathways to enable this (Desai, Dean, and Mitchell 2017). However, there is also evidence that there might be a specialised assembly pathway for some of the AD

components, especially the heavy chains. It has been shown that several dynein axonemal assembly factors are important for the stability of heavy chains in particular (Omran et al. 2008; Moore et al. 2013; Mitchison et al. 2012; Patel-King et al. 2019). The increased number of heavy chain specific co-chaperones could be due to the length and complexity of these proteins in comparison to the smaller intermediate and light chains. It has been shown that longer proteins often require more chaperones (Gong et al. 2009). They also take longer to translate making them more prone to misfolding, therefore they often require co-translational folding and assembly. It's been shown that co-translational folding and assembly is a process common to large or complex molecular assemblies (Kamenova et al. 2019). It's possible that ADs, large molecular complexes themselves, are also co-translationally assembled and this happens in assembly factories. The presence of high concentrations of chaperones and assembly factors in phase separated particles with intermediate and intermediate light chain AD proteins suggests that these factories may exist to aid in the assembly of large macromolecular complexes (Huizar et al. 2018). However, it has not been shown whether the heavy chains also localise to these so-called dynein assembly particles (DynAPs) and whether there is translational regulation of any of the AD subunits. Interestingly, the closely related cytoplasmic dynein heavy chain protein DYNC1H1 is found in moving translational factories (Pichon et al. 2016), which suggests that AD heavy chains could also undergo localised translation. The DynAPs also contain dynein assembly factors ZMYND10 and HEATR2, which have been shown to be important for the stability of heavy chain AD proteins, suggesting that the heavy chain dyneins also localise to these assembly particles (Mali et al. 2018, Huizar et al. 2018). To determine whether the heavy chains are translated at these particles requires tracking where the heavy chain AD proteins are translated and what the candidate heavy chain mRNA is interacting with.

4.2 Creation and characterisation of the *SNAP-Dnah5* mouse line.

As explained in **Chapter 3** the decision was taken to bypass the creation of a library of tagged ADs in *Drosophila* and to instead focus on targeting a mouse AD directly, obviating the need for a high throughput tagging method. Dynein Axonemal Heavy Chain 5 (*Dnah5*) was chosen as the target for fusion with the SNAP tag. *Dnah5* is the largest of the mammalian AD heavy chains and is a class 3 (γ OAD in *Chlamydomonas*) ODA component (Kollmar 2016). It is also the most commonly

mutated gene in PCD, resulting in ODA defects and loss of ciliary motility (Hornef et al. 2006; Davis et al. 2019). It was chosen because it is widely expressed in motile ciliated tissues, aside from sperm flagella, (Olbrich et al. 2002, Mali et al. 2018) and along the entire length of the axoneme (Oltean et al. 2018; Dougherty et al. 2016), making it useful as a fluorescent reporter of rescue in development of therapeutics for PCD, including genome editing. It is also a powerful tool to study fundamental mechanisms of AD biology like turnover and proteostasis.

Guide sequences were designed to target the N-terminus of *Dnah5*, because the N-terminal tail is unstructured (Kollmar 2016) and the N terminus of the closely related mouse *Dnah11* has already been functionally tagged with GFP (McGrath et al. 2003). Three guide sequences were designed that targeted downstream of the start codon in the 1st exon of *Dnah5*, these were tested *in vitro* against a PCR amplified region of *Dnah5* containing exon 1, see **Figure 4.1 A)** and **B)**. The guide named *Dnah5* N2 was the most efficient and was used to design a repair template to insert the SNAP tag into the 1st exon of *Dnah5*. The repair template consisted of a plasmid with ~800 bp of homology up and down stream of the SNAP tag insertion site between the last two codons of exon 1, as shown in **Figure 4.1 B)**. This was injected, by Margaret Keighren (Dr. P. Mill Lab University of Edinburgh), as plasmid DNA into mouse embryos with guide *Dnah5* N2 and Cas9 nuclease protein, as diagrammed in **Figure 4.1 C)**. After three rounds of injections, 23 mice were born and screened by PCRs, which flanked the site of the SNAP insertion, two of these mice had the tag inserted. However, only one mouse, shown in the gel in **Figure 4.1 D)**, was taken forward for further experiments because the other mouse had multiple bands from the PCR, suggesting potential mosaicism (data not shown). While the mouse chosen appeared to produce a slightly larger PCR product than the plasmid control it was of the expected size for an insertion of SNAP at the locus. The smaller bands produced by some of the founders could be due to homozygous deletions in *Dnah5*, but as multiple mutant alleles in *Dnah5* in mice have already been reported to result in a PCD-like phenotype (Tan et al. 2007), these animals were not kept for breeding.

The founder mouse, 1394, was sequenced outside the homology arms and analysis focused on the SNAP tag insertion site. Unexpectedly, the animal had altered sequence around both N- and C-termini junctions of the tag with exon 1, as shown in **Figure 4.2 A)** and **B)**. The changes in sequence resulted in the deletion

of one and the substitution of four amino acids from either end of the SNAP tag exon 1 fusion. While this was not expected or ideal, the alterations were not predicted to be detrimental to the activity or stability of the tagged protein, as determined by their positions in the protein (Mollwitz et al. 2012). Meanwhile, the founder had already been bred with wild type females to produce heterozygous offspring. To show that the SNAP-DNAH5 protein was stably expressed tracheal lysates were isolated from these offspring and treated with SNAP-cell SiR-647 fluorescent dye before being immunoprecipitated with an anti-SNAP antibody. The lysates were then run in a denaturing polyacrylamide gel and imaged for fluorescence, however no fluorescence could be detected. The gels were then blotted with anti-SNAP antibody, samples corresponding to the mice with the SNAP tag insertion showed a correctly sized high molecular weight band whereas the wild type littermates did not. The blots were also analysed using anti-DNAH5 (gift from Dr. H. Takeda, University of Tokyo) antibody and an enrichment in the *SNAP-Dnah5* mouse IP was seen but not in the wild type mice, **Figure 4.2 C)**. Given the high molecular weights of both native DNAH5 (529 kDa) and SNAP-DNAH5 (547 kDa), it was not possible to discern size differences in heterozygous samples. Together, this showed that the SNAP-DNAH5 protein is stably expressed in the tracheas of the tagged mice.

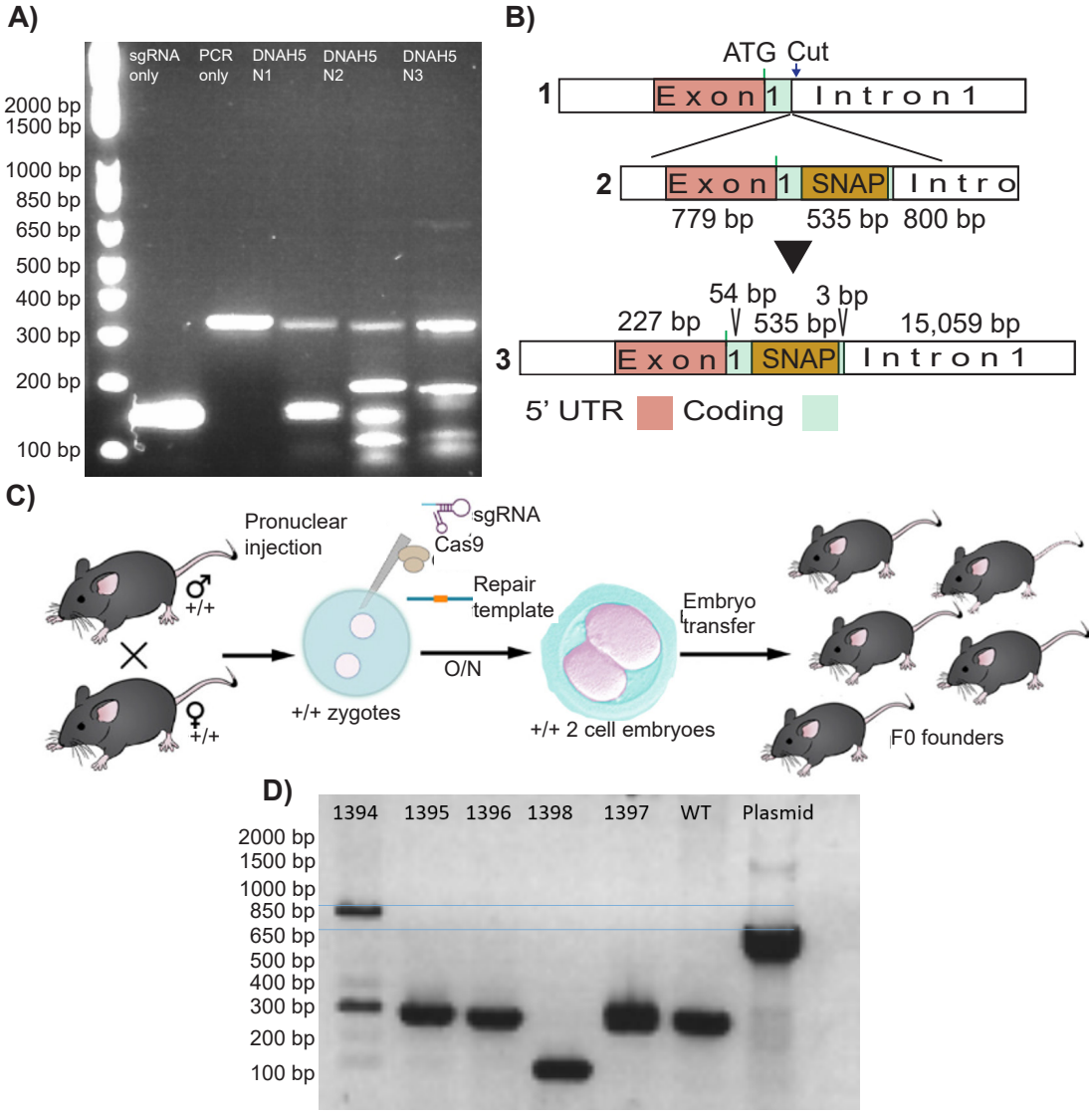

Figure 4.1 Mouse injection and founder PCRs

A) *In vitro* digest of a PCR product from the 1st exon of mouse *Dnah5* shows that while all three guide RNAs were capable of cutting N1 and N2 seemed to be the more efficient. Therefore guide N2 was selected as the *Dnah5* targeting guide to be used for tagging.
B) Cartoon 1 shows the cut site for guide N2 at the start of intron 1, underneath is the repair template (2) with the length of the homology arms. The position of SNAP in exon 1 of *Dnah5* is shown (3) with the lengths of the exon and intron included.
C) The schematic shows how the SNAP-DNAH5 mouse was generated by injection of a repair plasmid (2). This was injected into mouse zygotes with Cas9 nuclease and *Dnah5* N2 RNA in a complex. The zygotes were implanted into mice and the resultant offspring were the F0 founder generation. This was done by M. Keighren (P. Mill lab UoE).
D) These F0 mice were genotyped using a PCR that spanned the cut site and produced a band of 842 bp if the tag was present and a band of 249 bp if it was absent. The plasmid lane is the positive control, which seems to migrate lower than the expected size (blue line). The results show that founder 1394 is likely to have the SNAP tag inserted into the 1st exon while 1398 has a deletion.

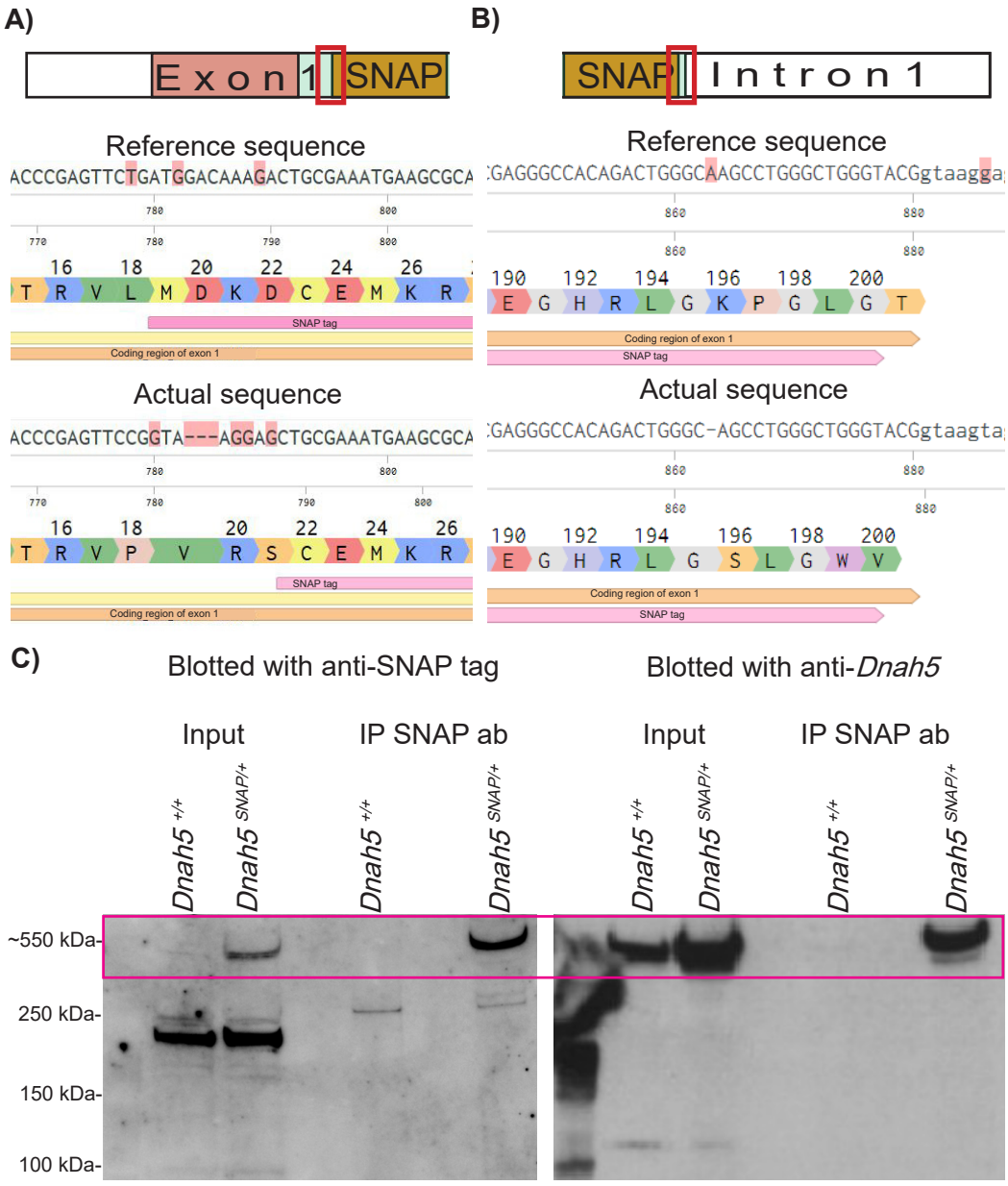

Figure 4.2 Sequence alignment and immunoblotting of *Dnah5* $^{Snap/+}$ mice.

A) Sequencing of the 5' junction of the SNAP tag inserted into *Dnah5*, red boxed region of the diagram above, showed that there was a deletion of 1 amino acid and changes to 4 others. The alignment shows the correct sequence at the top and the actual sequence underneath, the pink bar is the SNAP tag coding region and the orange bar is the coding region of exon 1. Altered bases are highlighted in red.
B) Sequencing of the 3' end of the SNAP tag junction, red boxed area, showed that there was a loss of 1 amino acid and 5 amino acid changes.
C) Using the anti-SNAP tag antibody for immunoprecipitation from *Dnah5* $^{SNAP/+}$ tracheal lysates shows that they have a protein (boxed area) recognised by the anti-SNAP tag antibody which the *Dnah5* $^{+/+}$ do not. The band corresponds to one created by blotting the immunoblot with anti-DNAH5 antibody. This band is not present in the IP lane of *Dnah5* $^{+/+}$ mice. Input is 10% of the total lysate used for pulldown.

After establishing that the *SNAP-Dnah5* mice expressed SNAP tagged DNAH5 in the correct organ they were bred to homozygosity to test the functionality of SNAP-DNAH5. The primary reason for using the SNAP tag is for imaging DNAH5 dynamics, as such it was important to verify that the SNAP tag bound to the fluorescent dyes and that the fluorescence localised to the axoneme of motile ciliated cells. To test whether this was the case, mouse tracheal epithelial cells (mTECs) were cultured from the *SNAP-Dnah5* mice. These were then incubated with SNAP-cell SiR-647 cell permeable dye before being fixed and stained with antibodies for DNAI2 and the SNAP tag. The images shown in **Figure 4.3 A)** demonstrate that the SNAP tag antibody co-localises with the SNAP dye and with DNAI2 but only in the *SNAP-Dnah5* cells. This demonstrates that the tag is functional and that the fusion protein is localising to the motile cilia in the tracheal epithelia of these mice. In order to further prove that the SNAP tagged DNAH5 is fully functional and able to generate full movement in the cilia, the homozygously tagged DNAH5 and control mTECs were imaged with high speed video microscopy. Selected stills from some of these videos are shown in **Figure 4.3 B)**, these videos were then used to calculate the frequency of ciliary beat in these cells. By taking ten separate areas of motile ciliated cells and counting the number of beats per second in each it was established that the mean beat frequency was not statistically significant between the mTECs from the *SNAP-Dnah5* mice and wild type mice, as shown in the graph in **Figure 4.3 C)**. The axoneme structure of homozygous and wild type mTECs was also compared with transmission electron microscopy (TEM) of transverse sections as shown in **Figure 4.3 D)**. Analysis of multiple sections from three homozygous and three wild type transwells showed that there was no significant difference between the number of AD arms between the two genotypes, **Figure 4.3 D)**. Furthermore, mice homozygous for *SNAP-Dnah5* do not exhibit PCD-like symptoms, such as hydrocephaly, and are viable. This shows that the SNAP-DNAH5 fusion protein retains its ability to drive the functional beating of cilia in these mice.

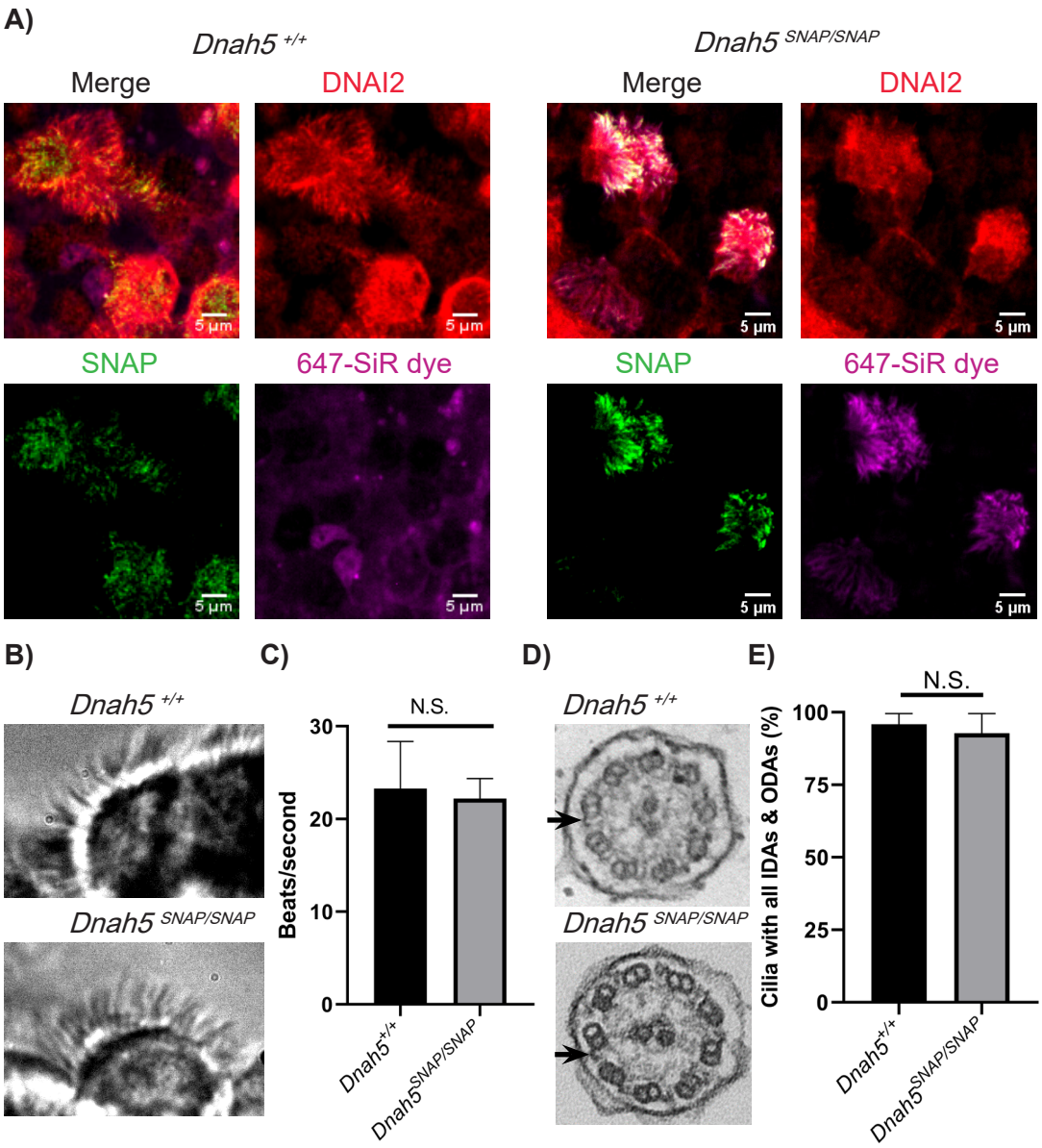

Figure 4.3 Showing SNAP-DNAH5 fusion functionality

A) The images show immunofluorescence of mTECs. The top left panel for each genotype shows a merge of channels with the anti-DNAI2 antibody (red), anti-SNAP antibody (green) and SNAP-Cell 647-SiR (magenta).
B) Still images from highspeed brightfield video microscopy of cilia beat in mTECs from SNAP tagged and wildtype mice (obtained by A. Shoemark UoD).
C) The graph shows that there was no significant diference in the freqeuncy of ciliary beat between the two genotypes. Unpaired t test (two-tailed) P = 0.5883, error bars = SD, n = 10 images.
D) TEM of transverse sections through mTEC axonemes, the arrowheads indicate the ODAs (made and analysed by Dr. A. Shoemark and Dr. F. Daudvohra. R.B.).
E) The graph shows that there was no significant difference in the percentage of cilia that retained the normal number of IDAs and ODAs between the two genotypes. Unpaired t test (two-tailed) P = 0.5, error bars = SD, n = 3 transwells.

4.3 Uncovering the dynamics of mammalian axonemal dynein docking using the *SNAP-Dnah5* mouse.

After confirming the non-disruptive and functional tagging of the *SNAP-Dnah5* mouse line, it was used for pulse-chase imaging to investigate the turnover and docking of ADs. Although SNAP has been used to look at protein dynamics and turnover for many years (Torné et al. 2018; Jansen et al. 2007; Stenoien et al. 2007), it does not appear that SNAP pulse-chase imaging has been attempted with an endogenous tag in primary cells. The main advantage of studying endogenously tagged protein dynamics as opposed to overexpression is that the studied protein is more likely to have the same rates of turnover and trafficking when expressed at the physiologically relevant level. It's also necessary to have a tag integrated into the genome when the protein is expressed in a restricted subset of cells that cannot easily be transfected, as is the case for *Dnah5*. Therefore, the *SNAP-Dnah5* mouse is ideally suited to study AD turnover and protein dynamics in mammals. The pulse chase experiment was designed to try and observe whether there was turnover of the dynein protein complexes in the motile axoneme, using the mTEC system which had previously been optimised for imaging with the cell permeable SNAP dyes, **Figure 4.3 A)**. The mTECs were incubated first with SNAP-cell SiR-647 for 2 days, the extended incubation time and reduced concentration was found to be beneficial for reducing background, then the dye was washed off and replaced with SNAP-Cell TMR-Star 7 days later. The long chase period is because of the expectation that there would be almost no turnover of the AD complexes (Georgikou et al. 2017), therefore to maximise the chances of recording turnover a period of a week was left before adding the second dye, this procedure is diagrammed in **Figure 4.4 A)**. The potential outcomes for where the newly translated AD might dock are also shown in **Figure 4.4 A)**, it's likely that turnover would happen all along the axoneme in mature cilia and that in the developing cilium ADs would dock towards the tip.

A)

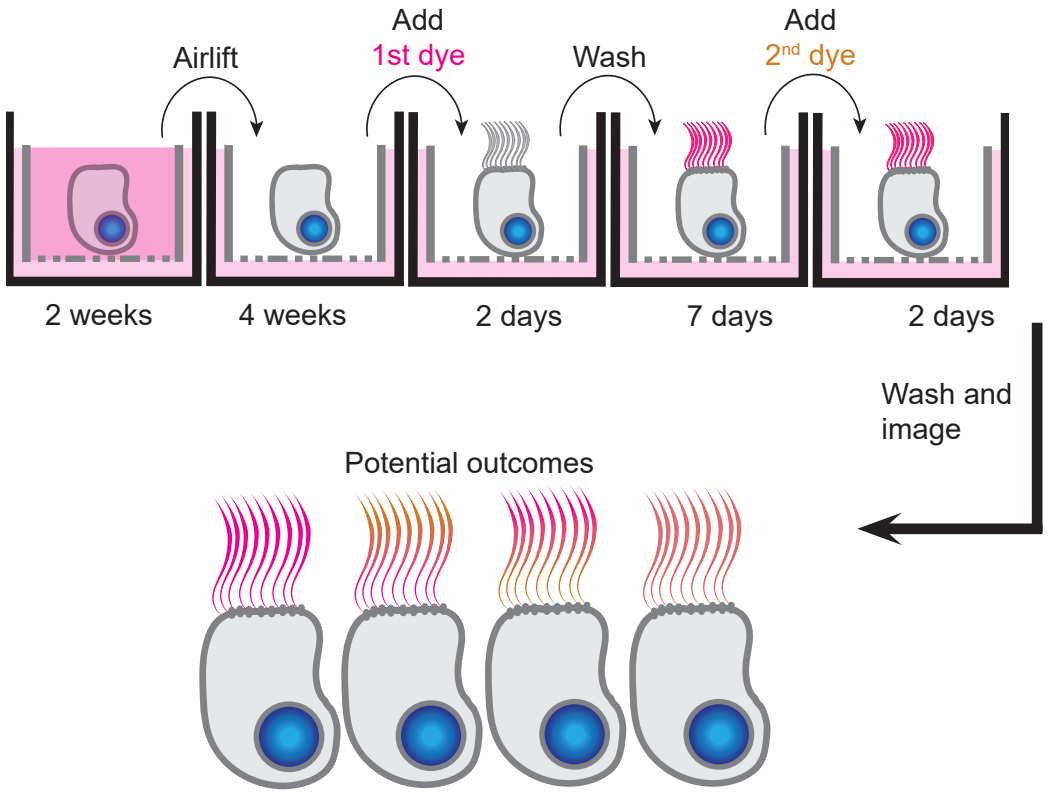

B)

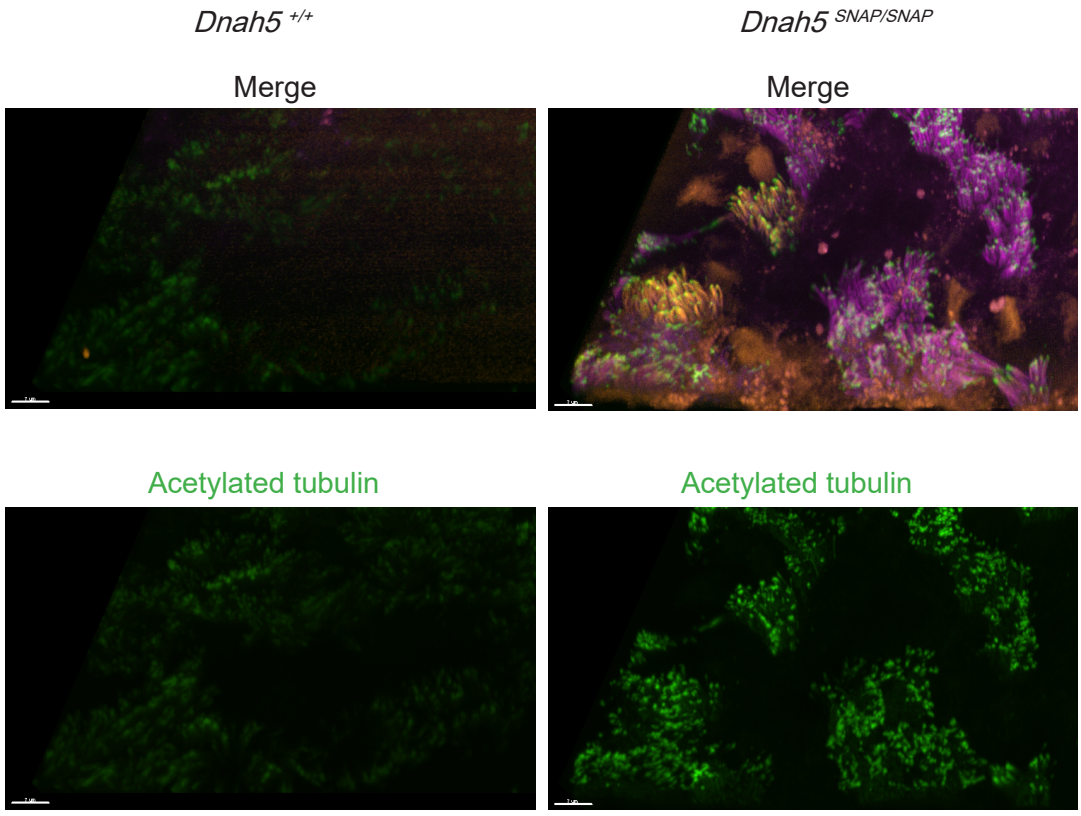

Continued on next page

B)

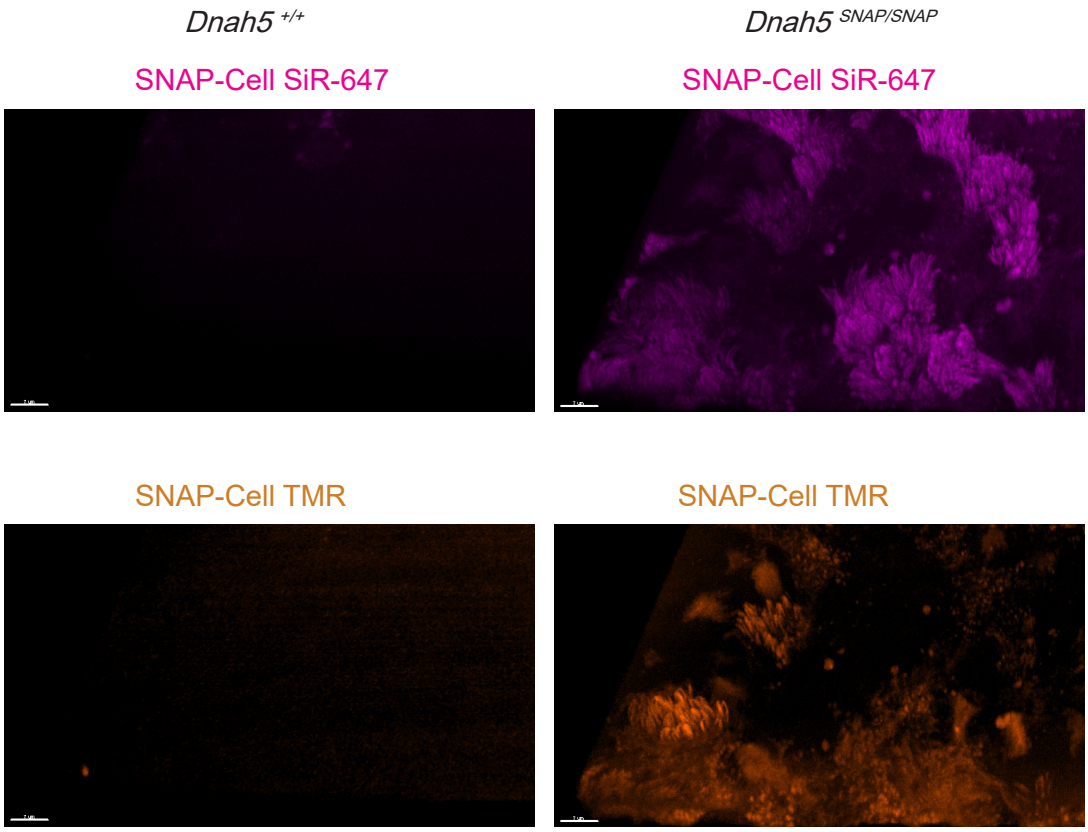

Figure 4.4 Tracking DNAH5 over time using SNAP dye pulse imaging

A) The diagram shows the protocol undertaken to investigate protein turnover in ciliated mTECs, these cells are proliferated before being airlifted to differentiate them. The first dye added is SNAP-Cell SiR-647 (magenta) 28 days after airlift and is left for 2 days before being washed out and is replaced 7 days later with SNAP-Cell TMR (orange) which is washed off after 2 days. The potential outcomes for where the newly translated protein is localised are shown, described from left to right these are; no turnover (no incorporation of new dye), newly translated protein is incorporated at the tip of the cilia, newly translated protein is incorporated at the base of the axoneme newly translated protein is incorporated all along the axoneme.
B) Images of mTECs 28 days post airlift, acetylated tubulin stains the axoneme (green), the 1st dye is SNAP-cell SiR-647 (magenta), 2nd dye is SNAP-cell TMR (orange). mTECs from *Dnah5* $^{+/+}$ mice shown on the left have no SNAP dye staining whereas *Dnah5* $^{SNAP/SNAP}$ cells are stained mostly with the 1st dye and have variable incorporation of the 2nd dye. Scale bars are 7 μm.

The mTECs were 28 days post airlift, a point at which all cells should be fully differentiated (You, Richer, Huang 2002; Kubo et al. 2008; Vladar and Brody 2013), however it is possible due to culture conditions that the mTECs were not all entirely differentiated. This may explain why the images of the pulse-chase mTECs show that, while the majority of cilia have very little TMR staining a few cells seem to have cilia predominately stained with TMR, Figure 4.4 B). This suggests the cells brightly stained with TMR may have still been assembling their mature cilia when the first dye was washed out resulting in a small amount of SiR SNAP incorporation in the DNAH5 present. However, DNAH5 synthesised after SiR SNAP was washed out would be stained with TMR as shown in Figure 4.4 B). As suggested by previous studies (Oltean et al. 2018), the newly synthesised ADs appear to dock towards the tip of the cilia in mouse tracheal epithelial cells. It also suggests that the time taken for a mature cilia to form is longer than expected, as it can be seen that the cilia with the TMR stained DNAH5 appear to be shorter than those of the neighbouring cell with DNAH5 stained only with the first dye, SiR-647, suggesting it is still not fully matured even at the end point of the experiment, as shown in Figure 4.5 A).

Further examination of these images shows that DNAH5 stained with the first dye is localised at the bottom of the cilia while the top is predominately stained with the second dye, **Figure 4.5 A)**. The total length of the axoneme populated by the newly translated DNAH5 was measured for each of the cilia in two cells which had predominately TMR stained DNAH5. This was then divided by the total time taken between washing out the first dye and washing out the second dye. Doing this gives a rough approximation of the speed at which docking is occurring in the motile axoneme, which was calculated to be ~17 nm/hour, as shown in **Figure 4.5 B)**. This is considerably faster than the rate calculated from previous experiments in *Chlamydomonas* (Viswanadha et al. 2014) which put the rate of docking at approximately 5.4 nm/hour. However, this is a very preliminary result and the measurement was taken over a long time period. The most effective way to measure the rate of AD docking would be to take multiple measurements with shorter time points and different mTEC cultures.

A)

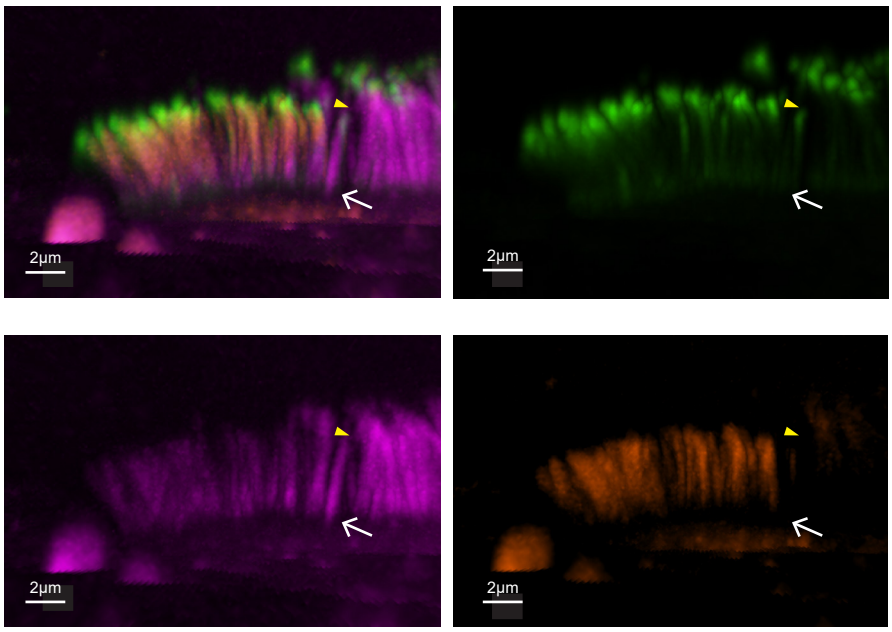

B)

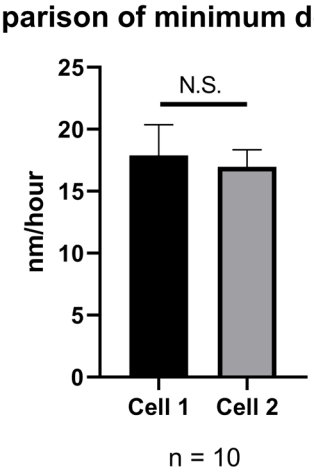

Figure 4.5 Pulse chase imaging showing ODA docking towards the ciliary tip

A) Oblique slices of mTECs stained with acetylated tubulin (green), SNAP-cell SiR-647 (magenta) and SNAP-cell TMR (orange). Clockwise from top left; merge of all channels, acetylated tubulin, SNAP-cell SiR-647 dye, SNAP-cell TMR. The images demonstrate that in the cilia of the left hand cell, indicated by white arrow, the newly translated SNAP-cell TMR stained DNAH5 is localised at the top of the cilia while the older SNAP-cell SiR-647 stained DNAH5 is localised towards the base.This is in contrast to the neighbouring cell which has no SNAP-cell TMR stained DNAH5 and slightly longer cilia (yellow arrowheads), suggesting the cilia are more mature.
B) Measuring the length of the DNAH5 stained with SNAP-cell TMR indicates the amount of docked axonemal dynein along the axonemes of the cell. When this is divided by the total amount of time since 1st dye was washed out it indicates the minimum rate at which axonemal dyneins dock along the axoneme. This was done for 10 cilia in 2 different cells and a student's two tailed t-test indicated no significant difference P = 0.59.

In order to examine the turnover of DNAH5 in the tracheal epithelial cilia, *SNAP-Dnah5* mTECs were cultured for longer in an air-liquid interface (ALI), 42 days, before adding the first dye, SNAP-cell SiR-647. The cells were then left for up to 32 days before adding the second dye (SNAP-cell TMR star), fixing and staining with a marker of mature cilia, SENTAN (Kubo et al. 2008). The cilia in transwells 4 days post airlift were all SENTAN positive, as shown in **Figure 4.6 A)**, suggesting the cells were mature. Surprisingly, SNAP-cell SiR 647 was brightest in the transwells which had been incubated for 32 days at 37 °C with the dye. These cells demonstrated weak TMR staining of the cilia, suggesting low levels of DNAH5 turnover on the axoneme after 32 days. In contrast to the staining seen in the growing axonemes in **Figure 4.5** the TMR dye was not localised towards the ciliary tip but was distributed along the entire length, indicating DNAH5 is being replaced equally across the axoneme instead of being deposited in newly assembled areas. While some turnover was observed the chase period after the initial pulse would need to be extended for longer to determine whether there would be a complete replacement of the older SNAP SiR-647 labelled DNAH5.

A)

4 days post pulse

Dnah5 $^{+/+}$

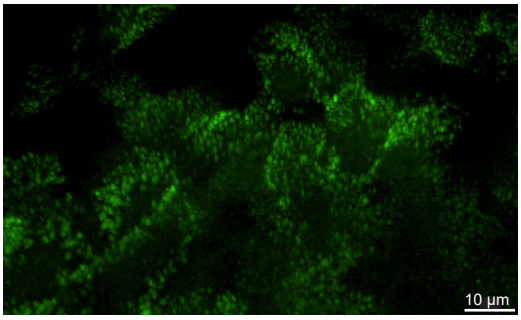

B)

32 days post pulse

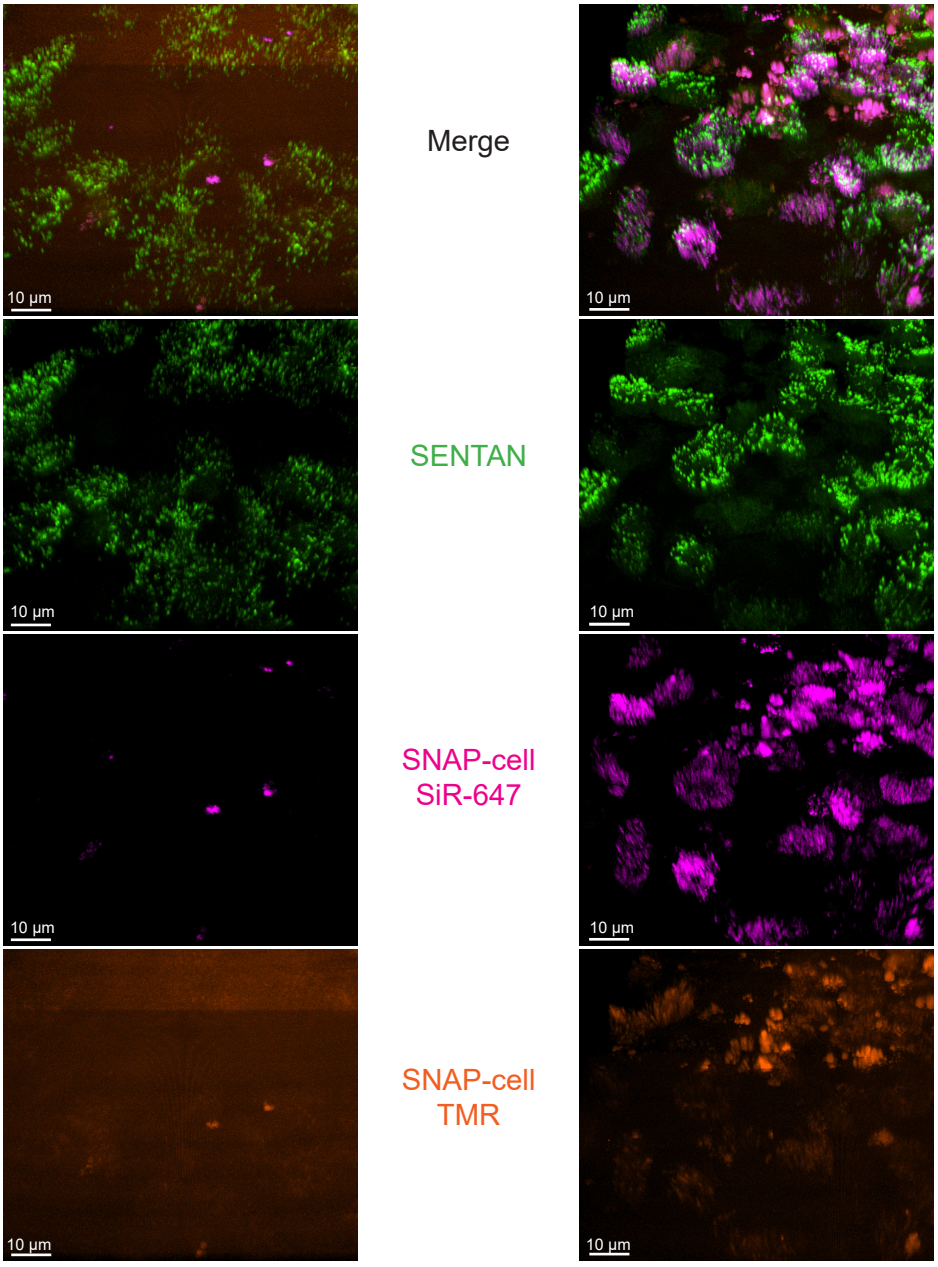

Continued on next page

C)

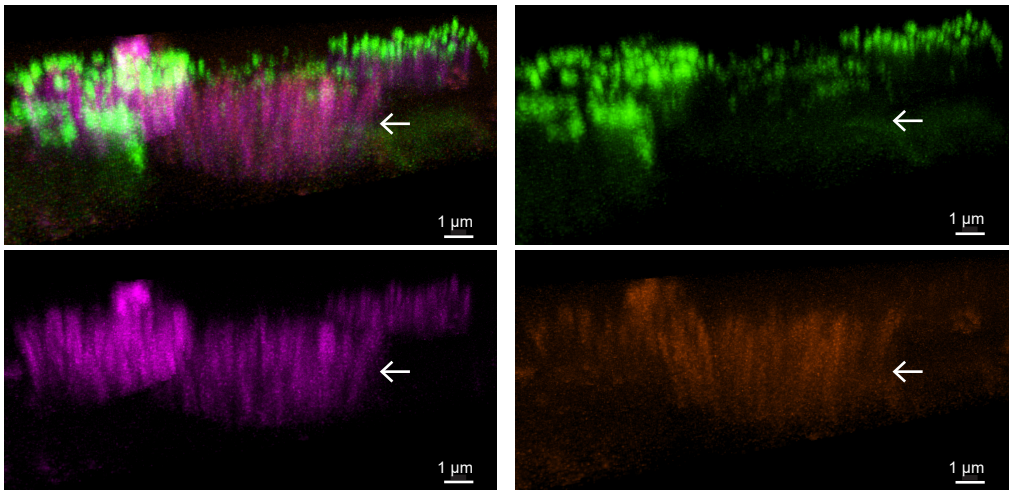

Figure 4.6 Pulse chase imaging to observe DNAH5 turnover in mature cilia

A) An image showing 42 day post airlift *Dnah5*$^{+/+}$ mTECs, 4 days after pulsing with SNAP-cell SiR 647 dye (magenta). Imaged transwells were densely packed with mature cilia, as indicated by SENTAN staining at their tips (green). Only the green channel is shown.
B) These images are of mTECs differentiated at the same time as those shown in the image above but chased 32 days after the initial dye pulse with SNAP-cell TMR dye (orange). The *Dnah5*$^{+/+}$ mTECs do not have cilia stained with the SNAP dyes whereas the *Dnah5*$^{SNAP/SNAP}$ mTECs do, the cilia are marked with SENTAN as in **A)**.
C) Oblique slices of the *Dnah5*$^{SNAP/SNAP}$ mTECs shown in **B)** demonstrate that there may be limited turnover of DNAH5 at this stage, as indicated by TMR staining in the axonemes of some cells (white arrow). However, the majority of axonemes are still brightly stained with the 1st dye suggesting very slow turnover.

4.4 Defining the SNAP-DNAH5 interactome: novel potential regulators of heavy chain axonemal dynein transcripts.

In addition to using the SNAP tag for quantitative imaging, SNAP affinity purification was used to identify novel interactors during dynein heavy chain translation, folding and cytoplasmic pre-assembly as well as trafficking. Importantly as the SNAP tag is at the N-terminus it will fold first, before DNAH5, allowing for the identification of the earliest interactors during heavy chain translation and folding.

While the main transcriptional regulators of the motile ciliary machinery are known, reviewed as part of (Reiter and Leroux 2017), it is less well known whether there is a post-transcriptional or translational regulatory pathway involved. However, due to the length of the *Dnah5* transcript, 268,300 bp, a single RNA polymerase takes approximately 45 minutes to transcribe it (Jonkers and Lis 2015). When the time taken for splicing and export is considered then it's likely that in order to make the required ~900,000 ODAs the multi motile ciliated cells would maximise the translation of the mRNA as much as possible to save time spent on transcription. Cells have adapted to overcome these kinds of transcriptional challenges by regulating transcripts, either through storage in P-bodies and stress granules (Standart and Weil 2018), or by changing how and where they are translated (Béthune et al. 2019; Fujii et al. 2017) or via altering transcript stability (Zhao, Roundtree, and He 2016; Hafezqorani et al. 2016).

Some preliminary evidence to support the post-transcriptional regulation of *Dnah5* has come from the use of the *SNAP-Dnah5* mouse to find DNAH5 interactors. mTECs were cultured from *SNAP-Dnah5* and wild type littermates before being lysed and immunoprecipitated using the anti-SNAP tag antibody. These samples were sent for mass spectrometry analysis, which was performed by Dr. Alex von Kriegsheim and Dr. Alfonso Bolado (Proteomics Core, University of Edinburgh). The results from three transwells, 28 days post airlift, of each genotype are shown in **Figure 4.7**. The volcano plot shows that DNAH5 is the most enriched protein from the pulldown in the SNAP tagged animals, suggesting that the SNAP antibody has specifically enriched for DNAH5 and its interactors. There were also known AD interactors found in the pulldown, including the assembly factor SPAG1 (Knowles, Ostrowski, et al. 2013) and the heat shock chaperone HSP90aa1 (Hartill et al. 2018; Mali et al. 2018) as well as novel interactors. Several of these

interactors are RNA binding and transcriptional or translational regulators, lending support to the hypothesis that there may be some co-localisation of the *Dnah5* transcript and its protein. These interactors were; Transcription Elongation Factor 1 A (TCEA1) which helps RNA polymerase II transcribe difficult sequences (Yang et al. 2018), Eukaryotic Translation Initiation Factor 2 Subunit 3 structural gene Y-linked (EIF2S3Y) which is a Y chromosome encoded translation initiation factor essential for spermatogenesis (Matsubara et al. 2015), TRNA Methyltransferase Subunit 11-2 (TRMTS112) which methylates rRNA and tRNA as well as proteins (Gu et al. 2012) and AlkB Homolog 5 (ALKBH5) which demethylates mRNA (Zheng et al. 2013).

The association with ALKBH5, which has been shown to be important for the removal of the most abundant mRNA modification, m^6A, is of particular interest (reviewed in (Zhao, Roundtree, and He 2016). ALKBH5 is essential for spermatogenesis in mice and is highly expressed in both the testes and lungs (Zheng et al. 2013), both organs that express AD genes. Furthermore, ALKBH5 has been found to be important for the correct splicing and expression of longer transcripts (Tang et al. 2018), although there is no evidence that it is directly responsible for regulating the heavy chain AD mRNA.

While it is interesting to find RNA regulatory proteins being pulled down with DNAH5, it is also perplexing how this might occur especially for nuclear localised factors. The presence of SPAG1 and HSP90 are good indicators that these cells are still assembling ADs at the late stages of differentiation as was suggested by the pulse-chase imaging shown in **Figure 4.5 A)**. However, there were many other expected parts of the outer dynein complex which were not significantly enriched, such as DNAI1 which was just below the threshold, casting doubt on the validity of these results. These issues will be discussed further in **Section 4.5**, however as a preliminary result the identification of assembly factors with a translation initiation factor and mRNA regulators lends further weight to the suggestion that there might be a co-localisation of the *Dnah5* transcript and protein in assembly factories.

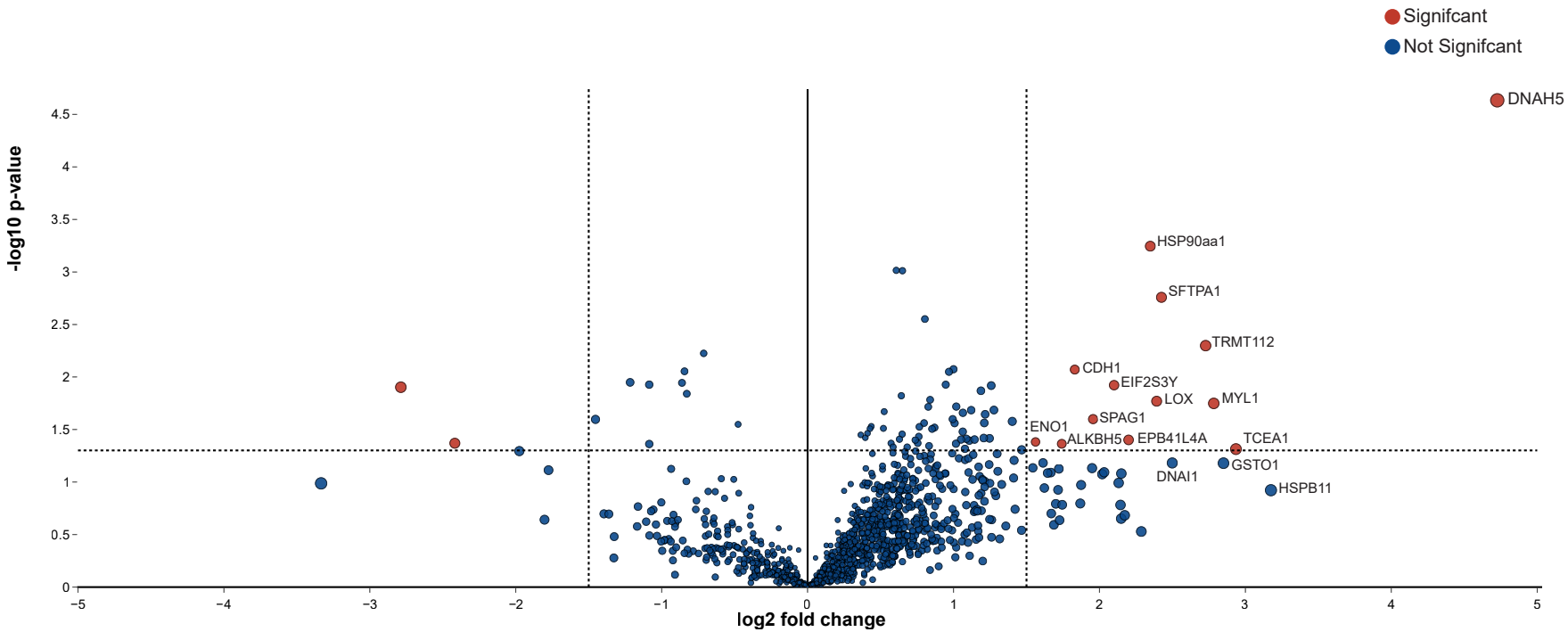

Figure 4.7 Mass spectrometry analysis of SNAP-DNAH5 co-immunoprecipitation from mTECs.

The graph shows the Log2 fold change in the intensity of interactors immunoprecipitated with anti-SNAP antibody in *Dnah5* $^{+/+}$ over *Dnah5* $^{SNAP/SNAP}$ mTECs from 3 replicates on the x axis and the -log10 p-value plotted on the y axis. A significance threshold of 1.3 and a fold change threshold of 1.5 was set. Interactors which are significantly enriched over these thresholds are indicated by a red dot with the ones enriched in the *Dnah5* $^{SNAP/SNAP}$ sample on the right of the midline and *Dnah5* $^{+/+}$ on the left. This analysis was done by Dr. A. von Kriegshiem and Dr. A. Bolado at the University of Edinburgh. Full peptide sequence and coverage is shown in **Appendix 2**.

To investigate whether there is specific subcellular localisation of *Dnah5* transcripts and if they co-localise with DNAH5 protein, mTECs were analysed using single molecule RNA fluorescent in situ hybridisation (smRNA FISH). They were also co-stained with the anti-DNAH5 antibody, however no DNAH5-like staining could be detected and no difference between secondary only controls and experimental samples was observed, in mTECs. Although early experiments demonstrated potential co-localisation of *Dnah5* transcript and protein in tracheal cryo-sections, **Figure 4.8 G)**, this result could not be replicated. This suggests the protocol needs to be optimised in order to preserve epitope antigenicity, which appears to be compromised under the in situ protocol conditions. Moreover, very bright autofluorescence was detectable in all channels at cytoplasmic granular structures which did not degrade with treatment of RNAse A whereas the probe signal did, **Figure 4.8 A) - D)**. Therefore puncta which fluoresced in all channels were discounted and only those which were solely positive for *Dnah5* were regarded as real. *Dnah5* RNA was detected in few but large (~0.55 μm^3) clusters in the cytoplasm and nucleus of mTECs early on in the ciliogenesis program, 4 days post airlift, **Figure 4.8 A)**. Imaging also demonstrated that very few of the cells at this stage seemed to have detectable expression of *Dnah5*. This localisation is in contrast to the control probe, *Gapdh*, which seems to be highly expressed in all cells in small (0.12 μm^3) puncta and ubiquitously cytoplasmic in localisation **Figure 4.8 C)**.

In order to better determine the structure of these clusters and to give an indication of how many transcripts there might be in them the cells were imaged with super resolution stimulated emission depletion (STED) microscopy, **Figure 4.8 E)** – **F)**, with Dr. Alison Dunn (ESRIC Heriot-Watt University). This showed that the clusters were made up of multiple transcripts and were of variable shape and size, however the density and shape of the transcripts made it hard to quantify their number accurately. Due to the difficulties of using immunofluorescence in conjunction with FISH to determine the localisation of DNAH5 mRNA and protein, the *SNAP-Dnah5* mouse was used with cell permeable SNAP dye to image DNAH5 protein in the cytoplasm. Unfortunately, in spite of the SNAP dye working via covalent enzymatic coupling to the target protein, obviating the requirement for the preservation of antigenicity, cytoplasmic DNAH5 was not distinguishable, although some cilia were very faintly stained in a few cells. Fortunately, this proved to be a useful landmark of the apical surface, such that on imaging the cells transversely the large clusters

of *Dnah5* transcript could be seen to be localised nearer the apical side of the cell, **Figure 4.8 H)**. While this preliminary data will need further verification it is reminiscent of the observed localisation of DynAPs (Huizar et al. 2018) and suggests translational regulation may occur in these ‘assembly factories’.

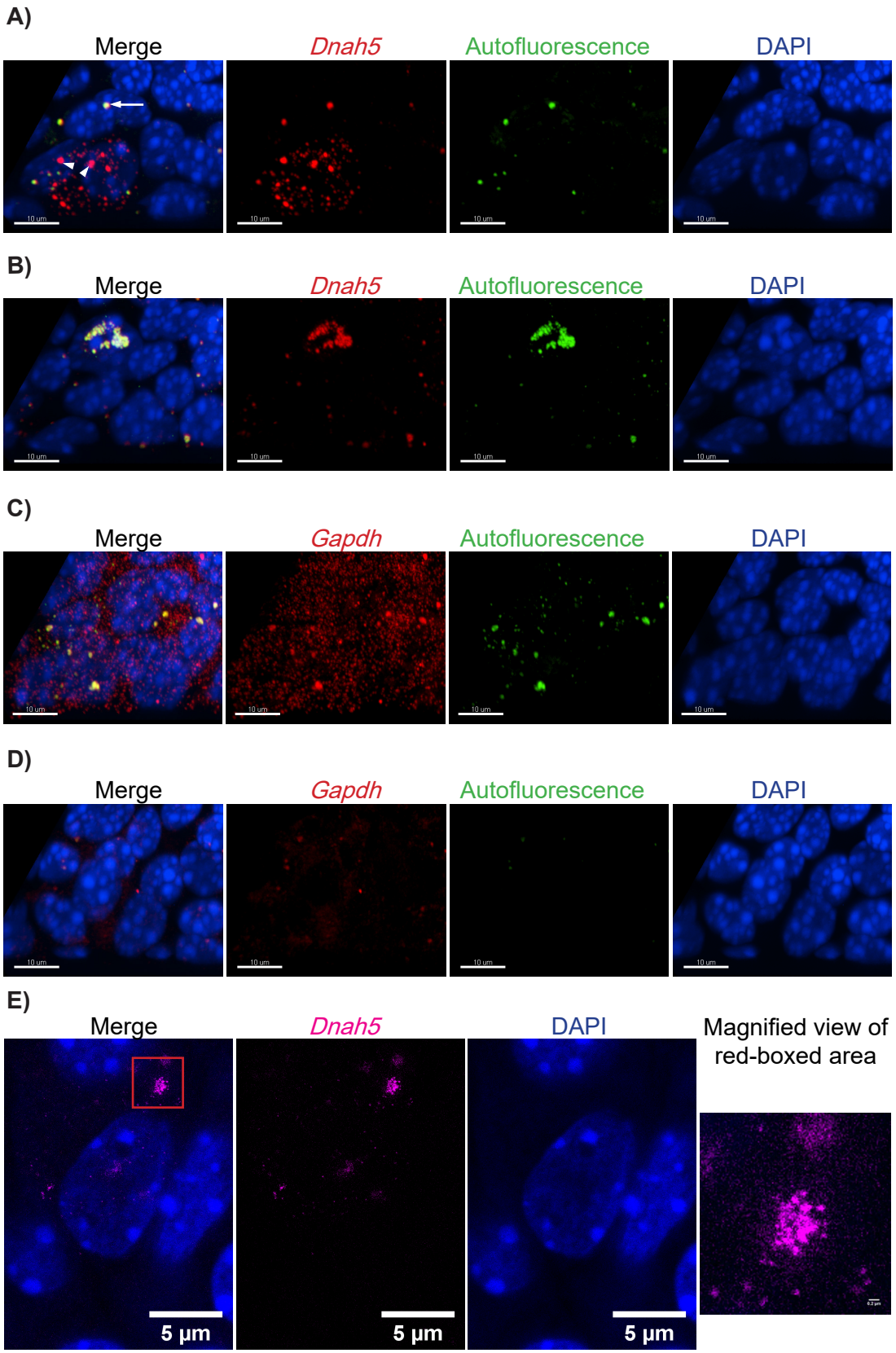

Continued on next page

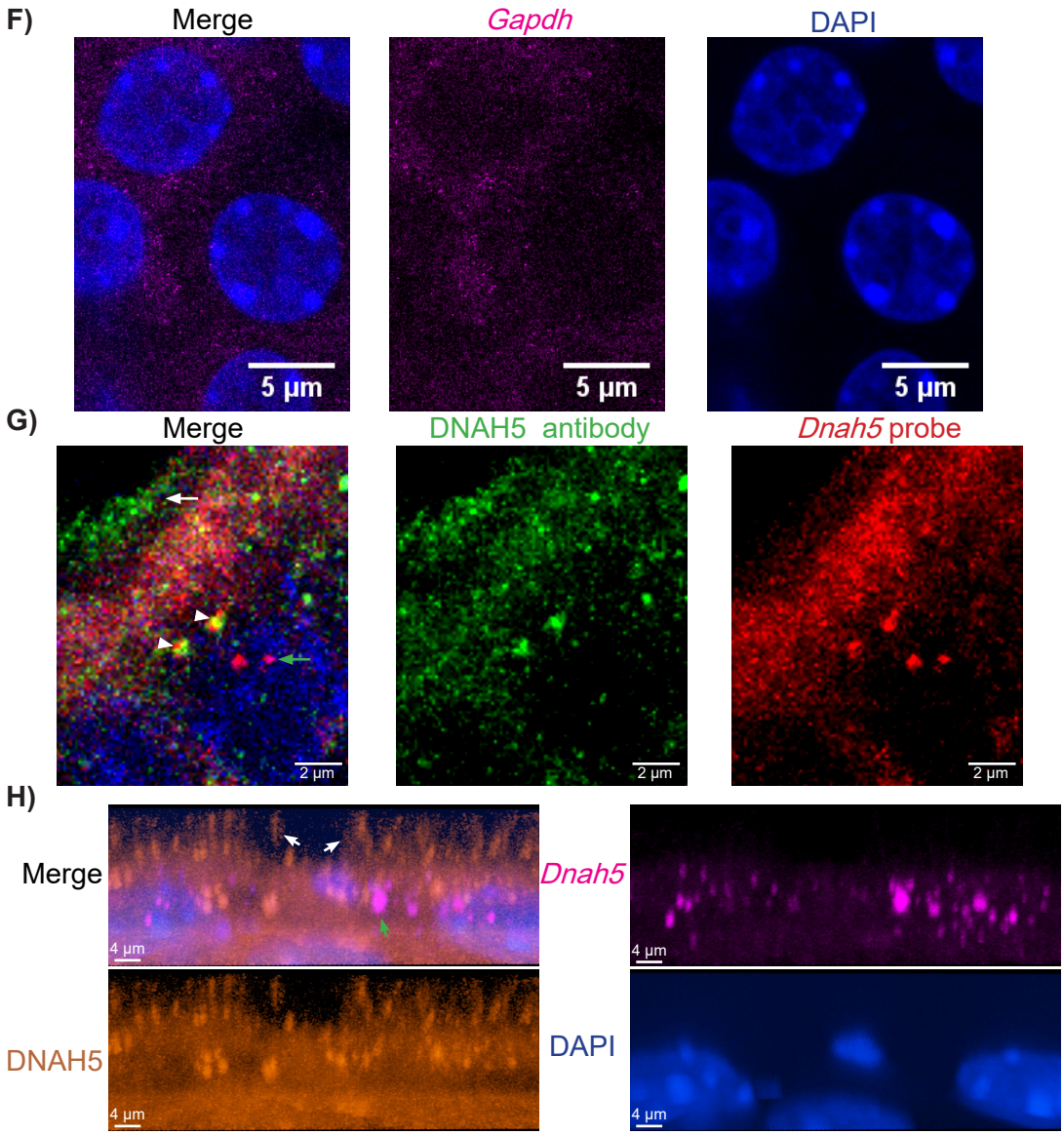

Figure 4.8 Localisation of *Dnah5* transcripts to large apically localised clusters

A) mTECs stained with probes against *Dnah5* in red, anti-DNAH5 antibody in green and DAPI in blue. The majority of the green and red spots are autofluorescence, indicated by the white arrow. Clusters of transcript are indicated by white arrowheads.
B) *Dnah5* staining disappears in mTECs that have been treated with Rnase A.
C) mTECs stained with probes against *Gapdh* in red.
D) Rnase A treatment removes *Gapdh* signal.
E) STED super resolution of *Dnah5* transcript clusters in magenta.
F) STED super resolution of *Gapdh* transcript in magenta. STED by A. Dunn (HW).
G) A tracheal cryosection stained with DNAH5 antibody (green), *Dnah5* probe (red) and DAPI (blue). Nuclear *Dnah5* is indicated by a green arrow, the cilia are indicated by a white arrow and potential sites of co-localised DNAH5 protein and transcript are indicated by the white arrowheads.
H) Transverse view of a *SNAP-Dnah5* mTEC transwell stained with cell permeable SNAP dye TMR-Star (red), with *Dnah5* probe (magenta) and DAPI (blue). The cilia are highlighted by white arrows and the *Dnah5* transcripts by a green arrow.

4.5 Discussion

These results taken together show that the *SNAP-Dnah5* mouse exhibits normal AD and SNAP tag function. This makes it the second endogenously tagged heavy chain dynein in mice, the first being GFP tagged *Dnah11* as mentioned earlier (Mcgrath et al. 2003). However, the advantage of the SNAP tag is that it can be used for more than just fluorescent imaging, such as pulse-chase imaging to observe protein turnover and AD docking as demonstrated. Additionally, now there are two tagged AD heavy chains, these mice can be inter-crossed to allow comparisons to be made in terms of endogenous localisation, dynamics and interaction partners. This is of particular interest for *Dnah11* which has been shown to not require assembly factors *DNAAF1* and *DNAAF3* (Dougherty et al. 2016) suggesting it might have a different assembly pathway to *Dnah5* which is affected by the loss of these assembly factors. Close examination of the individual proteins that make up the diverse array of large and complex ADs will illuminate the pathways involved in their regulation and assembly.

Using the *SNAP-Dnah5* mouse to calculate the docking rate of the ADs along the axoneme requires more experiments in order to make a more accurate measurement. As previously mentioned, measuring the length of newly docked dyneins along the axoneme at regular intervals over a shorter time period would give a more accurate reading of the rate of docking. Another possible method to do this would be to follow in the footsteps of previous work on *Chlamydomonas* where cells with a temperature sensitive kinesin-2 motor were mixed with I1 dynein deficient cells at permissive and restrictive temperatures (Viswanadha et al. 2014). This showed that the dynein was carried to the tip by IFT where they are released and diffuse through the axonemal shaft filling up docking sites closest to the tip first, in already assembled cilia. This may also reflect the situation in mature ciliated cells if genome editing were to correct any defects in the assembly machinery, as in PCD the ODAs are often absent. While there are no temperature sensitive mutants in mice it is possible to reversibly inhibit dynein assembly using the FKBP8 inhibitor DM-CHX (Mali et al. 2018) which would allow the axoneme to assemble without the dyneins. Taking measurements at regular timepoints from the moment of drug washout would allow the rate of docking in assembled cilia to be accurately calculated and compared to the assembling axoneme.

It remains an important and open question as to whether there is AD turnover in mammalian ciliated cells, which this mouse model will be a powerful tool to analyse. Currently *SNAP-Dnah5* mTECs are being cultured to repeat the experiment shown in **Figure 4.6** leaving a longer time between the addition of dyes. It is expected that eventually the older DNAH5, bound to the 1st dye will be replaced by new DNAH5, bound to the 2nd dye. Although it's possible that the rate of turnover is so slow that the cells will die before this happens to enough ODAs for it to be perceptible.

Besides the ability to image AD docking and turnover the *SNAP-Dnah5* mouse has also been shown to be useful for finding protein interaction partners via mass spectrometry. While it is possible to use the activity of the SNAP tag to covalently bind to beads for pulldown of interacting proteins it requires the tag to be enzymatically active after cell lysis. Attempts to use the benzylguanine modified beads to pull SNAP-DNAH5 down from cell lysates resulted in no enrichment of DNAH5 suggesting that the lysis conditions were either not harsh enough to extract the protein or inhibited the enzymatic activity of the SNAP tag. Therefore the SNAP-DNAH5 fusion was pulled down using the SNAP tag antibody, which did result in enrichment of DNAH5 however as previously discussed did not enrich for AD proteins and other known axonemal interactors. Nevertheless some of the proteins pulled down were known interactors and one of the novel interactors, ALKBH5, has been shown to be important in spermatogenesis and highly expressed in lungs. However, as previously discussed there was no detection of AD transcripts amongst the genes that were differentially expressed (Zheng et al. 2013; Tang et al. 2018), although that could be due to the heavy chain axonemal dyneins having a low number of transcripts, as suggested by the smRNA FISH results and published single cell RNA sequencing data (Plasschaert et al. 2018; Montoro et al. 2018). It is possible that these genes were affected in both the lungs and testes, where ALKBH5 expression is the highest, as levels of total m^{6}A methylation were shown to be increased in both these organs. The potential that ALKBH5 may regulate heavy chain transcription is supported by the fact that it has been shown to be important for maintaining accurate splicing of long transcripts as well as preventing nuclear export. However, ALKBH5 as an mRNA demethylase has been shown to function in the nucleus whereas DNAH5 is localised to the cytoplasm and cilia. Maintaining efficient splicing activity of very long transcripts with multiple exons, such as *Dnah5* which has 79 exons, is likely to be crucial for

their stability and efficient translation. Alternately, it has recently been shown that ALKBH5 interacts with the DEAD-box RNA helicase DDX3 (Shah et al. 2017) which shuttles between the nucleus and the cytoplasm, and is a component of the cytoplasmic granules such as stress granules and P-bodies (Hilliker et al. 2011; Kanai, Dohmae, and Hirokawa 2004; Lai, Lee, and Tarn 2008). However, it has not been established where this interaction occurs and it could be purely nuclear. This interaction needs to be confirmed with further pulldowns, either using the antibody or potentially with benzylguanine modified biotin and streptavidin to bypass the need for this gentle lysis and the anti-SNAP tag antibody.

The potential for post-transcriptional regulation of the AD subunits in P-bodies, stress granules or a similar phase separated organelle is supported by the discovery of DynAPs, which contain AD subunits and their assembly factors (Huizar et al. 2018). These particles were shown to contain some of the components found in similar types of foci. Whilst the RNA content of these particles was not investigated, it is possible the transcripts for AD components are also located here. As the RNA FISH in **Figure 4.8** shows *Dnah5* transcripts cluster in foci not entirely dissimilar in their localisation to the DynAPs however without being able to find out what proteins they are co-localised with it is not possible to speculate as to their nature. Nevertheless, post-transcriptional regulation and localised translation could be ways for the motile ciliated cell to cope with the heavy transcriptional toll of creating nearly a million axonemal dynein proteins. It has been shown previously that sperm cells store their transcripts for translation in order to complete spermatogenesis (Schäfer et al. 1995), while this is due to the genomic changes in the cell it is an example of how post-transcriptional control can aid in a cell's differentiation. Therefore, finding out the localisation of DNAH5 as well as other proteins is of paramount importance in establishing the function of these transcript clusters. The *SNAP-Dnah5* mouse will help to accomplish this and will hopefully prove useful for many other studies into AD biology.

5 Improving the efficiency of specific genomic editing with CRISPR/Cas9

5.1 Introduction

5.1.1 Reporters of DNA repair pathway

The mammalian cell has many different ways to repair DNA damage; for the purposes of genome editing these can be simplified into two main types: those that use a homologous sequence of DNA to repair the damaged strand or strands known as Homology Directed Repair (HDR), and those that do not referred to as Non-Homologous End Joining (NHEJ). The details of these repair systems have been reviewed previously in **Section 1.7**; the focus of this short introduction will be on the fluorescent reporter systems which have been developed to differentiate between these pathways.

Fluorescent reporters of genome editing repair outcomes began with the Traffic Light Reporter (TLR) system, which was initially developed using the SceI meganuclease (Certo et al. 2011) and has been adapted for use with other editing nucleases including Cas9 (Chu et al. 2015). It uses two out of frame fluorescent proteins in the same coding sequence, the upstream *EGFP* (+1) is separated from the downstream *mCherry* (+3) by a T2A peptide cleavage sequence. When supplied with a repair template with homology for *EGFP* that shifts it to the correct frame, the cells express EGFP whereas when there is no template, errors introduced by NHEJ can shift *mCherry* into frame. This kind of reporter requires a large repair template and is similar to the mTmG CRISPR reporter system developed in this lab, **Figure 5.1 A)**, as well as another recently published reporter that also uses the mTmG mouse (Alapati et al. 2019).

Another strategy relies on the ability to alter the fluorescence spectra of fluorescent proteins by changing single amino acid sequences. The most commonly used reporter utilises EGFP and the closely related blue fluorescent protein (BFP) which can be interchanged by introducing a single nucleotide polymorphism with a homology repair template (Richardson et al. 2016; Glaser, McColl, and Vadolas 2016). If there is error prone DNA repair as a result of NHEJ it can result in the loss of fluorescence of EGFP or BFP, depending on which fluorophore is being converted to which. The advantage of this type of system over the TLR type is that it only requires a short exogenous piece of DNA to convert the fluorescence of the

reporter protein, which allows for the use of cheap and easily synthesised single stranded DNA repair templates.

5.1.2 Attempts to improve CRISPR/Cas9 induced HDR

One of the main uses for the reporter systems mentioned in **Section 5.1.1** is testing the effectiveness of various approaches to improve the efficiency of HDR in genome editing. Mammalian cells have relatively low levels of homology directed repair, preferentially using the error-prone NHEJ pathway (Orthwein et al. 2015), making gene correction or replacement harder. Therefore, research to aid in the incorporation of exogenous DNA sequences into targeted regions of the genome is key to the success of gene therapy. With the development of the RNA guided editing system CRISPR/Cas9 for use in mammals the targeting of the genomic site has become easier, however repairing to the wild type sequence is still a challenge. The use of small molecules to alter the bias of the endogenous repair pathways towards HDR has shown that inhibitors of the NHEJ pathway can increase the levels of HDR (Maruyama et al. 2015; Srivastava et al. 2012; Robert et al. 2015; Leahy et al. 2004) and similarly activators of HDR can also increase HDR efficiency (Pinder, Salsman, and Dellaire 2015; Jayathilaka et al. 2008; Jun Song et al. 2016). This was predicted from genetic inhibition (Chu et al. 2015; Certo et al. 2011) and overexpression of proteins suspected to be important for DNA repair (Pinder, Salsman, and Dellaire 2015). Blind screens using a library of drugs have also uncovered drugs which seem to increase HDR through unknown mechanisms (Yu et al. 2015). Additional methods to increase HDR include changing the length, symmetry and chemistry of the repair template (Richardson et al. 2018; Paix et al. 2017; Liang et al. 2017), controlling the stage of the cell cycle at which editing occurs (Lin et al. 2014; Yang et al. 2016; Gutschner et al. 2016) and fusing Cas9 to proteins important for HDR (Rees, Yeh, and Liu 2019), amongst other approaches.

Another method which has been used to improve HDR of targeted double stranded DNA breaks has been to directly attach the DNA repair template to the editing complex. This has been shown to increase the efficiency of HDR in yeast cells (32 fold) and human cells (16 fold), edited with the meganuclease SceI and repair guided by a DNA repair template that binds to SceI with an aptamer (Ruff et al. 2014). Further experiments using CRISPR/Cas9 with a guide RNA that is covalently attached to the repair template have been conducted (Lee et al. 2017),

slightly increasing the efficiency of HDR. A study where a benzylguanine modified repair template was tethered to Cas9 by the SNAP tag concluded this was mainly due to the repair template being transported to the nucleus by the Cas9 nuclease, (Savic et al. 2018). Similar types of Cas9-fusions have been developed which bind to biotinylated DNA (Gu, Posfai, and Rossant 2018; Carlson-Stevermer et al. 2017) or covalently attach to single stranded DNA via a viral replication protein (Aird et al. 2018). Some of these strategies to improve the efficiency of specific repair of CRISPR induced double stranded DNA breaks were tested in order to develop a genome editing therapy for PCD.

5.2 Developing fluorescent reporters of genome editing outcomes.

In order to develop a gene editing therapy for PCD, attempts to improve the efficiency of specific repair pathways were trialled in an *in vivo* reporter of DNA repair. The mTmG system was developed to act as a Cre-mediated lineage tracer (Muzumdar et al. 2007). This has been adapted to be used as a fluorescent reporter of genome editing outcome by the Mill lab, **Figure 5.1 A)**. By directing an RNA targeted nuclease, such as Cas9, to the two identical LoxP containing regions that flank the *mTomato* gene, one can distinguish non-edited (membrane Tomato) from edited cells (other). If the ends of both cut sites are repaired by NHEJ, this can cause the downstream *mEGFP* to be expressed, or throw the *mTomato* gene out of frame causing loss of fluorescence. By including a repair template that changes localisation signal on EGFP from the MARCKS membrane tag to a H2B nuclear signal, one can distinguish NHEJ (membrane EGFP) from HDR (nuclear EGFP). Furthermore, by addition of a plasmid or mini circle encoding a nuclear localised BFP flanked by target sites for the mTmG LoxP guides, one can report the efficiency of Homology Independent Targeted Integration (HITI), a method that uses NHEJ to integrate DNA into a targeted site and has been used for gene editing therapy in mice (Suzuki et al. 2016). When the guides are expressed with the nuclease then the *BFP* gene is linearised and can be inserted in the place of *mTomato* by NHEJ, **Figure 5.1 A)**.

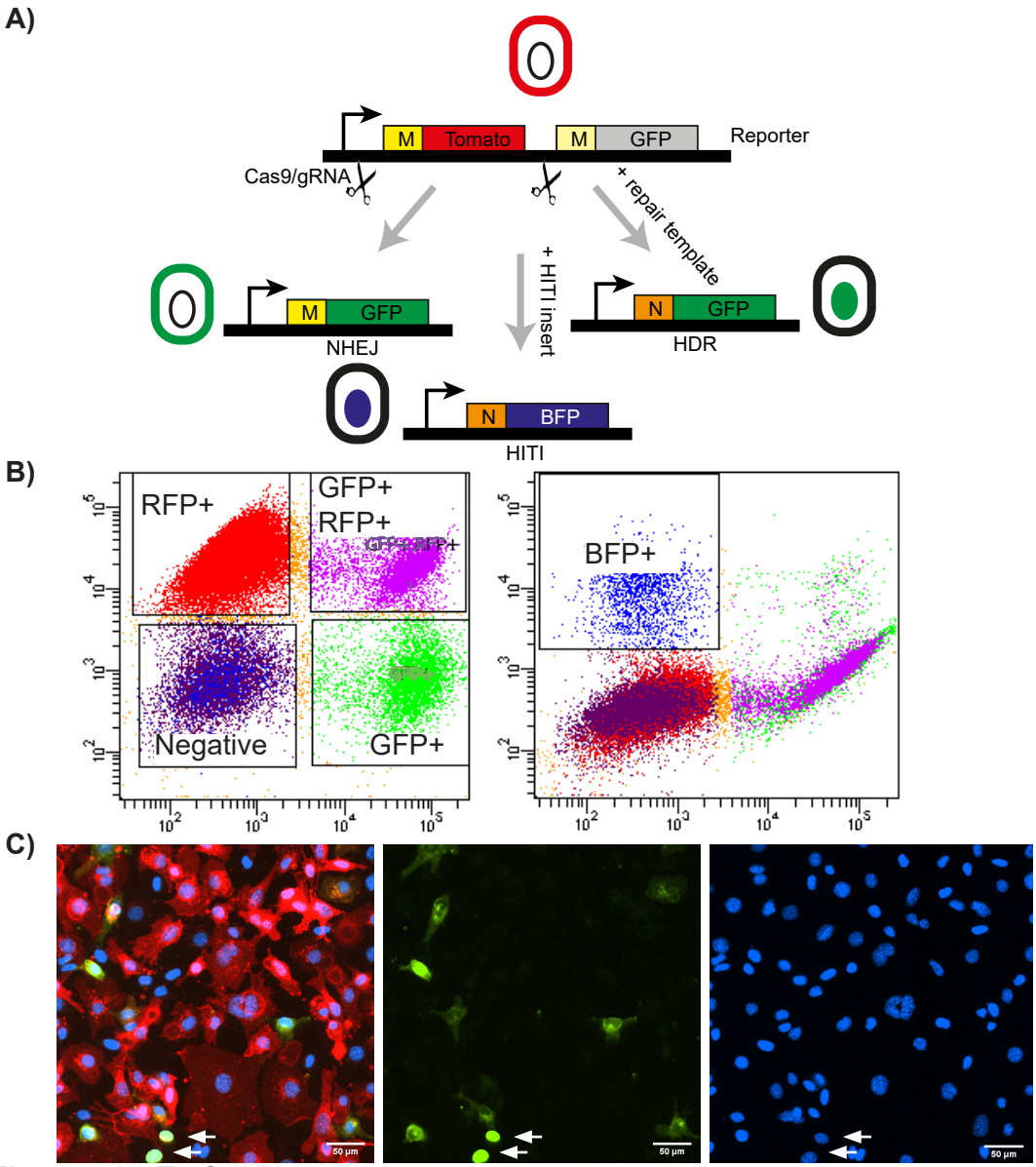

Figure 5.1 mTmG editing reporter system

A) This diagram shows the mTmG reporter sytem, which consists of a gene cassette with a red fluorescent protein dimer (*Tomato*) gene upstream of a green fluorescent protein gene under the control of a promoter (right angled arrow). Both fluorescent proteins have a MARCKs tag, M in yellow box, which localises them to the plasma membrane. The cells do not express GFP unless the tomato sequence with its strong stop is removed by the action of Cas9 targeted to flanking Loxp site containing sequences. If there is no repair template NHEJ will likely result in green membrane fluorescence or no fluorescence if errors are introduced, if a repair template with homology is added then the fluorescence will be nuclear GFP, if DNA with nuclear localised BFP is added and integrated via NHEJ then there will be nuclear BFP.
B) FACS plots showing the different editing outcomes, negative and double positive cells are the result of error prone repair and genomic instability.
C) Images of edited mTmG MEFs stained with blue nuclear stain. Images left to right, composite, GFP, nuclear stain. The white arrowheads indicate GFP positive nuclei, representing HDR.

This mTmG reporter system was used to test various conditions with immortalised mouse embryonic fibroblasts heterozygous for mTmG (referred to as mTmG MEFs). The changes in fluorescence can be measured using FACS, **Figure 5.1 B)**, while the change in localisation is analysed using imaging, **Figure 5.1 C)**. The FACS plots show that some of the cells express both EGFP and Tomato, as the mice are heterozygous for mTmG, this is likely due to genomic instability in the immortalised cells resulting in polyploidy and multiple copies of the *mTmG* locus.

One limitation of the mTmG reporter system is the relatively large repair template needed, due to the double cut sites and large deletions required to see changes in fluorescence. This is not an accurate representation of gene therapy in patients, which will usually be repairing a small mutation, therefore a second reporter system was developed, which relies on much shorter repair templates. This fluorescent reporter switches from non-fluorescent EGFP to fluorescent EGFP by repairing a single amino acid (68A>G), **Figure 5.2 A)**. The single nucleotide change was made using site directed mutagenesis, which converts a cytosine to a guanine, removing a PAM site and changing the 68th amino acid from glycine to alanine as indicated, **Figure 5.2 B)**. Glycine 68 is an essential part of the EGFP chromophore, therefore when altered it causes EGFP to lose fluorescence (Heim, Prasher, and Tsien 1994). The non-fluorescent EGFP^{68A} and the control fluorescent EGFP^{WT} constructs were integrated into the Flp-In™ HEK 293 T-REx cell line (HEK 293), using the Flp recombinase and Hygromycin selection, allowing integration of a single copy into a defined genetic locus to control expression levels, **Figure 5.2 C)**. After selection, clonal populations were isolated and screened by PCR for integration and the positive colonies were then checked for expression using reverse transcription PCR, demonstrating expression of either non-fluorescent EGFP^{68A} or fluorescent EGFP^{WT} in seven out of eight cell lines, **Figure 5.2 D)**. The fluorescent EGFP^{WT} cell lines were used as positive controls for the FACS experiments. Guide RNA and single stranded repair DNA was designed that would target the EGFP^{68A} reporter. The FACS plots of the positive and negative controls are shown in **Figure 5.2 E)**, the gates shown in these plots were used to identify which cells had undergone HDR. This shows that the single amino acid change is sufficient to stop EGFP fluorescence.

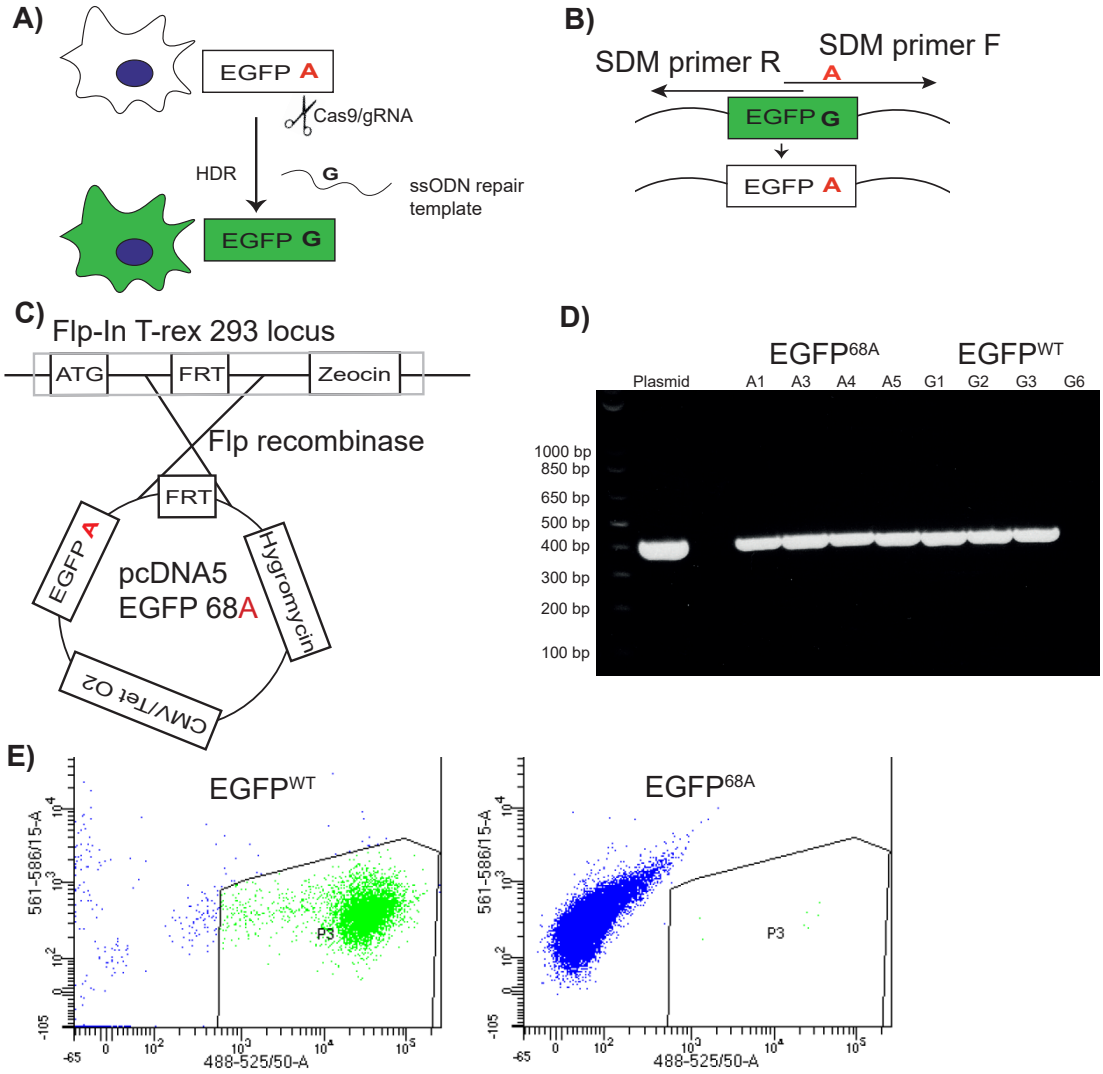

Figure 5.2 EGFP alanine 68 reporter system generation

A) The principle of the EGFP alanine 68 reporter system is to measure HDR by editing the non-fluorescent EGFP allele, shown as a blank box with A, in HEK293 cells using Cas9 and EGFP targeting guides with a single stranded repair template that converts alanine 68 to glycine 68, green box with G, making the cells EGFP fluorescent.
B) EGFP was mutagenised using site directed mutagenesis, with primers SDM F and R to create an EGFP with alanine at position 68 ($EGFP^{68A}$), rendering it non-fluorescent.
C) Both the 68G and 68A eGFP (pcDNA5) plasmids were then integrated into Flp-In T-rex 293 cells using Flp recombinase. Colonies of cells were then selected using the Hygromycin resistance marker.
D) Reverse transcription PCR was performed after inducing expression with Doxycyline. The plasmid used for integration was used as a positive control, A1-5 refer to $EGFP^{68A}$ cells and G1-6 to $EGFP^{WT}$ cells, all but one of the colonies seem to express EGFP.
E) EGFP fluorescence was measured with FACS, the plots shown acted as positive and negative controls for editing experiments. Green fluorescence is measured on the X axis and blue is on the Y (for cell viability). Each dot is a cell and the green gated population (P3) represents the GFP positive cells, 93% of the viable cells in $EGFP^{WT}$.

5.3 Testing putative small molecule modulators of genome editing using the mTmG reporter system.

The mTmG system was used to test small molecules which had previously been shown in published work to improve the efficiency of HDR. Two of the small molecules used were inhibitors of NHEJ, Scr7 an inhibitor of DNA Ligase IV (Srivastava et al. 2012) and Nu7441 an inhibitor of DNA dependent protein kinase (Leahy et al. 2004). A blind screen of compounds to find chemicals to increase HDR efficiency identified two other molecules (Yu et al. 2015), Brefeldin-A (Brf-A), an inhibitor of ADP-ribosylation factor 1 (Benabdi et al. 2017), and L755,501, an agonist of the β3 adrenergic receptor (Parmee et al. 1998). RS-1, an activator of the homologous recombination pathway protein Rad51 (Jayathilaka et al. 2008), was also tested using the mTmG system. Despite previous reports suggesting the molecules increased the efficiency of HDR (Maruyama et al. 2015; Robert et al. 2015; Jun Song et al. 2016; Pinder, Salsman, and Dellaire 2015; Yu et al. 2015), analysis of the levels of HDR in control and drug treated mTmG MEFs showed no significant differences, **Figure 5.3 A)**. The experiment was repeated to include more replicates in order to gain statistical power, the HITI repair construct was also included to measure the effect of small molecules on the efficiency of HITI.

Repeating the small molecule treatments with five replicates failed to produce results for HDR due to an issue which resulted in detachment of the MEFs from the plate prior to imaging. However, there were differences in the percentages of different types of fluorescence between the cells treated with certain small molecules measured by FACS. The DNA dependent protein kinase inhibitor (DNAPKcs) Nu7441 seemed to have the most effect on the editing outcomes in MEFs, which were measured as a percentage of total editing (non-red cells). It increased the percentage of GFP positive cells from 27% in the DMSO control to 31%, **Figure 5.3 B)**, while decreasing BFP positive cells from 9% to 6%, **Figure 5.3 C)**. It also seemed to increase the proportion of negative cells from 41% to 44%, **Figure 5.3 D)** and decrease the number of double positive cells from 25% to 18%, **Figure 5.3 E)**. This led to an overall increase in total visible editing in the Nu7441 cells from 39% to 50%, **Figure 5.3 F)**. The increase in the number of GFP positive cells suggests that Nu7441 might be increasing the number of GFP positive nuclei through the HDR pathway however it could also be the result of NHEJ and expression of the membrane localised GFP. Similarly the decrease in BFP positive cells is to be expected, given that HITI relies on NHEJ. The effects

on the negative and yellow cells is harder to explain. While Nu7441 had the clearest effect, Brf-A seemed to have an opposite effect decreasing total editing from 39% to 35% as well as the proportion of negative cells from 40% to 32%, **Figures 5.3 F) and D)**. It also increased the percentage of yellow cells from 25 to 33, again the opposite effect to Nu7441 as shown in **Figure 5.3 E)**. However, Brf-A did not significantly decrease the percentage of GFP positive cells and had a similar effect on the proportion of BFP positive cells, decreasing them from 9% to 7%. Overall, the changes in the efficiency of HDR caused by these small molecules suggest that they are not likely to be useful for genome editing therapy. However, their effectiveness is likely to be cell type dependent and the efficiency may be different in the target tissue. The effects of the small molecules on the choice of DNA repair pathway will be discussed further in **Section 5.6**.

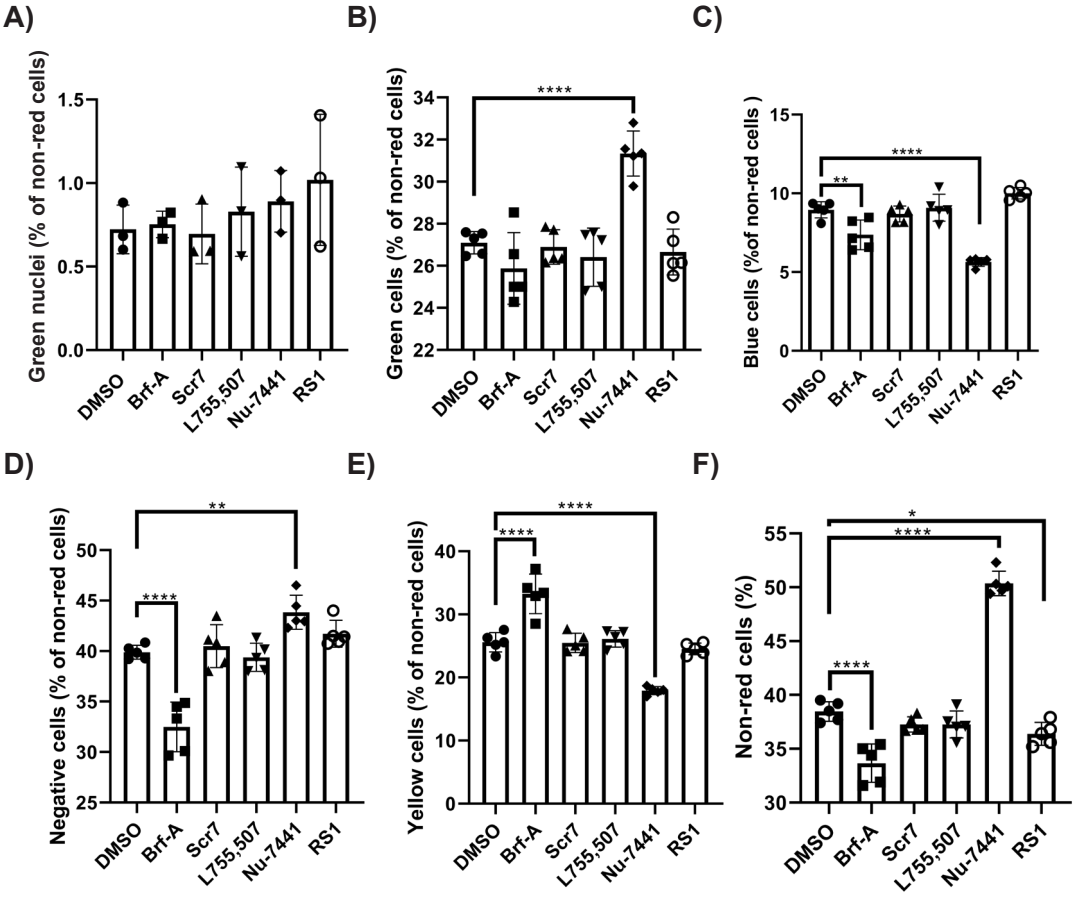

Figure 5.3 The effect of published small molecules on editing outcomes

A) The bar chart shows the percentage of green nuclei as a percentage of total non-red fluorescent cells, as measured by imaging, no significant differences were noted. The individual points represent technical replicates, significant diferences between the DMSO vehicle control and the treated cells are highlighted by black lines. Significance was tested using one way ANOVA and Dunnett's multiple comparisons, 0.0021 < P < 0.05 = *, 0.0002 < P < 0.0021 = **, 0.0001 < P < 0.0002 = ***, P < 0.0001 = ****. n= 3

B) Nu7741 increases the percentage of green (GFP+) cells as a percentage of all non-red fluorescent cells as measured by FACS. n =5

C) Brf-A increases and Nu7441 decreases the percentage of Blue cells (BFP+) cells as a percentage of all non-red fluorescent cells as measured by FACS. n =5

D) Nu7441 increases and Brf-A decreases the percentage of non-fluorescent cells as a percentage of all non-red fluorescent cells as measured by FACS. n= 5

E) Brf-A increases and Nu7441 decreases the percentage of yellow cells (GFP+ RFP+) as a percentage of all non-red fluorescent cells as measured by FACS. n =5

F) Nu7441 increases the percentage of all non-red fluorescent cells as measured by FACS while RS1 and Brf-A decrease it. n =5

5.4 Testing the effect of linked guide RNA on HDR efficiency.

Directly attaching the DNA repair template to the editing complex has been shown to increase the efficiency of HDR (Ruff et al. 2014; Lee et al. 2017). For this method, a short repair template is required, which is not possible in the mTmG system, so here we used the EGFP^{68A} reporter system described in **Section 5.2** to assess genome editing efficiency improvements.

The idea to link the repair template DNA to the guide RNA to improve HDR efficiency was trialled initially using a method based on sequence complementarity between the 3' end of the single guide RNA and the 5' end of the ssDNA repair template, however this proved unsuccessful (data not shown). The approach was changed to use Click chemistry to link the nucleic acids when it was published in 2017 (Lee et al. 2017), however instead of linkage at the 5' end of the guide RNA DNA was attached at the 3' end of the sgRNA. This is predicted to be closer to the editing site and would be in the correct orientation to allow for complementary binding to the target region (Nishimasu et al. 2014).

As shown in **Figure 5.4 A)** the 5' end of the DNA repair template was modified with a DBCO molecule and the 3' end of the guide RNA was modified with an azide group. The same groups were used previously to attach guide RNA and repair DNA using Click chemistry (Lee et al. 2017). The Click reaction is designed to be a very thermodynamically favourable one, which can be conducted with simple reaction conditions (Agard, Prescher, and Bertozzi 2004), however in order to get a good yield these conditions were optimised. One way to improve the ligation of two nucleic acids is to use a short piece of DNA complementary to both sequences, known as a splint, which binds them both and brings the ends closer together. Three different splints were designed each was complementary to the 3' end of the guide RNA and to the 5' end of the repair DNA. The lengths of the homology arms were either 16 nucleotides in the case of splint number 1 or 20 nucleotides in the case of splint numbers 2 and 3. Splint 3, shown in **Figure 5.4 A)** had a flexible hexa-ethylene glycol (HEG) linker between the homology arms which helps to avoid steric hindrance of the splint in the Click reaction. The different types of splints and concentrations of nucleic acids used to optimise the reaction are shown in **Table 5.1**. The reactions were heated and cooled to allow for annealing and were left at 25 °C overnight, the resulting products were then analysed on a polyacrylamide gel with the reaction reagents, shown in **Figure 5.4 B)**. The yield

of the various conditions was calculated using gel densitometry to measure the intensity of the RNA and DNA bands by themselves and then dividing the intensity of the product band by this. These measurements showed that condition 4 had the best yield with 81% of the DNA and RNA being linked together.

Reaction	sgRNA (μM)	Repair DNA (μM)	Splint	Splint (μM)
1	10	30		
2	10	30	1	30
3	10	30	2	30
4	10	30	3	30
5	10	10		
6	10	10	1	10
7	10	10	2	10
8	10	10	3	10
9	10	20		
10	10	20	1	20
11	10	20	2	20
12	10	20	3	20
13	30	10		
14	30	10	1	30
15	30	10	2	30
16	30	10	3	30

Table 5.1 Click reactions to link guide RNA and repair DNA

The table shows the 16 different reaction conditions, numbered 1-16, used to optimise the Click chemistry mediated linkage of the modified guide RNA and repair DNA. The concentrations for each reagent added are given in micromolar. Splints are numbered 1 – 3 with splint 1 having 16 nucleotide homology arms and no HEG linker, splint 2 having 20 nucleotide homology arms and no HEG linker and splint 3 having 20 nucleotide homology arms and a HEG linker.

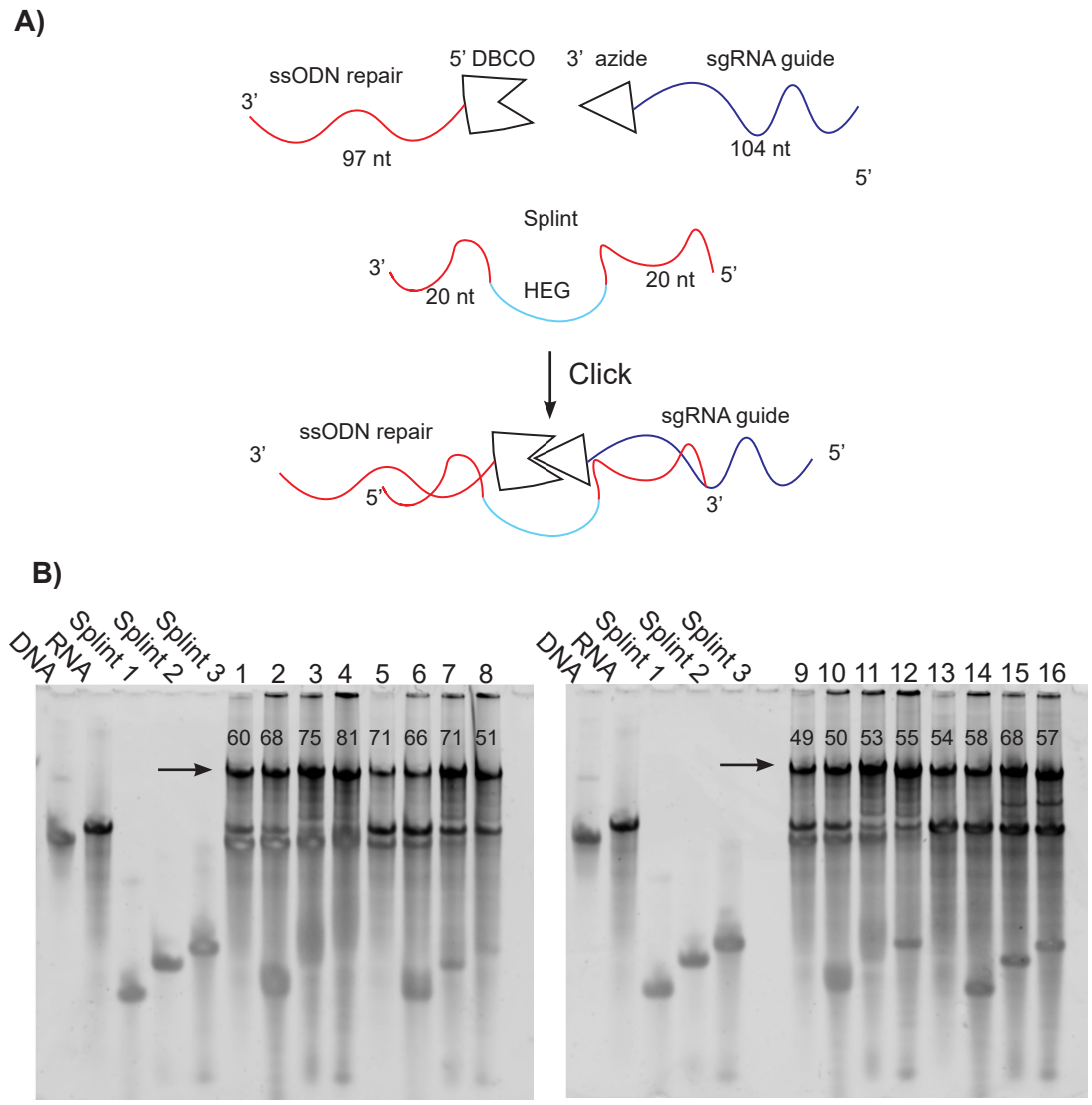

Figure 5.4 Click chemistry to make linked RNA-DNA

A) The diagram demonstrates the reagents that were used to make the combined guide RNA and repair template complex used. Single stranded repair template DNA with a 5' DBCO modification was added to single stranded guide RNA with a 3' azide modification, this is combined with a single stranded DNA oligonucleotide that has 20 bp homology arms that are complementary to the ends of the RNA and DNA to be joined. The homology arms are seperated by the addition of Hexa-Ethylene-Glycol (HEG). These then form a covalent bond and become joined.
B) These gels show the results of optimisation for the click reaction with different concentrations of DNA and RNA and different splints as detailed in **Table 5.1**. The black arrow indicates the product produced after the reaction, this is the linked RNA-DNA. Reaction 4 was the most efficient so this was used to produce the RNA-DNA in later reactions.

To verify the ability of EGFP^{68A} to report on genome editing induced HDR, cells were transfected with the Cas9 guide RNP complex with repair template DNA. These had significantly more EGFP positive cells than the controls, 0.08% compared with 0.03% for the untransfected cells, **Figures 5.5 A)** and **C)**. This shows that the EGFP alanine 68 reporter system is able to measure the level of HDR in transfected cells. To test whether linkage of the guide and repair could improve the efficiency of HDR, EGFP^{68A} cells were transfected with gel purified covalently linked guide RNA and repair DNA, unpurified linked RNA and repair DNA and unreacted RNA and DNA. The cells were also transfected with purified linked RNA and repair DNA mixed with complementary single stranded DNA that extended the 3' end of the repair template. However, the percentage of HDR was negligible in all samples, as shown in **Figure 5.5 D)**. This suggests that the linkage of the guide RNA and repair DNA template does not improve the efficiency of HDR. However, the overall levels of HDR appear to be very low when compared to the mTmG reporter system for example (~1.5%), suggesting that the reporter system was not performing effectively as discussed in **Section 5.6**.

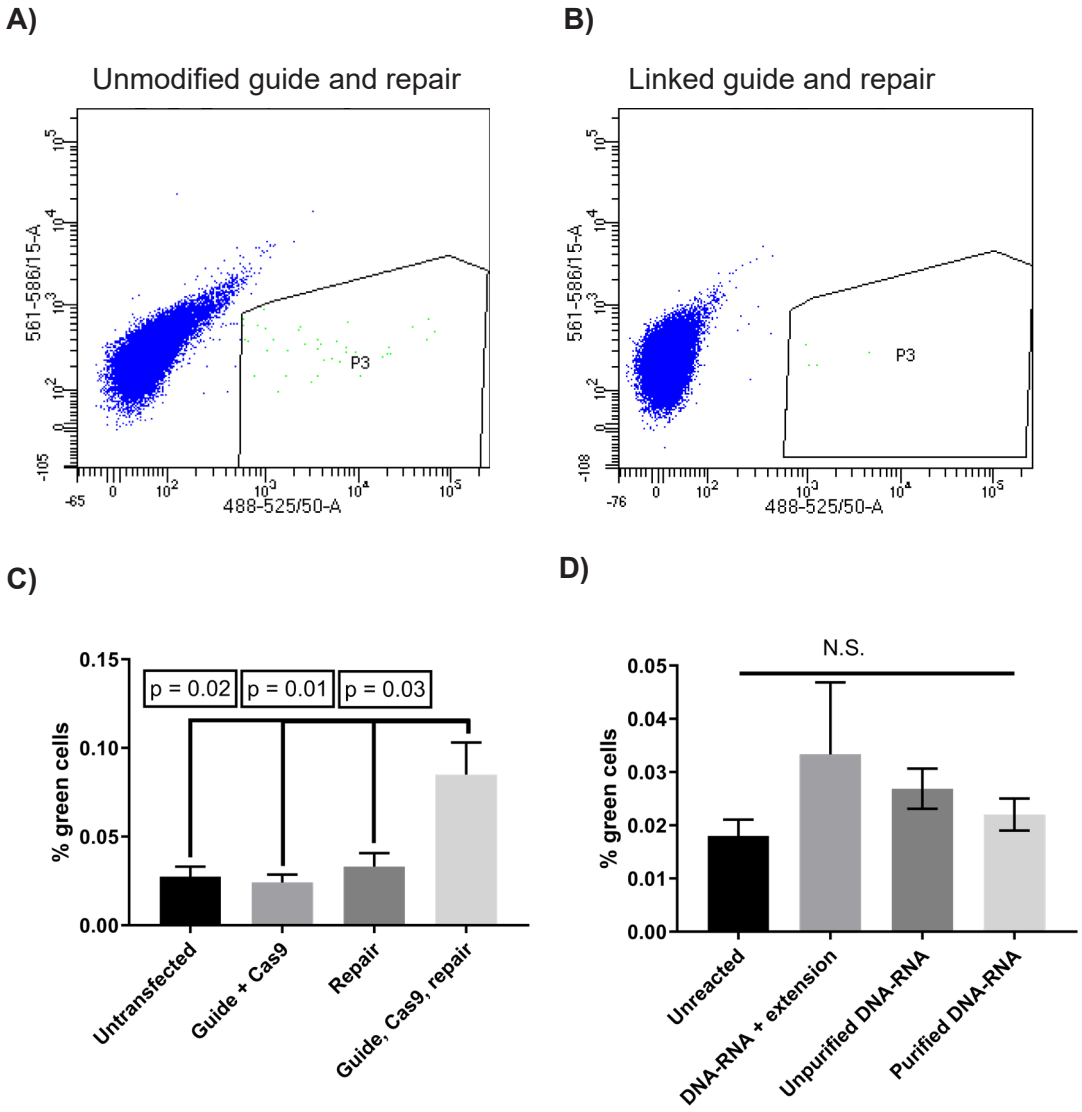

Figure 5.5 Testing the effect of covalently linked guide and repair template on HDR

A) This FACS plot shows EGFP^{68A} cells which have been transfected with Cas9, guide RNA and ssODN repair template, green fluorescence is measured on the X axis and blue is on the Y (for cell viability). Each dot is a cell and the green gated population (P3) represents the GFP positive cells, in this sample 0.08% of the living single cells are GFP positive.
B) The plot shows the EGFP^{68A} cells which have been transfected with Cas9 and covalently linked guide RNA and repair DNA, the percentage of green cells is lower at 0.03%.
C) This graph shows the results of control transfections of EGFP^{68A} cells, including the one analysed in the FACS plot in A). The cells transfected with guide RNA, Cas9 protein and single stranded DNA repair template had significantly more green cells as a percentage of the total than the cells transfected with each component separately, according to one way ANOVA and Dunnett's multiple comparisons.
D) No significant increase in the percentage of GFP positive cells was observed when comparing linked RNA-DNA complexes to the unlinked complexes, according to one way ANOVA and Dunnett's multiple comparisons.

5.5 An AAV based approach to increase the efficiency of HDR by tethering of the repair template to Cas9.

Adeno-associated virus (AAV) is a common vector used for delivery of DNA *in vivo*. It consists of a viral capsid and single stranded DNA genome that expresses two genes Cap, which encodes the capsid subunits VP1 to VP3 and *Rep*, encoding the 4 replication proteins Rep78, Rep68, Rep52 and Rep40. The genome is enclosed by T shaped inverted terminal repeats (ITRs) which are recognised by the cell's DNA synthesis machinery and used as primers to synthesise complementary DNA, reviewed in (Wang, Tai, and Gao 2019). It was shown that Rep78's N terminal 244 amino acids is sufficient to bind to the ITRs of the AAV genome and is what mediates its integration into the *AAVS1* site in the human genome (Cathomen, Collete, and Weitzman 2000). It was also shown that the fusion of this protein domain to transposases increased the efficiency of transposition into the *AAVS1* site up to 15 fold (Ammar et al. 2012).

Given that AAV is one of the most commonly used vectors for gene therapy and is targeted to the nucleus it is likely to be a good method for the delivery of repair template DNA for genome editing. If the Cas9 nuclease fused to Rep78's N-terminal domain could bind and deliver the repair template to the target site it might increase the efficiency of specific repair. This fusion protein is shown binding to the ITRs of an AAV genome containing the Histone 2B GFP repair template in **Figure 5.6 A)**. The linker which attaches the Rep78 N terminal domain to the C terminus of the Cas9 protein was used previously to make a Cas9-RFP fusion (Mircetic et al. 2017).mTmG MEFs were transfected with the Cas9-Rep78 fusion and wild type Cas9, then transduced with the Histone 2B repair template in an AAV2/2 vector. The results show that fusion of Cas9 to Rep78 increases the efficiency of HDR with an AAV based repair template by approximately 30% but not enough to be statistically significant, **Figure 5.6 B)**. Indicating that this increase is most likely due to random variation than Cas9-Rep78. The potential reasons for Cas9-Rep78 having no significant effect are discussed below in **Section 5.6**.

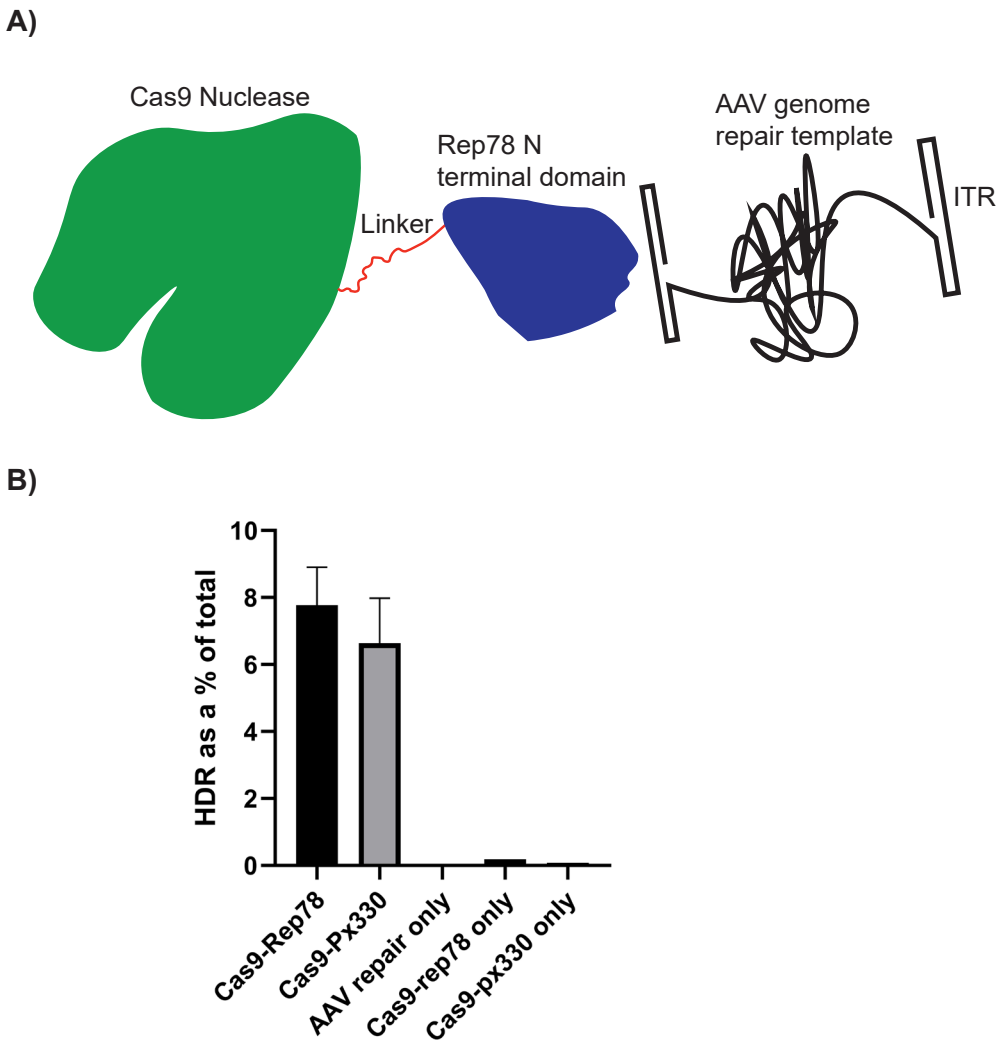

Figure 5.6 Testing the effect of Cas9-rep78 on AAV mediated repair

A) The diagram shows Cas9 *S.p.* (green) fused to the N terminal 244 amino acids of the AAV2/2 Rep78 protein (blue) via a linker sequence (red). The Rep78 protein is then shown binding to the AAV genome (black), specifically to the ITRs which flank the homologous repair sequence.
B) The bar chart compares HDR, measured as green nuclei by imaging, as a percentage of the total of non-red fluorescent cells (as measured by FACS) between cells transfected with unmodified Cas9 (Cas9-px330) and Cas9-Rep78. No significant difference is found when testing with a two-tailed student's T test. n = 5 replicates for the test samples, n = 1 for negative controls.

5.6 Discussion

In this chapter, two methods of linking the Cas9 nuclease editing complex to the DNA repair template were used to try to improve the efficiency of HDR. The first method trialled, the covalent linkage of the guide RNA with the repair DNA, did not improve the efficiency of HDR. However, it's possible that the fluorescent reporter system developed to test this was not functioning correctly when this was tested. This is evidenced by the much reduced percentage of GFP positive cells in samples transfected with the unmodified guide repair DNA than those transfected with modified DNA and RNA. This could have been due to the effect of the modifications on the function of the guide RNA or on the DNA repair template, however this is unlikely to be the case given that there seemed to be no adverse effect of these modifications in the original publication (Lee et al. 2017). The azide group was attached at the 3' end of the tracrRNA portion of the single guide RNA here, differing from previously published work which tethered at the 5' end of crRNA, however this would not be expected to make a difference as altering the 3' tail of the tracrRNA or sgRNA does not seem to effect its ability to mediate Cas9 cleavage (Cheng et al. 2016).

The baseline level of editing in the EGFP alanine 68 reporter system was also a potential source of failure to report change as the level of editing was not consistent between experiments. It was also much lower than other reporter systems in HEK 293 cells, such as the BFP to EGFP reporter system which showed approximately 17% conversion of BFP to EGFP (Lee et al. 2017) compared to less than 0.1% in the EGFP alanine 68 reporter system. This suggests that the locus was not very amenable to editing or HDR.

While no change in HDR could be demonstrated using these methods it was encouraging that the efficiency of the Click reaction could be increased by using splinting to bring the nucleic acids together. Using this optimised method the yield of the final RNA-DNA product was increased from 60% to 81% which is over double that reported in previous publications (Lee et al. 2017). As suggested earlier covalent linkage of the guide RNA and DNA may have increased the efficiency of HDR but it was undetectable using the reporter system developed, **Figure 5.2**. The same experiment was tried with the BFP to EGFP reporter system, however the linkage of sgRNA and repair DNA for the BFP to EGFP (data not shown)

sequences could not be achieved. It's unclear why it was not possible to link the nucleic acids, it's possible it could be due to errors in synthesis of the constituents.

The second method to attach the Cas9 editing complex to the repair template DNA by fusion of Cas9 to Rep78 is a novel approach. However, it did not seem to result in any increase to the efficiency of HDR. This could be because the AAV replication proteins act as a hetero tetramer and as such Rep78 requires the other three subunits. Indeed, making the Rep78 N-terminal domain tetrameric was suggested to improve its ability to bind to the ITRs of the AAV genome (Cathomen, Collete, and Weitzman 2000). A new Cas9-Rep78 with a tetramerization domain is currently being made and tested for its ability to improve HDR efficiency with AAV mediated repair. If successful this method is directly applicable to genome editing therapy and only requires modification of the Cas9 nuclease and use of an AAV vector, which is already widely used for gene editing repair.

The effect of small molecules on the CRISPR mediated editing observed in **Section 5.3** did not recapitulate the increase in HDR efficiency shown in the published literature. Some publications agree with these findings: Scr7 does not increase HDR in certain cell types (Yang et al. 2016; Song et al. 2016; Zhang et al. 2017) and similarly one study showed L755,501 and RS-1 do not affect the efficiency of HDR (Zhang et al. 2017). While there was no effect on the HDR efficiency as observed in the experiment with three replicates, there was an effect on the DNA repair pathways of transfected cells when using Nu7441 and Brf-A. The increase in GFP positive cells observed with the treatment of Nu7441 points towards a potential increase in GFP positive nuclei. However, the increase in percentage of GFP positive cells in FACS measurements (4%) cannot be explained by what was observed in the previous experiment for the increase in HDR seen with Nu7441, only a ~0.3% increase. There was also a large increase in the number of non-fluorescent cells suggesting that Nu7441 may have promoted large deletions or insertions causing loss of fluorescence. If the NHEJ pathway was inhibited by Nu7441, as is predicted by its mechanism of action and by the decrease in HITI induced BFP positive cells, then its possible alternative DSB DNA repair pathways could have been employed. Blocking NHEJ using the DNA-PKCs inhibitor Wortmannin was shown to increase the levels of Microhomology Mediated End Joining (MMEJ) (Sharma et al. 2015). It's unclear why this would result in the increased loss of fluorescence or gain of GFP expression, it's possible that the

homology present in the HDR template resulted in it being ligated directly to the 5' of Tomato which would destroy the guide site and push the Tomato gene out of frame. However, without deep sequencing of the treated cells the exact editing outcomes cannot be determined. As for the increase in the double positive and decrease in all other populations in the Brf-A treated cells it's possible that Brf-A sensitised the cells to DSBs, as there was an increase in cell death in these cells after transfection. Potentially the more transformed polyploid cells were better able to survive this sensitisation and could escape DNA damage induced death, however without knowing Brf-A's mechanism of action on DNA repair it is hard to conclude the reason for these results. It is likely that the failure to increase HDR efficiency using these small molecules lies in the differences between the cell types and reporter systems used. To investigate this more fully it would be necessary to try different cell types from the mTmG reporter and compare the effects, however this is beyond the scope of this project.

6 Conclusions and future directions

6.1 *SNAP-Dnah5* mice as part of a new motile ciliated toolset

The research described in **Chapter 4** demonstrates the effectiveness of endogenous gene tagging with an adaptable protein tag. The techniques employed to accomplish this result are particularly important for use with dynein heavy chains, which are often too large to for transient gene expression and transgenesis. As such, most tagging studies have focused on the much more manageably sized intermediate chains, which are often essential for the assembly of axonemal dynein (AD) complexes. However, it is the heavy chains which seem to require the most assistance for assembly and function (King 2016). Therefore, using fusion tags to pull down these massive proteins will help identify many of the components involved in assembly of the ADs. Isolated AD complexes could also be used for structural analysis using high resolution cryogenic electron microscopy, providing details about different dynein complexes during their trafficking, pre-assembly and axoneme docked forms.

While it was not possible to conclusively identify DNAH5 interactors in the immunoprecipitation reactions shown in **Chapter 4** (**Figure 4.7**)**,** further optimisation continues to help to identify more interactors. As discussed in **Section 4.5,** a potential way to improve these pulldowns would be to add benzylguanine-modified biotin to the cells, thereby covalently labelling the SNAP-DNAH5 protein with biotin. This approach has been used before to pulldown SNAP-tagged proteins in cell lines (Siwek et al. 2018) and will remove any non-specific interactors of the SNAP antibodies which may be hindering the current experiments. Biotinylation of SNAP-tagged flagella proteins has also been used for Cryo-EM to study the structure of nexin dynein regulatory complexes *in situ* in the axoneme (Song et al. 2015). Preliminary results from streptavidin pulldown of biotin labelled SNAP-DNAH5 suggest this approach does work. However, results from these pulldowns need further analysis by mass spectrometry to assess whether streptavidin biotin pulldowns give a better enrichment for DNAH5 and may confirm the interactors in **Figure 4.7**.

While using the SNAP tag to pulldown SNAP-DNAH5 was at least partially successful and will be improved through optimisation, this was not the case for live imaging of SNAP-DNAH5. Despite SNAP-DNAH5 being labelled in live cultured cells with cell permeable fluorescent dyes which could be imaged after fixation, no

fluorescence could be seen in the *SNAP-Dnah5* live cells. This is in contrast to live imaging of *PCM1*^{SNAP} cells, suggesting it is not the chemistry or dyes themselves that are precluding the imaging. It is more likely to be something specific to the MTECs and/or how they are cultured. For example, it could be due to the rapid movement of the cilia in live culture, reducing the time that each position is exposed to the imaging laser. Additionally, imaging SNAP-DNAH5 in the cytoplasm of mTEC cultures was particularly challenging, as the membrane they grow on is highly auto-fluorescent which makes cytoplasmically localised DNAH5 hard to detect. These problems are mainly due to the brightness of the fluorescent dyes, or low 'signal-to-noise' when used live. It is possible that with further optimisation of the imaging and staining protocols these issues could be overcome. An alternative solution would be to use primary cells from the *GFP-Dnah11* mouse to optimise live imaging of tagged ADs (McGrath et al. 2003). The advantage of using *GFP-Dnah11* is that it does not rely on the addition of dyes for fluorescence and therefore reduces the number of variables that need to be optimised for live cell imaging. If it is possible to image GFP-DNAH11 in live cells, then the same conditions could be used for SNAP-DNAH5 imaging, allowing the concentration and incubation time of the fluorescent dye to be optimised independently of other variables.

The advantage of being able to track the movement of AD components live in motile ciliated cells was demonstrated by recent research which used fluorescently tagged DNAAFs and dynein intermediate chains to show that these factors are concentrated in cytoplasmic phase separated dynein assembly particles (DynAPs) (Huizar et al. 2018). The limitation of this study was that these genes were overexpressed which may result in erroneous interactions and force the proteins to phase separate. However, if these results could be recapitulated with endogenously tagged proteins it would reinforce their findings. It would also be interesting to compare the localisation of two different heavy chains which are both part of the same complex yet have different requirements for DNAAFs (Dougherty et al. 2016). It might be that DNAH11 is recruited to the axoneme independently of DNAH5 as part of another complex, being able to identify the interactors of both proteins via pulldown and mass spectrometry would help to identify these complexes. The combination of the existing *GFP-Dnah11* mouse and the newly created *SNAP-Dnah5* line will help to define how mammalian cells are able to recognise a diverse array of dynein heavy chains, where they are assembled into

dynein arms and how they are trafficked into distinct regions of the axoneme. It is likely that each β-DHC of the ODA has its own adaptor for transport or docking, these could be identified using the methods described with not only DNAH5 and DNAH11 (proximal) but also DNAH9 (distal).

Therefore further endogenous tagging of the AD components will help to uncover the complex mechanisms underlying the assembly and regulation of these molecular machines.

6.2 Learning from failure: a potential application for high throughput endogenous tagging in immortalised cell lines

It is clear that the initial objective to create a library of endogenously tagged genes in different fly lines did not succeed, however the methodology was shown to work in immortalised mammalian cell lines, see **Chapter 3**. As such a similar approach for the primary cilia and centriolar proteome might prove useful in primary ciliated cells. Fluorescently tagged centriolar proteins have already given the field valuable insights into how centriole length is maintained in fly embryos (Aydogan et al. 2018). Similarly a transgenic tricistronic fluorescent Arl13b and the Fucci system (Sakaue-Sawano et al. 2008) have provided a way to link dynamic processes such as ciliogenesis and the cell cycle (Ford et al. 2018). Therefore tagged proteins are a valuable tool to investigate the fundamental mechanisms involved in the formation and function of primary cilia and centrioles.

The *PCM1*^{SNAP} HEK 293 cell line could be used for similar purposes as the *SNAP-Dnah5* mouse cells, namely to isolate centriolar satellites and identify interactors, although this was recently done (Gheiratmand et al. 2019; Quarantotti et al. 2019). The turnover of these proteins could also be measured in the same 'pulse-chase' manner as described in **Chapter 4**. This would demonstrate whether PCM1 really is the stable scaffold of centriolar satellites or if it has a more transitory role. This could also be used to investigate whether distinct populations of centriolar satellites with differing stability exist. However, although HEK 293 cells are a robust cell line and are amenable to genetic manipulation they have an abnormal karyotype (Stepanenko and Dmitrenko 2015). Therefore tagging PCM1 in a more physiologically relevant cell line, such as h-TERT immortalised RPE-1 cells (Bodnar et al. 1998), would provide more relevant information. Similarly live cell imaging could be more easily achieved in cells using a bright fluorescent tag, which with the generic tagging strategy is easy to change (Lackner et al. 2015). An

interesting possibility would be to observe the movement of PCM1 in relation to ciliogenesis as it has been suggested that the centriolar satellites are important for this process (Hori and Toda 2016). This could be achieved via endogenous tagging of PCM1 in the already established Arl13b Fucci cells. While PCM1 is an important part of centriolar satellites it would also be useful to be able to track the movement of other proteins in the cell as well. Tagging centriole and cilia associated proteins would further help delineate when and where satellites interact with these structures.

High throughput endogenous tagging could also be applied to the various IFT complex proteins to help define what their interactors are as well as to observe where they are localised and when they are expressed. Although much of this has already been achieved with overexpression studies the use of endogenous tagging reduces the level of background interactions.

While the high throughput strategy employed proved ineffective for tagging fly embryos, it may yet be applicable for studying cilia related processes in immortalised cell lines by creating a library of tagged genes.

6.3 The role of translation in regulating the axonemal dyneins

As previously discussed in **Chapter 4**, translational regulation of large heavy chain dyneins is a way in which motile ciliated cells might control how many ADs they produce. It is clear from the results shown in **Chapter 4** that the AD heavy chains are still being produced at least 28 days after the initiation of differentiation in mTECs, indicating that translation happens over a long period of time. This is in contrast to the levels of the transcript which appear to remain relatively low (Plasschaert et al. 2018; Montoro et al. 2018), **Figure 4.8**. The low number of *Dnah5* transcripts could be a result of their unusual length, 268,300 bp, which would take approximately ~45 minutes to transcribe at the fastest estimated transcription speed of a single RNA polymerase II (RNAP II) (Jonkers and Lis 2015). Splicing at the 79 exons present and nuclear export would also contribute to the time taken to produce the *Dnah5* mRNA. Therefore it's possible that the cell makes a few transcripts which are then highly translated in the cytoplasm by polysomes. The storage of mRNA for later translation is conducted by liquid-liquid phase separated organelles such as stress granules and processing bodies (P-bodies). Stress granules are a molecular response to sudden stresses such as

heat-shock, they consist of stalled pre-initiation complexes and a variety of RNA binding proteins. In contrast, the P-bodies consist of free mRNAs and RNA binding proteins, some of which are shared with stress granules (Ivanov, Kedersha, and Anderson 2019). The localisation of the *Dnah5* transcript in motile ciliated mouse cells in large clusters suggests they are being sequestered deliberately. However, without further analysis of the protein composition of these clusters it is unclear whether these are cytoplasmic granules, polysomes (i.e. translation factories) or something else. The results of the SNAP-DNAH5 pulldown, **Figure 4.7**, do suggest an interaction with ALKBH5, the m^6A demethylase. Recent studies have suggested that demethylation of certain mRNAs can result in their sequestration into stress granules by G3BP1 and G3BP2, which ensures their stability (Edupuganti et al. 2017). G3BP1 has been shown to co-localise with DNAAFs and dynein subunits in DynAPs (Huizar et al. 2018), combined with the interaction between DNAH5 and ALKBH5 this suggests there could be active regulation of translation complexes. Furthermore isolation of P-bodies and profiling of their mRNA suggests that longer transcripts, such as *Dnah5*, are preferentially recruited here (Hubstenberger et al. 2017).

The methodology used by Hubstenberger et al. could be used to isolate cytoplasmic granules containing the axonemal dynein proteins. In this study they used a fluorescently tagged protein component of P-bodies and isolated all fluorescent granules from cells that were of a certain size. If the axonemal dyneins are in liquid-liquid phase separated granules such as P-bodies then this approach may allow for their isolation and characterisation by mass spec and RNA sequencing.

In conclusion, the smRNA FISH evidence demonstrates an unusual clustering of few *Dnah5* transcripts in mTECs and preliminary IP interaction studies suggest there may be translational control by ALKBH5. However, the findings of this project need to be validated with analysis of additional pulldowns and imaging of DNAAFs, DNAH5 and translational regulation proteins simultaneously with the *Dnah5* transcripts in motile ciliated cells.

6.4 Axonemal dynein turnover and the relevance to PCD genome editing therapy

The pulse-chase experiments shown in **Chapter 4** demonstrate the remarkable stability of the SNAP conjugated dyes and of DNAH5 in the axoneme. This is the

first study to investigate the turnover of AD proteins in the mammalian cilia; it suggests that there may be low levels of turnover. The replacement of ODAs along the length of the mature axoneme is consistent with findings from other organisms (Piperno, Mead, and Henderson 1996; Stephens 1997; Viswanadha et al. 2014; Dai et al. 2018). However, as discussed in **Chapter 4** the incubation times need to be increased to assess whether there really is replacement of DNAH5 on the axoneme. It is expected that the DNAH5 proteins stained with the initial dye would eventually be completely replaced by the newly synthesised protein if there is turnover of these complexes. In a scenario where this is the case it would be interesting to see whether this is due to continual transcription of the AD subunits or if it comes from translation of existing transcripts, which would lend weight to the sequestration model proposed in the previous section.

The pulse-chase assessment of turnover indicates that any therapeutic rescue of ODA assembly in mature ciliated mTECs would not result in their large scale docking onto the axoneme for at least 32 days but probably much longer. However, as previously discussed in **Section 4.5**, the situation may be different in an axoneme devoid of ODAs to begin with. Therefore to assess the feasibility of genome editing directed at mature ciliated cells in PCD patients the cells could be treated with DM-CHX to prevent assembly of ADs for varying periods of time. The DM-CHX inhibits AD formation but allows the cilia to form without them. This would better reflect the mixed population of mature and maturing cells within the respiratory epithelium. While it would be good to be able to correct mutations in the mature ciliated epithelial population, which makes up ~50% of the airways, these cells do not have an indefinite lifespan, with the respiratory epithelium being replaced every 30 to 50 days (Bowden 1983; Rawlins et al. 2007). The rate of replacement may be even faster in PCD patients where cycles of chronic infection and inflammation lead to areas of the epithelial layer being damaged (Look et al. 2001). For a lasting cure, the optimal target cell type for genome editing is the basal (stem cell) population in the airway epithelium which replenishes the ciliated cells (Boers, Ambergen, and Thunnissen 1998). Gene correction in these cycling cells would help to ensure that rescue would be permanent, as long as the pool of corrected cells remained actively cycling. In addition to the reduced usefulness of a strategy that targets the mature ciliated cells it would also be more difficult to achieve because they are differentiated and have very low levels of HDR.

Measuring the effectiveness of any genome editing in the restoration of the ODAs could be done by assessing the restoration of axonemally localised SNAP-DNAH5 fluorescence in treated mTECs. It could be used to optimise the best approach to genome editing specifically aimed at PCD mutations affecting ODAs in the same way as the existing fluorescent reporter systems discussed in **Chapter 5,** reducing the variability and cost associated with immunofluorescence for dynein antibodies. However, this would be more effective if the fluorescence was seen in live cells because rescue could be assessed more immediately than in fixed cells.

6.5 Engineering Cas proteins for better genome editing

As was explained in **Chapter 5,** the CRISPR/Cas system has been altered in many ways to improve its ability to make specific changes in mammalian genomes. One approach has been to rationally design Cas9 fusions which perform in more desirable ways, for example to improve HDR (Rees, Yeh, and Liu 2019; Savic et al. 2018; Gu, Posfai, and Rossant 2018; Aird et al. 2018) or to convert single bases through chemical modification (Komor et al. 2016). The Cas9-Rep78 fusion protein designed in this project would be another example of these rationally designed molecules. The advantage of this Cas9 fusion being that it is designed to work in conjunction with a commonly used gene therapy vector and therefore has immediate applicability to therapeutic genome editing. However, further optimisation is required to increase the efficiency of HDR in this system. Despite the number of rationally designed Cas9 nucleases constantly increasing they are still reliant on the use of Cas9 as an intact unit to recognise the guide RNAs and target them to the correct place in the genome, even if the nuclease domains are not required (Komor et al. 2016). This represents an area which could be further optimised to reduce the size of vectors and make any protein targetable to a specific position in the genome via fusion of the minimal RNA targeting domain.

While researchers have been attempting to rationally design a Cas nuclease which is able to mediate efficient and targeted gene therapy it has been discovered that a similar system may already exist (Klompe et al. 2019). In this study they found that a bacterial transposon, Tn6677, can use the CRISPR/Cas system of *E. coli* to insert itself into the genome. Furthermore this system can be altered to insert other sequences at different locations and does so with high levels of efficiency, ~52%. Therefore it may be useful for future gene therapy applications such as gene

replacement or HITI. However, it will also need to be simplified to reduce the number of factors involved and optimised for use in mammals.

The potential for the CRISPR/Cas systems to revolutionise the treatment of genetic disorders such as PCD is huge and it is clear that there is still a lot to discover and much optimisation to be done.

6.6 Concluding remarks

This project has uncovered some hitherto unknown aspects of the dynein heavy chain DNAH5, such as where its transcripts localise in the cytoplasm, the rate at which it docks onto the axoneme and how long it stays there. This work has also helped to establish the use of a universal tagging strategy that will be useful to this lab for future studies. Furthermore the creation of the *SNAP-Dnah5* mouse line will provide useful information about motile cilia biology and adds to the list of endogenously tagged dynein genes available. The repertoire of attempted Cas9 fusion proteins also has a new addition with the creation of Cas9-Rep78, which will hopefully prove to be useful in the development of genome editing therapy for PCD.

While many more experiments are required to validate these preliminary results, this project has laid the groundwork for these investigations, which ask broader questions about how intricate molecular complexes are regulated and assembled.

7 Bibliography

Adams, G M, Bessie Huang, and D J Luck. 1982. “Temperature-Sensitive, Assembly-Defective Flagella Mutants of Chlamydomonas Reinhardtii.” *Genetics* 100 (4): 579–57986.

Adams, Stephen R., Robert E. Campbell, Larry A. Gross, Brent R. Martin, Grant K. Walkup, Yong Yao, Juan Llopis, and Roger Y. Tsien. 2002. “New Biarsenical Ligands and Tetracysteine Motifs for Protein Labeling in Vitro and in Vivo: Synthesis and Biological Applications.” *Journal of the American Chemical Society* 124 (21): 6063–76. https://doi.org/10.1021/ja017687n.

Afzelius, Bjorn A., and Unne Stenram. 2006. “Prevalence and Genetics of Immotile-Cilia Syndrome and Left-Handedness.” *International Journal of Developmental Biology* 50 (6): 571–73. https://doi.org/10.1387/ijdb.052132ba.

Afzelius, Björn A. 1976. “A Human Syndrome Caused by Immotile Cilia.” *Science* 193 (4250): 317–19. https://doi.org/10.1126/science.1084576.

Agard, Nicholas J., Jennifer A. Prescher, and Carolyn R. Bertozzi. 2004. “A Strain-Promoted [3 + 2] Azide-Alkyne Cycloaddition for Covalent Modification of Biomolecules in Living Systems.” *Journal of the American Chemical Society* 126 (46): 15046–47. https://doi.org/10.1021/ja044996f.

Ahmed, Iltaf, Kirti Mittal, Taimoor I. Sheikh, Nasim Vasli, Muhammad Arshad Rafiq, Anna Mikhailov, Mehrnaz Ohadi, et al. 2014. “Identification of a Homozygous Splice Site Mutation in the Dynein Axonemal Light Chain 4 Gene on 22q13.1 in a Large Consanguineous Family from Pakistan with Congenital Mirror Movement Disorder.” *Human Genetics* 133 (11): 1419–29. https://doi.org/10.1007/s00439-014-1475-8.

Ahmed, Noveera T, Chunlei Gao, Ben F Lucker, Douglas G Cole, and David R Mitchell. 2008. “ODA16 Aids Axonemal Outer Row Dynein Assembly through an Interaction with the Intraflagellar Transport Machinery.” *Journal of Cell Biology* 183 (2): 313–22. https://doi.org/10.1083/jcb.200802025.

Ahmed, Noveera T, and David R Mitchell. 2005. “ODA16p, a Chlamydomonas Flagellar Protein Needed for Dynein Assembly.” *Molecular Biology of the Cell* 16 (10): 5004–12. https://doi.org/10.1091/mbc.e05-07-0627.

Aird, Eric J., Klaus N. Lovendahl, Amber St. Martin, Reuben S. Harris, and Wendy R. Gordon. 2018. “Increasing Cas9-Mediated Homology-Directed Repair Efficiency through Covalent Tethering of DNA Repair Template.” *Communications Biology* 1 (1): 54. https://doi.org/10.1038/s42003-018-0054-2.

Alapati, Deepthi, William J. Zacharias, Heather A. Hartman, Avery C. Rossidis, John D. Stratigis, Nicholas J. Ahn, Barbara Coons, et al. 2019. “In Utero Gene Editing for Monogenic Lung Disease.” *Science Translational Medicine* 11 (488): eaav8375. https://doi.org/10.1126/scitranslmed.aav8375.

Alfaro-Cervello, Clara, Mario Soriano-Navarro, Zaman Mirzadeh, Arturo Alvarez-Buylla, and Jose Manuel Garcia-Verdugo. 2012. “Biciliated Ependymal Cell Proliferation Contributes to Spinal Cord Growth.” *Journal of Comparative Neurology* 520 (15): 3528–52. https://doi.org/10.1002/cne.23104.

Ammar, Ismahen, Andreas Gogol-Döring, Csaba Miskey, Wei Chen, Toni Cathomen, Zsuzsanna Izsvák, and Zoltán Ivics. 2012. “Retargeting Transposon Insertions by the Adeno-Associated Virus Rep Protein.” *Nucleic Acids Research* 40 (14): 6693–6712. https://doi.org/10.1093/nar/gks317.

Auclair, Walter, and Barry W. Siegel. 1966. “Cilia Regeneration in the Sea Urchin Embryo: Evidence for a Pool of Ciliary Proteins.” *Science* 154 (3751): 913–15. https://doi.org/10.1126/science.154.3751.913.

Auer, Thomas O., Karine Duroure, Anne De Cian, Jean Paul Concordet, and Filippo Del Bene. 2014. “Highly Efficient CRISPR/Cas9-Mediated Knock-in in Zebrafish by Homology-Independent DNA Repair.” *Genome Research* 24 (1): 142–53. https://doi.org/10.1101/gr.161638.113.

Austin-Tse, Christina, Jan Halbritter, Maimoona A. Zariwala, Renée M. Gilberti, Heon Yung Gee, Nathan Hellman, Narendra Pathak, et al. 2013. “Zebrafish Ciliopathy Screen plus Human Mutational Analysis Identifies C21orf59 and CCDC65 Defects as Causing Primary Ciliary Dyskinesia.” *American Journal of Human Genetics* 93 (4): 672–86. https://doi.org/10.1016/j.ajhg.2013.08.015.

Awata, Junya, Kangkang Song, Jianfeng Lin, Stephen M. King, Michael J. Sanderson, Daniela Nicastro, and George B. Witman. 2015. “DRC3 Connects the N-DRC to Dynein g to Regulate Flagellar Waveform.” *Molecular Biology of the Cell* 26 (15): 2788–2800. https://doi.org/10.1091/mbc.E15-01-0018.

Aydogan, Mustafa G., Alan Wainman, Saroj Saurya, Thomas L. Steinacker, Anna Caballe, Zsofia A. Novak, Janina Baumbach, Nadine Muschalik, and Jordan W. Raff. 2018. “A Homeostatic Clock Sets Daughter Centriole Size in Flies.” *Journal of Cell Biology* 217 (4): 1233–48. https://doi.org/10.1083/jcb.201801014.

Barrangou, Rodolphe, Christophe Fremaux, Hélène Deveau, Melissa Richards, Patrick Boyaval, Sylvain Moineau, Dennis A. Romero, and Philippe Horvath. 2007. “CRISPR Provides Acquired Resistance against Viruses in Prokaryotes.” *Science* 315 (5819): 1709–12. https://doi.org/10.1126/science.1138140.

Bebenek, Katarzyna, Lars C. Pedersen, and Thomas A. Kunkel. 2014. “Structure-Function Studies of DNA Polymerase λ.” *Biochemistry* 53 (17): 2781–92. https://doi.org/10.1021/bi4017236.

Bell, C. W., E. Fronk, and I. R. Gibbons. 1979. “Polypeptide Subunits of Dynein 1 from Sea Urchin Sperm Flagella.” *Journal of Supramolecular and Cellular Biochemistry* 11 (3): 311–17. https://doi.org/10.1002/jss.400110305.

Belles-Isles, M, C Chapeau, D White, and C Gagnon. 1986. “Isolation and Characterization of Dynein ATPase from Bull Spermatozoa.” *Biochemical Journal* 240 (3): 863–69. https://doi.org/10.1042/bj2400863.

Benabdi, Sarah, François Peurois, Agata Nawrotek, Jahnavi Chikireddy, Tatiana Cañeque, Takao Yamori, Isamu Shiina, et al. 2017. “Family-Wide Analysis of the Inhibition of Arf Guanine Nucleotide Exchange Factors with Small Molecules: Evidence of Unique Inhibitory Profiles.” *Biochemistry* 56 (38): 5125–33. https://doi.org/10.1021/acs.biochem.7b00706.

Benashski, Sharon E., Ramila S. Patel-King, and Stephen M. King. 1999. “Light Chain 1 from the Chlamydomonas Outer Dynein Arm Is a Leucine-Rich Repeat Protein Associated with the Motor Domain of the γ Heavy Chain.” *Biochemistry* 38 (22): 7253–64. https://doi.org/10.1021/bi990466y.

Benbahouche, Nour El Houda, Ioannis Iliopoulos, István Török, Joachim Marhold, Julien Henri, Andrey V. Kajava, Robert Farkaš, et al. 2014. “Drosophila Spag Is the Homolog of RNA Polymerase II-Associated Protein 3 (RPAP3) and Recruits the Heat Shock Proteins 70 and 90 (Hsp70 and Hsp90) during the Assembly of Cellular Machineries.” *Journal of Biological Chemistry* 289 (9): 6236–47.

https://doi.org/10.1074/jbc.M113.499608.

Bertocci, Barbara, Annie De Smet, Jean-Claude Weill, and Claude-Agnès Reynaud. 2006. “Nonoverlapping Functions of DNA Polymerases Mu, Lambda, and Terminal Deoxynucleotidyltransferase during Immunoglobulin V(D)J Recombination in Vivo.” *Immunity* 25 (1): 31–41. https://doi.org/10.1016/j.immuni.2006.04.013.

Béthune, Julien, Ralf Peter Jansen, Michael Feldbrügge, and Kathi Zarnack. 2019. “Membrane-Associated RNA-Binding Proteins Orchestrate Organelle-Coupled Translation.” *Trends in Cell Biology* 29 (2): 178–88. https://doi.org/10.1016/j.tcb.2018.10.005.

Beucher, Andrea, Julie Birraux, Leopoldine Tchouandong, Olivia Barton, Atsushi Shibata, Sandro Conrad, Aaron A. Goodarzi, Andrea Krempler, Penny A. Jeggo, and Markus Löbrich. 2009. “ATM and Artemis Promote Homologous Recombination of Radiation-Induced DNA Double-Strand Breaks in G2.” *EMBO Journal* 28 (21): 3413–27. https://doi.org/10.1038/emboj.2009.276.

Blyth, M., and D. Wellesley. 2008. “Ectopic Pregnancy in Primary Ciliary Dyskinesia.” *Journal of Obstetrics and Gynaecology* 28 (3): 358. https://doi.org/10.1080/01443610802058742.

Boch, Jens, and Ulla Bonas. 2010. “Xanthomonas AvrBs3 Family-Type III Effectors: Discovery and Function.” *Annual Review of Phytopathology* 48 (1): 419–36. https://doi.org/10.1146/annurev-phyto-080508-081936.

Boch, Jens, Heidi Scholze, Sebastian Schornack, Angelika Landgraf, Simone Hahn, Sabine Kay, Thomas Lahaye, Anja Nickstadt, and Ulla Bonas. 2009. “Breaking the Code of DNA Binding Specificity of TAL-Type III Effectors.” *Science* 326 (5959): 1509–12. https://doi.org/10.1126/science.1178811.

Bodnar, Andrea G., Michel Ouellette, Maria Frolkis, Shawn E. Holt, Choy Pik Chiu, Gregg B. Morin, Calvin B. Harley, Jerry W. Shay, Serge Lichtsteiner, and Woodring E. Wright. 1998. “Extension of Life-Span by Introduction of Telomerase into Normal Human Cells.” *Science* 279 (5349): 349–52. https://doi.org/10.1126/science.279.5349.349.

Boers, James E., Anton W. Ambergen, and Frederik B.J.M. Thunnissen. 1998. “Number and Proliferation of Basal and Parabasal Cells in Normal Human

Airway Epithelium.” *American Journal of Respiratory and Critical Care Medicine* 157 (6): 2000–2006.

Bonnefoy, Serge, Christopher M. Watson, Kristin D. Kernohan, Moara Lemos, Sebastian Hutchinson, James A. Poulter, Laura A. Crinnion, et al. 2018. “Biallelic Mutations in LRRC56, Encoding a Protein Associated with Intraflagellar Transport, Cause Mucociliary Clearance and Laterality Defects.” *American Journal of Human Genetics* 103 (5): 727–39. https://doi.org/10.1016/j.ajhg.2018.10.003.

Boon, Mieke, Kris De Boeck, Harry Cuppens, Julia Wallmeier, Niki Tomas Loges, Heike Olbrich, Gerard W. Dougherty, et al. 2014. “MCIDAS Mutations Result in a Mucociliary Clearance Disorder with Reduced Generation of Multiple Motile Cilia.” *Nature Communications* 5: 4418. https://doi.org/10.1038/ncomms5418.

Bowden, D H. 1983. “Cell Turnover in the Lung.” *American Review of Respiratory Disease* 128 (2 II Suppl.): S46-8. https://doi.org/10.1164/arrd.1983.128.2P2.S46.

Bowman, A B, R S Patel-King, S E Benashski, J M McCaffery, L S Goldstein, and S M King. 1999. “Drosophila Roadblock and Chlamydomonas LC7: A Conserved Family of Dynein-Associated Proteins Involved in Axonal Transport, Flagellar Motility, and Mitosis.” *The Journal of Cell Biology* 146 (1): 165–80. http://www.ncbi.nlm.nih.gov/pubmed/10402468.

Brokaw, C J, and R Kamiya. 1987. “Bending Patterns of Chlamydomonas Flagella: IV. Mutants with Defects in Inner and Outer Dynein Arms Indicate Differences in Dynein Arm Function.” *Cell Motility and the Cytoskeleton* 8 (1): 68–75. https://doi.org/10.1002/cm.970080110.

Brokaw, Charles J. 1994. “Control of Flagellar Bending: A New Agenda Based on Dynein Diversity.” *Cell Motility and the Cytoskeleton*. https://doi.org/10.1002/cm.970280303.

Brouns, Stan J. J., Matthijs M. Jore, Magnus Lundgren, Edze R. Westra, Rik J. H. Slijkhuis, Ambrosius P. L. Snijders, Mark J. Dickman, Kira S. Makarova, Eugene V. Koonin, and John van der Oost. 2008. “Small CRISPR RNAs Guide Antiviral Defense in Prokaryotes.” *Science* 321 (5891): 960–64.

Brow, David A., and Christine Guthrie. 1988. “Spliceosomal RNA U6 Is Remarkably

Conserved from Yeast to Mammals." *Nature* 334 (6179): 213–18. https://doi.org/10.1038/334213a0.

Buchner, Johannes, and Jing Li. 2013. "Structure, Function and Regulation of the Hsp90 Machinery." *Biomedical Journal* 36 (3): 106. https://doi.org/10.4103/2319-4170.113230.

Bukowy-Bieryłło, Zuzanna, Ewa Ziętkiewicz, Niki Tomas Loges, Mariana Wittmer, Maclej Geremek, Heike Olbrich, Manfred Fliegauf, et al. 2013. "RPGR Mutations Might Cause Reduced Orientation of Respiratory Cilia." *Pediatric Pulmonology* 48 (4): 352–63. https://doi.org/10.1002/ppul.22632.

Burgess, S a, D a Carter, S D Dover, and D M Woolley. 1991. "The Inner Dynein Arm Complex: Compatible Images from Freeze-Etch and Thin Section Methods of Microscopy." *Journal of Cell Science* 100 (2): 319–28.

Burgess, Stan A., Matt L. Walker, Hitoshi Sakakibara, Peter J. Knight, and Kazuhiro Oiwa. 2003. "Dynein Structure and Power Stroke." *Nature* 421 (6924): 715–18. https://doi.org/10.1038/nature01377.

Caggese, C., R. Moschetti, G. Ragone, P. Barsanti, and R. Caizzi. 2001. "Dtctex-1 , the Drosophila Melanogaster Homolog of a Putative Murine t-Complex Distorter Encoding a Dynein Light Chain, Is Required for Production of Functional Sperm." *Molecular Genetics and Genomics* 265 (3): 436–44. https://doi.org/10.1007/s004380000431.

Cao, Haishi, Baowei Chen, Thomas C. Squier, and M. Uljana Mayer. 2006. "CrAsH: A Biarsenical Multi-Use Affinity Probe with Low Non-Specific Fluorescence." *Chemical Communications*, no. 24: 2601–3. https://doi.org/10.1039/b602699k.

Cao, Haishi, Yijia Xiong, Ting Wang, Baowei Chen, Thomas C. Squier, and M. Uljana Mayer. 2007. "A Red Cy3-Based Biarsenical Fluorescent Probe Targeted to a Complementary Binding Peptide." *Journal of the American Chemical Society* 129 (28): 8672–73. https://doi.org/10.1021/ja070003c.

Carlson-Stevermer, Jared, Amr A. Abdeen, Lucille Kohlenberg, Madelyn Goedland, Kaivalya Molugu, Meng Lou, and Krishanu Saha. 2017. "Assembly of CRISPR Ribonucleoproteins with Biotinylated Oligonucleotides via an RNA Aptamer for Precise Gene Editing." *Nature Communications* 8 (1): 1711. https://doi.org/10.1038/s41467-017-01875-9.

Casey, Diane M, Kazuo Inaba, Gregory J Pazour, Saeko Takada, Ken-ichi Wakabayashi, Curtis G Wilkerson, Ritsu Kamiya, and George B Witman. 2003. “DC3, the 21-KDa Subunit of the Outer Dynein Arm-Docking Complex (ODA-DC), Is a Novel EF-Hand Protein Important for Assembly of Both the Outer Arm and the ODA-DC.” *Molecular Biology of the Cell* 14 (9): 3650–63. https://doi.org/10.1091/mbc.e03-01-0057.

Cathomen, T, D Collete, and M D Weitzman. 2000. “A Chimeric Protein Containing the N Terminus of the Adeno-Associated Virus Rep Protein Recognizes Its Target Site in an in Vivo Assay.” *Journal of Virology* 74 (5): 2372–82. http://www.ncbi.nlm.nih.gov/pubmed/10666268.

Certo, Michael T., Byoung Y. Ryu, James E. Annis, Mikhail Garibov, Jordan Jarjour, David J. Rawlings, and Andrew M. Scharenberg. 2011. “Tracking Genome Engineering Outcome at Individual DNA Breakpoints.” *Nature Methods* 8 (8): 671–76. https://doi.org/10.1038/nmeth.1648.

Chang, Howard H.Y., and Michael R. Lieber. 2016. “Structure-Specific Nuclease Activities of Artemis and the Artemis: DNA-PKcs Complex.” *Nucleic Acids Research*. Oxford University Press. https://doi.org/10.1093/nar/gkw456.

Chang, Howard H.Y., Nicholas R. Pannunzio, Noritaka Adachi, and Michael R. Lieber. 2017. “Non-Homologous DNA End Joining and Alternative Pathways to Double-Strand Break Repair.” *Nature Reviews Molecular Cell Biology*. Nature Publishing Group. https://doi.org/10.1038/nrm.2017.48.

Chang, Howard H.Y., Go Watanabe, and Michael R. Lieber. 2015. “Unifying the DNA End-Processing Roles of the Artemis Nuclease: Ku-Dependentartemis Resection Atbluntdnaends.” *Journal of Biological Chemistry* 290 (40): 24036–50. https://doi.org/10.1074/jbc.M115.680900.

Check, Erika. 2002. “A Tragic Setback.” *Nature*. Nature Publishing Group. https://doi.org/10.1038/420116a.

Chen, Yuxin, Muzi Zhao, Saiqun Wang, Jie Chen, Yun Wang, Qinhong Cao, Wenbin Zhou, et al. 2009. “A Novel Role for DYX1C1, a Chaperone Protein for Both Hsp70 and Hsp90, in Breast Cancer.” *Journal of Cancer Research and Clinical Oncology* 135 (9): 1265–76. https://doi.org/10.1007/s00432-009-0568-6.

Cheng, Albert W, Nathaniel Jillette, Phoebe Lee, Dylan Plaskon, Yasuhiro Fujiwara,

Wenbo Wang, Aziz Taghbalout, and Haoyi Wang. 2016. “Casilio: A Versatile CRISPR-Cas9-Pumilio Hybrid for Gene Regulation and Genomic Labeling.” *Cell Research* 26: 254–57. https://doi.org/10.1038/cr.2016.3.

Chhin, Brigitte, Didier Negre, Olivier Merrot, Jacqueline Pham, Yves Tourneur, Denis Ressnikoff, Martine Jaspers, Mark Jorissen, Francois Loïc Cosset, and Patrice Bouvagnet. 2009. “Ciliary Beating Recovery in Deficient Human Airway Epithelial Cells after Lentivirus Ex Vivo Gene Therapy.” *PLoS Genetics* 5 (3). https://doi.org/10.1371/journal.pgen.1000422.

Chih, Ben, Peter Liu, Yvonne Chinn, Cecile Chalouni, Laszlo G Komuves, Philip E Hass, Wendy Sandoval, and Andrew S Peterson. 2012. “A Ciliopathy Complex at the Transition Zone Protects the Cilia as a Privileged Membrane Domain.” *Nature Cell Biology* 14 (1): 61–72. https://doi.org/10.1038/ncb2410.

Cho, Kyeong Jee, Shin Hye Noh, Soo Min Han, Won Il Choi, Hye Youn Kim, Seyoung Yu, Joon Suk Lee, et al. 2018. “ZMYND10 Stabilizes Intermediate Chain Proteins in the Cytoplasmic Pre-Assembly of Dynein Arms.” *PLoS Genetics* 14 (3). https://doi.org/10.1371/journal.pgen.1007316.

Choksi, Semil P., Gilbert Lauter, Peter Swoboda, and Sudipto Roy. 2014. “Switching on Cilia: Transcriptional Networks Regulating Ciliogenesis.” *Development (Cambridge, England)* 141 (7): 1427–41. https://doi.org/10.1242/dev.074666.

Chu, Van Trung, Timm Weber, Benedikt Wefers, Wolfgang Wurst, Sandrine Sander, Klaus Rajewsky, and Ralf Kühn. 2015. “Increasing the Efficiency of Homology-Directed Repair for CRISPR-Cas9-Induced Precise Gene Editing in Mammalian Cells.” *Nature Biotechnology* 33 (5): 543–48. https://doi.org/10.1038/nbt.3198.

Cole, D G, D R Diener, A L Himelblau, P L Beech, J C Fuster, and J L Rosenbaum. 1998. “Chlamydomonas Kinesin-II-Dependent Intraflagellar Transport (IFT): IFT Particles Contain Proteins Required for Ciliary Assembly in Caenorhabditis Elegans Sensory Neurons.” *The Journal of Cell Biology* 141 (4): 993–1008. https://doi.org/10.1083/jcb.141.4.993.

Cong, Le, and Feng Zhang. 2014. “Genome Engineering Using Crispr-Cas9 System.” In *Chromosomal Mutagenesis: Second Edition*, 8:197–217. NIH Public Access. https://doi.org/10.1007/978-1-4939-1862-1_10.

Cox, David Benjamin Turitz, Randall Jeffrey Platt, and Feng Zhang. 2015.

"Therapeutic Genome Editing: Prospects and Challenges." *Nature Medicine*. https://doi.org/10.1038/nm.3793.

Craige, Branch, Che Chia Tsao, Dennis R Diener, Yuqing Hou, Karl Ferdinand Lechtreck, Joel L Rosenbaum, and George B Witman. 2010. "CEP290 Tethers Flagellar Transition Zone Microtubules to the Membrane and Regulates Flagellar Protein Content." *Journal of Cell Biology* 190 (5): 927–40. https://doi.org/10.1083/jcb.201006105.

Dai, Jin, Francesco Barbieri, David R. Mitchell, and Karl F. Lechtreck. 2018. "In Vivo Analysis of Outer Arm Dynein Transport Reveals Cargo-Specific Intraflagellar Transport Properties." *Molecular Biology of the Cell* 29 (21): 2553–65. https://doi.org/10.1091/mbc.e18-05-0291.

Davis, Stephanie D., Margaret Rosenfeld, Hye Seung Lee, Thomas W. Ferkol, Scott D. Sagel, Sharon D. Dell, Carlos Milla, et al. 2019. "Primary Ciliary Dyskinesia: Longitudinal Study of Lung Disease by Ultrastructure Defect and Genotype." *American Journal of Respiratory and Critical Care Medicine* 199 (2): 190–98. https://doi.org/10.1164/rccm.201803-0548OC.

Dean, Anudariya B, and David R Mitchell. 2013. "Chlamydomonas ODA10 Is a Conserved Axonemal Protein That Plays a Unique Role in Outer Dynein Arm Assembly." *Mol Biol Cell* 24 (23): 3689–96. https://doi.org/10.1091/mbc.E13-06-0310.

Dellinger, O. P. 1909. "The Cilium as a Key to the Structure of Contractile Protoplasm." *Journal of Morphology* 20 (2): 171–210. https://doi.org/10.2753/JEI0021-3624470403.

Deltcheva, Elitza, Krzysztof Chylinski, Cynthia M. Sharma, Karine Gonzales, Yanjie Chao, Zaid A. Pirzada, Maria R. Eckert, Jörg Vogel, and Emmanuelle Charpentier. 2011. "CRISPR RNA Maturation by Trans-Encoded Small RNA and Host Factor RNase III." *Nature* 471 (7340): 602–7. https://doi.org/10.1038/nature09886.

Dentler, W. L. 1980. "Structures Linking the Tips of Ciliary and Flagellar Microtubules to the Membrane." *Journal of Cell Science* VOL.42 (1): 207–20.

Dentler, W. L., and J. L. Rosenbaum. 1977. "Flagellar Elongation and Shortening in Chlamydomonas. III. Structures Attached to the Tips of Flagellar Microtubules

and Their Relationship to the Directionality of Flagellar Microtubule Assembly." *Journal of Cell Biology* 74 (3): 747–59. https://doi.org/10.1083/jcb.74.3.747.

Desai, Paurav B., Anudariya B. Dean, and David R. Mitchell. 2017. "Cytoplasmic Preassembly and Trafficking of Axonemal Dyneins." In *Dyneins: The Biology of Dynein Motors: Second Edition*, 141–61. https://doi.org/10.1016/B978-0-12-809471-6.00004-8.

DiBella, Linda M., Sharon E. Benashski, Hugo W. Tedford, Alistair Harrison, Ramila S. Patel-King, and Stephen M. King. 2001. "The Tctex1/Tctex2 Class of Dynein Light Chains." *Journal of Biological Chemistry* 276 (17): 14366–73. https://doi.org/10.1074/jbc.m011456200.

DiBella, Linda M, Oksana Gorbatyuk, Miho Sakato, Ken-ichi Wakabayashi, Ramila S Patel-King, Gregory J Pazour, George B Witman, and Stephen M King. 2005. "Differential Light Chain Assembly Influences Outer Arm Dynein Motor Function." *Molecular Biology of the Cell* 16 (12): 5661–74. https://doi.org/10.1091/mbc.e05-08-0732.

DiBella, Linda M, Miho Sakato, Ramila S Patel-King, Gregory J Pazour, and Stephen M King. 2004. "The LC7 Light Chains of Chlamydomonas Flagellar Dyneins Interact with Components Required for Both Motor Assembly and Regulation." *Molecular Biology of the Cell* 15 (10): 4633–46. https://doi.org/10.1091/mbc.e04-06-0461.

Dick, T, K Ray, H K Salz, and W Chia. 1996. "Cytoplasmic Dynein (Ddlc1) Mutations Cause Morphogenetic Defects and Apoptotic Cell Death in Drosophila Melanogaster." *Molecular and Cellular Biology* 16 (5): 1966–77. https://doi.org/10.1128/mcb.16.5.1966.

Diggle, Christine P., Daniel J. Moore, Girish Mali, Petra zur Lage, Aouatef Ait-Lounis, Miriam Schmidts, Amelia Shoemark, et al. 2014. "HEATR2 Plays a Conserved Role in Assembly of the Ciliary Motile Apparatus." *PLoS Genetics* 10 (9). https://doi.org/10.1371/journal.pgen.1004577.

Dirksen, Ellen Roter, and Peter Satir. 1972. "Ciliary Activity in the Mouse Oviduct as Studied by Transmission and Scanning Electron Microscopy." *Tissue and Cell* 4 (3): 389–403. https://doi.org/10.1016/S0040-8166(72)80017-X.

Doan, Phuong, Anzhelika Karjalainen, Jerome G. Chandraseelan, Ossi Sandberg,

Olli Yli-Harja, Tomi Rosholm, Robert Franzen, Nuno R. Candeias, and Meenakshisundaram Kandhavelu. 2016. “Synthesis and Biological Screening for Cytotoxic Activity of N-Substituted Indolines and Morpholines.” *European Journal of Medicinal Chemistry* 120 (10): 296–303. https://doi.org/10.1186/gb-2006-7-10-r100.

Doench, John G, Nicolo Fusi, Meagan Sullender, Mudra Hegde, Emma W Vaimberg, Katherine F Donovan, Ian Smith, et al. 2016. “Optimized SgRNA Design to Maximize Activity and Minimize Off-Target Effects of CRISPR-Cas9.” *Nature Biotechnology* 34 (2): 184–91. https://doi.org/10.1038/nbt.3437.

Dong, Fenglan, Kyosuke Shinohara, Yanick Botilde, Ryo Nabeshima, Yasuko Asai, Akemi Fukumoto, Toshiaki Hasegawa, et al. 2014. “Pih1d3 Is Required for Cytoplasmic Preassembly of Axonemal Dynein in Mouse Sperm.” *Journal of Cell Biology* 204 (2): 203–13. https://doi.org/10.1083/jcb.201304076.

Doudna, Jennifer A, Emmanuelle Charpentier, S. Scherer, R. W. Davis, Y. S. Rong, K. G. Golic, O. Smithies, et al. 2014. “Genome Editing. The New Frontier of Genome Engineering with CRISPR-Cas9.” *Science* 346 (6213): 1258096. https://doi.org/10.1126/science.1258096.

Dougherty, Gerard W., Niki T. Loges, Judith A. Klinkenbusch, Heike Olbrich, Petra Pennekamp, Tabea Menchen, Johanna Raidt, et al. 2016. “DNAH11 Localization in the Proximal Region of Respiratory Cilia Defines Distinct Outer Dynein Arm Complexes.” *American Journal of Respiratory Cell and Molecular Biology* 55 (2): 213–24. https://doi.org/10.1165/rcmb.2015-0353OC.

Duquesnoy, Philippe, Estelle Escudier, Laetitia Vincensini, Judy Freshour, Anne Marie Bridoux, André Coste, Antoine Deschildre, et al. 2009. “Loss-of-Function Mutations in the Human Ortholog of Chlamydomonas Reinhardtii ODA7 Disrupt Dynein Arm Assembly and Cause Primary Ciliary Dyskinesia.” *American Journal of Human Genetics* 85 (6): 890–96. https://doi.org/10.1016/j.ajhg.2009.11.008.

Duriez, B., P. Duquesnoy, E. Escudier, A.-M. Bridoux, D. Escalier, I. Rayet, E. Marcos, A.-M. Vojtek, J.-F. Bercher, and S. Amselem. 2007. “A Common Variant in Combination with a Nonsense Mutation in a Member of the Thioredoxin Family Causes Primary Ciliary Dyskinesia.” *Proceedings of the National Academy of Sciences* 104 (9): 3336–41.

https://doi.org/10.1073/pnas.0611405104.

Dutcher, Susan K. 1995. “Flagellar Assembly in Two Hundred and Fifty Easy-to-Follow Steps.” *Trends in Genetics*. https://doi.org/10.1016/S0168-9525(00)89123-4.

Edupuganti, Raghu R., Simon Geiger, Rik G.H. Lindeboom, Hailing Shi, Phillip J. Hsu, Zhike Lu, Shuang Yin Wang, et al. 2017. “N6-Methyladenosine (M6A) Recruits and Repels Proteins to Regulate MRNA Homeostasis.” *Nature Structural and Molecular Biology* 24 (10): 870–78. https://doi.org/10.1038/nsmb.3462.

Edwards, Beatrice Freya Lucy, Richard John Wheeler, Amy Rachel Barker, Flávia Fernandes Moreira-Leite, Keith Gull, and Jack Daniel Sunter. 2018. “Direction of Flagellum Beat Propagation Is Controlled by Proximal/Distal Outer Dynein Arm Asymmetry.” *Proceedings of the National Academy of Sciences of the United States of America* 115 (31): E7341–50. https://doi.org/10.1073/pnas.1805827115.

Eenjes, Evelien, Tinne C.J. Mertens, Marjon J. Buscop-Van Kempen, Yolanda Van Wijck, Christian Taube, Robbert J Rottier, and Pieter S Hiemstra. 2018. “A Novel Method for Expansion and Differentiation of Mouse Tracheal Epithelial Cells in Culture.” *Scientific Reports* 8 (1): 7349. https://doi.org/10.1038/s41598-018-25799-6.

Elgeti, J., and G. Gompper. 2013. “Emergence of Metachronal Waves in Cilia Arrays.” *Proceedings of the National Academy of Sciences* 110 (12): 4470–75. https://doi.org/10.1073/pnas.1218869110.

Espindola, Foued S., Daniel M. Suter, Leticia B.E. Partata, Tracy Cao, Joseph S. Wolenski, Richard E. Cheney, Stephen M. King, and Mark S. Mooseker. 2000. “The Light Chain Composition of Chicken Brain Myosin-Va: Calmodulin, Myosin-II Essential Light Chains, and 8-KDa Dynein Light Chain/PIN.” *Cell Motility and the Cytoskeleton* 47 (4): 269–81. https://doi.org/10.1002/1097-0169(200012)47:4<269::AID-CM2>3.3.CO;2-7.

Failly, M, L Bartoloni, a Letourneau, a Munoz, E Falconnet, C Rossier, M M de Santi, et al. 2009. “Mutations in DNAH5 Account for Only 15% of a Non-Preselected Cohort of Patients with Primary Ciliary Dyskinesia.” *Journal of*

Medical Genetics 46 (4): 281–86. https://doi.org/10.1136/jmg.2008.061176.

Fassad, Mahmoud R., Amelia Shoemark, Pierrick le Borgne, France Koll, Mitali Patel, Mellisa Dixon, Jane Hayward, et al. 2018. “C11orf70 Mutations Disrupting the Intraflagellar Transport-Dependent Assembly of Multiple Axonemal Dyneins Cause Primary Ciliary Dyskinesia.” *American Journal of Human Genetics* 102 (5): 956–72. https://doi.org/10.1016/j.ajhg.2018.03.024.

Fassad, Mahmoud R., Amelia Shoemark, Marie Legendre, Robert A. Hirst, France Koll, Pierrick le Borgne, Bruno Louis, et al. 2018. “Mutations in Outer Dynein Arm Heavy Chain DNAH9 Cause Motile Cilia Defects and Situs Inversus.” *American Journal of Human Genetics* 103 (6): 984–94. https://doi.org/10.1016/j.ajhg.2018.10.016.

Fawcett, Don W., and Keith R. Porter. 1954. “A Study of the Fine Structure of Ciliated Epithelia.” *Journal of Morphology* 94 (2): 221–81. https://doi.org/10.1002/jmor.1050940202.

Fliegauf, Manfred, Heike Olbrich, Judit Horvath, Johannes H Wildhaber, Maimoona A Zariwala, Marcus Kennedy, Michael R Knowles, and Heymut Omran. 2005. “Mislocalization of DNAH5 and DNAH9 in Respiratory Cells from Patients with Primary Ciliary Dyskinesia.” *American Journal of Respiratory and Critical Care Medicine* 171 (12): 1343–49. https://doi.org/10.1164/rccm.200411-1583OC.

Fok, Agnes K., Hali Wang, Akiko Katayama, Marilynn S. Aihara, and Richard D. Allen. 1994. “22S Axonemal Dynein Is Preassembled and Functional Prior to Being Transported to and Attached on the Axonemes.” *Cell Motility and the Cytoskeleton* 29 (3): 215–24. https://doi.org/10.1002/cm.970290304.

Follit, John A, Richard A Tuft, Kevin E Fogarty, and Gregory J Pazour. 2006. “The Intraflagellar Transport Protein IFT20 Is Associated with the Golgi Complex and Is Required for Cilia Assembly.” *Molecular Biology of the Cell* 17 (9): 3781–92. https://doi.org/10.1091/mbc.e06-02-0133.

Ford, Matthew J., Patricia L. Yeyati, Girish R. Mali, Margaret A. Keighren, Scott H. Waddell, Heidi K. Mjoseng, Adam T. Douglas, et al. 2018. “A Cell/Cilia Cycle Biosensor for Single-Cell Kinetics Reveals Persistence of Cilia after G1/S Transition Is a General Property in Cells and Mice.” *Developmental Cell* 47 (4): 509-523.e5. https://doi.org/10.1016/j.devcel.2018.10.027.

Fowkes, M E, and D R Mitchell. 1998. “The Role of Preassembled Cytoplasmic Complexes in Assembly of Flagellar Dynein Subunits.” *Molecular Biology of the Cell* 9 (9): 2337–47. https://doi.org/10.1091/MBC.9.9.2337.

Friedmann, Theodore, and Richard Roblin. 1972. “Gene Therapy for Human Genetic Disease?” *Science* 175 (4025): 949–55. https://doi.org/10.1126/science.175.4025.949.

Fujii, Kotaro, Zhen Shi, Olena Zhulyn, Nicolas Denans, and Maria Barna. 2017. “Pervasive Translational Regulation of the Cell Signalling Circuitry Underlies Mammalian Development.” *Nature Communications* 8: 14443. https://doi.org/10.1038/ncomms14443.

Furuta, Akane, Toshiki Yagi, Haru Aki Yanagisawa, Hideo Higuchi, and Ritsu Kamiya. 2009. “Systematic Comparison of in Vitro Motile Properties between Chlamydomonas Wild-Type and Mutant Outer Arm Dyneins Each Lacking One of the Three Heavy Chains.” *Journal of Biological Chemistry* 284 (9): 5927–35. https://doi.org/10.1074/jbc.M807830200.

Gao, Chunlei, Guangliang Wang, Jeffrey D Amack, and David R Mitchell. 2010. “Oda16/Wdr69 Is Essential for Axonemal Dynein Assembly and Ciliary Motility during Zebrafish Embryogenesis.” *Developmental Dynamics* 239 (8): 2190–97. https://doi.org/10.1002/dvdy.22355.

Garcia-Gonzalo, Francesc R, Kevin C Corbit, Maré Salomé Sirerol-Piquer, Gokul Ramaswami, Edgar A Otto, Thomas R Noriega, Allen D Seol, et al. 2011. “A Transition Zone Complex Regulates Mammalian Ciliogenesis and Ciliary Membrane Composition.” *Nature Genetics* 43 (8): 776–84. https://doi.org/10.1038/ng.891.

Garneau, Josiane E., Marie Ève Dupuis, Manuela Villion, Dennis A. Romero, Rodolphe Barrangou, Patrick Boyaval, Christophe Fremaux, Philippe Horvath, Alfonso H. Magadán, and Sylvain Moineau. 2010. “The CRISPR/Cas Bacterial Immune System Cleaves Bacteriophage and Plasmid DNA.” *Nature* 468 (7320): 67–71. https://doi.org/10.1038/nature09523.

Gatti, J L, S M King, A G Moss, and G B Witman. 1989. “Outer Arm Dynein from Trout Spermatozoa. Purification, Polypeptide Composition, and Enzymatic Properties.” *Journal of Biological Chemistry* 264 (19): 11450–57.

http://www.ncbi.nlm.nih.gov/pubmed/2525558.

Gautier, Arnaud, Alexandre Juillerat, Christian Heinis, Ivan Reis Corrêa, Maik Kindermann, Florent Beaufils, and Kai Johnsson. 2008. “An Engineered Protein Tag for Multiprotein Labeling in Living Cells.” *Chemistry and Biology* 15 (2): 128–36. https://doi.org/10.1016/j.chembiol.2008.01.007.

Georgikou, Christina, Laetitia Vincensini, Sebastian Hutchinson, Cher-Pheng Ooi, Eloïse Bertiaux, Thierry Blisnick, and Philippe Bastin. 2017. “Flagellar Incorporation of Proteins Follows at Least Two Different Routes in Trypanosomes.” *Biology of the Cell* 110 (2): 33–47. https://doi.org/10.1111/boc.201700052.

Gheiratmand, Ladan, Etienne Coyaud, Gagan D Gupta, Estelle MN Laurent, Monica Hasegan, Suzanna L Prosser, João Gonçalves, Brian Raught, and Laurence Pelletier. 2019. “Spatial and Proteomic Profiling Reveals Centrosome-independent Features of Centriolar Satellites.” *The EMBO Journal* 38 (June): e101109. https://doi.org/10.15252/embj.2018101109.

Glaser, Astrid, Bradley McColl, and Jim Vadolas. 2016. “GFP to BFP Conversion: A Versatile Assay for the Quantification of CRISPR/Cas9-Mediated Genome Editing.” *Molecular Therapy - Nucleic Acids* 5: e334. https://doi.org/10.1038/mtna.2016.48.

Gong, Yunchen, Yoshito Kakihara, Nevan Krogan, Jack Greenblatt, Andrew Emili, Zhaolei Zhang, and Walid A. Houry. 2009. “An Atlas of Chaperone-Protein Interactions in Saccharomyces Cerevisiae: Implications to Protein Folding Pathways in the Cell.” *Molecular Systems Biology* 5 (275). https://doi.org/10.1038/msb.2009.26.

Goodarzi, Aaron A., Yaping Yu, Enriqueta Riballo, Pauline Douglas, Sarah A. Walker, Ruiqiong Ye, Christine Härer, et al. 2006. “DNA-PK Autophosphorylation Facilitates Artemis Endonuclease Activity.” *EMBO Journal* 25 (16): 3880–89. https://doi.org/10.1038/sj.emboj.7601255.

Goodenough, Ursula, and John Heuser. 1984. “Structural Comparison of Purified Dynein Proteins with in Situ Dynein Arms.” *Journal of Molecular Biology* 180 (4): 1083–1118. https://doi.org/10.1016/0022-2836(84)90272-9.

Goodenough, Ursula W., and John E. Heuser. 1985. “Substructure of Inner Dynein

Arms, Radial Spokes, and the Central Pair/Projection Complex of Cilia and Flagella." *Journal of Cell Biology* 100 (6): 2008–18. https://doi.org/10.1083/jcb.100.6.2008.

Goodenough, Ursula W, Brian Gebhart, Valerie Mermall, David R Mitchell, and John E Heuser. 1987. "High-Pressure Liquid Chromatography Fractionation of Chlamydomonas Dynein Extracts and Characterization of Inner-Arm Dynein Subunits." *Journal of Molecular Biology* 194 (3): 481–94. https://doi.org/10.1016/0022-2836(87)90676-0.

Grawunder, Ulf, Matthias Wilm, Xiantuo Wu, Peter Kulesza, Thomas E. Wilson, Matthias Mann, and Michael R. Lieber. 1997. "Activity of DNA Ligase IV Stimulated by Complex Formation with XRCC4 Protein in Mammalian Cells." *Nature* 388 (6641): 492–95. https://doi.org/10.1038/41358.

Griffin, B A, S R Adams, and R Y Tsien. 1998. "Specific Covalent Labeling of Recombinant Protein Molecules inside Live Cells." *Science (New York, N.Y.)* 281 (5374): 269–72. http://www.ncbi.nlm.nih.gov/pubmed/9657724.

Grundy, Gabrielle J., Stuart L. Rulten, Zhihong Zeng, Raquel Arribas-Bosacoma, Natasha Iles, Katie Manley, Antony Oliver, and Keith W. Caldecott. 2013. "APLF Promotes the Assembly and Activity of Non-Homologous End Joining Protein Complexes." *EMBO Journal* 32 (1): 112–25. https://doi.org/10.1038/emboj.2012.304.

Gu, Bin, Eszter Posfai, and Janet Rossant. 2018. "Efficient Generation of Targeted Large Insertions by Microinjection into Two-Cell-Stage Mouse Embryos." *Nature Biotechnology* 36 (7): 632–37. https://doi.org/10.1038/nbt.4166.

Gu, Jiafeng, Sicong Li, Xiaoshan Zhang, Ling Chi Wang, Doris Niewolik, Klaus Schwarz, Randy J. Legerski, Ebrahim Zandi, and Michael R. Lieber. 2010. "DNA-PKcs Regulates a Single-Stranded DNA Endonuclease Activity of Artemis." *DNA Repair* 9 (4): 429–37. https://doi.org/10.1016/j.dnarep.2010.01.001.

Gu, Tiantian, Hongjuan He, Yan Zhang, Zhengbin Han, Guangyuan Hou, Tiebo Zeng, Qi Liu, and Qiong Wu. 2012. "Trmt112 Gene Expression in Mouse Embryonic Development." *Acta Histochemica et Cytochemica* 45 (2): 113–19. https://doi.org/10.1267/ahc.11047.

Gutschner, Tony, Monika Haemmerle, Giannicola Genovese, Giulio F. Draetta, and Lynda Chin. 2016. “Post-Translational Regulation of Cas9 during G1 Enhances Homology-Directed Repair.” *Cell Reports* 14 (6): 1555–66. https://doi.org/10.1016/j.celrep.2016.01.019.

Habermacher, Geoffrey, and Winfield S. Sale. 1997. “Regulation of Flagellar Dynein by Phosphorylation of a 138-KD Inner Ann Dynein Intermediate Chain.” *Journal of Cell Biology* 136 (1): 167–76. https://doi.org/10.1083/jcb.136.1.167.

Hafezqorani, Saber, Atefeh Lafzi, Ruben G. De Bruin, Anton Jan Van Zonneveld, Eric P. Van Der Veer, Yesim Aydln Son, and Hilal Kazan. 2016. “Modeling the Combined Effect of RNA-Binding Proteins and MicroRNAs in Post-Transcriptional Regulation.” *Nucleic Acids Research* 44 (9): e83–92. https://doi.org/10.1093/nar/gkw048.

Hannah, William B., Suzanne DeBrosse, BreAnna Kinghorn, Steven Strausbaugh, Moira L. Aitken, Margaret Rosenfeld, Whitney E. Wolf, Michael R. Knowles, and Maimoona A. Zariwala. 2019. “The Expanding Phenotype of OFD1 -related Disorders: Hemizygous Loss-of-function Variants in Three Patients with Primary Ciliary Dyskinesia.” *Molecular Genetics & Genomic Medicine*, no. e911. https://doi.org/10.1002/mgg3.911.

Hartill, Verity L., Glenn van de Hoek, Mitali P. Patel, Rosie Little, Christopher M. Watson, Ian R. Berry, Amelia Shoemark, et al. 2018. “DNAAF1 Links Heart Laterality with the AAA+ ATPase RUVBL1 and Ciliary Intraflagellar Transport.” *Human Molecular Genetics* 27 (3): 529–45. https://doi.org/10.1093/hmg/ddx422.

Hastie, Annette T., David T. Dicker, Susan T. Hingley, Friedrich Kueppers, Michael L. Higgins, and George Weinbaurn. 1986. “Isolation of Cilia from Porcine Tracheal Epithelium and Extraction of Dynein Arms.” *Cell Motility and the Cytoskeleton* 6 (1): 25–34. https://doi.org/10.1002/cm.970060105.

Hedges, S Blair, Joel Dudley, and Sudhir Kumar. 2006. “TimeTree: A Public Knowledge-Base of Divergence Times among Organisms.” *Bioinformatics* 22 (23): 2971–72. https://doi.org/10.1093/bioinformatics/btl505.

Heim, Roger, Douglas C. Prasher, and Roger Y. Tsien. 1994. “Wavelength Mutations and Posttranslational Autoxidation of Green Fluorescent Protein.”

Proceedings of the National Academy of Sciences of the United States of America 91 (26): 12501–4. https://doi.org/10.1073/pnas.91.26.12501.

Hendrickson, Triscia W, Catherine A Perrone, Paul Griffin, Kristin Wuichet, Joshua Mueller, Pinfen Yang, Mary E Porter, and Winfield S Sale. 2004. “IC138 Is a WD-Repeat Dynein Intermediate Chain Required for Light Chain Assembly and Regulation of Flagellar Bending.” *Molecular Biology of the Cell* 15 (12): 5431–42. https://doi.org/10.1091/mbc.e04-08-0694.

Heuser, Thomas, Milen Raytchev, Jeremy Krell, Mary E. Porter, and Daniela Nicastro. 2009. “The Dynein Regulatory Complex Is the Nexin Link and a Major Regulatory Node in Cilia and Flagella.” *Journal of Cell Biology* 187 (6): 921–33. https://doi.org/10.1083/jcb.200908067.

Hilliker, Angela, Zhaofeng Gao, Eckhard Jankowsky, and Roy Parker. 2011. “The DEAD-Box Protein Ded1 Modulates Translation by the Formation and Resolution of an EIF4F-MRNA Complex.” *Molecular Cell* 43 (6): 962–72. https://doi.org/10.1016/j.molcel.2011.08.008.

Hisanaga, Shin Ichi, and Hikoichi Sakai. 1983. “Cytoplasmic Dynein of the Sea Urchin Egg. II. Purification, Characterization and Interactions with Microtubules and Ca-Calmodulin.” *Journal of Biochemistry* 93 (1): 87–98. https://doi.org/10.1093/oxfordjournals.jbchem.a134182.

Hjeij, Rim, Alexandros Onoufriadis, Christopher M Watson, Christopher E Slagle, Nikolai T Klena, Gerard W Dougherty, Magorzata Kurkowiak, et al. 2014. “CCDC151 Mutations Cause Primary Ciliary Dyskinesia by Disruption of the Outer Dynein Arm Docking Complex Formation.” *American Journal of Human Genetics* 95 (3): 257–74. https://doi.org/10.1016/j.ajhg.2014.08.005.

Hong, Dong Hyun, Basil Pawlyk, Maxim Sokolov, Katherine J. Strissel, Jun Yang, Brian Tulloch, Alan F. Wright, Vadim Y. Arshavsky, and Tiansen Li. 2003. “RPGR Isoforms in Photoreceptor Connecting Cilia and the Transitional Zone of Motile Cilia.” *Investigative Ophthalmology and Visual Science* 44 (6): 2413–21. https://doi.org/10.1167/iovs.02-1206.

Horani, Amjad, Todd E. Druley, Maimoona A. Zariwala, Anand C. Patel, Benjamin T. Levinson, Laura G. Van Arendonk, Katherine C. Thornton, et al. 2012. “Whole-Exome Capture and Sequencing Identifies HEATR2 Mutation as a Cause of

Primary Ciliary Dyskinesia." *American Journal of Human Genetics* 91 (4): 685–93. https://doi.org/10.1016/j.ajhg.2012.08.022.

Horani, Amjad, Thomas W. Ferkol, David Shoseyov, Mollie G. Wasserman, Yifat S. Oren, Batsheva Kerem, Israel Amirav, et al. 2013. "LRRC6 Mutation Causes Primary Ciliary Dyskinesia with Dynein Arm Defects." *PLoS ONE* 8 (3). https://doi.org/10.1371/journal.pone.0059436.

Horani, Amjad, Alessandro Ustione, Tao Huang, Amy L. Firth, Jiehong Pan, Sean P. Gunsten, Jeffrey A. Haspel, David W. Piston, and Steven L. Brody. 2018. "Establishment of the Early Cilia Preassembly Protein Complex during Motile Ciliogenesis." *Proceedings of the National Academy of Sciences* 115 (6): E1221–28. https://doi.org/10.1073/pnas.1715915115.

Hori, Akiko, and Takashi Toda. 2016. "Regulation of Centriolar Satellite Integrity and Its Physiology." *Cellular and Molecular Life Sciences*. Birkhauser Verlag AG. https://doi.org/10.1007/s00018-016-2315-x.

Hornef, Nada, Heike Olbrich, Judit Horvath, Maimoona A. Zariwala, Manfred Fliegauf, Niki Tomas Loges, Johannes Wildhaber, et al. 2006. "DNAH5 Mutations Are a Common Cause of Primary Ciliary Dyskinesia with Outer Dynein Arm Defects." *American Journal of Respiratory and Critical Care Medicine* 174 (2): 120–26. https://doi.org/10.1164/rccm.200601-084OC.

Horváth, Judit, Manfred Fliegauf, Heike Olbrich, Andreas Kispert, Stephen M. King, Hannah Mitchison, Maimoona A. Zariwala, et al. 2005. "Identification and Analysis of Axonemal Dynein Light Chain 1 in Primary Ciliary Dyskinesia Patients." *American Journal of Respiratory Cell and Molecular Biology* 33 (1): 41–47. https://doi.org/10.1165/rcmb.2004-0335OC.

Hou, Yuqing, Hongmin Qin, John A. Follit, Gregory J. Pazour, Joel L. Rosenbaum, and George B. Witman. 2007. "Functional Analysis of an Individual IFT Protein: IFT46 Is Required for Transport of Outer Dynein Arms into Flagella." *Journal of Cell Biology* 176 (5): 653–65. https://doi.org/10.1083/jcb.200608041.

Hsu, Patrick D, David A Scott, Joshua A Weinstein, F Ann Ran, Silvana Konermann, Vineeta Agarwala, Yinqing Li, et al. 2013. "DNA Targeting Specificity of RNA-Guided Cas9 Nucleases." *Nature Biotechnology* 31 (9): 827–32. https://doi.org/10.1038/nbt.2647.

Huang, B., M. R. Rifkin, and D. J.L. Luck. 1977. “Temperature Sensitive Mutations Affecting Flagellar Assembly and Function in Chlamydomonas Reinhardtii.” *Journal of Cell Biology* 72 (1): 67–85. https://doi.org/10.1083/jcb.72.1.67.

Hubstenberger, Arnaud, Maïté Courel, Marianne Bénard, Sylvie Souquere, Michèle Ernoult-Lange, Racha Chouaib, Zhou Yi, et al. 2017. “P-Body Purification Reveals the Condensation of Repressed MRNA Regulons.” *Molecular Cell* 68 (1): 144-157.e5. https://doi.org/10.1016/j.molcel.2017.09.003.

Huizar, Ryan L, Chanjae Lee, Alexander A Boulgakov, Amjad Horani, Fan Tu, Edward M Marcotte, Steven L Brody, and John B Wallingford. 2018. “A Liquid-like Organelle at the Root of Motile Ciliopathy.” *ELife* 7 (e38497). https://doi.org/10.7554/elife.38497.

Huw, Ling Yuh, Andrew S. Goldsborough, Keith Willison, and Karen Artzt. 1995. “Tctex2: A Sperm Tail Surface Protein Mapping to the t-Complex.” *Developmental Biology* 170 (1): 183–94. https://doi.org/10.1006/dbio.1995.1206.

Ide, Takahiro, Mikito Owa, Stephen M. King, Ritsu Kamiya, and Ken Ichi Wakabayashi. 2013. “Protein-Protein Interactions between Intermediate Chains and the Docking Complex of Chlamydomonas Flagellar Outer Arm Dynein.” *FEBS Letters* 587 (14): 2143–49. https://doi.org/10.1016/j.febslet.2013.05.058.

Imtiaz, Faiqa, Rabab Allam, Khushnooda Ramzan, and Moeenaldeen Al-Sayed. 2015. “Variation in DNAH1 May Contribute to Primary Ciliary Dyskinesia.” *BMC Medical Genetics* 16 (14). https://doi.org/10.1186/s12881-015-0162-5.

Inaba, Kazuo, O Kagami, and K Ogawa. 1999. “Tctex2-Related Outer Arm Dynein Light Chain Is Phosphorylated at Activation of Sperm Motility.” *Biochemical and Biophysical Research Communications* 256 (1): 177–83. https://doi.org/10.1006/bbrc.1999.0309.

Inaba, Kazuo. 2011. “Sperm Flagella: Comparative and Phylogenetic Perspectives of Protein Components.” *Molecular Human Reproduction*. https://doi.org/10.1093/molehr/gar034.

Inaba, Kazuo. 2018. “Biochemical Purification of Axonemal and Cytoplasmic Dyneins.” In *Dyneins: Dynein Mechanics, Dysfunction, and Disease: Second Edition*, 2:88–111. Elsevier. https://doi.org/10.1016/B978-0-12-809470-

9.00004-7.

Inaba, Kazuo, Toshiko Mohri, and Hideo Mohri. 2005. “B-Band Protein in Sea Urchin Sperm Flagella.” *Cell Motility and the Cytoskeleton* 10 (4): 506–17. https://doi.org/10.1002/cm.970100407.

Inaba, Yasuko, Kyosuke Shinohara, Yanick Botilde, Ryo Nabeshima, Katsuyoshi Takaoka, Rieko Ajima, Lynda Lamri, et al. 2016. “Transport of the Outer Dynein Arm Complex to Cilia Requires a Cytoplasmic Protein Lrrc6.” *Genes to Cells* 21 (7): 728–39. https://doi.org/10.1111/gtc.12380.

Ishikawa, Hiroaki, Takahiro Ide, Toshiki Yagi, Xue Jiang, Masafumi Hirono, Hiroyuki Sasaki, Haruaki Yanagisawa, et al. 2014. “TTC26/DYF13 Is an Intraflagellar Transport Protein Required for Transport of Motility-Related Proteins into Flagella.” *ELife* 2014 (3): e01566. https://doi.org/10.7554/eLife.01566.

Ishikawa, Takashi. 2017. “Axoneme Structure from Motile Cilia.” *Cold Spring Harbor Perspectives in Biology* 9 (1). https://doi.org/10.1101/cshperspect.a028076.

Ishikawa, Takashi, Hitoshi Sakakibara, and Kazuhiro Oiwa. 2007. “The Architecture of Outer Dynein Arms in Situ.” *Journal of Molecular Biology* 368 (5): 1249–58. https://doi.org/10.1016/j.jmb.2007.02.072.

Ishino, Y, H Shinagawa, K Makino, M Amemura, and A. Nakatura. 1987. “Nucleotide Sequence of the Iap Gene, Responsible for Alkaline Phosphatase Isoenzyme Conversion in Escherichia Coli, and Identification of the Gene Product.” *Journal of Bacteriology* 169 (12): 5429–33. https://doi.org/10.1128/jb.169.12.5429-5433.1987.

Ivanov, Pavel, Nancy Kedersha, and Paul Anderson. 2019. “Stress Granules and Processing Bodies in Translational Control.” *Cold Spring Harbor Perspectives in Biology*. NLM (Medline). https://doi.org/10.1101/cshperspect.a032813.

Jaffe, Kimberly M., Daniel T. Grimes, Jodi Schottenfeld-Roames, Michael E. Werner, Tse Shuen J. Ku, Sun K. Kim, Jose L. Pelliccia, Nicholas F.C. Morante, Brian J. Mitchell, and Rebecca D. Burdine. 2016. “C21orf59/Kurly Controls Both Cilia Motility and Polarization.” *Cell Reports* 14 (8): 1841–49. https://doi.org/10.1016/j.celrep.2016.01.069.

Jaffrey, Samie R., and Solomon H. Snyder. 1996. “PIN: An Associated Protein

Inhibitor of Neuronal Nitric Oxide Synthase." *Science* 274 (5288): 774–77. https://doi.org/10.1126/science.274.5288.774.

Jain, Raksha, Jiehong Pan, James A. Driscoll, Jeffrey W. Wisner, Tao Huang, Sean P. Gunsten, Yingjian You, and Steven L. Brody. 2010. "Temporal Relationship between Primary and Motile Ciliogenesis in Airway Epithelial Cells." *American Journal of Respiratory Cell and Molecular Biology* 43 (6): 731–39. https://doi.org/10.1165/rcmb.2009-0328OC.

Jansen, Lars E.T., Ben E. Black, Daniel R. Foltz, and Don W. Cleveland. 2007. "Propagation of Centromeric Chromatin Requires Exit from Mitosis." *Journal of Cell Biology* 176 (6): 795–805. https://doi.org/10.1083/jcb.200701066.

Jayathilaka, Krishanthi, Sean D Sheridan, Tyler D Bold, Katarzyna Bochenska, Hillary L Logan, Ralph R Weichselbaum, Douglas K Bishop, and Philip P Connell. 2008. "A Chemical Compound That Stimulates the Human Homologous Recombination Protein RAD51." *Proceedings of the National Academy of Sciences of the United States of America* 105 (41): 15848–53. https://doi.org/10.1073/pnas.0808046105.

Jerber, Julie, Dominique Baas, Fabien Soulavie, Brigitte Chhin, Elisabeth Cortier, Christine Vesque, Joëlle Thomas, and Bénédicte Durand. 2014. "The Coiled-Coil Domain Containing Protein CCDC151 Is Required for the Function of IFT-Dependent Motile Cilia in Animals." *Human Molecular Genetics* 23 (3): 563–77. https://doi.org/10.1093/hmg/ddt445.

Jiang, Guo Qiang, Xue Feng Yao, and Chun Ming Liu. 2013. "A Simple CELI Endonuclease-Based Protocol for Genotyping Both SNPs and InDels." *Plant Molecular Biology Reporter* 31 (6): 1325–35. https://doi.org/10.1007/s11105-013-0606-z.

Jinek, Martin, Krzysztof Chylinski, Ines Fonfara, Michael Hauer, Jennifer A Doudna, and Emmanuelle Charpentier. 2012. "A Programmable Dual-RNA-Guided DNA Endonuclease in Adaptive Bacterial Immunity." *Science (New York, N.Y.)* 337 (6096): 816–21. https://doi.org/10.1126/science.1225829.

Johnson, K A, and J S Wall. 1983. "Structure and Molecular Weight of the Dynein ATPase." *The Journal of Cell Biology* 96 (3): 669–78. https://doi.org/10.1083/jcb.96.3.669.

Jonkers, Iris, and John T. Lis. 2015. “Getting up to Speed with Transcription Elongation by RNA Polymerase II.” *Nature Reviews Molecular Cell Biology*. Nature Publishing Group. https://doi.org/10.1038/nrm3953.

Jordan, Mareike A., Dennis R. Diener, Ludek Stepanek, and Gaia Pigino. 2018. “The Cryo-EM Structure of Intraflagellar Transport Trains Reveals How Dynein Is Inactivated to Ensure Unidirectional Anterograde Movement in Cilia.” *Nature Cell Biology* 20 (11): 1250–55. https://doi.org/10.1038/s41556-018-0213-1.

Kakihara, Yoshito, and Walid A. Houry. 2012. “The R2TP Complex: Discovery and Functions.” *Biochimica et Biophysica Acta - Molecular Cell Research* 1823 (1): 101–7. https://doi.org/10.1016/j.bbamcr.2011.08.016.

Kamenova, Ivanka, Pooja Mukherjee, Sascha Conic, Florian Mueller, Farrah El-Saafin, Paul Bardot, Jean Marie Garnier, et al. 2019. “Co-Translational Assembly of Mammalian Nuclear Multisubunit Complexes.” *Nature Communications* 10 (1). https://doi.org/10.1038/s41467-019-09749-y.

Kamiya, R. 1988. “Mutations at Twelve Independent Loci Result in Absence of Outer Dynein Arms in Chlamydomonas Reinhardtii.” *Journal of Cell Biology* 107 (6 I): 2253–58. https://doi.org/10.1083/jcb.107.6.2253.

Kamiya, R., E. Kurimoto, and E. Muto. 1991. “Two Types of Chlamydomonas Flagellar Mutants Missing Different Components of Inner-Arm Dynein.” *Journal of Cell Biology* 112 (3): 441–47. https://doi.org/10.1083/jcb.112.3.441.

Kanai, Yoshimitsu, Naoshi Dohmae, and Nobutaka Hirokawa. 2004. “Kinesin Transports RNA: Isolation and Characterization of an RNA-Transporting Granule.” *Neuron* 43 (4): 513–25. https://doi.org/10.1016/j.neuron.2004.07.022.

Kartagener, M. 1933. “Zur Pathogenese Der Bronchiektasien.” *Beiträge Zur Klinik Der Tuberkulose Und Spezifischen Tuberkulose-Forschung* 83 (4): 489–501. https://doi.org/10.1007/BF02141468.

Kato, Takako, Osamu Kagami, Toshiki Yagi, and Ritsu Kamiya. 1993. “Isolation of Two Species of Chlamydomonas Reinhardtii Flagellar Mutants, Ida5 and Ida6, That Lack a Newly Identified Heavy Chain of the Inner Dynein Arm.” *Cell Structure and Function* 18 (6): 371–77. https://doi.org/10.1247/csf.18.371.

Kee, Hooi Lynn, John F. Dishinger, T. Lynne Blasius, Chia Jen Liu, Ben Margolis,

and Kristen J. Verhey. 2012. “A Size-Exclusion Permeability Barrier and Nucleoporins Characterize a Ciliary Pore Complex That Regulates Transport into Cilia.” *Nature Cell Biology* 14 (4): 431–37. https://doi.org/10.1038/ncb2450.

Keppler, Antje, Susanne Gendreizig, Thomas Gronemeyer, Horst Pick, Horst Vogel, and Kai Johnsson. 2003. “A General Method for the Covalent Labeling of Fusion Proteins with Small Molecules in Vivo.” *Nature Biotechnology* 21 (1): 86–89. https://doi.org/10.1038/nbt765.

Kersey, Paul Julian, James E. Allen, Alexis Allot, Matthieu Barba, Sanjay Boddu, Bruce J. Bolt, Denise Carvalho-Silva, et al. 2018. “Ensembl Genomes 2018: An Integrated Omics Infrastructure for Non-Vertebrate Species.” *Nucleic Acids Research* 46 (D1): D802–8. https://doi.org/10.1093/nar/gkx1011.

Khelifa, Mariem Ben, Charles Coutton, Raoudha Zouari, Thomas Karaouzène, John Rendu, Marie Bidart, Sandra Yassine, et al. 2014. “Mutations in DNAH1, Which Encodes an Inner Arm Heavy Chain Dynein, Lead to Male Infertility from Multiple Morphological Abnormalities of the Sperm Flagella.” *American Journal of Human Genetics* 94 (1): 95–104. https://doi.org/10.1016/j.ajhg.2013.11.017.

Kim, Na Yong, Jin Young Baek, Hong Seok Choi, In Sik Chung, Sungho Shin, Jung Ihn Lee, Jung Yun Choi, and Jai Myung Yang. 2012. “Short-Hairpin RNA-Mediated Gene Expression Interference in Trichoplusia Ni Cells.” *Journal of Microbiology and Biotechnology* 22 (2): 190–98. https://doi.org/10.4014/jmb.1108.08045.

King, Stephen M., C G Wilkerson, and G B Witman. 1991. “The Mr 78,000 Intermediate Chain of Chlamydomonas Outer Arm Dynein Interacts with Alpha-Tubulin in Situ.” *The Journal of Biological Chemistry* 266 (13): 8401–7. http://www.ncbi.nlm.nih.gov/pubmed/1827120.

King, Stephen M. 2016. “Axonemal Dynein Arms.” *Cold Spring Harbor Perspectives in Biology* 8 (11). https://doi.org/10.1101/cshperspect.a028100.

King, Stephen M. 2018. “Composition and Assembly of Axonemal Dyneins.” In *Dyneins*, 162–201. https://doi.org/10.1016/b978-0-12-809471-6.00005-x.

King, Stephen M., Elisa Barbarese, James F. Dillman, Ramila S. Patel-King, John H. Carson, and K. Kevin Pfister. 1996. “Brain Cytoplasmic and Flagellar Outer Arm Dyneins Share a Highly Conserved M(r) 8,000 Light Chain.” *Journal of*

Biological Chemistry 271 (32): 19358–66. https://doi.org/10.1074/jbc.271.32.19358.

King, Stephen M., James F. Dillman, Sharon E. Benashski, R. John Lye, Ramila S. Patel-King, and K. Kevin Pfister. 1996. “The Mouse T-Complex-Encoded Protein Tctex-1 Is a Light Chain of Brain Cytoplasmic Dynein.” *Journal of Biological Chemistry* 271 (50): 32281–87. https://doi.org/10.1074/jbc.271.50.32281.

King, Stephen M., and Ramila S. Patel-King. 2015. “The Oligomeric Outer Dynein Arm Assembly Factor CCDC103 Is Tightly Integrated within the Ciliary Axoneme and Exhibits Periodic Binding to Microtubules.” *Journal of Biological Chemistry* 290 (12): 7388–7401. https://doi.org/10.1074/jbc.M114.616425.

King, Stephen M. 2016. “Axonemal Dynein Arms.” *Cold Spring Harbor Perspectives in Biology* 8 (11): a028100. https://doi.org/10.1101/cshperspect.a028100.

Klompe, Sanne E., Phuc L. H. Vo, Tyler S. Halpin-Healy, and Samuel H. Sternberg. 2019. “Transposon-Encoded CRISPR–Cas Systems Direct RNA-Guided DNA Integration.” *Nature* 571 (June): 219–225. https://doi.org/10.1038/s41586-019-1323-z.

Knowles, Michael R., Margaret W. Leigh, Lawrence E. Ostrowski, Lu Huang, Johnny L. Carson, Milan J. Hazucha, Weining Yin, et al. 2013. “Exome Sequencing Identifies Mutations in CCDC114 as a Cause of Primary Ciliary Dyskinesia.” *American Journal of Human Genetics* 92 (1): 99–106. https://doi.org/10.1016/j.ajhg.2012.11.003.

Knowles, Michael R., Lawrence E. Ostrowski, Niki T. Loges, Toby Hurd, Margaret W. Leigh, Lu Huang, Whitney E. Wolf, et al. 2013. “Mutations in SPAG1 Cause Primary Ciliary Dyskinesia Associated with Defective Outer and Inner Dynein Arms.” *American Journal of Human Genetics* 93 (4): 711–20. https://doi.org/10.1016/j.ajhg.2013.07.025.

Kobayashi, Daisuke, Anshin Asano-Hoshino, Takashi Nakakura, Toshiyuki Nishimaki, Satoshi Ansai, Masato Kinoshita, Motoyuki Ogawa, Haruo Hagiwara, and Takahiko Yokoyama. 2017. “Loss of Zinc Finger MYND-Type Containing 10 (Zmynd10) Affects Cilia Integrity and Axonemal Localization of Dynein Arms, Resulting in Ciliary Dysmotility, Polycystic Kidney and Scoliosis

in Medaka (Oryzias Latipes).” *Developmental Biology* 430 (1): 69–79. https://doi.org/10.1016/j.ydbio.2017.08.016.

Kolberg, Katharina, Christiane Puettmann, Alessa Pardo, Jenny Fitting, and Stefan Barth. 2013. “SNAP-Tag Technology: A General Introduction.” *Current Pharmaceutical Design* 19 (30): 5406–13. http://www.ncbi.nlm.nih.gov/pubmed/23431982.

Kollmar, Martin. 2016. “Fine-Tuning Motile Cilia and Flagella: Evolution of the Dynein Motor Proteins from Plants to Humans at High Resolution.” *Molecular Biology and Evolution* 33 (12): 3249–67. https://doi.org/10.1093/molbev/msw213.

Komor, Alexis C, Yongjoo B Kim, Michael S Packer, John A Zuris, David R Liu, Supplementary Information, and Rna-programmed Dna. 2016. “CRISPR/Cas9 Cytidine Deaminase Fusion c to t Single Strand Conversion.” *Nature*. https://doi.org/10.1038/nature17946.

Kon, Takahide, Takuji Oyama, Rieko Shimo-Kon, Kenji Imamula, Tomohiro Shima, Kazuo Sutoh, and Genji Kurisu. 2012. “The 2.8 Å Crystal Structure of the Dynein Motor Domain.” *Nature* 484 (7394): 345–50. https://doi.org/10.1038/nature10955.

Koressaar, Triinu, and Maido Remm. 2007. “Enhancements and Modifications of Primer Design Program Primer3.” *Bioinformatics* 23 (10): 1289–91. https://doi.org/10.1093/bioinformatics/btm091.

Kott, Esther, Philippe Duquesnoy, Bruno Copin, Marie Legendre, Florence Dastot-Le Moal, Guy Montantin, Ludovic Jeanson, et al. 2012. “Loss-of-Function Mutations in LRRC6, a Gene Essential for Proper Axonemal Assembly of Inner and Outer Dynein Arms, Cause Primary Ciliary Dyskinesia.” *American Journal of Human Genetics* 91 (5): 958–64. https://doi.org/10.1016/j.ajhg.2012.10.003.

Koutoulis, Anthony, Gregory J. Pazour, Curtis G. Wilkerson, Kazuo Inaba, Hong Sheng, Saeko Takada, and George B. Witman. 1997. “The Chlamydomonas Reinhardtii ODA3 Gene Encodes a Protein of the Outer Dynein Arm Docking Complex.” *Journal of Cell Biology* 137 (5): 1069–80. https://doi.org/10.1083/jcb.137.5.1069.

Kozminski, K. G., K. A. Johnson, P. Forscher, and J. L. Rosenbaum. 1993. “A

Motility in the Eukaryotic Flagellum Unrelated to Flagellar Beating." *Proceedings of the National Academy of Sciences* 90 (12): 5519–23. https://doi.org/10.1073/pnas.90.12.5519.

Krawczyński, Maciej R, Hanna Dmeńska, and Michał Witt. 2004. "Apparent X-Linked Primary Ciliary Dyskinesia Associated with Retinitis Pigmentosa and a Hearing Loss." *Journal of Applied Genetics* 45 (1): 107–10. http://www.ncbi.nlm.nih.gov/pubmed/14960774.

Kubo, A., A. Yuba-Kubo, S. Tsukita, S. Tsukita, and M. Amagai. 2008. "Sentan: A Novel Specific Component of the Apical Structure of Vertebrate Motile Cilia." *Molecular Biology of the Cell* 19 (12): 5338–46. https://doi.org/10.1091/mbc.e08-07-0691.

Kubo, Akiharu, Hiroyuki Sasaki, Akiko Yuba-Kubo, Shoichiro Tsukita, and Nobuyuki Shiina. 1999. "Centriolar Satellites: Molecular Characterization, ATP-Dependent Movement toward Centrioles and Possible Involvement in Ciliogenesis." *Journal of Cell Biology* 147 (5): 969–79. https://doi.org/10.1083/jcb.147.5.969.

Kuhn, Charles, and Wayne Engleman. 1978. "The Structure of the Tips of Mammalian Respiratory Cilia." *Cell and Tissue Research* 186 (3): 491–98. https://doi.org/10.1007/BF00224937.

Kurosawa, Aya, Hideki Koyama, Shinichi Takayama, Kensuke Miki, Dai Ayusawa, Michihiko Fujii, Susumu Iiizumi, and Noritaka Adachi. 2008. "The Requirement of Artemis in Double-Strand Break Repair Depends on the Type of DNA Damage." *DNA and Cell Biology* 27 (1): 55–61. https://doi.org/10.1089/dna.2007.0649.

Lackner, Daniel H., Alexia Carré, Paloma M. Guzzardo, Carina Banning, Ramu Mangena, Tom Henley, Sarah Oberndorfer, et al. 2015. "A Generic Strategy for CRISPR-Cas9-Mediated Gene Tagging." *Nature Communications* 6: 10237. https://doi.org/10.1038/ncomms10237.

Lader, Eric, Hae Sook Ha, Michael O'Neill, Karen Artzt, and Dorothea Bennett. 1989. "Tctex-1: A Candidate Gene Family for a Mouse t Complex Sterility Locus." *Cell* 58 (5): 969–79. https://doi.org/10.1016/0092-8674(89)90948-3.

Lage, Petra zur, Fay G. Newton, and Andrew P. Jarman. 2019. "Survey of the

Ciliary Motility Machinery of Drosophila Sperm and Ciliated Mechanosensory Neurons Reveals Unexpected Cell-Type Specific Variations: A Model for Motile Ciliopathies." *Frontiers in Genetics* 10 (FEB): 24. https://doi.org/10.3389/fgene.2019.00024.

Lage, Petra Zur, Panagiota Stefanopoulou, Katarzyna Styczynska-Soczka, Niall Quinn, Girish Mali, Alex Von Kriegsheim, Pleasantine Mill, and Andrew P. Jarman. 2018. "Ciliary Dynein Motor Preassembly Is Regulated by Wdr92 in Association with HSP90 Co-Chaperone, R2TP." *Journal of Cell Biology* 217 (7): 2583–98. https://doi.org/10.1083/jcb.201709026.

Lai, M.-C., Y.-H. W. Lee, and W.-Y. Tarn. 2008. "The DEAD-Box RNA Helicase DDX3 Associates with Export Messenger Ribonucleoproteins as Well AsTip-Associated Protein and Participates in Translational Control." *Molecular Biology of the Cell* 19 (9): 3847–58. https://doi.org/10.1091/mbc.e07-12-1264.

Lai, Michele, Massimo Pifferi, Andrew Bush, Martina Piras, Angela Michelucci, Maria Di Cicco, Ambra del Grosso, et al. 2016. "Gene Editing of DNAH11 Restores Normal Cilia Motility in Primary Ciliary Dyskinesia." *Journal of Medical Genetics* 53 (4): 242–49. https://doi.org/10.1136/jmedgenet-2015-103539.

Leahy, Justin J.J., Bernard T. Golding, Roger J. Griffin, Ian R. Hardcastle, Caroline Richardson, Laurent Rigoreau, and Graeme C.M. Smith. 2004. "Identification of a Highly Potent and Selective DNA-Dependent Protein Kinase (DNA-PK) Inhibitor (NU7441) by Screening of Chromenone Libraries." *Bioorganic and Medicinal Chemistry Letters* 14 (24): 6083–87. https://doi.org/10.1016/j.bmcl.2004.09.060.

Lechtreck, Karl Ferdinand, Philippe Delmotte, Michael L. Robinson, Michael J. Sanderson, and George B. Witman. 2008. "Mutations in Hydin Impair Ciliary Motility in Mice." *Journal of Cell Biology* 180 (3): 633–43. https://doi.org/10.1083/jcb.200710162.

Ledbetter, Myron C., and Keith R. Porter. 1964. "Morphology of Microtubules of Plant Cells." *Science* 144 (3620): 872–74. https://doi.org/10.1126/science.144.3620.872.

Lee, Kunwoo, Vanessa A Mackley, Anirudh Rao, Anthony T Chong, Mark A Dewitt, Jacob E Corn, and Niren Murthy. 2017. "Synthetically Modified Guide RNA and

Donor DNA Are a Versatile Platform for CRISPR-Cas9 Engineering." *ELife* 6 (May): e25312. https://doi.org/10.7554/eLife.25312.

Lee, Lance. 2013. "Riding the Wave of Ependymal Cilia: Genetic Susceptibility to Hydrocephalus in Primary Ciliary Dyskinesia." *Journal of Neuroscience Research*. https://doi.org/10.1002/jnr.23238.

Leeuwenhoek, A. van. 1676. "Letter of October 9, 1676 to the Royal Society." *Philos Trans R Soc Lond B* 12 (12): 821–31.

Leigh, Margaret W., Amjad Horani, BreAnna Kinghorn, Michael G. O'Connor, Maimoona A. Zariwala, and Michael R. Knowles. 2019. "Primary Ciliary Dyskinesia (PCD): A Genetic Disorder of Motile Cilia." *Translational Science of Rare Diseases* 4 (1–2): 51–75. https://doi.org/10.3233/TRD-190036.

Li, You, Hisato Yagi, Ezenwa Obi Onuoha, Rama Rao Damerla, Richard Francis, Yoshiyuki Furutani, Muhammad Tariq, et al. 2016. "DNAH6 and Its Interactions with PCD Genes in Heterotaxy and Primary Ciliary Dyskinesia." *PLoS Genetics* 12 (2). https://doi.org/10.1371/journal.pgen.1005821.

Liang, Xiquan, Jason Potter, Shantanu Kumar, Namritha Ravinder, and Jonathan D. Chesnut. 2017. "Enhanced CRISPR/Cas9-Mediated Precise Genome Editing by Improved Design and Delivery of GRNA, Cas9 Nuclease, and Donor DNA." *Journal of Biotechnology* 241: 136–46. https://doi.org/10.1016/j.jbiotec.2016.11.011.

Lieber, Michael R. 2016. "Mechanisms of Human Lymphoid Chromosomal Translocations." *Nature Reviews Cancer*. Nature Publishing Group. https://doi.org/10.1038/nrc.2016.40.

Lin, Steven, Brett T. Staahl, Ravi K. Alla, and Jennifer A. Doudna. 2014. "Enhanced Homology-Directed Human Genome Engineering by Controlled Timing of CRISPR/Cas9 Delivery." *ELife* 3: e04766. https://doi.org/10.7554/eLife.04766.

Liu, Zhongmei, Hiroko Takazaki, Yuki Nakazawa, Miho Sakato, Toshiki Yagi, Takuo Yasunaga, Stephen M. King, and Ritsu Kamiya. 2008. "Partially Functional Outer-Arm Dynein in a Novel Chlamydomonas Mutant Expressing a Truncated γ Heavy Chain." *Eukaryotic Cell* 7 (7): 1136–45. https://doi.org/10.1128/EC.00102-08.

Lo, Kevin W.H., John M. Kogoy, Bareza A. Rasoul, Stephen M. King, and K. Kevin Pfister. 2007. “Interaction of the DYNLT (TCTEX1/RP3) Light Chains and the Intermediate Chains Reveals Novel Intersubunit Regulation during Assembly of the Dynein Complex.” *Journal of Biological Chemistry* 282 (51): 36871–78. https://doi.org/10.1074/jbc.M705991200.

Loges, Niki T., Dinu Antony, Ales Maver, Matthew A. Deardorff, Elif Yýlmaz Güleç, Alper Gezdirici, Tabea Nöthe-Menchen, et al. 2018. “Recessive DNAH9 Loss-of-Function Mutations Cause Laterality Defects and Subtle Respiratory Ciliary-Beating Defects.” *American Journal of Human Genetics* 103 (6): 995–1008. https://doi.org/10.1016/j.ajhg.2018.10.020.

Loges, Niki Tomas, Heike Olbrich, Lale Fenske, Huda Mussaffi, Judit Horvath, Manfred Fliegauf, Heiner Kuhl, et al. 2008. “DNAI2 Mutations Cause Primary Ciliary Dyskinesia with Defects in the Outer Dynein Arm.” *American Journal of Human Genetics* 83 (5): 547–58. https://doi.org/10.1016/j.ajhg.2008.10.001.

Look, Dwight C., Michael J. Walter, Michael R. Williamson, Liyi Pang, Yingjian You, J. Nicholas Sreshta, Joyce E. Johnson, Dani S. Zander, and Steven L. Brody. 2001. “Effects of Paramyxoviral Infection on Airway Epithelial Cell Foxj1 Expression, Ciliogenesis, and Mucociliary Function.” *American Journal of Pathology* 159 (6): 2055–69. https://doi.org/10.1016/S0002-9440(10)63057-X.

Los, Georgyi V., Lance P. Encell, Mark G. McDougall, Danette D. Hartzell, Natasha Karassina, Chad Zimprich, Monika G. Wood, et al. 2008. “HaloTag: A Novel Protein Labeling Technology for Cell Imaging and Protein Analysis.” *ACS Chemical Biology* 3 (6): 373–82. https://doi.org/10.1021/cb800025k.

Lu, Jun, and Arne Holmgren. 2014. “The Thioredoxin Antioxidant System.” *Free Radical Biology and Medicine* 66: 75–87. https://doi.org/10.1016/j.freeradbiomed.2013.07.036.

Lucas, Jane S, Angelo Barbato, Samuel A Collins, Myrofora Goutaki, Laura Behan, Daan Caudri, Sharon Dell, et al. 2017. “European Respiratory Society Guidelines for the Diagnosis of Primary Ciliary Dyskinesia.” *European Respiratory Journal*. https://doi.org/10.1183/13993003.01090-2016.

Luck, D. J.L. 1984. “Genetic and Biochemical Dissection of the Eucaryotic Flagellum.” *Journal of Cell Biology* 98 (3): 789–94.

https://doi.org/10.1083/jcb.98.3.789.

Maeder, Morgan L, and Charles A Gersbach. 2016. “Genome-Editing Technologies for Gene and Cell Therapy.” *Molecular Therapy* 24 (3): 430–46. https://doi.org/10.1038/mt.2016.10.

Makarova, Kira S., Nick V. Grishin, Svetlana A. Shabalina, Yuri I. Wolf, and Eugene V. Koonin. 2006. “A Putative RNA-Interference-Based Immune System in Prokaryotes: Computational Analysis of the Predicted Enzymatic Machinery, Functional Analogies with Eukaryotic RNAi, and Hypothetical Mechanisms of Action.” *Biology Direct* 1 (March): 7. https://doi.org/10.1186/1745-6150-1-7.

Mali, Girish R, Patricia L Yeyati, Seiya Mizuno, Daniel O Dodd, Peter A Tennant, Margaret A Keighren, Petra zur Lage, et al. 2018. “ZMYND10 Functions in a Chaperone Relay during Axonemal Dynein Assembly.” *ELife* 7 (e34389). https://doi.org/10.7554/elife.34389.

Mali, Prashant, Luhan Yang, Kevin M Esvelt, John Aach, Marc Guell, James E DiCarlo, Julie E Norville, and George M Church. 2013. “RNA-Guided Human Genome Engineering via Cas9.” *Science (New York, N.Y.)* 339 (6121): 823–26. https://doi.org/10.1126/science.1232033.

Manton, Irene. 1952. “The Fine Structure of Plant Cilia.” In *Symp. Soc. Exp. Biol*, 6:306–19.

Manton, Irene, and Bryan Clarke. 1952. “An Electron Microscope Study of the Spermatozoid of Fucus Serratus.” *Journal of Experimental Botany* 3 (9): 265–75. https://doi.org/10.1093/oxfordjournals.aob.a083292.

Marshall, W. F., and J. L. Rosenbaum. 2001. “Intraflagellar Transport Balances Continuous Turnover of Outer Doublet Microtubules: Implications for Flagellar Length Control.” *The Journal of Cell Biology* 155 (3): 405–14. https://doi.org/10.1083/jcb.200106141.

Maruyama, Takeshi, Stephanie K Dougan, Matthias C Truttmann, Angelina M Bilate, Jessica R Ingram, and Hidde L Ploegh. 2015. “Increasing the Efficiency of Precise Genome Editing with CRISPR-Cas9 by Inhibition of Nonhomologous End Joining.” *Nature Biotechnology* 33 (5): 538–42. https://doi.org/10.1038/nbt.3190.

Mastronarde, David N., Eileen T. O'Toole, Kent L. McDonald, J. Richard McIntosh, and Mary E. Porter. 1992. "Arrangement of Inner Dynein Arms in Wild-Type and Mutant Flagella of Chlamydomonas." *Journal of Cell Biology* 118 (5): 1145–62. https://doi.org/10.1083/jcb.118.5.1145.

Matsubara, Yohei, Tomoko Kato, Kenichi Kashimada, Hiromitsu Tanaka, Zhou Zhi, Shizuko Ichinose, Shuki Mizutani, et al. 2015. "TALEN-Mediated Gene Disruption on y Chromosome Reveals Critical Role of EIF2S3Y in Mouse Spermatogenesis." *Stem Cells and Development* 24 (10): 1164–70. https://doi.org/10.1089/scd.2014.0466.

Mazor, Masha, Soliman Alkrinawi, Vered Chalifa-Caspi, Esther Manor, Val C. Sheffield, Micha Aviram, and Ruti Parvari. 2011. "Primary Ciliary Dyskinesia Caused by Homozygous Mutation in DNAL1, Encoding Dynein Light Chain 1." *American Journal of Human Genetics* 88 (5): 599–607. https://doi.org/10.1016/j.ajhg.2011.03.018.

McGrath, James, Stefan Somlo, Svetlana Makova, Xin Tian, and Martina Brueckner. 2003. "Two Populations of Node Monocilia Initiate Left-Right Asymmetry in the Mouse Asymmetric Expression of a Signaling Molecule Like." *Cell* 114: 61–73. https://ac.els-cdn.com/S0092867403005117/1-s2.0-S0092867403005117-main.pdf?_tid=0b730fac-b7f7-11e7-8de4-00000aacb35f&acdnat=1508765914_7dd8a55cacd89a36159229224bca3f21.

Meindl, A., K. Dry, K. Herrmann, F. Manson, A. Ciccodicola, A. Edgar, M. R.S. Carvalho, et al. 1996. "A Gene (RPGR) with Homology to the RCC1 Guanine Nucleotide Exchange Factor Is Mutated in X-Linked Retinitis Pigmentosa (RP3)." *Nature Genetics* 13 (1): 35–42. https://doi.org/10.1038/ng0596-35.

Miller, Jeffrey C., Siyuan Tan, Guijuan Qiao, Kyle A. Barlow, Jianbin Wang, Danny F. Xia, Xiangdong Meng, et al. 2011. "A TALE Nuclease Architecture for Efficient Genome Editing." *Nature Biotechnology* 29 (2): 143–50. https://doi.org/10.1038/nbt.1755.

Mimitou, Eleni P., and Lorraine S. Symington. 2010. "Ku Prevents Exo1 and Sgs1-Dependent Resection of DNA Ends in the Absence of a Functional MRX Complex or Sae2." *EMBO Journal* 29 (19): 3358–69. https://doi.org/10.1038/emboj.2010.193.

Mircetic, Jovan, Iris Steinebrunner, Li Ding, Ji-Feng Fei, Aliona Bogdanova, David Drechsel, and Frank Buchholz. 2017. “Purified Cas9 Fusion Proteins for Advanced Genome Manipulation.” *Small Methods* 1 (4): 1600052. https://doi.org/10.1002/smtd.201600052.

Mitchell, D. R., and Y. Kang. 1991. “Identification of Oda6 as a Chlamydomonas Dynein Mutant by Rescue with the Wild-Type Gene.” *Journal of Cell Biology* 113 (4): 835–42. https://doi.org/10.1083/jcb.113.4.835.

Mitchell, David R, and Joel L Rosenbaum. 1986. “Protein-Protein Interactions in the 18S ATPase of Chlamydomonas Outer Dynein Arms.” *Cell Motility* 6 (5): 510–20. https://doi.org/10.1002/cm.970060510.

Mitchison, Hannah M., and Enza Maria Valente. 2017. “Motile and Non-Motile Cilia in Human Pathology: From Function to Phenotypes.” *Journal of Pathology* 241 (2): 294–309. https://doi.org/10.1002/path.4843.

Mitchison, Hannah M, Miriam Schmidts, Niki T Loges, Judy Freshour, Athina Dritsoula, Rob A Hirst, Christopher O’Callaghan, et al. 2012. “Mutations in Axonemal Dynein Assembly Factor DNAAF3 Cause Primary Ciliary Dyskinesia.” *Nature Genetics* 44 (4): 381–89. https://doi.org/10.1038/ng.1106.

Mollwitz, Birgit, Elizabeth Brunk, Simone Schmitt, Florence Pojer, Michael Bannwarth, Marc Schiltz, Ursula Rothlisberger, and Kai Johnsson. 2012. “Directed Evolution of the Suicide Protein O 6-Alkylguanine-DNA Alkyltransferase for Increased Reactivity Results in an Alkylated Protein with Exceptional Stability.” *Biochemistry* 51 (5): 986–94. https://doi.org/10.1021/bi2016537.

Montoro, Daniel T., Adam L. Haber, Moshe Biton, Vladimir Vinarsky, Brian Lin, Susan E. Birket, Feng Yuan, et al. 2018. “A Revised Airway Epithelial Hierarchy Includes CFTR-Expressing Ionocytes.” *Nature* 560 (7718): 319–24. https://doi.org/10.1038/s41586-018-0393-7.

Moon, Andrea F., John M. Pryor, Dale A. Ramsden, Thomas A. Kunkel, Katarzyna Bebenek, and Lars C. Pedersen. 2014. “Sustained Active Site Rigidity during Synthesis by Human DNA Polymerase μ.” *Nature Structural and Molecular Biology* 21 (3): 253–60. https://doi.org/10.1038/nsmb.2766.

Moore, A., E. Escudier, G. Roger, A. Tamalet, B. Pelosse, S. Marlin, A. Clément, et

al. 2006. “RPGR Is Mutated in Patients with a Complex X Linked Phenotype Combining Primary Ciliary Dyskinesia and Retinitis Pigmentosa.” *Journal of Medical Genetics* 43 (4): 326–33. https://doi.org/10.1136/jmg.2005.034868.

Moore, Daniel J., Alexandros Onoufriadis, Amelia Shoemark, Michael A. Simpson, Petra I. zur Lage, Sandra C. de Castro, Lucia Bartoloni, et al. 2013. “Mutations in ZMYND10, a Gene Essential for Proper Axonemal Assembly of Inner and Outer Dynein Arms in Humans and Flies, Cause Primary Ciliary Dyskinesia.” *The American Journal of Human Genetics*. Vol. 93. https://doi.org/10.1016/j.ajhg.2013.07.009.

Moscou, Matthew J., and Adam J. Bogdanove. 2009. “A Simple Cipher Governs DNA Recognition by TAL Effectors.” *Science* 326 (5959): 1501. https://doi.org/10.1126/science.1178817.

Moss, A. G., J. L. Gatti, and G. B. Witman. 1992. “The Motile β/IC1 Subunit of Sea Urchin Sperm Outer Arm Dynein Does Not Form a Rigor Bond.” *Journal of Cell Biology* 118 (5): 1177–88. https://doi.org/10.1083/jcb.118.5.1177.

Munier, Annie, Catherine Serres, Marie-Louise Kann, Mathieu Boissan, Corinne Lesaffre, Jacqueline Capeau, Jean-Pierre Fouquet, and Marie-Lise Lacombe. 2003. “Nm23/NDP Kinases in Human Male Germ Cells: Role in Spermiogenesis and Sperm Motility?” *Experimental Cell Research* 289 (2): 295–306. https://doi.org/10.1016/s0014-4827(03)00268-4.

Munye, Mustafa M., Aristides D. Tagalakis, Josephine L. Barnes, Rachel E. Brown, Robin J. McAnulty, Steven J. Howe, and Stephen L. Hart. 2016. “Minicircle DNA Provides Enhanced and Prolonged Transgene Expression Following Airway Gene Transfer.” *Scientific Reports* 6 (March): 23125. https://doi.org/10.1038/srep23125.

Muzumdar, Mandar Deepak, Bosiljka Tasic, Kazunari Miyamichi, Ng Li, and Liqun Luo. 2007. “A Global Double-Fluorescent Cre Reporter Mouse.” *Genesis* 45 (9): 593–605. https://doi.org/10.1002/dvg.20335.

Nachury, Maxence V., and David U. Mick. 2019. “Establishing and Regulating the Composition of Cilia for Signal Transduction.” *Nature Reviews Molecular Cell Biology*. Nature Publishing Group. https://doi.org/10.1038/s41580-019-0116-4.

Nakade, Shota, Takuya Tsubota, Yuto Sakane, Satoshi Kume, Naoaki Sakamoto,

Masanobu Obara, Takaaki Daimon, et al. 2014. “Microhomology-Mediated End-Joining-Dependent Integration of Donor DNA in Cells and Animals Using TALENs and CRISPR/Cas9.” *Nature Communications* 5 (11): 118–33. https://doi.org/10.1038/ncomms6560.

Neesen, J, R Kirschner, M Ochs, A Schmiedl, B Habermann, C Mueller, A F Holstein, T Nuesslein, I Adham, and W Engel. 2001. “Disruption of an Inner Arm Dynein Heavy Chain Gene Results in Asthenozoospermia and Reduced Ciliary Beat Frequency.” *Human Molecular Genetics* 10 (11): 1117–28. https://doi.org/10.1093/hmg/10.11.1117.

Nicastro, Daniela, Cindi Schwartz, Jason Pierson, Richard Gaudette, Mary E. Porter, and J. Richard McIntosh. 2006. “The Molecular Architecture of Axonemes Revealed by Cryoelectron Tomography.” *Science* 313 (5789): 944–48. https://doi.org/10.1126/science.1128618.

Nicholas, Matthew P., Peter Höök, Sibylle Brenner, Caitlin L. Wynne, Richard B. Vallee, and Arne Gennerich. 2015. “Control of Cytoplasmic Dynein Force Production and Processivity by Its C-Terminal Domain.” *Nature Communications* 6: 6206. https://doi.org/10.1038/ncomms7206.

Nishimasu, Hiroshi, F Ann Ran, Patrick D Hsu, Silvana Konermann, Soraya I. Shehata, Naoshi Dohmae, Ryuichiro Ishitani, Feng Zhang, and Osamu Nureki. 2014. “Crystal Structure of Cas9 in Complex with Guide RNA and Target DNA.” *Cell* 156 (5): 935–49. https://doi.org/10.1016/j.cell.2014.02.001.

Nonaka, Shigenori, Hidetaka Shiratori, Yukio Saijoh, and Hiroshi Hamada. 2002. “Determination of Left-Right Patterning of the Mouse Embryo by Artificial Nodal Flow.” *Nature* 418 (6893): 96–99. https://doi.org/10.1038/nature00849.

O’Callaghan, C., P. Chetcuti, and E. Moya. 2010. “High Prevalence of Primary Ciliary Dyskinesia in a British Asian Population.” *Archives of Disease in Childhood* 95 (1): 51–52. https://doi.org/10.1136/adc.2009.158493.

O’Callaghan, Chris, Kulvinder Sikand, and Mark A. Chilvers. 2012. “Analysis of Ependymal Ciliary Beat Pattern and Beat Frequency Using High Speed Imaging: Comparison with the Photomultiplier and Photodiode Methods.” *Cilia* 1 (8). https://doi.org/10.1186/2046-2530-1-8.

Oda, Toshiyuki, Tatsuki Abe, Haruaki Yanagisawa, and Masahide Kikkawa. 2016.

"Docking-Complex-Independent Alignment of Chlamydomonas Outer Dynein Arms with 24-Nm Periodicity in Vitro." *Journal of Cell Science* 129 (8): 1547–51. https://doi.org/10.1242/jcs.184598.

Oda, Toshiyuki, Nobutaka Hirokawa, and Masahide Kikkawa. 2007. "Three-Dimensional Structures of the Flagellar Dynein-Microtubule Complex by Cryoelectron Microscopy." *Journal of Cell Biology* 177 (2): 243–52. https://doi.org/10.1083/jcb.200609038.

Oda, Toshiyuki, Haruaki Yanagisawa, Ritsu Kamiya, and Masahide Kikkawa. 2014. "A Molecular Ruler Determines the Repeat Length in Eukaryotic Cilia and Flagella." *Science (New York, N.Y.)* 346 (6211): 857–60. https://doi.org/10.1126/science.1260214.

Ogawa, K., H. Takai, A. Ogiwara, E. Yokota, T. Shimizu, K. Inaba, and H. Mohri. 1996. "Is Outer Arm Dynein Intermediate Chain 1 Multifunctional?" *Molecular Biology of the Cell* 7 (12): 1895–1907. https://doi.org/10.1091/mbc.7.12.1895.

Ogawa, K, and I R Gibbons. 1976. "Dynein 2. A New Adenosine Triphosphatase from Sea Urchin Sperm Flagella." *The Journal of Biological Chemistry* 251 (18): 5793–5801. http://www.ncbi.nlm.nih.gov/pubmed/134996.

Olbrich, Heike, Karsten Häffner, Andreas Kispert, Alexander Völkel, Andreas Volz, Gürsel Sasmaz, Richard Reinhardt, et al. 2002. "Mutations in DNAH5 Cause Primary Ciliary Dyskinesia and Randomization of Left-Right Asymmetry." *Nature Genetics* 30 (2): 143–44. https://doi.org/10.1038/ng817.

Olcese, Chiara, Mitali P. Patel, Amelia Shoemark, Santeri Kiviluoto, Marie Legendre, Hywel J. Williams, Cara K. Vaughan, et al. 2017. "X-Linked Primary Ciliary Dyskinesia Due to Mutations in the Cytoplasmic Axonemal Dynein Assembly Factor PIH1D3." *Nature Communications* 8. https://doi.org/10.1038/ncomms14279.

Olstad, Emilie W., Christa Ringers, Jan N. Hansen, Adinda Wens, Cecilia Brandt, Dagmar Wachten, Emre Yaksi, and Nathalie Jurisch-Yaksi. 2019. "Ciliary Beating Compartmentalizes Cerebrospinal Fluid Flow in the Brain and Regulates Ventricular Development." *Current Biology* 29 (2): 229-241.e6. https://doi.org/10.1016/j.cub.2018.11.059.

Oltean, Alina, Andrew J. Schaffer, Philip V. Bayly, and Steven L. Brody. 2018.

"Quantifying Ciliary Dynamics during Assembly Reveals Stepwise Waveform Maturation in Airway Cells." *American Journal of Respiratory Cell and Molecular Biology* 59 (4): 511–22. https://doi.org/10.1165/rcmb.2017-0436OC.

Omran, Heymut, Daisuke Kobayashi, Heike Olbrich, Tatsuya Tsukahara, Niki T. Loges, Haruo Hagiwara, Qi Zhang, et al. 2008. "Ktu/PF13 Is Required for Cytoplasmic Pre-Assembly of Axonemal Dyneins." *Nature* 456 (7222): 611–16. https://doi.org/10.1038/nature07471.

Onoufriadis, Alexandros, Tamara Paff, Dinu Antony, Amelia Shoemark, Dimitra Micha, Bertus Kuyt, Miriam Schmidts, et al. 2013. "Splice-Site Mutations in the Axonemal Outer Dynein Arm Docking Complex Gene CCDC114 Cause Primary Ciliary Dyskinesia." *American Journal of Human Genetics* 92 (1): 88–98. https://doi.org/10.1016/j.ajhg.2012.11.002.

Orthwein, Alexandre, Sylvie M. Noordermeer, Marcus D. Wilson, Sébastien Landry, Radoslav I. Enchev, Alana Sherker, Meagan Munro, et al. 2015. "A Mechanism for the Suppression of Homologous Recombination in G1 Cells." *Nature* 528 (7582): 422–26. https://doi.org/10.1038/nature16142.

Ostrowski, L. E., W. Yin, M. Patel, J. Sechelski, T. Rogers, K. Burns, B. R. Grubb, and J. C. Olsen. 2014. "Restoring Ciliary Function to Differentiated Primary Ciliary Dyskinesia Cells with a Lentiviral Vector." *Gene Therapy* 21 (3): 253–61. https://doi.org/10.1038/gt.2013.79.

Owa, Mikito, Akane Furuta, Jiro Usukura, Fumio Arisaka, Stephen M King, George B Witman, Ritsu Kamiya, and Ken-ichi Wakabayashi. 2014. "Cooperative Binding of the Outer Arm-Docking Complex Underlies the Regular Arrangement of Outer Arm Dynein in the Axoneme." *Proceedings of the National Academy of Sciences* 111 (26): 9461–66. https://doi.org/10.1073/pnas.1403101111.

Padma, Potturi, Akiko Hozumi, Kazuo Ogawa, and Kazuo Inaba. 2001. "Molecular Cloning and Characterization of a Thioredoxin/Nucleoside Diphosphate Kinase Related Dynein Intermediate Chain from the Ascidian, Ciona Intestinalis." *Gene* 275 (1): 177–83. https://doi.org/10.1016/S0378-1119(01)00661-8.

Paff, Tamara, Niki T. Loges, Isabella Aprea, Kaman Wu, Zeineb Bakey, Eric G. Haarman, Johannes M.A. Daniels, et al. 2017. "Mutations in PIH1D3 Cause X-

Linked Primary Ciliary Dyskinesia with Outer and Inner Dynein Arm Defects." *American Journal of Human Genetics*. https://doi.org/10.1016/j.ajhg.2016.11.019.

Paix, Alexandre, Andrew Folkmann, Daniel H Goldman, Heather Kulaga, Michael J Grzelak, Dominique Rasoloson, Supriya Paidemarry, Rachel Green, Randall R Reed, and Geraldine Seydoux. 2017. "Precision Genome Editing Using Synthesis-Dependent Repair of Cas9-Induced DNA Breaks." *Proceedings of the National Academy of Sciences* 114 (50): E10745–54. https://doi.org/10.1073/pnas.1711979114.

Panizzi, Jennifer R., Anita Becker-Heck, Victoria H. Castleman, Dalal A. Al-Mutairi, Yan Liu, Niki T. Loges, Narendra Pathak, et al. 2012. "CCDC103 Mutations Cause Primary Ciliary Dyskinesia by Disrupting Assembly of Ciliary Dynein Arms." *Nature Genetics* 44 (6): 714–19. https://doi.org/10.1038/ng.2277.

Pannunzio, Nicholas R., Go Watanabe, and Michael R. Lieber. 2018. "Nonhomologous DNA End-Joining for Repair of DNA Double-Strand Breaks." *Journal of Biological Chemistry*. American Society for Biochemistry and Molecular Biology Inc. https://doi.org/10.1074/jbc.TM117.000374.

Parmee, Emma R., Hyun O. Ok, Mari R. Candelore, Laurie Tota, Liping Deng, Catherine D. Strader, Matthew J. Wyvratt, Michael H. Fisher, and Ann E. Weber. 1998. "Discovery of L-755,507: A Subnanomolar Human B3 Adrenergic Receptor Agonist." *Bioorganic and Medicinal Chemistry Letters*. https://doi.org/10.1016/S0960-894X(98)00170-X.

Patel-King, Ramila S., Miho Sakato-Antoku, Maya Yankova, and Stephen M. King. 2019. "WDR92 Is Required for Axonemal Dynein Heavy Chain Stability in Cytoplasm." *Molecular Biology of the Cell*, mbc.E19-03-0139. https://doi.org/10.1091/mbc.e19-03-0139.

Patel-King, Ramila S, Oksana Gorbatyuk, Sachiko Takebe, and Stephen M King. 2004. "Flagellar Radial Spokes Contain a Ca2+-Stimulated Nucleoside Diphosphate Kinase." *Molecular Biology of the Cell* 15 (8): 3891–3902. https://doi.org/10.1091/mbc.e04-04-0352.

Patel-King, Ramila S, and Stephen M King. 2009. "An Outer Arm Dynein Light Chain Acts in a Conformational Switch for Flagellar Motility." *Journal of Cell Biology*

186 (2): 283–95. https://doi.org/10.1083/jcb.200905083.

Pazour, G J, A Koutoulis, S E Benashski, B L Dickert, H Sheng, R S Patel-King, S M King, and G B Witman. 1999. “LC2, the Chlamydomonas Homologue of the t Complex-Encoded Protein Tctex2, Is Essential for Outer Dynein Arm Assembly.” *Molecular Biology of the Cell* 10 (10): 3507–20. https://doi.org/10.1091/mbc.10.10.3507.

Pazour, Gregory J., Bethany L. Dickert, Yvonne Vucica, E. Scott Seeley, Joel L. Rosenbaum, George B. Witman, and Douglas G. Cole. 2000. “Chlamydomonas IFT88 and Its Mouse Homologue, Polycystic Kidney Disease Gene Tg737, Are Required for Assembly of Cilia and Flagella.” *Journal of Cell Biology* 151 (3): 709–18. https://doi.org/10.1083/jcb.151.3.709.

Pedersen, Lotte B, and Joel L Rosenbaum. 2008. “Chapter Two Intraflagellar Transport (IFT). Role in Ciliary Assembly, Resorption and Signalling.” *Current Topics in Developmental Biology*. https://doi.org/10.1016/S0070-2153(08)00802-8.

Pennarun, Gaëlle, Estelle Escudier, Catherine Chapelin, Anne-Marie Bridoux, Valère Cacheux, Gilles Roger, Annick Clément, Michel Goossens, Serge Amselem, and Bénédicte Duriez. 2002. “Loss-of-Function Mutations in a Human Gene Related to Chlamydomonas Reinhardtii Dynein IC78 Result in Primary Ciliary Dyskinesia.” *The American Journal of Human Genetics* 65 (6): 1508–19. https://doi.org/10.1086/302683.

Piatti, Gioia, Maria Margherita De Santi, Sara Torretta, Lorenzo Pignataro, Daniela Soi, and Umberto Ambrosetti. 2017. “Cilia and Ear: A Study on Adults Affected by Primary Ciliary Dyskinesia.” *Annals of Otology, Rhinology and Laryngology* 126 (4): 322–27. https://doi.org/10.1177/0003489417691299.

Pichon, Xavier, Amandine Bastide, Adham Safieddine, Racha Chouaib, Aubin Samacoits, Eugenia Basyuk, Marion Peter, Florian Mueller, and Edouard Bertrand. 2016. “Visualization of Single Endogenous Polysomes Reveals the Dynamics of Translation in Live Human Cells.” *The Journal of Cell Biology* 214 (6): 769 LP – 781. https://doi.org/10.1083/jcb.201605024.

Pinder, Jordan, Jayme Salsman, and Graham Dellaire. 2015. “Nuclear Domain ‘knock-in’ Screen for the Evaluation and Identification of Small Molecule

Enhancers of CRISPR-Based Genome Editing." *Nucleic Acids Research* 43 (19): 9379–92. https://doi.org/10.1093/nar/gkv993.

Piperno, G., and Z. Ramanis. 1991. "The Proximal Portion of Chlamydomonas Flagella Contains a Distinct Set of Inner Dynein Arms." *Journal of Cell Biology* 112 (4): 701–9. https://doi.org/10.1083/jcb.112.4.701.

Piperno, G, Z Ramanis, E F Smith, and W S Sale. 1990. "Three Distinct Inner Dynein Arms in Chlamydomonas Flagella: Molecular Composition and Location in the Axoneme." *Journal of Cell Biology* 110 (2): 379–89. https://doi.org/10.1083/jcb.110.2.379.

Piperno, Gianni, Kara Mead, and Scott Henderson. 1996. "Inner Dynein Arms but Not Outer Dynein Arms Require the Activity of Kinesin Homologue Protein KHP1FLA10 to Reach the Distal Part of Flagella in Chlamydomonas." *Journal of Cell Biology* 133 (2): 371–79. https://doi.org/10.1083/jcb.133.2.371.

Plasschaert, Lindsey W., Rapolas Žilionis, Rayman Choo-Wing, Virginia Savova, Judith Knehr, Guglielmo Roma, Allon M. Klein, and Aron B. Jaffe. 2018. "A Single-Cell Atlas of the Airway Epithelium Reveals the CFTR-Rich Pulmonary Ionocyte." *Nature*. Nature Publishing Group. https://doi.org/10.1038/s41586-018-0394-6.

Port, F., H.-M. Chen, T. Lee, and S. L. Bullock. 2014. "Optimized CRISPR/Cas Tools for Efficient Germline and Somatic Genome Engineering in Drosophila." *Proceedings of the National Academy of Sciences* 111 (29): E2967–76. https://doi.org/10.1073/pnas.1405500111.

Porter, Mary E., and Winfield S. Sale. 2000. "The 9 + 2 Axoneme Anchors Multiple Inner Arm Dyneins and a Network of Kinases and Phosphatases That Control Motility." *Journal of Cell Biology*. https://doi.org/10.1083/jcb.151.5.F37.

Price, Michael E., and Joseph H. Sisson. 2019. "Redox Regulation of Motile Cilia in Airway Disease." *Redox Biology*, 101146. https://doi.org/10.1016/j.redox.2019.101146.

Quadros, Rolen M., Hiromi Miura, Donald W. Harms, Hisako Akatsuka, Takehito Sato, Tomomi Aida, Ronald Redder, et al. 2017. "Easi-CRISPR: A Robust Method for One-Step Generation of Mice Carrying Conditional and Insertion Alleles Using Long SsDNA Donors and CRISPR Ribonucleoproteins." *Genome*

Biology 18 (1). https://doi.org/10.1186/s13059-017-1220-4.

Quarantotti, Valentina, Jia-Xuan Chen, Julia Tischer, Carmen Gonzalez Tejedo, Evaggelia K Papachristou, Clive S D'Santos, John V Kilmartin, Martin L Miller, and Fanni Gergely. 2019. "Centriolar Satellites Are Acentriolar Assemblies of Centrosomal Proteins." *The EMBO Journal* 38 (June): e101082. https://doi.org/10.15252/embj.2018101082.

Raidt, Johanna, Claudius Werner, Tabea Menchen, Gerard W. Dougherty, Heike Olbrich, Niki T. Loges, Ralf Schmitz, Petra Pennekamp, and Heymut Omran. 2015. "Ciliary Function and Motor Protein Composition of Human Fallopian Tubes." *Human Reproduction* 30 (12): 2871–80. https://doi.org/10.1093/humrep/dev227.

Ran, F. Ann, Le Cong, Winston X. Yan, David A. Scott, Jonathan S. Gootenberg, Andrea J. Kriz, Bernd Zetsche, et al. 2015. "In Vivo Genome Editing Using Staphylococcus Aureus Cas9." *Nature* 520 (7546): 186–90. https://doi.org/10.1038/nature14299.

Rawlins, Emma L., Lawrence E. Ostrowski, Scott H. Randell, and Brigid L.M. Hogan. 2007. "Lung Development and Repair: Contribution of the Ciliated Lineage." *Proceedings of the National Academy of Sciences of the United States of America* 104 (2): 410–17. https://doi.org/10.1073/pnas.0610770104.

Rees, Holly A., Wei Hsi Yeh, and David R. Liu. 2019. "Development of HRad51–Cas9 Nickase Fusions That Mediate HDR without Double-Stranded Breaks." *Nature Communications* 10 (1): 2212. https://doi.org/10.1038/s41467-019-09983-4.

Reiter, Jeremy F., and Michel R. Leroux. 2017. "Genes and Molecular Pathways Underpinning Ciliopathies." *Nature Reviews Molecular Cell Biology* 18 (9): 533–47. https://doi.org/10.1038/nrm.2017.60.

Richardson, Chris D., Katelynn R. Kazane, Sharon J. Feng, Elena Zelin, Nicholas L. Bray, Axel J. Schäfer, Stephen N. Floor, and Jacob E. Corn. 2018. "CRISPR–Cas9 Genome Editing in Human Cells Occurs via the Fanconi Anemia Pathway." *Nature Genetics* 50 (8): 1132–39. https://doi.org/10.1038/s41588-018-0174-0.

Richardson, Christopher D, Graham J Ray, Mark A Dewitt, Gemma L Curie, and

Jacob E Corn. 2016. “Enhancing Homology-Directed Genome Editing by Catalytically Active and Inactive CRISPR-Cas9 Using Asymmetric Donor DNA.” *Nature Biotechnology* 34 (3): 339–44. https://doi.org/10.1038/nbt.3481.

Rimmer, Joanne. 2018. “The Sense of Smell in Primary Ciliary Dyskinesia.” *Thorax*, October 1, 2018. https://doi.org/10.1136/thoraxjnl-2018-211620.

Robert, Francis, Mathilde Barbeau, Sylvain Éthier, Josée Dostie, and Jerry Pelletier. 2015. “Pharmacological Inhibition of DNA-PK Stimulates Cas9-Mediated Genome Editing.” *Genome Medicine* 7 (1): 93. https://doi.org/10.1186/s13073-015-0215-6.

Roberts, Anthony J., Naoki Numata, Matt L. Walker, Yusuke S. Kato, Bara Malkova, Takahide Kon, Reiko Ohkura, et al. 2009. “AAA+ Ring and Linker Swing Mechanism in the Dynein Motor.” *Cell* 136 (3): 485–95. https://doi.org/10.1016/j.cell.2008.11.049.

Roseman, R.R., V. Pirrotta, and P.K. Geyer. 1993. “The Su(Hw) Protein Insulates Expression of the Drosophila Melanogaster White Gene from Chromosomal Position-Effects.” *The EMBO Journal* 12 (2): 435–42. https://doi.org/10.1002/j.1460-2075.1993.tb05675.x.

Ruff, Patrick, Kyung Duk Koh, Havva Keskin, Rekha B Pai, and Francesca Storici. 2014. “Aptamer-Guided Gene Targeting in Yeast and Human Cells.” *Nucleic Acids Research* 42 (7): e61. https://doi.org/10.1093/nar/gku101.

Sadek, Christine M., Anastasios E. Damdimopoulos, Markku Pelto-Huikko, Jan Åke Gustafsson, Giannis Spyrou, and Antonio Miranda-Vizuete. 2001. “Sptrx-2, a Fusion Protein Composed of One Thioredoxin and Three Tandemly Repeated NDP-Kinase Domains Is Expressed in Human Testis Germ Cells.” *Genes to Cells* 6 (12): 1077–90. https://doi.org/10.1046/j.1365-2443.2001.00484.x.

Sadek, Christine M., Alberto Jiménez, Anastasios E. Damdimopoulos, Thomas Kieselbach, Magnus Nord, Jan Åke Gustafsson, Giannis Spyrou, et al. 2003. “Characterization of Human Thioredoxin-like 2: A Novel Microtubule-Binding Thioredoxin Expressed Predominantly in the Cilia of Lung Airway Epithelium and Spermatid Manchette and Axoneme.” *Journal of Biological Chemistry* 278 (15): 13133–42. https://doi.org/10.1074/jbc.M300369200.

Sakakibara, H., S. Takada, Stephen M. King, G. B. Witman, and R. Kamiya. 1993.

"A Chlamydomonas Outer Arm Dynein Mutant with a Truncated β Heavy Chain." *Journal of Cell Biology* 122 (3): 653–61. https://doi.org/10.1083/jcb.122.3.653.

Sakato, Miho, and Stephen M. King. 2003. "Calcium Regulates ATP-Sensitive Microtubule Binding by Chlamydomonas Outer Arm Dynein." *Journal of Biological Chemistry* 278 (44): 43571–79. https://doi.org/10.1074/jbc.M305894200.

Sakaue-Sawano, Asako, Hiroshi Kurokawa, Toshifumi Morimura, Aki Hanyu, Hiroshi Hama, Hatsuki Osawa, Saori Kashiwagi, et al. 2008. "Visualizing Spatiotemporal Dynamics of Multicellular Cell-Cycle Progression." *Cell* 132 (3): 487–98. https://doi.org/10.1016/j.cell.2007.12.033.

Sale, Winfield S., and Peter Satir. 1977. "The Termination of the Central Microtubules from the Cilia of Tetrahymena Pyriformis." *Cell Biology International Reports* 1 (1): 45–49. https://doi.org/10.1016/0309-1651(77)90008-X.

Sale, Winfield S, Ursula W Goodenough, and John E Heuser. 1985. "The Substructure of Isolated and in Situ Outer Dynein Arms of Sea Urchin Sperm Flagella." *Journal of Cell Biology* 101 (4): 1400–1412. https://doi.org/10.1083/jcb.101.4.1400.

Sallmyr, Annahita, and Alan E. Tomkinson. 2018. "Repair of DNA Double-Strand Breaks by Mammalian Alternative End-Joining Pathways." *Journal of Biological Chemistry*. American Society for Biochemistry and Molecular Biology Inc. https://doi.org/10.1074/jbc.TM117.000375.

Samant, Sadhana A., Olugbemiga Ogunkua, Ling Hui, John Fossella, and Stephen H. Pilder. 2002. "The t Complex Distorter 2 Candidate Gene, Dnahc8, Encodes at Least Two Testis-Specific Axonemal Dynein Heavy Chains That Differ Extensively at Their Amino and Carboxyl Termini." *Developmental Biology* 250 (1): 24–43. https://doi.org/10.1006/dbio.2002.0769.

Sapranauskas, Rimantas, Giedrius Gasiunas, Christophe Fremaux, Rodolphe Barrangou, Philippe Horvath, and Virginijus Siksnys. 2011. "The Streptococcus Thermophilus CRISPR/Cas System Provides Immunity in Escherichia Coli." *Nucleic Acids Research* 39 (21): 9275–82. https://doi.org/10.1093/nar/gkr606.

Satir, Peter. 1965. “STUDIES ON CILIA : II. Examination of the Distal Region of the Ciliary Shaft and the Role of the Filaments in Motility.” *The Journal of Cell Biology* 26 (3): 805–34. https://doi.org/10.1083/jcb.26.3.805.

Satir, Peter. 1992. “Mechanisms of Ciliary Movement: Contributions from Electron Microscopy.” *Scanning Microscopy* 6 (2): 573–79.

Satir, Peter. 1995. “Landmarks in Cilia Research from Leeuwenhoek to Us.” *Cell Motil. Cytoskel.* 32 (2): 90–94. https://doi.org/10.1002/cm.970320203.

Savic, Natasa, Femke C.A.S. Ringnalda, Helen Lindsay, Christian Berk, Katja Bargsten, Yizhou Li, Dario Neri, et al. 2018. “Covalent Linkage of the DNA Repair Template to the CRISPR-Cas9 Nuclease Enhances Homology-Directed Repair.” *ELife* 7: e33761. https://doi.org/10.7554/eLife.33761.

Sawamoto, Kazunobu, Hynek Wichterle, Oscar Gonzalez-Perez, Jeremy A. Cholfin, Masayuki Yamada, Nathalie Spassky, Noel S. Murcia, et al. 2006. “New Neurons Follow the Flow of Cerebrospinal Fluid in the Adult Brain.” *Science* 311 (5761): 629–32. https://doi.org/10.1126/science.1119133.

Schäfer, Mireille, Karim Nayernia, Wolfgang Engel, and Ulrich Schäfer. 1995. “Translational Control in Spermatogenesis.” *Developmental Biology* 172 (2): 344–52. https://doi.org/10.1006/dbio.1995.8049.

Schindelin, Johannes, Ignacio Arganda-Carreras, Erwin Frise, Verena Kaynig, Mark Longair, Tobias Pietzsch, Stephan Preibisch, et al. 2012. “Fiji: An Open-Source Platform for Biological-Image Analysis.” *Nature Methods* 9 (7): 676–82. https://doi.org/10.1038/nmeth.2019.

Schlager, Max A, Ha Thi Hoang, Linas Urnavicius, Simon L Bullock, and Andrew P Carter. 2014. “In Vitro Reconstitution of a Highly Processive Recombinant Human Dynein Complex.” *The EMBO Journal* 33 (17): 1855–68. https://doi.org/10.15252/embj.201488792.

Schmidt, Helgo, Emma S. Gleave, and Andrew P. Carter. 2012. “Insights into Dynein Motor Domain Function from a 3.3-Å Crystal Structure.” *Nature Structural and Molecular Biology* 19 (5): 492–97. https://doi.org/10.1038/nsmb.2272.

Schmidt, Helgo, Ruta Zalyte, Linas Urnavicius, and Andrew P. Carter. 2015.

"Structure of Human Cytoplasmic Dynein-2 Primed for Its Power Stroke." *Nature* 518 (7539): 435–38. https://doi.org/10.1038/nature14023.

Schmidts, Miriam, Yuqing Hou, Claudio R. Cortés, Dorus A. Mans, Celine Huber, Karsten Boldt, Mitali Patel, et al. 2015. "TCTEX1D2 Mutations Underlie Jeune Asphyxiating Thoracic Dystrophy with Impaired Retrograde Intraflagellar Transport." *Nature Communications* 6: 7074. https://doi.org/10.1038/ncomms8074.

Sears, Patrick R., Kristin Thompson, Michael R. Knowles, and C. William Davis. 2013. "Human Airway Ciliary Dynamics." *American Journal of Physiology-Lung Cellular and Molecular Physiology* 304 (3): L170–83. https://doi.org/10.1152/ajplung.00105.2012.

Shah, Abdullah, Farooq Rashid, Hassaan Mehboob Awan, Shanshan Hu, Xiaolin Wang, Liang Chen, and Ge Shan. 2017. "The DEAD-Box RNA Helicase DDX3 Interacts with M6A RNA Demethylase ALKBH5." *Stem Cells International* 2017: 8596135. https://doi.org/10.1155/2017/8596135.

Shah, Alok S., Ben Shahar Yehuda, Thomas O. Moninger, Joel N. Kline, and Michael J. Welsh. 2009. "Motile Cilia of Human Airway Epithelia Are Chemosensory." *Science* 325 (5944): 1131–34. https://doi.org/10.1126/science.1173869.

Shapiro, Adam J., Stephanie D. Davis, Thomas Ferkol, Sharon D. Dell, Margaret Rosenfeld, Kenneth N. Olivier, Scott D. Sagel, et al. 2014. "Laterality Defects Other than Situs Inversus Totalis in Primary Ciliary Dyskinesia: Insights into Situs Ambiguus and Heterotaxy." *Chest* 146 (5): 1176–86. https://doi.org/10.1378/chest.13-1704.

Shapiro, Adam J., Maimoona A. Zariwala, Thomas Ferkol, Stephanie D. Davis, Scott D. Sagel, Sharon D. Dell, Margaret Rosenfeld, et al. 2016. "Diagnosis, Monitoring, and Treatment of Primary Ciliary Dyskinesia: PCD Foundation Consensus Recommendations Based on State of the Art Review." *Pediatric Pulmonology* 51 (2): 115–32. https://doi.org/10.1002/ppul.23304.

Sharma, S., S. M. Javadekar, M. Pandey, M. Srivastava, R. Kumari, and S. C. Raghavan. 2015. "Homology and Enzymatic Requirements of Microhomology-Dependent Alternative End Joining." *Cell Death & Disease* 6: e1697.

https://doi.org/10.1038/cddis.2015.58.

Shih, Juliann, Russ Hodge, and Miguel A. Andrade-Navarro. 2015. “Comparison of Inter- and Intraspecies Variation in Humans and Fruit Flies.” *Genomics Data* 3: 49–54. https://doi.org/10.1016/j.gdata.2014.11.010.

Shoemark, Amelia, and Jane S Lucas. 2018. *Diagnosis of Primary Ciliary Dyskinesia: Current Practice and Future Perspectives*. *Bronchiectasis*. 81st ed. European Respiratory Society.

Siewert, A.K. 1904. “Ueber Einen Fall van Bronchiectasie Bei Einem Patienten Mito Situs Inversus Viscerum.” *Berlin Klin Wochen Schr* 6: 139–41.

Singla, Veena, and Jeremy F. Reiter. 2006. “The Primary Cilium as the Cell’s Antenna: Signaling at a Sensory Organelle.” *Science*. https://doi.org/10.1126/science.1124534.

Singla, Veena, Miriam Romaguera-Ros, Jose Manuel Garcia-Verdugo, and Jeremy F. Reiter. 2010. “Ofd1, a Human Disease Gene, Regulates the Length and Distal Structure of Centrioles.” *Developmental Cell* 18 (3): 410–24. https://doi.org/10.1016/j.devcel.2009.12.022.

Siwek, Wojciech, Mariluz Gómez-Rodríguez, Daniel Sobral, Ivan R. Corrêa, and Lars E.T. Jansen. 2018. “Time-ChIP: A Method to Determine Long-Term Locus-Specific Nucleosome Inheritance.” In *Methods in Molecular Biology*, 1832:131–58. Humana Press Inc. https://doi.org/10.1007/978-1-4939-8663-7_7.

Sloboda, Roger D. 2005. “Intraflagellar Transport and the Flagellar Tip Complex.” *Journal of Cellular Biochemistry*. https://doi.org/10.1002/jcb.20323.

Smith, Elizabeth F., and Pinfen Yang. 2004. “The Radial Spokes and Central Apparatus: Mechano-Chemical Transducers That Regulate Flagellar Motility.” *Cell Motility and the Cytoskeleton*. https://doi.org/10.1002/cm.10155.

Sneeden, Jessica L., Sara M. Grossi, Inger Tappin, Jerard Hurwitz, and Wolf Dietrich Heyer. 2013. “Reconstitution of Recombination-Associated DNA Synthesis with Human Proteins.” *Nucleic Acids Research* 41 (9): 4913–25. https://doi.org/10.1093/nar/gkt192.

Soares, Helena, Bruno Carmona, Sofia Nolasco, Luís Viseu Melo, and João

Gonçalves. 2019. “Cilia Distal Domain: Diversity in Evolutionarily Conserved Structures.” *Cells* 8 (2): 160. https://doi.org/10.3390/cells8020160.

Solinger, Jachen A., Konstantin Kiianitsa, and Wolf Dietrich Heyer. 2002. “Rad54, a Swi2/Snf2-like Recombinational Repair Protein, Disassembles Rad51:DsDNA Filaments.” *Molecular Cell* 10 (5): 1175–88. https://doi.org/10.1016/S1097-2765(02)00743-8.

Song, Jikui, Robert C. Tyler, Min S. Lee, Ejan M. Tyler, and John L. Markley. 2005. “Solution Structure of Isoform 1 of Roadblock/LC7, a Light Chain in the Dynein Complex.” *Journal of Molecular Biology* 354 (5): 1043–51. https://doi.org/10.1016/j.jmb.2005.10.017.

Song, Jun, Dongshan Yang, Jie Xu, Tianqing Zhu, Y. Eugene Chen, and Jifeng Zhang. 2016. “RS-1 Enhances CRISPR/Cas9- and TALEN-Mediated Knock-in Efficiency.” *Nature Communications* 7: 10548. https://doi.org/10.1038/ncomms10548.

Song, Kangkang, Junya Awata, Douglas Tritschler, Raqual Bower, George B. Witman, Mary E. Porter, and Daniela Nicastro. 2015. “In Situ Localization of N and C Termini of Subunits of the Flagellar Nexin-Dynein Regulatory Complex (N-DRC) Using SNAP Tag and Cryo-Electron Tomography.” *Journal of Biological Chemistry* 290 (9): 5341–53. https://doi.org/10.1074/jbc.M114.626556.

Sorokin, S. 1962. “Centrioles and the Formation of Rudimentary Cilia by Fibroblasts and Smooth Muscle Cells.” *The Journal of Cell Biology* 15: 363–77. https://doi.org/10.1083/jcb.15.2.363.

Sorokin, S P. 1968. “Reconstructions of Centriole Formation and Ciliogenesis in Mammalian Lungs.” *Journal of Cell Science* 3 (2): 207–30. http://www.ncbi.nlm.nih.gov/pubmed/5661997.

Srivastava, Mrinal, Mridula Nambiar, Sheetal Sharma, Subhas S. Karki, G. Goldsmith, Mahesh Hegde, Sujeet Kumar, et al. 2012. “An Inhibitor of Nonhomologous End-Joining Abrogates Double-Strand Break Repair and Impedes Cancer Progression.” *Cell* 151 (7): 1474–87. https://doi.org/10.1016/j.cell.2012.11.054.

Standart, Nancy, and Dominique Weil. 2018. “P-Bodies: Cytosolic Droplets for

Coordinated MRNA Storage.” *Trends in Genetics* 34 (8): 612–26. https://doi.org/10.1016/j.tig.2018.05.005.

Stenoien, David L., Tatyana V. Knyushko, Monica P. Londono, Lee K. Opresko, M. Uljana Mayer, Scott T. Brady, Thomas C. Squier, and Diana J. Bigelow. 2007. “Cellular Trafficking of Phospholamban and Formation of Functional Sarcoplasmic Reticulum during Myocyte Differentiation.” *American Journal of Physiology-Cell Physiology* 292 (6): C2084–94. https://doi.org/10.1152/ajpcell.00523.2006.

Stepanek, Ludek, and Gaia Pigino. 2016. “Microtubule Doublets Are Double-Track Railways for Intraflagellar Transport Trains.” *Science* 352 (6286): 721–24. https://doi.org/10.1126/science.aaf4594.

Stepanenko, A. A., and V. V. Dmitrenko. 2015. “HEK293 in Cell Biology and Cancer Research: Phenotype, Karyotype, Tumorigenicity, and Stress-Induced Genome-Phenotype Evolution.” *Gene*. Elsevier. https://doi.org/10.1016/j.gene.2015.05.065.

Stephens, R. E. 1997. “Synthesis and Turnover of Embryonic Sea Urchin Ciliary Proteins during Selective Inhibition of Tubulin Synthesis and Assembly.” *Molecular Biology of the Cell* 8 (11): 2187–98. https://doi.org/10.1091/mbc.8.11.2187.

Supp, Dorothy M., S. Steven Potter, Martina Brueckner, James McGrath, JoMichelle Corrales, Michael R. Kuehn, Linda A. Lowe, and David P. Witte. 1999. “Targeted Deletion of the ATP Binding Domain of Left-Right Dynein Confirms Its Role in Specifying Development of Left-Right Asymmetries.” *Development* 126 (23): 5495–5504.

Susalka, Stephen J., Karina Nikulina, Mark W. Salata, Patricia S. Vaughan, Stephen M. King, Kevin T. Vaughan, and K. Kevin Pfister. 2002. “The Roadblock Light Chain Binds a Novel Region of the Cytoplasmic Dynein Intermediate Chain.” *Journal of Biological Chemistry* 277 (36): 32939–46. https://doi.org/10.1074/jbc.M205510200.

Suzuki, Keiichiro, Yuji Tsunekawa, Reyna Hernandez-Benitez, Jun Wu, Jie Zhu, Euiseok J. Kim, Fumiyuki Hatanaka, et al. 2016. “In Vivo Genome Editing via CRISPR/Cas9 Mediated Homology-Independent Targeted Integration.” *Nature*,

November. https://doi.org/10.1038/nature20565.

Symington, Lorraine S. 2014. “End Resection at Double-Strand Breaks: Mechanism and Regulation.” *Cold Spring Harbor Perspectives in Biology* 6 (8). https://doi.org/10.1101/cshperspect.a016436.

Ta-Shma, Asaf, Rim Hjeij, Zeev Perles, Gerard W. Dougherty, Ibrahim Abu Zahira, Stef J.F. Letteboer, Dinu Antony, et al. 2018. “Homozygous Loss-of-Function Mutations in MNS1 Cause Laterality Defects and Likely Male Infertility.” *PLoS Genetics* 14 (8). https://doi.org/10.1371/journal.pgen.1007602.

Tagalakis, Aristides D., Robin J. McAnulty, James Devaney, Stephen E. Bottoms, John B. Wong, Martin Elbs, Michele J. Writer, et al. 2008. “A Receptor-Targeted Nanocomplex Vector System Optimized for Respiratory Gene Transfer.” *Molecular Therapy* 16 (5): 907–15. https://doi.org/10.1038/mt.2008.38.

Takada, Saeko, Curtis G Wilkerson, Ken-ichi Wakabayashi, Ritsu Kamiya, and George B Witman. 2002. “The Outer Dynein Arm-Docking Complex: Composition and Characterization of a Subunit (Oda1) Necessary for Outer Arm Assembly.” *Molecular Biology of the Cell* 13 (3): 1015–29. https://doi.org/10.1091/mbc.01-04-0201.

Tan, Serena Y, Julie Rosenthal, Xiao-qing Zhao, Richard J Francis, Bishwanath Chatterjee, Steven L Sabol, Kaari L Linask, et al. 2007. “Heterotaxy and Complex Structural Heart Defects in a Mutant Mouse Model of Primary Ciliary Dyskinesia” 117 (12). https://doi.org/10.1172/JCI33284.3742.

Tanaka, Y., Z. Zhang, and N. Hirokawa. 1995. “Identification and Molecular Evolution of New Dynein-like Protein Sequences in Rat Brain.” *Journal of Cell Science* 108 (5): 1883–93.

Tang, Chong, Rachel Klukovich, Hongying Peng, Zhuqing Wang, Tian Yu, Ying Zhang, Huili Zheng, Arne Klungland, and Wei Yan. 2018. “ALKBH5-Dependent M6A Demethylation Controls Splicing and Stability of Long 3′-UTR MRNAs in Male Germ Cells.” *Proceedings of the National Academy of Sciences* 115 (2): E325–33. https://doi.org/10.1073/pnas.1717794115.

Tanner, C. A., P. Rompolas, R. S. Patel-King, O. Gorbatyuk, K.-i. Wakabayashi, G. J. Pazour, and S. M. King. 2008. “Three Members of the LC8/DYNLL Family

Are Required for Outer Arm Dynein Motor Function." *Molecular Biology of the Cell* 19 (9): 3724–34. https://doi.org/10.1091/mbc.e08-04-0362.

Tarkar, Aarti, Niki T. Loges, Christopher E. Slagle, Richard Francis, Gerard W. Dougherty, Joel V. Tamayo, Brett Shook, et al. 2013. "DYX1C1 Is Required for Axonemal Dynein Assembly and Ciliary Motility." *Nature Genetics* 45 (9): 995–1003. https://doi.org/10.1038/ng.2707.

Taschner, Michael, and Esben Lorentzen. 2016. "The Intraflagellar Transport Machinery." *Cold Spring Harbor Perspectives in Biology* 8 (10). https://doi.org/10.1101/cshperspect.a028092.

Taschner, Michael, André Mourão, Mayanka Awasthi, Jerome Basquin, and Esben Lorentzen. 2017. "Structural Basis of Outer Dynein Arm Intraflagellar Transport by the Transport Adaptor Protein ODA16 and the Intraflagellar Transport Protein IFT46." *Journal of Biological Chemistry*. https://doi.org/10.1074/jbc.M117.780155.

Thomas, Clare E., Anja Ehrhardt, and Mark A. Kay. 2003. "Progress and Problems with the Use of Viral Vectors for Gene Therapy." *Nature Reviews Genetics*. https://doi.org/10.1038/nrg1066.

Thurmond, Jim, Joshua L. Goodman, Victor B. Strelets, Helen Attrill, L. Sian Gramates, Steven J. Marygold, Beverley B. Matthews, et al. 2019. "FlyBase 2.0: The next Generation." *Nucleic Acids Research* 47 (D1): D759–65. https://doi.org/10.1093/nar/gky1003.

Tilley, Ann E., Matthew S. Walters, Renat Shaykhiev, and Ronald G. Crystal. 2015. "Cilia Dysfunction in Lung Disease." *Annual Review of Physiology* 77 (1): 379–406. https://doi.org/10.1146/annurev-physiol-021014-071931.

Torné, Júlia, Guillermo A. Orsi, Dominique Ray-Gallet, and Geneviève Almouzni. 2018. "Imaging Newly Synthesized and Old Histone Variant Dynamics Dependent on Chaperones Using the SNAP-Tag System." In *Methods in Molecular Biology*, 1832:207–21. https://doi.org/10.1007/978-1-4939-8663-7_11.

Travis, Sue M, and David L Nelson. 1988. "Purification and Properties of Dyneins from Paramecium Cilia." *BBA - General Subjects* 966 (1): 73–83. https://doi.org/10.1016/0304-4165(88)90130-4.

Tuomanen, Elaine. 1990. “Adjuncts to the Therapy of Bacterial Meningitis.” *Pediatric Infectious Disease Journal* 9 (10): 781–82. https://doi.org/10.1097/00006454-199010000-00041.

Turriziani, Benedetta, Amaya Garcia-Munoz, Ruth Pilkington, Cinzia Raso, Walter Kolch, and Alexander von Kriegsheim. 2014. “On-Beads Digestion in Conjunction with Data-Dependent Mass Spectrometry: A Shortcut to Quantitative and Dynamic Interaction Proteomics.” *Biology* 3 (2): 320–32. https://doi.org/10.3390/biology3020320.

Ueno, H., T. Yasunaga, C. Shingyoji, and K. Hirose. 2008. “Dynein Pulls Microtubules without Rotating Its Stalk.” *Proceedings of the National Academy of Sciences* 105 (50): 19702–7. https://doi.org/10.1073/pnas.0808194105.

Untergasser, Andreas, Ioana Cutcutache, Triinu Koressaar, Jian Ye, Brant C. Faircloth, Maido Remm, and Steven G. Rozen. 2012. “Primer3-New Capabilities and Interfaces.” *Nucleic Acids Research* 40 (15). https://doi.org/10.1093/nar/gks596.

Vanaken, Gert Jan, Laurence Bassinet, Mieke Boon, Rahma Mani, Isabelle Honoré, Jean Francois Papon, Harry Cuppens, et al. 2017. “Infertility in an Adult Cohort with Primary Ciliary Dyskinesia: Phenotype-Gene Association.” *European Respiratory Journal*. European Respiratory Society. https://doi.org/10.1183/13993003.00314-2017.

Viswanadha, Rasagnya, Emily L. Hunter, Ryosuke Yamamoto, Maureen Wirschell, Lea M. Alford, Susan K. Dutcher, and Winfield S. Sale. 2014. “The Ciliary Inner Dynein Arm, I1 Dynein, Is Assembled in the Cytoplasm and Transported by IFT before Axonemal Docking.” *Cytoskeleton* 71 (10): 573–86. https://doi.org/10.1002/cm.21192.

Vladar, Eszter K., and Steven L. Brody. 2013. “Analysis of Ciliogenesis in Primary Culture Mouse Tracheal Epithelial Cells.” In *Methods in Enzymology*, 525:285–309. https://doi.org/10.1016/B978-0-12-397944-5.00014-6.

Wada, Shigeo, Makoto Okuno, and Hideo Mohri. 1991. “Inner Arm Dynein Atpase Fraction of Sea Urchin Sperm Flagella Causes Active Sliding of Axonemal Outer Doublet Microtubule.” *Biochemical and Biophysical Research Communications* 175 (1): 173–78. https://doi.org/10.1016/S0006-

291X(05)81216-1.

Wakabayashi, Ken Ichi, and Stephen M. King. 2006. “Modulation of Chlamydomonas Reinhardtii Flagellar Motility by Redox Poise.” *Journal of Cell Biology*. https://doi.org/10.1083/jcb.200603019.

Wakabayashi, Ken Ichi, Saeko Takada, George B. Witman, and Ritsu Kamiya. 2001. “Transport and Arrangement of the Outer-Dynein-Arm Docking Complex in the Flagella of Chlamydomonas Mutants That Lack Outer Dynein Arms.” *Cell Motility and the Cytoskeleton* 48 (4): 277–86. https://doi.org/10.1002/cm.1015.

Wallmeier, Julia, Dalal A. Al-Mutairi, Chun Ting Chen, Niki Tomas Loges, Petra Pennekamp, Tabea Menchen, Lina Ma, et al. 2014. “Mutations in CCNO Result in Congenital Mucociliary Clearance Disorder with Reduced Generation of Multiple Motile Cilia.” *Nature Genetics* 46 (6): 646–51. https://doi.org/10.1038/ng.2961.

Wallmeier, Julia, Hidetaka Shiratori, Gerard W. Dougherty, Christine Edelbusch, Rim Hjeij, Niki T. Loges, Tabea Menchen, et al. 2016. “TTC25 Deficiency Results in Defects of the Outer Dynein Arm Docking Machinery and Primary Ciliary Dyskinesia with Left-Right Body Asymmetry Randomization.” *The American Journal of Human Genetics*. Vol. 99. https://doi.org/10.1016/j.ajhg.2016.06.014.

Wang, Dan, Phillip W.L. Tai, and Guangping Gao. 2019. “Adeno-Associated Virus Vector as a Platform for Gene Therapy Delivery.” *Nature Reviews Drug Discovery* 18 (5): 358–78. https://doi.org/10.1038/s41573-019-0012-9.

Wei, Qing, Kun Ling, and Jinghua Hu. 2015. “The Essential Roles of Transition Fibers in the Context of Cilia.” *Current Opinion in Cell Biology*. Elsevier Ltd. https://doi.org/10.1016/j.ceb.2015.04.015.

Whitfield, Marjorie, Lucie Thomas, Emilie Bequignon, Alain Schmitt, Laurence Stouvenel, Guy Montantin, Sylvie Tissier, et al. 2019. “Mutations in DNAH17, Encoding a Sperm-Specific Axonemal Outer Dynein Arm Heavy Chain, Cause Isolated Male Infertility Due to Asthenozoospermia.” *The American Journal of Human Genetics* 105 (1): 198–212. https://doi.org/10.1016/j.ajhg.2019.04.015.

Wiedemann, I., A. Maehlmeyer, S. Jansen, A. R. Sharifi, and C. Knorr. 2018. “SNP g.1007A>G within the Porcine DNAL4 Gene Affects Sperm Motility Traits and

Percentage of Midpiece Abnormalities." *Reproduction in Domestic Animals* 53 (2): 401–13. https://doi.org/10.1111/rda.13120.

Wilkerson, Curtis G., Stephen M. King, Anthony Koutoulis, Gregory J. Pazour, and George B. Witman. 1995. "The 78,000 Mr Intermediate Chain of Chlamydomonas Outer Arm Dynein Is a WD-Repeat Protein Required for Arm Assembly." *Journal of Cell Biology* 129 (1): 169–78. https://doi.org/10.1083/jcb.129.1.169.

Wilkes, David E, Hadley E Watson, David R Mitchell, and David J Asai. 2008. "Twenty-Five Dyneins in Tetrahymena: A Re-Examination of the Multidynein Hypothesis." *Cell Motility and the Cytoskeleton* 65 (4): 342–51. https://doi.org/10.1002/cm.20264.

Wirschell, Maureen, Triscia Hendrickson, and Winfield S. Sale. 2007. "Keeping an Eye on I1:I1 Dynein as a Model for Flagellar Dynein Assembly and Regulation." *Cell Motility and the Cytoskeleton* 64 (8): 569–79. https://doi.org/10.1002/cm.20211.

Wirth, Thomas, Nigel Parker, and Seppo Ylä-Herttuala. 2013. "History of Gene Therapy." *Gene* 525 (2): 162–69. https://doi.org/10.1016/j.gene.2013.03.137.

Wong, L. B., I. F. Miller, and D. B. Yeates. 1993. "Nature of the Mammalian Ciliary Metachronal Wave." *Journal of Applied Physiology* 75 (1): 458–67. https://doi.org/10.1152/jappl.1993.75.1.458.

Wright, William Douglass, Shanaya Shital Shah, and Wolf Dietrich Heyer. 2018. "Homologous Recombination and the Repair of DNA Double-Strand Breaks." *Journal of Biological Chemistry*. American Society for Biochemistry and Molecular Biology Inc. https://doi.org/10.1074/jbc.TM118.000372.

Yagi, Toshiki, Itsushi Minoura, Akiko Fujiwara, Ryo Saito, Takuo Yasunaga, Masafumi Hirono, and Ritsu Kamiya. 2005. "An Axonemal Dynein Particularly Important for Flagellar Movement at High Viscosity: Implications from a New Chlamydomonas Mutant Deficient in the Dynein Heavy Chain Gene DHC9." *Journal of Biological Chemistry* 280 (50): 41412–20. https://doi.org/10.1074/jbc.M509072200.

Yang, Diane, Marissa A Scavuzzo, Jolanta Chmielowiec, Robert Sharp, Aleksandar Bajic, and Malgorzata Borowiak. 2016. "Enrichment of G2/M Cell Cycle Phase

in Human Pluripotent Stem Cells Enhances HDR-Mediated Gene Repair with Customizable Endonucleases." *Scientific Reports* 6 (February): 21264. https://doi.org/10.1038/srep21264.

Yang, Pinfen, and Winfield S. Sale. 2000. "Casein Kinase I Is Anchored on Axonemal Doublet Microtubules and Regulates Flagellar Dynein Phosphorylation and Activity." *Journal of Biological Chemistry* 275 (25): 18905–12. https://doi.org/10.1074/jbc.M002134200.

Yang, Taomei, Haoran Cui, Mingxin Wen, Johannes Zuber, Scott C. Kogan, and Guangwei Wei. 2018. "TCEA1 Regulates the Proliferative Potential of Mouse Myeloid Cells." *Experimental Cell Research* 370 (2): 551–60. https://doi.org/10.1016/j.yexcr.2018.07.020.

Yokota, Etsuo, and Issei Mabuchi. 1994. "Isolation and Characterization of a Novel Dynein That Contains C and A Heavy Chains from Sea Urchin Sperm Flagellar Axonemes." *Journal of Cell Science* 107 (2): 345–51.

You Y, Richer EJ, Huang T, Brody SL. 2002. "Growth and Differntiation of Mouse Tracheal Epithelial Cells: Selection of a Proliferative Population." *Am J Physiol Lung Cell Mol Physiol* 283 (1): L1315–21. https://doi.org/10.1016/j.jacr.2010.07.010.

You, Yingjian, Edward J. Richer, Tao Huang, and Steven L. Brody. 2002. "Growth and Differentiation of Mouse Tracheal Epithelial Cells: Selection of a Proliferative Population." *American Journal of Physiology-Lung Cellular and Molecular Physiology* 283 (6): L1315–21. https://doi.org/10.1152/ajplung.00169.2002.

Young, Samantha A.M., Haruhiko Miyata, Yuhkoh Satouh, Hirotaka Kato, Kaori Nozawa, Ayako Isotani, R. John Aitken, Mark A. Baker, and Masahito Ikawa. 2015. "CRISPR/Cas9-Mediated Rapid Generation of Multiple Mouse Lines Identified Ccdc63 as Essential for Spermiogenesis." *International Journal of Molecular Sciences* 16 (10): 24732–50. https://doi.org/10.3390/ijms161024732.

Yu, Chen, Yanxia Liu, Tianhua Ma, Kai Liu, Shaohua Xu, Yu Zhang, Honglei Liu, et al. 2015. "Small Molecules Enhance Crispr Genome Editing in Pluripotent Stem Cells." *Cell Stem Cell* 16 (2): 142–47. https://doi.org/10.1016/j.stem.2015.01.003.

Zariwala, Maimoona A, Heon Yung Gee, Małgorzata Kurkowiak, Dalal A Al-Mutairi, Margaret W Leigh, Toby W Hurd, Rim Hjeij, et al. 2013. “ZMYND10 Is Mutated in Primary Ciliary Dyskinesia and Interacts with LRRC6.” *American Journal of Human Genetics* 93 (2): 336–45. https://doi.org/10.1016/j.ajhg.2013.06.007.

Zepp, Jarod A., and Edward E. Morrisey. 2019. “Cellular Crosstalk in the Development and Regeneration of the Respiratory System.” *Nature Reviews Molecular Cell Biology*. Nature Publishing Group. https://doi.org/10.1038/s41580-019-0141-3.

Zhang, Jian Ping, Xiao Lan Li, Guo Hua Li, Wanqiu Chen, Cameron Arakaki, Gary D. Botimer, David Baylink, et al. 2017. “Efficient Precise Knockin with a Double Cut HDR Donor after CRISPR/Cas9-Mediated Double-Stranded DNA Cleavage.” *Genome Biology* 18 (1): 35–53. https://doi.org/10.1186/s13059-017-1164-8.

Zhang, Kai, Helen E. Foster, Arnaud Rondelet, Samuel E. Lacey, Nadia Bahi-Buisson, Alexander W. Bird, and Andrew P. Carter. 2017. “Cryo-EM Reveals How Human Cytoplasmic Dynein Is Auto-Inhibited and Activated.” *Cell* 169 (7): 1303-1314.e18. https://doi.org/10.1016/j.cell.2017.05.025.

Zhao, Boxuan Simen, Ian A. Roundtree, and Chuan He. 2016. “Post-Transcriptional Gene Regulation by MRNA Modifications.” *Nature Reviews Molecular Cell Biology* 18 (1): 31–42. https://doi.org/10.1038/nrm.2016.132.

Zhao, L., S. Yuan, Y. Cao, S. Kallakuri, Y. Li, N. Kishimoto, L. DiBella, and Z. Sun. 2013. “Reptin/Ruvbl2 Is a Lrrc6/Seahorse Interactor Essential for Cilia Motility.” *Proceedings of the National Academy of Sciences* 110 (31): 12697–702. https://doi.org/10.1073/pnas.1300968110.

Zheng, Guanqun, John Arne Dahl, Yamei Niu, Peter Fedorcsak, Chun Min Huang, Charles J. Li, Cathrine B. Vågbø, et al. 2013. “ALKBH5 Is a Mammalian RNA Demethylase That Impacts RNA Metabolism and Mouse Fertility.” *Molecular Cell* 49 (1): 18–29. https://doi.org/10.1016/j.molcel.2012.10.015.

Zhou, Jian, Fang Yang, N. Adrian Leu, and P. Jeremy Wang. 2012. “MNS1 Is Essential for Spermiogenesis and Motile Ciliary Functions in Mice.” *PLoS Genetics* 8 (3). https://doi.org/10.1371/journal.pgen.1002516.

Zietkiewicz, Ewa, Zuzanna Bukowy-Bieryllo, Alicja Rabiasz, Patrycja Daca-Roszak,

Alina Wojda, Katarzyna Voelkel, Ewa Rutkiewicz, Andrzej Pogorzelski, Margarida Rasteiro, and Michal Witt. 2019. “CFAP300 : Mutations in Slavic Primary Ciliary Dyskinesia Patients and a Role in Ciliary Dynein Arms Trafficking.” *American Journal of Respiratory Cell and Molecular Biology*, March, rcmb.2018-0260OC. https://doi.org/10.1165/rcmb.2018-0260OC.

Appendix 1

No.	Name	Nucleotide sequence (5' to 3')
9	GFP forward	AGAACTCTTGCTTGCTTTGCT
10	GFP reverse	TCCTTGAAGTCGATGCCCTT
11	SDM EGFP_G67A_+XhoI_f	GACCACCCTGACCTACgccGTGCAGTG CTTCtcgaggTACCCCGACCA
12	SDM EGFP_G67A_+XhoI_r	GTAGGTCAGGGTGGTCACGAGGGTGG GCCAGGGCACGGG
13	SNAP BAMH1 cloning F +0 ORF	AAAGGATCCGGCGGAAGCGGAGACAA AGA
14	SNAP HindIII cloning r +0 ORF	AAAAAGCTTACCCAGCCCAGGCTTGC CCA
15	SNAP BAMH1 cloning F +1 ORF	AAAGGATCCGGGCGGAAGCGGAGACA AAGA
16	SNAP HindIII cloning r +1 ORF	AAAAAGCTTTCACCCAGCCCAGGCTTG CCCA
17	SNAP BAMH1 cloning F +2 ORF	AAAGGATCCGAGGCGGAAGCGGAGAC AAAGA
18	SNAP HindIII cloning r +2 ORF	AAAAAGCTTTACCCAGCCCAGGCTTGC CCA
19	SNAP sequencing forward	CTGAATGGCGAATGGGAGC
20	SNAP sequencing reverse	CTCTCCAGGGCTGCCAAG
21	pMA-tia1L + GGSGSNAP no stop or start 240-261 undefined	Ccaacttaatcgccttgcagca
22	pMA-tia1L + GGSGSNAP no stop or start 357-377 undefined	AGACGGTTTTTCGCCCTTTGAC
23	pMA-tia1L + GGSGSNAP no stop or start 720-741 undefined	TGACCTCTCCGAACTTCACCAC

24	pMA-tia1L + GGSGSNAP no stop or start 888-906 undefined	GGGCTCGCCGTGAAAGAGT
31	eGFP1-F	TAATACGACTCACTATAGGTACCTCGA GAAGCACTGCA
32	eGFP1-R	TTCTAGCTCTAAAACTGCAGTGCTTCT CGAGGTAC
33	eGFP2-F	TAATACGACTCACTATAGGTAGGTCAG GGTGGTCACGA
34	eGFP2-R	TTCTAGCTCTAAAACTCGTGACCACCC TGACCTAC
35	N-1F cg6971	ACAAACCTGCTGAATTCCTGA
36	N-1R cg6971	CCGTTTGGGGCCTTTTCAT
37	SNAPNR cg6971	GAAGATGATACGGTGCAGGC
38	C-1F cg6971	GGCGCATGAGGAAAAGGAAA
39	C-1R cg6971	AACGCATAGACCACACTCCA
40	SNAPCR cg6971	CGCTTCATTTCGCAGTCTTTG
41	CEL1 eGFP forward	Ataaccatggtgagcaaggg
42	CEL1 eGFP reverse	Tctgcttgtcggccatgata
43	PCM1 ex2_f	Agtgcttcaaagattgtattgct
44	PCM1-ex3_f	GTGCCCAACAGAAGAAAGCA
45	PCM1 ex38_f	tcattccaaagGCAGATCTAAGA
46	PCM1 ex39_f	Tgaatcagaaacgcctcacc
47	Primer SNAP_r	CTCAGGCTGGTGAAAGTAGG
48	PCM1 del_f2	Ttcaagcatgcagactggtg
49	PCM1 del_r39	GGGGAGAAATGACCACACCT
50	PCM1 del_f3	Tcctggtttgatacaggcca
51	PCM1 del_r38	Gtctccatctcctgacctcg
52	PCM1 notdel_f	Ccagttgacttggttgcctc
53	PCM1 notdel_r	Gagtctcgttctgtcaccca
54	C-2F cg6971	GCTCAACGCCTACTTTCACC
55	SNAPCR2 cg6971	AACGCATAGACCACACTCCA
13	PCM1-ex3_r	TAATTCTGCCTGCTCTGGGA

54	DNAH5nterm F	AGTCACCCACATGCATGAGA
55	DNAH5nterm R	Tgcagcacgtcagagactta
56	DNAH5cterm F	Acctggcttgtgttctgaga
57	DNAH5cterm R	CCAGCACTGACAGAGAAACG
60	Pma-tia1l seq F	Gctgcaaggcgattaagttg
61	Pma-tia1l seq R	Gaaggaatcatgggaaataggcc
64	EcoRI Rep78 R	GAATTCctggatccactgcttctccg
65	Linker Rep78 F	GCGCGCCGGGATCCGCTGGCTCCGC TGCTGGTTCTGGCatgccggggttttacgagat
66	FseI Rep78 F	AAAGGCCGGCCAGGCAAAAAAGAAAA AGGCGCCGGGATCCGCTGGCTC
67	Stop Rep78 R	AAAAGAATTCTTActggatccactg
80	Cas9-Rep F	CTTTGACACCACCATCGACC
81	Cas9-Rep R	AGGAAAGGACAGTGGGAGTG
82	MCS F BamHI	GATCCgctagcgcggccgcgtcgacgaattca
83	MCS R HindIII	agcttgaattcgtcgacgcggccgcgctagcG
98	Mouse DNAH5_N_F	GCTCAACGCCTACTTTCACC
99	Mouse DNAH5_N_R	Ttgtcttgtggccccatttg
100	Mouse DNAH5_N_F 1	GAAATCCCGTGCCCATTCTG
101	Mouse DNAH5_N_R 1	Cccatttccctgctctacca
102	Mouse DNAH5_N_F 2	CGGAGAGGTCATCAGCTACA
103	Mouse DNAH5_N_R 2	Gtgtcatctggcttgttccc

Table A1 Primer sequences

The table above shows the primer sequences used in this project in the 5’ to 3’ orientation.

Appendix 2

Gene names	Peptides	Sequence coverage [%]
Dnah5	29	7.7
Eif2s3y	17	42.8
Tcea1	12	39.9
Hsp90aa1	8	12.3
Spag1	7	9.4
Eno1	5	17.1
Alkbh5	4	14.4
Sftpa1	3	14.9
Cdh1	2	3.6
Lox	2	8.8
Epb41l4a	2	4.4
Trmt112	2	20
Myl1;Myl3	1	8.5

Table A2.1 Peptide number and sequence coverage of enriched proteins

The table above lists the gene names, number of peptides used to identify and the percentage of the sequence covered by the peptides of the proteins enriched in the SNAP antibody pulldown, shown in **Figure 4.7**, as measured by mass spectrometry.

Gene names	Sequence
Dnah5	ANLIVQENR
Dnah5	ASDVQNELGALQPSFR
Dnah5	ASPTDTESTIVMR
Dnah5	ASPTDTESTIVMRVLRDMNLSK
Dnah5	DAPEATGETPEEADAEMPK
Dnah5	DEIDEINSDLTPIMK
Dnah5	EKEDTIMTFIAQNPLLPEFESR
Dnah5	EVITSMDR
Dnah5	EVSFNTLDTADGGLLNSVR
Dnah5	GFSEEVQDALIK
Dnah5	HILAMQDLQK
Dnah5	IMDIFTTFK
Dnah5	INELHNDLQR
Dnah5	IVFEPHNIDNASPATVSR
Dnah5	LEQPMQLFQQHPFVLR
Dnah5	LNIPNLGIEEK
Dnah5	LPNPAYTPEISAR
Dnah5	LYEPIASLNHLR
Dnah5	MDQLFAVGGLR
Dnah5	MPPAIEQLMFPHLAR
Dnah5	NISDNKEIVK
Dnah5	SPTDFEWLK
Dnah5	SYLSFIQGYK
Dnah5	TAQAPEHWVLR
Dnah5	TLTFSGFK
Dnah5	VGSIALYTADLK
Dnah5	VLFELMPVIR
Dnah5;Dnah8	YPLLIDPQTQGK

Dnah5;Dnah8;Dnah7b;Dnah1;Dnah11;Dnah10;Dnah12;Dnah3;Dnah2;Dnah17;Dnah9	LVITPLTDR
Eif2s3x;Eif2s3y	AISGVHTVR
Eif2s3x;Eif2s3y	DFTSEPR
Eif2s3x;Eif2s3y	HILILQNK
Eif2s3x;Eif2s3y	IDPTLCR
Eif2s3x;Eif2s3y	IVLTNPVCTEVGEK
Eif2s3x;Eif2s3y	IVSLFAEHNDLQYAAPGGLIGVGTK
Eif2s3x;Eif2s3y	LIGWGQIR
Eif2s3x;Eif2s3y	LKHILILQNK
Eif2s3x;Eif2s3y	LMCKPIFSK
Eif2s3x;Eif2s3y	LSKNEVLMVNIGSLSTGGR
Eif2s3x;Eif2s3y	NEVLMVNIGSLSTGGR
Eif2s3x;Eif2s3y	QATINIGTIGHVAHGK
Eif2s3x;Eif2s3y	QDLATLDVTK
Eif2s3x;Eif2s3y	SFDVNKPGCEVDDLKGGVAGGSILK
Eif2s3x;Eif2s3y	VGQEIEVRPGIVSK
Eif2s3y	AGGEAGVTLGQPHLSR
Eif2s3y	LDDSSCPRPECYR
Tcea1	APSTSDSVR
Tcea1	DTYVSSFPR
Tcea1	EESSSSSNVSSR
Tcea1	KQSTDEEVTSLAK
Tcea1	LLDGPSTDKDPEEK
Tcea1	MEDEVVR
Tcea1	MTAEEMASDELK
Tcea1	MTAEEMASDELKEMR
Tcea1	NCTYTQVQTR
Tcea1	QSTDEEVTSLAK

Tcea1	SADEPMTTFVVCNECGNR
Tcea1	TGGTQTDLFTCGK
Hsp90aa1;Hsp90ab1	ADLINNLGTIAK
Hsp90aa1;Hsp90ab1	GVVDSEDLPLNISR
Hsp90aa1;Hsp90ab1	YIDQEELNK
Hsp90aa1	ALLFVPR
Hsp90aa1	DQVANSAFVER
Hsp90aa1	ELISNSSDALDK
Hsp90aa1	LGIHEDSQNR
Hsp90aa1	NPDDITNEEYGEFYK
Spag1	ACAIYTNR
Spag1	ALELHPFSVKPLLR
Spag1	IETAGLTEK
Spag1	LPPIPAVPTSEPLR
Spag1	LQEAVDDLRK
Spag1	SGEEGYYPELTEFCEK
Spag1	SLSALPTAIAYNNR
Eno1	AGYTDQVVIGMDVAASEFYR
Eno1	DATNVGDEGGFAPNILENK
Eno1	EALELLK
Eno1	GVSQAVEHINK
Eno1	LAMQEFMILPVGASSFR
Alkbh5	EAAAAAAAAVAAAAAAAAAAEPYPASGTTK
Alkbh5	IDEVVSR
Alkbh5	LFSQDECSK
Alkbh5	VSEPVLSLPVR
Sftpa1	AGGHIAAPR
Sftpa1	NPEENEAIASITK
Sftpa1	VFSTNGQSVNFDTIR

Cdh1	DTANWLEINPETGAIFTR
Cdh1	DTGVISVLTSGLDR
Lox	ASFCLEDTSCDYGYHR
Lox	VSVNPSYLVPESDYTNNVVR
Epb41l4a	ITANTENGENEGTTK
Epb41l4a	SSDAQGSGGSTVHQR
Trmt112	INPVEFNPEFVAR
Trmt112	LLTHNLLSSHVR
Myl1;Myl3	VFDKEGNGTVMGAELR

Table A2.2 Amino acid sequences of enriched peptides

The table shows the gene names of the proteins enriched by pulling down SNAP-DNAH5 with the SNAP antibody and the amino acid sequences of the corresponding used to identify them.